UNIVERSITY OF CALIFORNIA
RIVERSIDE

Using Hsp40 Affinity to Profile Destabilized Proteomes

A Dissertation submitted in partial satisfaction
of the requirements for the degree of

Doctor of Philosophy

in

Chemistry

by

Guy Mitsuo Quanrud

March 2022

Dissertation Committee:
Dr. Joseph Genereux, Chairperson
Dr. Yinsheng Wang
Dr. Min Xue

The Dissertation of Guy Mitsuo Quanrud is approved:

Committee Chairperson

University of California, Riverside

ACKNOWLEDGEMENTS

The scientific journey of graduating from UCR with a Doctor of Philosophy in Chemistry has been a difficult challenge. I would not be able to make it this far without the help of many individuals and I would like to thank them here.

First, I would like to thank Hoi Ting Wu. I met her during the second half of my graduate career at UCR and since then, she became the essential backbone and support for my schooling, my career, and my life. Not only has she helped with mass spectrometry, but she has also guided me through difficult challenges and gave me confidence and strength to become a more cheerful and better student at work and at home. I am forever grateful for having her in my life and I will always try to do the same for her. I also would like to thank her family for their support as well.

Many other graduate students also contributed to my graduate studies. Yana Lyon, Dylan Riggs, James Bonner, Lance Talbert, and Tyler Lambeth and the rest of the Julian lab all contributed to the start of my career at UCR. Yana Lyon and Dylan Riggs continued to not just support me as I progressed through but were also sources of constant help and assistance in the Genereux lab. I am forever grateful for their contributions and support. From the Hooley lab, where I first started, Lauren Halloway and Paul Bogie both watched over me even though I worked on a separate floor. I am also very appreciative of their guidance as well as the friendships I had with the rest of organic and inorganic chemistry department through teaching and meetings. This includes very talented and very fun people such as Taylor Alexander, Ryan Stanton, Jessica Rodriguez, and Jan P. Scheifers.

My family has also been very supportive along my journey. My parents and little brother Noah have always cheered me on from San Jose, Ca. My older brother Kent has been an inspiration as he is the first Quanrud to achieve a PhD. They have watched me grown from my undergraduate studies at Albion College through my graduate studies at Northeastern University and UCR and they never lost faith in my work. I will always be appreciative of that.

I would like to thank the Genereux Lab for transforming me into the graduate student that I am today. Maureen Montoya and Liangyong Mei were integral into transitioning me into the exciting Hsp40 chaperone project. Khanh Ngyuen and Mateo Espinoza were also very helpful in the lab. Ziqi Lyu became an integral part of the lab especially during difficult times and has been always very helpful in all my projects. I also thank every undergraduate for assisting me in my projects. This includes Michaela Sabbah, Mohammad Awad, Sunil Balamurugan, and Enrique Felix. Macon Abernathy, a honorary member of the Genereux Lab, was really helpful in driving our studies in Manganese and Vanadium as well as contributing to our studies in Hsp40 chaperones. I am so fortunate to work with him during my last year at UCR.

I would like to thank the staff at UCR. My committee members Dr. Yingsheng Wang and Dr. Min Xue have always provided assistance such as sharing equipment and given me guidance throughout my journey. I would also thank Dr. Rena Hayashi as she was my teaching boss. She always provided me with a lot of assistance gave me lots of encouragement in teaching undergraduates in organic chemistry.

Finally, I would like thank my Principal Investigator, Joseph Genereux. He is

responsible for the skillset and knowledge I have gained in proteomics, chemistry, and biochemistry. I was very fortunate that he trusted me to expand upon his research on Hsp40 chaperones as well as represent him in many conferences and seminar talks. He thus has helped me become successful in graduate school and in my career in chemistry as well.

To everyone I have discussed and to the ones I haven't mentioned, I say thank you again.

The Material in Chapter 2 was previously published. It is reprinted with permission from *Anal. Chem.* **2021,** 93 (50), 1690-16946.

ABSTRACT OF THE DISSERTATION

Using Hsp40 Affinity to Profile Destabilized Proteomes

by

Guy Mitsuo Quanrud

Doctor of Philosophy, Graduate Program in Chemistry
University of California, Riverside, March 2022
Dr. Joseph Genereux, Chairperson

Proteins in their native or optimal conformational states can perform essential cellular functions to assist in the stability of the proteome and the overall health of the cell. However, if a protein misfolds, it instead can gain a new toxic function. Misfolded proteins can aggregate into more stable toxic precursors that can cause cellular degradation and ultimately induce health disorders such as Parkinson's Disease, Alzheimer's Disease, and Huntington's Disease.

Cellular stresses are significant factors in protein misfolding. These stimuli can change protein structure through several mechanisms such as covalent modification of cysteines or oxidation of methionine residues. The immediate consequence of post-translational modifications of a protein from stress is difficulty in refolding. The long term consequence is that these altered proteins can instead gain new toxic functions as they proceed to aggregate. Therefore, changes to protein structures induced by stresses can create cellular havoc as the cell scrambles to recover from the affected misfolded proteins.

Several analytical assays can measure the effects of stress on protein stability. Fluorescence assays show direct changes to a protein based on gain or loss of signal. Mass Spectrometry surveys entire proteomes by measuring a protein's ability to react after exposure to a cellular stress. Herein, we describe a quantitative proteomics approach that measures proteins binding to Hsp40 chaperone DNAJB8, a protein quality control factor designed to recognize misfolded proteins. We aimed to use the chaperone to identify destabilized proteins and deduce toxic cellular mechanisms arising from environmental stresses. We found several ribosomal proteins such as TAR DNA-Binding protein (TDP-43) and Pyruvate Dehydrogenase E1 subunit (PDHA1) misfolded after arsenite exposure. Later, we found potential biomarkers in GAPDH and PARK7 involved in driving the cellular toxicity of propachlor. Led by limited proteolysis, we conducted several validation experiments to show that DNAJ8 recognized significantly destabilized proteins after exposure to environmental toxins. In total, we hope to show the effectiveness of this approach in exploring how environmental toxins can impact cellular proteostasis and identifying the resulting susceptible proteome.

Table of Contents

LIST OF FIGURES

LIST OF SCHEMES

TABLES

Chapter 1: Introduction to Protein Misfolding and DNAJB8

1.1 The Relationship Between Protein Folding and Protein Activity

The nature of how a protein folds can often reflect how it functions. Proteins ideally perform many beneficial roles to cells such as transporting nutrients and molecules for energy, regulating other proteins to keep cell compartments functional, or attacking foreign molecules to provide protection[1,2,3]. Proteins perform these roles when in their optimal conformational state, i.e. the folded state, or when oscillating between energetically favorable structural states[4,5]. Proteins in these conformational states are unhindered in performing their desired tasks in helping to maintain cellular health.

This relationship between protein folding and protein activity can be effectively visualized by assessing the cellular activity of a Green Fluorescent Protein (GFP) against its degree of folding as seen in **Scheme 1**[6]. The GFP functions most effectively as a fluorescent protein with complete formation of the beta barrel surrounding the chromophore in the middle[7,8]. This beta barrel provides structural stability for the protein by protecting the fluorophore against premature quenching by solvent[9,10,11]. In the energy landscape of the GFP, this state is illustrated as the most energetically favored structure[6]. This structure both is its native state and also the most thermodynamically favored state at equilibrium[6] (**Scheme 1**). It is not easy for the GFP to reach this native state. The energy landscape of the GFP shows that the GFP can also fold into several slightly less energetically favorable states. These states can represent kinetically favorable folded structures for GFP based on the rate of folding from the nascent polypeptide[12].

Thus, the GFP can undergo several folding pathways before folding completely into its native state (**Scheme 1**).

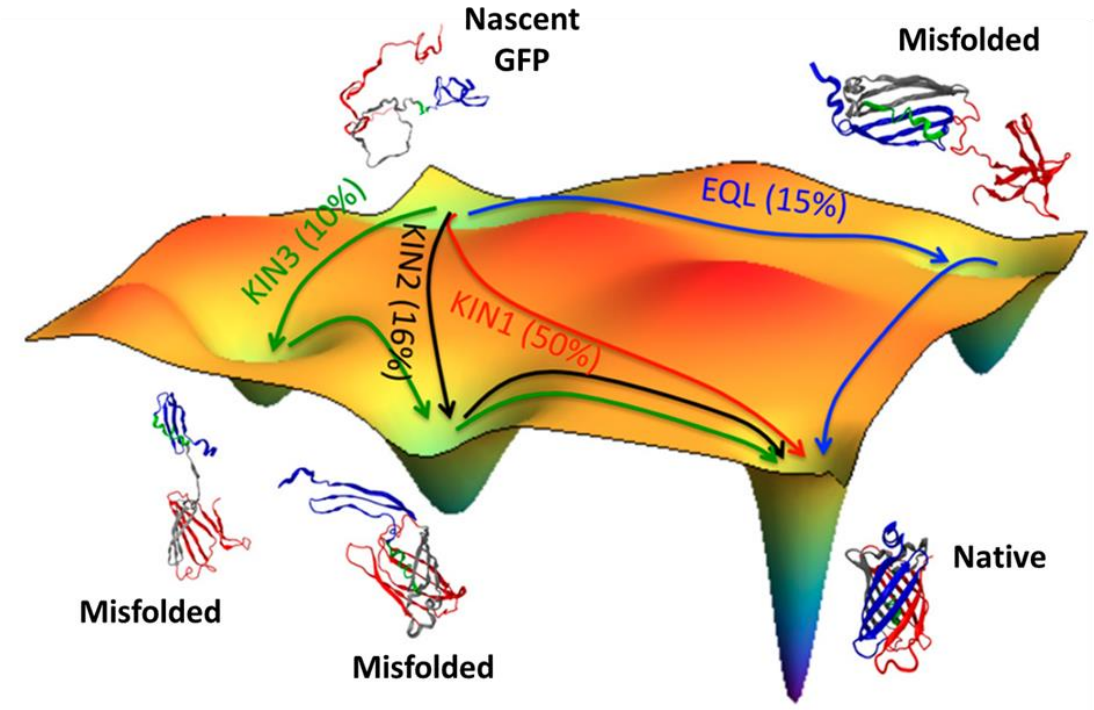

Scheme 1: Representative Folding States For a Protein: Folding landscape of Green Fluorescent Protein (GFP) is shown. The flux or arrows represent the different paths of folding that GFP can take before it can reach its native state. The native state of GFP can be seen with the largest energy potential as shown and labeled. Other energy potentials seen represent different folding states of GFP. GFP energy diagram was calculated based on Brownian simulations from Reddy et al. 2012[6].

In the energy landscape of the GFP, roughly 15% of the nascent polypeptide GFP will achieve their native state following normal folding pathways at equilibrium, while 76% of the nascent polypeptide GFP will reach their native state following kinetic folding pathways[6]. The remaining 9% of the nascent polypeptide population will never

reach the native state[6]. The structure of the GFP also reflects how well the GFP can fluoresce. The conformational states of the GFP in which the beta barrel did not completely form fluoresce less, likely more due to chromophore quenching than due to the lack of complete protection[13,14].

Cellular stresses can make it difficult for proteins to reach or retain these stable conformations. A cellular stress is a stimulus that prompts the cell to try to recover and survive the distress[15]. Cellular stresses in the form of environmental toxins or toxicants for example can directly modify active cysteines or oxidize certain residues of proteins making forming the tertiary structure of a protein difficult[16,17]. Cellular stresses can thus misfold the protein and create a new folding pathway. The energy required for a protein to reach the native state from a protein misfolded state caused by a cellular stress becomes more endergonic and unfavorable[18,19]. Proteins once misfolded from cellular stresses can instead prefer to fold into a more stable misfolded state (**Scheme 2**)[20]. Proteins possibly modified by oxidative stress readily continue to misfold into more stable aggregates and amyloid fibers[20,21,22]. Cellular stresses thus change the nature of protein folding. Proteins may never reach the native state and instead form different misfolded structures that in turn hamper their true cellular function.

Ultimately, a misfolded protein affected by cellular stress can gain a new toxic function. Misfolded proteins become cellular stresses in forming toxic misfolded aggregates in several neurological diseases. In Huntington's disease, the protein huntingtin which phenotypically should support neuronal protection, is mutated such that there are multiple CAG repeats in its gene[23,24]. The ability of the huntingtin protein to

fold into native structures is impaired, and when this mutant is cleaved for degradation, a toxic larger polyglutamine fragment (polyQ) is released. This fragment can aggregate in the nucleus and disrupt essential transcription factors TBP and CBP[25,26].

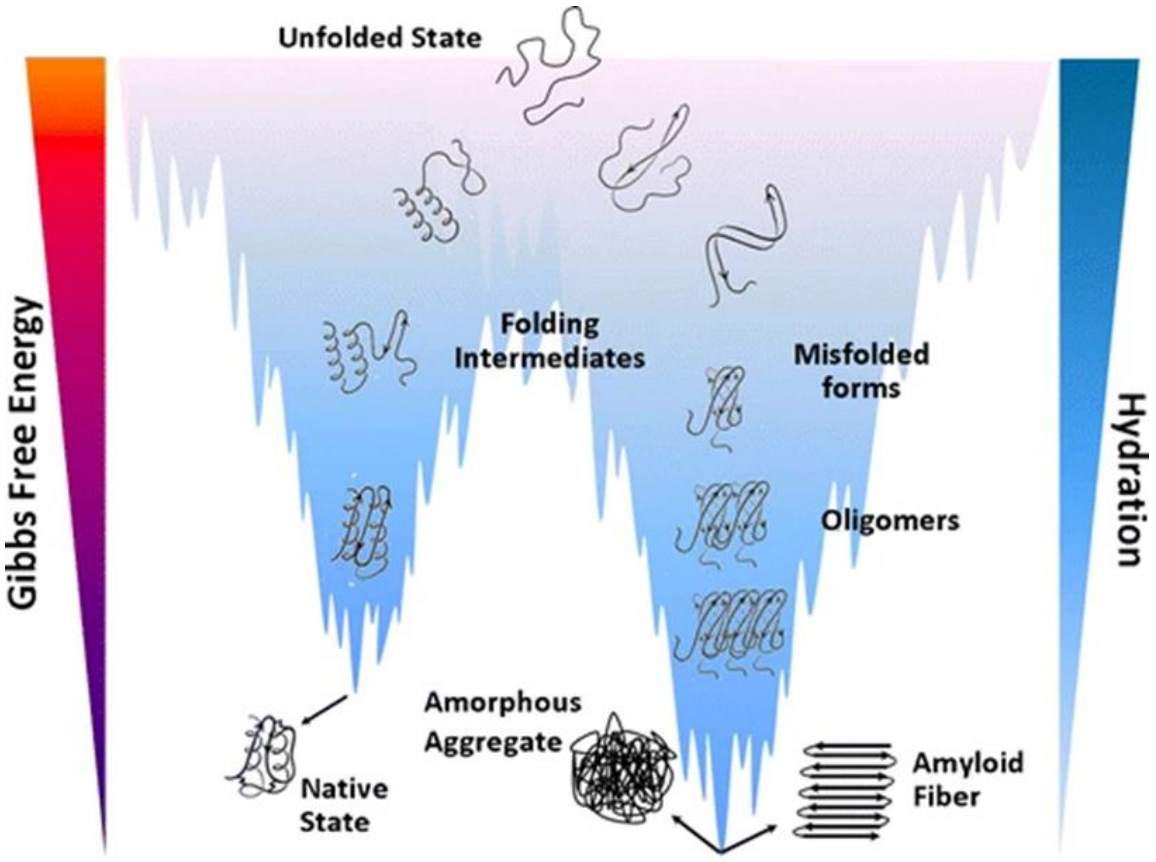

Scheme 2: New Energy Landscape for Misfolded Proteins. From an unfolded state, proteins can instead fold into more toxic forms as they are more energetically favorable. States with lower energy states are at the bottom of the protein-folding funnel. As they begin to form more of these disordered and misfolded structures, the less water soluble these proteins become. The protein-folding funnel diagram was taken from Cordeiro et al. 2014[20].

Ultimately, the toxic aggregates of PolyQ fragments disrupt cellular networks and damage medium spiny neurons (MSNs) to cause neurodegeneration[27]. Alpha-synuclein in

Parkinson's Disease misfolds and aggregates into toxic oligomers and ultimately lewy bodies[28]. Alpha-synuclein, instead of regulating neurotransmitters and regulating trafficking, misfolds due to environmental or hereditary factors and proceeds to form stable aggregates that cause neurodegeneration[27]. Two pathologies of Alzheimer's disease relate to the aggregation of the tau protein and beta actin[29,30,31]. Both misfolded proteins form more stable favorable toxic fibrils but also can co-aggregate with other proteins in the presence of oxidative stress[32,33]. Proteins gaining new toxic functions due to misfolding are highly evident in neurological diseases. Cellular stresses play a role in forming that toxic pathology.

Cellular stresses can modify the protein structure and thus change the trajectory of its functions. Proteins can lose or perform in a slightly less efficient manner by not folding into their optimal or native states. Cellular stress can unfortunately misfold the protein and influence them to gain a new toxic function. The loss of a function or the gain of new toxic functions by the misfolded protein can lead to immediate and long term cellular problems. The effects of cellular stress on protein misfolding motivates the desire to determine which proteins are most sensitive to change and ultimately determines the toxic pathology of the condition.

1.2 Analyzing Effects of Cellular Stresses on Individual Proteins

Proteins can be assessed in the presence of cellular stresses to determine how their function changes. These assays aim to determine if a protein misfolds after incubation with a cellular stressor.

Fluorescence assays can effectively analyze how a protein changes after exposure to cellular stresses. A protein can be fused to an AgHalo Tag and then screened against different stresses to determine if it misfolds[34,35]. The AgHalo tag is attached in a position where it will fluoresce if the protein aggregates. Proteins that misfold and aggregate due to a cellular stress and will gain a fluorescence signal. Proteins unaffected by a cellular stress will not fluoresce. Thus the AgHalo tag can assess protein misfolding and determine if it gains a toxic function by aggregating. Fluorescence Resonance Energy Transfer (FRET) can also be used to measure changes in the protein structure based on the position of the donor and acceptor. A protein can misfold due to a cellular stress, changing the distance between the donor and acceptor on the protein. This will lead to either gain or loss of FRET Signal[36]. Fluorescence assays can thus provide evidence of structural changes in proteins and sometimes indicate a change in protein functionality after treatment of a cellular stress.

Protein expression levels can be measured in response to cellular stress to evaluate protein stability. Misfolded proteins that cannot refold into their native or functional forms are often targeted for degradation pathways for protein turnover[37]. Cellular stress can increase the turnover rate of a protein by misfolding it. The cellular response could be to overexpress the protein or express proteins that can assist in refolding the protein[38,39,40]. RT-PCR for example can measure increases in mRNA of stress response proteins such as Hsp60 and Hsp70 after exposure to a stress, indicating the presence of misfolded proteins[41]. Proteins known to aggregate such as α-syn nuclein can have higher mRNA expression rates due to certain mutations[42]. These mutations can

cause the protein to misfold, sent to degradation and thus the cell responds by trying to express more α-syn nuclein. The levels of a protein can also be measured to determine misfolding by western blotting. Protein aggregation can be observed as large smears indicating that multiple proteins co-aggregated with the misfolded protein[43]. Specific interpretations of protein expression levels can indicate whether a protein misfolded due to a cellular stress and determine if the protein gained a new toxic function.

1.3 Simultaneous Detection of Multiple Misfolded Proteins

Quantitatively profiling the cellular stresses on protein misfolding for multiple proteins at once can be advantageous. For example, misfolded proteins influence the misfolding and aggregation of other proteins. Transcription factors in RNA synthesis such as ELK1, E3 ubiquitin ligase proteins HERC5, or chaperone proteins such as PARK7 are some of the many proteins involved in the regulation of alpha-synuclein[44,45]. If these proteins are misfolded from a cellular stress, they can lose their inherent function in regulating alpha-synuclein[46]. Assays that can screen how cellular stress can misfold multiple proteins can help narrow down which proteins are involved in the toxic mechanisms of the condition[46].

Bottom-up proteomic approaches can incorporate mass spectrometry to screen a misfolded proteome after treatment with a cellular stress[47,48,49]. These techniques can qualitatively identify peptides by using liquid chromatography for separation and then using tandem mass spectrometry to identify them based on size and sequence[50]. This platform can thus identify peptides from multiple misfolded proteins after treatment of

cellular stresses. Several strategies have utilized mass spectrometry to show how multiple proteins can structurally change in the presence of a stress/condition.

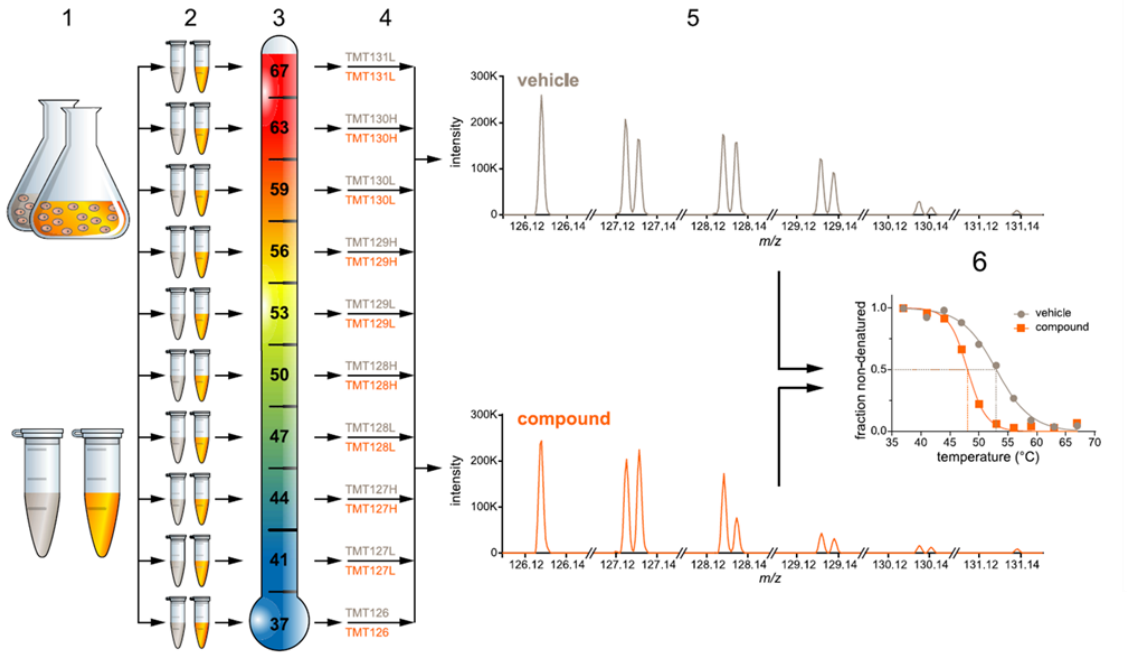

Scheme 3: Representative Bottom-Up Proteomics Approach to Assess Protein Misfolding by Cellular Thermal Shift Assay (CETSA). Two different conditions of a proteome are assessed. Each condition is aliquoted and subjected to different temperatures. Samples are then labeled with a different Tandem Mass Tag (TMT) label and pooled. Pooled samples are run and quantified by mass spectrometry. Peptides exhibiting differences in stability are shown by melting curves. Proteins are thus assessed for protein stability simultaneously by TMT Mass Spectrometry. CETSA scheme was taken from Savitski et al. 2014[54].

These techniques can specifically use changes in peptide abundance to suggest that a protein has become unmeasurable for quantification, possibly because of a change in structure due to misfolding[51,52,53].

The cellular thermal shift assay (CETSA), for example, quantifies protein stability

by exposing proteins to a panel of increasing temperatures and then measuring the peptides that remain soluble (**Scheme 3**)[54,55,56]. Proteins will misfold and aggregate at a given temperature[57]. When the protein aggregates, they become insoluble, and ideally become unable to be labeled for mass spectrometry quantification. CETSA utilizes this heating concept to show that aliquots from two different conditions (e.g drug treatment versus control) will have differences in the amount of soluble proteins remaining after incubation at higher temperatures. Drug treatment for example can stabilize the protein to make it less prone to aggregation at higher temperatures compared to the control. These soluble protein fractions after heat treatment are labeled by Tandem Mass Tags (TMT) and pooled together for a single LC-MS/MS run. The amount of protein remaining in each aliquot is measured based on the intensity of the respective reporter ion in the MS2[54,57]. Ideally peptides that show differences in their melting curves can indicate that the treatment prevents aggregation (**Scheme 3**)[54]**.** Although most CETSA applications examine the effects of ligands stabilized or protecting proteins from heat, CETSA can possibly profile the effects of different stresses. Cells treated with a stress can be more aggregation prone and thus less soluble at higher temperatures compared to the control.

Stability of Proteins from Rates of Oxidation (SPROX) follows a similar procedure to CETSA except it utilizes a gradient of oxidative conditions to quantitatively show changes in protein stability based on the oxidation of methionine residues[58,59,60]. Proteins after cellular treatment can misfold, and methionine residues may be more solvent exposed. Methionine oxidation of a peptide can be proportional to how exposed the peptide is to solvents, and $\Delta G_{folding}$ can be determined between different states of the

protein. Misfolded proteins due to a cellular stress can be more prone to oxidation of methionine residues. SPROX has ability to profile the effects of cellular stresses on proteins with methionine residues.

Other residues can also be probed to modify structural changes after cellular stresses. Cellular stresses in the form of small molecules can react with nucleophilic cysteine of proteins to modify their structure[61,62]. These post-translational modifications can inhibit proteins such as enzymes but also influence new toxic functions as modified proteins can aggregate[62,63,64]. Activity Based Protein Profiling (ABPP) utilizes the ability of nucleophilic cysteines in proteins to react with electrophilic probes to profile changes in protein structure[65,66,67,68]. If a cellular stress can modify a cysteine, the site will not be reactive toward the electrophilic probe. The probe can be tagged and labeled with a heavy or light antibody for quantitation and identification by LC-MS/MS[63]. ABPP thus provides identification of multiple proteins that can be misfolded by modification by a cellular stress. Lysine residues in proteins can also be probed to identify structural changes after cellular stresses. Lysine residues are often structurally located on the surface of proteins, and the hydrogens on the side chains are solvent exposed[69,70,71]. Covalent Protein Painting (CPP) is a bottom-up proteomics approach that labels surface exposed lysines in proteins for LC-MS/MS[72]. Proteins misfolded after incubation with a cellular stress will have higher quantified signals due to more labeling of the lysine residues.

Mass spectrometry can also incorporate label free techniques to identify misfolded proteins after incubation with a cellular stress. Limited Proteolysis (LiP) is a label free method used to show differences in protein states based on differences in

proteolytic digestions (**Scheme 4**)[73,74,75]. Similar to CPP, LiP takes advantage of how many more peptides in proteins can be exposed to the environment in a denatured state than in the native state by enzymatic digestion.

A broad specific enzyme such as Proteinase K (PK), for example, can digest peptides that are normally buried in the native state of a protein[76,77]. LiP thus incorporates an initial PK digestion before the trypsin digestion of the denatured and the native states of a protein. Proteins that misfold due to a cellular stress would be more susceptible to PK digestion and thus be more sensitive to the subsequent trypsin digest.

Proteins not treated by cellular stress are ideally more resistant to PK digestion. The presence of half tryptic peptides or loss of sensitivity of a particular tryptic peptide between two different conditions shows that the protein is sensitive to misfolding from a cellular stress[73,74]. LiP can thus identify which proteins are more sensitive to cellular stress and determine global or proximal regions where the protein misfolds based on enzymatic digestion.

Each of these bottom-up proteomic approaches utilize different aspects of protein folding to measure protein stability. Several of these methods can utilize the modification of side chains of amino acids, protein behavior in the presence of known stressors such as heat and oxidation, and the manner in which proteins are digested by enzymes to show the effects of cellular stresses. The requirements for each technique can be limiting. CETSA shifts proteins far from equilibrium by exposing them to increasing temperatures. This measurement of protein stability does not reflect proteins misfolding at normal cellular conditions.

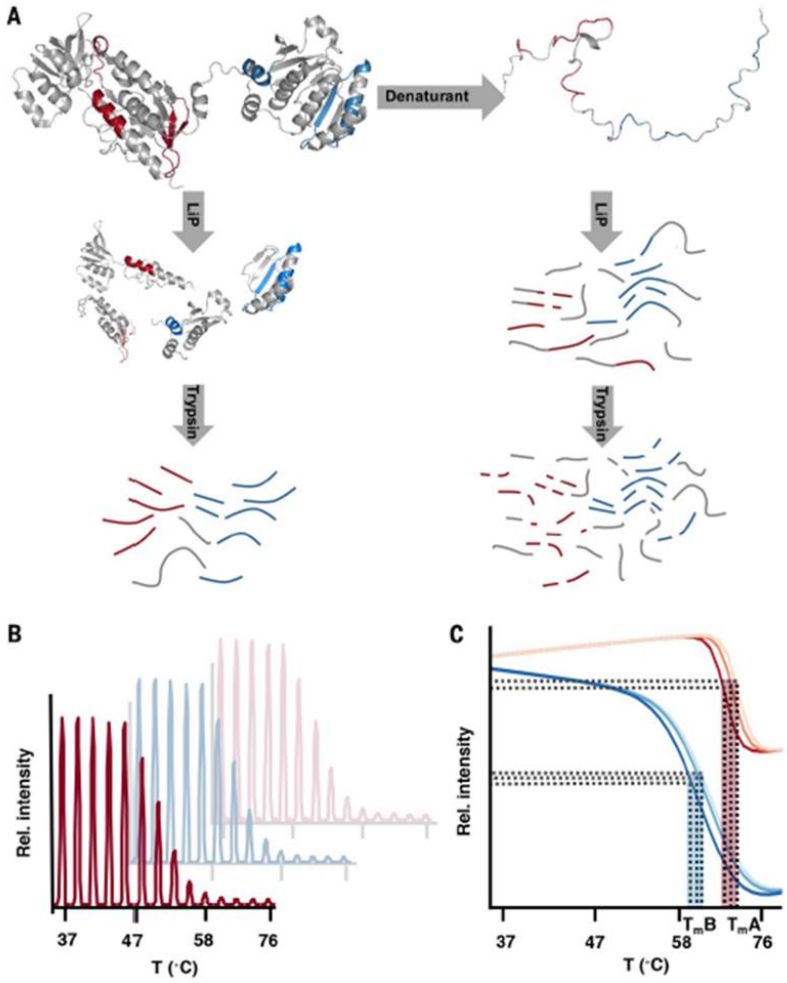

Scheme 4: Representative Bottom-Up label free method to assess protein stability by Limited Proteolysis (LiP). Proteins can be assessed by label free methods such as LiP. Two different states of a protein can be shown to have different digestion by incorporating a short proteolysis step before trypsin digest as shown in panel A. Targeting methods can be used to show differences in peptide abundances with native states being more resistant to digestion compared to denatured states as shown in panel B and C. LiP scheme was taken from Leuenberger et al. 2017[73].

LiP can be challenging to reproduce as a discovery method in assessing cellular stresses. LiP requires distinct and significant differences in PK sensitivity in a peptide of an observed protein to change structure. SPROX can only profile proteins with

methionine residues and further cannot the profile protein response to oxidative stress because it will prematurely oxidize the residue. When conducted in parallel, however, these techniques can be effective in profiling misfolded proteins. If a protein is found to be misfolded utilizing multiple bottom-up approaches, it reduces the possibility that a protein identified to misfold from a cellular stress is a false positive (type 1 error)[78,79]. Moreover, each technique can profile multiple proteins at once and thus discover proteins that can misfold and gain new toxic functions in a much quicker fashion.

1.4 Utilizing Protein-Protein Interactions to Probe Protein Misfolding

A different approach that does not aim at quantifying modified residues, misfolding due to heat, or showing differences in enzymatic digestion is to recognize a misfolded protein by protein-protein interactions. Cells have inherent protein quality factors in proteostasis that can recognize and interact with misfolded proteins. Proteostasis encompasses a network of pathways that controls protein integrity (**See Scheme 5**)[80,81,82]. In the presence of misfolded proteins, mutations, and exogenous compounds, protein quality control factors are released to help the cell respond and recover[83,84]. Misfolded proteins can be refolded by molecular chaperones released after the activation of heat shock factors[85,86,87]. Misfolded proteins can also be targeted for degradation pathways. Misfolded proteins can be degraded in lysosomes or ubiquitinated by E3 ligases and digested in the 26S proteasome for example[88,89]. Protein quality control factors thus encompass several protein interactors that have a binding affinity for misfolded proteins.

Molecular chaperones have been used for Affinity Purification Mass Spectrometry (AP-MS) to profile misfolded proteins in the presence of cellular stresses.

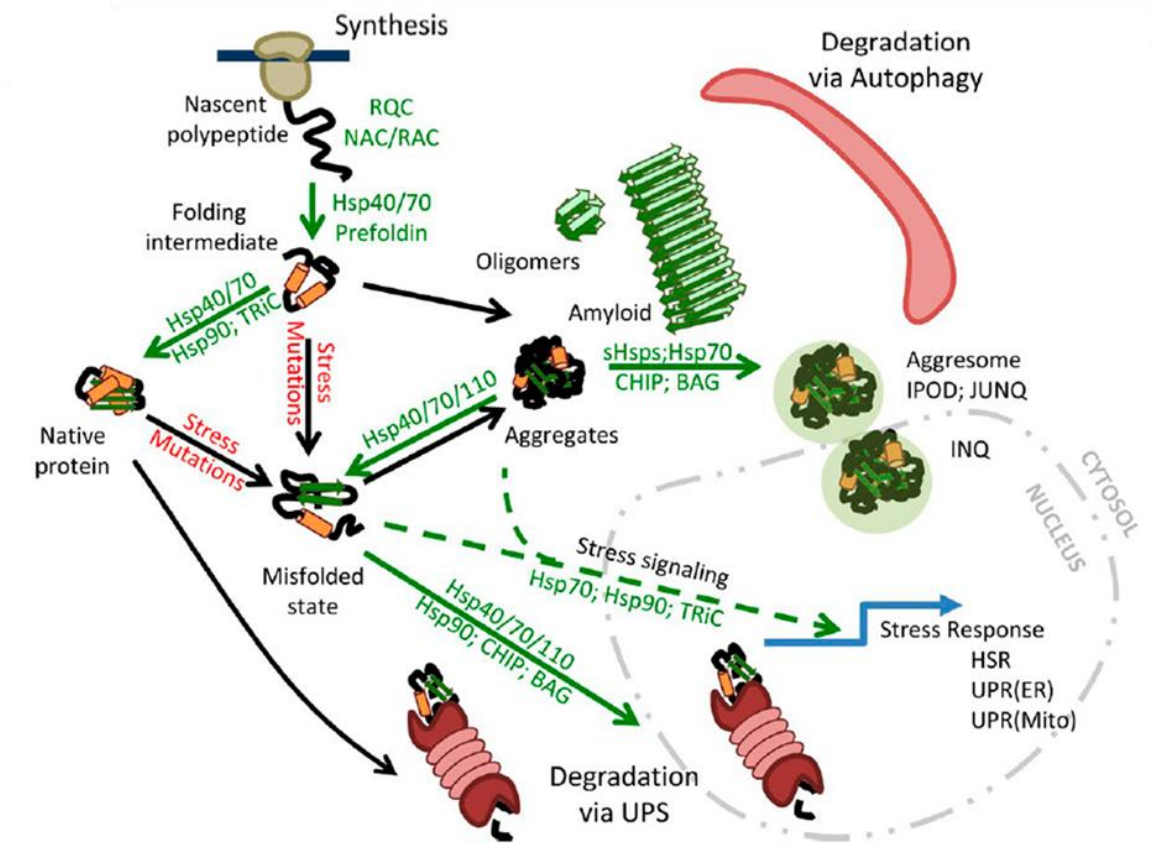

Scheme 5: Overview of Proteostasis. Nascent polypeptides can go through different stages of folding due to proteostasis. Proteostasis encompasses all folding pathways for a protein to reach its native state. Protein can misfolded due to stress, mutations. Cellular responses such as activation of chaperone (shown in green) are activated to attempt to refold the protein. Proteins can also be designated for degradation in pathways such as the Ubiquitin-Proteasome System (UPS) or to the Unfolded Protein Response (UPR) in the endoplasmic reticulum (ER). Scheme was taken from Klaips et al. 2018[84].

AP-MS strategies typically incorporate an epitope tag into a protein to create a bait for protein-protein interactions to be pulled down for purification and thus identified

and quantified by LC-MS/MS[90,91]. Chaperone proteins are excellent bait candidates for investigating the effects of cellular stresses as they adjust their conformation to maximize binding to interact with the entire proteome[92]. Heat Shock Protein 70 (Hsp70) and Heat Shock Protein (Hsp90) chaperone proteins have been tagged to pull down protein interactors after cellular exposure to a stress[93,94,95].

Hsp70 chaperone protein Ssa1 and Hsp90 chaperone Hsp82 were HIS_6 tagged and pulled down misfolded proteins from yeast lysate in response to cellular treatment of methanesulfonate, a DNA damaging agent[93]. Proteins that were more destabilized due to methanesulfonate can be recognized by the chaperone bait and be shown to be more abundant in treated samples compared to untreated samples[93]. Hsp90 has also been used to profile proteins against Hsp90 inhibitors and Hsp70 has also been used to profile misfolded proteins in the presence of mutated proteins[94,95]. The inherent biological phenotypes that chaperones use for protein recognition makes them desirable for identifying misfolded proteins after treatments with cellular stress.

There are other protein-protein interactions that can be used to study the effects of stresses on proteins. Misfolded proteins can be targeted and sent for degradation through the Endoplasmic Reticulum (ER)-associated protein degradation (ERAD) and then the Ubiquitin-Proteasome pathway (UPS)[96,97]. These pathways for misfolded proteins thus provide areas of the cell where sensors can be sent to identify proteins sent there possibly because they misfolded due to cellular stress.

Ascorbate Peroxidase 2 (APEX2) can be used as a labeling strategy for identifying misfolded proteins trafficking in cellular compartments such as the ER[98,99].

APEX2, as a peroxidase, can generate biotin-phenoxyl radicals after the addition of hydrogen peroxide and biotin phenol and can covalently modify proteins in near approximation[100]. The labeling strategy with APEX2 is to fuse the peroxidase to a protein of interest where it can label proteins with biotin phenol. The labeled proteins can then be enriched and quantified by LC-MS/MS[101]. APEX2, for example, has been fused to Ribosome-binding protein 1(RRBP1), an abundant ER-membrane bound protein to label proteins trafficking in and out of the ER[102]. In comparing two conditions of either incubation with cellular stress or without, proteins that misfold due to a cellular stress can be sent to the ER for degradation and thus be labeled by APEX2-RRBP1. These proteins do not appear labeled in the control condition. APEX2 can also be fused to known protein aggregators to determine co-aggregating proteins. Proteins that co-aggregate will misfold to form different conformational structures that allows them to interact with each other[103]. Alpha-syn nuclein was fused for APEX2 to discover proteins such as RNA-binding proteins that can interact, misfold, and possibly co-aggregate with the protein[104]. APEX2 labeling can thus be used to identify possible misfolded proteins based on cellular trafficking and protein-protein interactors. Heat shock protein 40 (Hsp40) chaperone proteins can be effective interactors for misfolded proteins. Hsp40 chaperones are protein quality control proteins involved in the protein misfolding response[105]. These proteins are localized to different parts of the cell and their role is to coordinate with Hsp70 chaperone partners to assist in refolding of a misfolded protein[105]. Hsp40 proteins can have an additional role in interacting directly with misfolded proteins and recruiting them to Hsp70 binding partners depending on their structure.

Type I and type II Hsp40 proteins have a distinct peptide binding region that can bind to proteins[105,106]. Having this region allows Type I and Type II Hsp40s to dimerize, use the peptide binding region to bind to a misfolded protein, and then lead them to Hsp70 protein for refolding[109,107].

This handoff has been studied in ERDJ3, a type II Hsp40 chaperone localized in the ER. In ERDJ3, the mutation of Histidine 31 to Glutamine halted the handoff of substrate kappa light chain to BiP, the Hsp70 binding partner in the ER[108,109]. This mutation in ERDJ3 prevented the formation of folding complex with BiP and possibly decreased stimulation of ATPase of BiP for substrate transfer[108]. Thus, the right type of Hsp40 proteins can be mutated to interact and retain proteins that are misfolded due to a cellular stress.

DNAJB8, a Hsp40 chaperone localized to the cytosol and nucleus, can be an ideal bait for misfolded proteins. DNAJB8 has a strong affinity for proteins due to its large structure covering a large substrate binding area[110]. DNAJB8 is also promiscuous in that it is not selective in the type of proteins it will bind to[109]. Finally, DNAJB8 can also be mutated at histidine 31 to glutamine to block substrate handoff to its binding partner HSPA1A[108]. Following similar strategies of protein interactors as discussed before, DNAJB8 can be used to identify misfolded proteins after an incubation of a cellular stress.

Pulldown experiments of a mutated ^{Flag}DNAJB8^{H31Q} combined with TMT proteomics were tested[111]. Cells transfected with ^{Flag}DNAJB^{H31Q} and with DSP crosslinking produced a large and significant client list in comparison to mock (GFP)

pulldowns[111]. Co-immunoprecipitated clients from DNAJB8^{H31Q} were fairly consistent between biological replicates, and 562 interactors were found to significantly bind to the bait after applying Pearson's correlation with a low false positive rate ($q_{BH} < .01$) after applying Benjamini-Hochberg analysis[111]. The workflow for immunoprecipitation using ^{Flag}DNAJB8^{H31Q} is also very facile and advantageous. Six 10 cm plates at once can be pooled for TMT-MudPIT runs allowing for a single MudPIT run to account for bait variability[111]. Overall, ^{Flag}DNAJB^{H31Q} can use its phenotypic biological recognition to recognize misfolded proteins after incubation of cellular stress. Proteins that misfold due to a cellular stress are more likely to bind to DNAJB8^{H31Q}, be co-immunoprecipitated, and then identified and quantified by LC-MS/MS.

1.5 Profiling Heavy Metals and Herbicides by DNAJB8^{H31Q}

Herein, the ^{Flag}DNAJB8^{H31Q} assay was thus used to assess the misfolded proteome in HEK293T cells after incubation from environmental stresses. The variety of stresses that can be profiled by ^{Flag}DNAJB8^{H31Q} provide an opportunity to explore new and existing mechanisms of toxicity and evaluate the capabilities of the chaperone of a sensor for misfolded proteins.

The ^{Flag}DNAJB8^{H31Q} assay was first used to profile the effects of arsenite and cadmium on HEK29T cells. Both metals are oxidative metals that cause protein misfolding. Arsenite is a heavy metal implicated in Amyotrophic Lateral Sclerosis (ALS) by initiating misfolding of RNA binding proteins such as TDP43[112,113]. LiP was optimized and added to the initial ^{Flag}DNAJB8^{H31Q} assessment of the arsenite sensitive

proteome to create a viable mass spec platform that can assess protein stability[114].

The success of the new mass spec platform prompted investigation into the effects of chloroacetanilides on the HEK293T proteome. These electrophiles are N-alkoxy alkyl-N-chloroacetyl substituted derivatives of aniline previously used as an agricultural weed agent[115,116]. The proteome after treatment with acetochlor, alachlor, and propachlor were first assessed using the ^{Flag}DNAJB8^{H31Q} AP-MS assay. Two significant interactors with ^{Flag}DNAJ8^{H31Q} after propachlor treatment were validated to be misfolded. The aggregated proteome after propachlor treatment was compared to the initial pulldowns from the chaperone.

Finally, the misfolded proteome after treatment of manganese was investigated. Manganese is a common contaminant in groundwater and its implications in terms of toxicity to cellular proteins remains a bit unexplored. Manganese can be toxic as it can promote alpha-syn aggregation in Parkinson's disease[117]. The AP-MS platform was used to assess long term incubation of Manganese and found several RNA processing proteins to be destabilized such as XRN2 and NKRF.

The overarching theme from each of these explorations is how uniquely DNAJB8 can offer insights into the effects of each environmental stressor on proteins. DNAJB8^{H31Q} can recognize misfolded proteins but also help elucidate mechanisms into how each environmental condition effects the cell. Each environmental stress produced a different misfolded proteome and several assays validated that the significant interactors with DNAJB8^{H31Q} were misfolded. DNAJB8^{H31Q} as a sensor protein should be able to contribute to how we can profile misfolded proteins and mechanisms of cellular stresses.

References

[1]Laganowsky, A.; Reading, E.; Allison, T. M.; Ulmschneider, M. B.; Degiacomi, M. T.; Baldwin, A. J.; Robinson, C. V. Membrane Proteins Bind Lipids Selectively to Modulate Their Structure and Function. *Nature* **2014**, *510* (7503), 172–175. https://doi.org/10.1038/nature13419.

[2]Fujisawa, T.; Filippakopoulos, P. Functions of Bromodomain-Containing Proteins and Their Roles in Homeostasis and Cancer. *Nat. Rev. Mol. Cell Biol.* **2017**, *18* (4), 246–262. https://doi.org/10.1038/nrm.2016.143.

[3]Pedemonte, N.; Galietta, L. J. V. Structure and Function of Tmem16 Proteins (Anoctamins). *Physiol. Rev.* **2014**, *94* (2), 419–459. https://doi.org/10.1152/physrev.00039.2011.

[4]Hoang, T. X.; Marsella, L.; Trovato, A.; Seno, F.; Banavar, J. R.; Maritan, A. Common Attributes of Native-State Structures of Proteins, Disordered Proteins, and Amyloid. *Proc. Natl. Acad. Sci. U. S. A.* **2006**, *103* (18), 6883–6888. https://doi.org/10.1073/pnas.0601824103.

[5]Wei, G.; Xi, W.; Nussinov, R.; Ma, B. Protein Ensembles: How Does Nature Harness Thermodynamic Fluctuations for Life? The Diverse Functional Roles of Conformational Ensembles in the Cell. *Chem. Rev.* **2016**, *116* (11), 6516–6551. https://doi.org/10.1021/acs.chemrev.5b00562.

[6]Reddy, G.; Liu, Z.; Thirumalai, D. Denaturant-Dependent Folding of GFP. *Proc. Natl. Acad. Sci. U. S. A.* **2012**, *109* (44), 17832–17838. https://doi.org/10.1073/pnas.1201808109.

[7]Yang, F.; Moss, L. G.; Phillips, G. N. The Molecular Structure of Green Fluorescent Protein The Molecular Structure of Green Fluorescent Protein. *Structure* **2011**, *14* (October), 1–14.

[8]Stepanenko, O. V.; Stepanenko, O. V.; Kuznetsova, I. M.; Verkhusha, V. V.; Turoverov, K. K. Beta-Barrel Scaffold of Fluorescent Proteins: Folding, Stability and Role in Chromophore Formation. *Int Rev Cell Mol Biol.* **2013**, *302*, 221–278. https://doi.org/10.1016/b978-0-12-407699-0.00004-2.

[9]Tsien, R. Y. The Green Fluorescent Protein. *Annu. Rev. Biochem.* **1998**, *67*, 509–544. https://doi.org/10.1146/annurev.biochem.67.1.509.

[10]Arpino, J. A. J.; Rizkallah, P. J.; Jones, D. D. Crystal Structure of Enhanced Green Fluorescent Protein to 1.35 Å Resolution Reveals Alternative Conformations for Glu222. *PLoS One* **2012**, *7* (10). https://doi.org/10.1371/journal.pone.0047132.

[11]Li, B.; Shahid, R.; Peshkepija, P.; Zimmer, M. Water Diffusion in and out of the β-Barrel of GFP and the Fast Maturing Fluorescent Protein, TurboGFP. *Chem. Phys.* **2012**, *392* (1), 143–148. https://doi.org/10.1016/j.chemphys.2011.11.001.

[12]Eaton, W. A. Modern Kinetics and Mechanism of Protein Folding: A Retrospective. *J. Phys. Chem. B* **2021**, *125* (14), 3452–3467. https://doi.org/10.1021/acs.jpcb.1c00206.
[13]Ganim, Z.; Rief, M. Mechanically Switching Single-Molecule Fluorescence of GFP by Unfolding and Refolding. *Proc. Natl. Acad. Sci. U. S. A.* **2017**, *114* (42), 11052–11056. https://doi.org/10.1073/pnas.1704937114.

[14]Izumi, M. Heat Shock Proteins Support Refolding and Shredding of Misfolded Proteins. *Plant Physiol.* **2019**, *180* (4), 1777–1778. https://doi.org/10.1104/pp.19.00711.

[15]Fulda, S.; Gorman, A. M.; Hori, O.; Samali, A. Cellular Stress Responses: Cell Survival and Cell Death. *Int. J. Cell Biol.* **2010**, *2010*. https://doi.org/10.1155/2010/214074.

[16]Tamás, M. J.; Sharma, S. K.; Ibstedt, S.; Jacobson, T.; Christen, P. Heavy Metals and Metalloids as a Cause for Protein Misfolding and Aggregation. *Biomolecules* **2014**, *4* (1), 252–267. https://doi.org/10.3390/biom4010252.

[17]Bateman, L. A.; Nguyen, T. B.; Roberts, A. M.; Miyamoto, D. K.; Ku, W. M.; Huffman, T. R.; Petri, Y.; Heslin, M. J.; Contreras, C. M.; Skibola, C. F.; Olzmann, J. A.; Nomura, D. K. Chemoproteomics-Enabled Covalent Ligand Screen Reveals a Cysteine Hotspot in Reticulon 4 That Impairs ER Morphology and Cancer Pathogenicity. *Chem. Commun.* **2017**, *53* (53), 7234–7237. https://doi.org/10.1039/c7cc01480e.

[18]Makareeva, E.; Aviles, N. A.; Leikin, S. Chaperoning Osteogenesis: New Protein-Folding-Disease Paradigms. *Trends Cell Biol.* **2012**, *21* (3), 168–176. https://doi.org/10.1016/j.tcb.2010.11.007.Chaperoning.

[19]Jha, S. K.; Udgaonkar, J. B. Free energy barriers in protein folding and unfolding reactions. *Current Science*, **2010**, *99(*4*)*, 457–475. http://www.jstor.org/stable/24109569.

[20]Cordeiro, Y.; Macedo, B.; Silva, J. L.; Gomes, M. P. B. Pathological Implications of Nucleic Acid Interactions with Proteins Associated with Neurodegenerative Diseases. *Biophys. Rev.* **2014**, *6* (1), 97–110. https://doi.org/10.1007/s12551-013-0132-0.

[21]Huang, W. J.; Zhang, X.; Chen, W. W. Role of Oxidative Stress in Alzheimer's Disease (Review). *Biomed. Reports* **2016**, *4* (5), 519–522. https://doi.org/10.3892/br.2016.630.

[22]Gella, A.; Durany, N. Oxidative Stress in Alzheimer Disease. *Cell Adhes. Migr.* **2009**, *3* (1), 88–93. https://doi.org/10.4161/cam.3.1.7402.

[23]McColgan, P.; Tabrizi, S. J. Huntington's Disease: A Clinical Review. *Eur. J. Neurol.* **2018**, *25* (1), 24–34. https://doi.org/10.1111/ene.13413.

[24]Barnat, M.; Capizzi, M.; Aparicio, E.; Boluda, S.; Wennagel, D.; Kacher, R.; Kassem, R.; Lenoir, S.; Agasse, F.; Bra, B. Y.; Liu, J. P.; Ighil, J.; Tessier, A.; Zeitli, S. O.; Duyckaerts, C.; Dommergues, M.; Durr, A.; Humbert, S. Huntington's Disease Alters Human Neurodevelopment. *Science (80-.).* **2020**, *369* (6505), 787–793. https://doi.org/10.1126/science.aax3338.

[25]Gella, A.; Durany, N. Oxidative Stress in Alzheimer Disease. *Cell Adhes. Migr.* **2009**, *3* (1), 88–93. https://doi.org/10.4161/cam.3.1.7402.

[26]Schaffar, G.; Breuer, P.; Boteva, R.; Behrends, C.; Tzvetkov, N.; Strippel, N.; Sakahira, H.; Siegers, K.; Hayer-Hartl, M.; Hartl, F. U. Cellular Toxicity of Polyglutamine Expansion Proteins: Mechanism of Transcription Factor Deactivation. *Mol. Cell* **2004**, *15* (1), 95–105. https://doi.org/10.1016/j.molcel.2004.06.029.

[27]Ehrlich, M. E. Huntington's Disease and the Striatal Medium Spiny Neuron: Cell-Autonomous and Non-Cell-Autonomous Mechanisms of Disease. *Neurotherapeutics* **2012**, *9* (2), 270–284. https://doi.org/10.1007/s13311-012-0112-2.

[28]Kingwell, K. Zeroing in on Neurodegenerative α-Synuclein. *Nat. Rev. Drug Discov.* **2017**, *16* (6), 371–373. https://doi.org/10.1038/nrd.2017.95.

[29]Shea, D.; Hsu, C. C.; Bi, T. M.; Paranjapye, N.; Childers, M. C.; Cochran, J.; Tomberlin, C. P.; Wang, L.; Paris, D.; Zonderman, J.; Varani, G.; Link, C. D.; Mullan, M.; Daggett, V. α-Sheet Secondary Structure in Amyloid β-Peptide Drives Aggregation and Toxicity in Alzheimer's Disease. *Proc. Natl. Acad. Sci. U. S. A.* **2019**, *116* (18), 8895–8900. https://doi.org/10.1073/pnas.1820585116.

[30]Šimić, G.; Babić Leko, M.; Wray, S.; Harrington, C.; Delalle, I.; Jovanov-Milošević, N.; Bažadona, D.; Buée, L.; de Silva, R.; Giovanni, G. Di; Wischik, C.; Hof, P. R. Tau Protein Hyperphosphorylation and Aggregation in Alzheimer's Disease and Other Tauopathies, and Possible Neuroprotective Strategies. *Biomolecules* **2016**, *6* (1), 2–28. https://doi.org/10.3390/biom6010006.

[31]Nisbet, R. M.; Polanco, J. C.; Ittner, L. M.; Götz, J. Tau Aggregation and Its Interplay with Amyloid-β. *Acta Neuropathol.* **2015**, *129* (2), 207–220. https://doi.org/10.1007/s00401-014-1371-2.

[32]Huang, W. J.; Zhang, X.; Chen, W. W. Role of Oxidative Stress in Alzheimer's Disease (Review). *Biomed. Reports* **2016**, *4* (5), 519–522. https://doi.org/10.3892/br.2016.630.

[33]Gella, A.; Durany, N. Oxidative Stress in Alzheimer Disease. *Cell Adhes. Migr.* **2009**, *3* (1), 88–93. https://doi.org/10.4161/cam.3.1.7402.

[34]Liu, Y.; Fares, M.; Dunham, N. P.; Gao, Z.; Miao, K.; Jiang, X.; Bollinger, S. S.; Boal, A. K.; Zhang, X. AgHalo: A Facile Fluorogenic Sensor to Detect Drug-Induced Proteome Stress. *Angew. Chemie - Int. Ed.* **2017**, *56* (30), 8672–8676. https://doi.org/10.1002/anie.201702417.

[35]Fares, M.; Li, Y.; Liu, Y.; Miao, K.; Gao, Z.; Zhai, Y.; Zhang, X. A Molecular Rotor-Based Halo-Tag Ligand Enables a Fluorogenic Proteome Stress Sensor to Detect Protein Misfolding in Mildly Stressed Proteome. *Bioconjug. Chem.* **2018**, *29* (1), 215–224. https://doi.org/10.1021/acs.bioconjchem.7b00763.

[36]Pollitt, S. K.; Pallos, J.; Shao, J.; Desai, U. A.; Ma, A. A. K.; Thompson, L. M.; Marsh, J. L.; Diamond, M. I. A Rapid Cellular FRET Assay of Polyglutamine Aggregation Identifies a Novel Inhibitor. *Neuron* **2003**, *40* (4), 685–694. https://doi.org/10.1016/S0896-6273(03)00697-4.

[37]Sun, Z.; Brodsky, J. L. The Degradation Pathway of a Model Misfolded Protein Is Determined by Aggregation Propensity. *Mol. Biol. Cell* **2018**, *29* (12), 1422–1434. https://doi.org/10.1091/mbc.E18-02-0117.

[38]Ross, A. B.; Langer, J. D.; Jovanovic, M. Proteome Turnover in the Spotlight: Approaches, Applications, and Perspectives. *Mol. Cell. Proteomics* **2021**, *20*, 100016. https://doi.org/10.1074/MCP.R120.002190.

[39]Eguchi, Y.; Makanae, K.; Hasunuma, T.; Ishibashi, Y.; Kito, K.; Moriya, H. Estimating the Protein Burden Limit of Yeast Cells by Measuring the Expression Limits of Glycolytic Proteins. *Elife* **2018**, *7*, 1–3. https://doi.org/10.7554/eLife.34595.

[40]Sun, Z.; Brodsky, J. L. The Degradation Pathway of a Model Misfolded Protein Is Determined by Aggregation Propensity. *Mol. Biol. Cell* **2018**, *29* (12), 1422–1434. https://doi.org/10.1091/mbc.E18-02-0117.

[41]Bowyer, J. F.; Davies, D. L. Changes in MRNA Levels for Heat-Shock/Stress Proteins (Hsp) and a Secretory Vesicle Associated Cysteine-String Protein (Csp1) after Amphetamine (AMPH) Exposure. *Ann. N. Y. Acad. Sci.* **1999**, *890*, 314–329. https://doi.org/10.1111/j.1749-6632.1999.tb08009.x.

[42]Guan, Y.; Zhao, X.; Liu, F.; Yan, S.; Wang, Y.; Du, C.; Cui, X.; Li, R.; Zhang, C. X. Pathogenic Mutations Differentially Regulate Cell-to-Cell Transmission of α-Synuclein. *Front. Cell. Neurosci.* **2020**, *14* (June), 1–18. https://doi.org/10.3389/fncel.2020.00159.

[43]Zhou, Y.; Shi, J.; Chu, D.; Hu, W.; Guan, Z.; Gong, C. X.; Iqbal, K.; Liu, F. Relevance of Phosphorylation and Truncation of Tau to the Etiopathogenesis of Alzheimer's Disease. *Front. Aging Neurosci.* **2018**, *10*, 1–10. https://doi.org/10.3389/fnagi.2018.00027.

[44]Iwata, A.; Miura, S.; Kanazawa, I.; Sawada, M.; Nukina, N. α-Synuclein Forms a Complex with Transcription Factor Elk-1. *J. Neurochem.* **2001**, *77* (1), 239–252. https://doi.org/10.1046/j.1471-4159.2001.00232.x.

[45]Im, E.; Yoo, L.; Hyun, M.; Shin, W. H.; Chung, K. C. Covalent ISG15 Conjugation Positively Regulates the Ubiquitin E3 Ligase Activity of Parkin. *Open Biol.* **2016**, *6* (8). https://doi.org/10.1098/rsob.160193.

[46]Hernandez, S. M.; Tikhonova, E. B.; Karamyshev, A. L. Protein-Protein Interactions in Alpha-Synuclein Biogenesis: New Potential Targets in Parkinson's Disease. *Front. Aging Neurosci.* **2020**, *12* (March), 1–8. https://doi.org/10.3389/fnagi.2020.00072.

[47]Gao, Y.; Yates, J. R. Protein Analysis by Shotgun Proteomics. *Mass Spectrom. Chem. Proteomics* **2019**, 1–38. https://doi.org/10.1002/9781118970195.ch1.

[48]Schubert, O. T.; Röst, H. L.; Collins, B. C.; Rosenberger, G.; Aebersold, R. Quantitative Proteomics: Challenges and Opportunities in Basic and Applied Research. *Nat. Protoc.* **2017**, *12* (7), 1289–1294. https://doi.org/10.1038/nprot.2017.040.

[49]Calloni, G.; Vabulas, R. M. *Proteome-Scale Studies of Protein Stability*; Elsevier Inc., 2020. https://doi.org/10.1016/b978-0-12-819132-3.00004-x.

[50]Kubota K., Kosaka T., Ichikawa K. (2009) Shotgun Protein Analysis by Liquid Chromatography-Tandem Mass Spectrometry. In: Tyther R., Sheehan D. (eds) Two-Dimensional Electrophoresis Protocols. Methods in Molecular Biology (Methods and Protocols), vol 519. Humana Press. https://doi.org/10.1007/978-1-59745-281-6_32

[51]Aggarwal, K.; Choe, L. H.; Lee, K. H. Shotgun Proteomics Using the ITRAQ Isobaric Tags. *Briefings Funct. Genomics Proteomics* **2006**, *5* (2), 112–120. https://doi.org/10.1093/bfgp/ell018.

[52]Zhang L., Elias J.E. (2017) Relative Protein Quantification Using Tandem Mass Tag Mass Spectrometry. In: Comai L., Katz J., Mallick P. (eds) Proteomics. Methods in Molecular Biology, vol 1550. Humana Press, New York, NY. https://doi.org/10.1007/978-1-4939-6747-6_14

[53]Thompson, A.; Schäfer, J.; Kuhn, K.; Kienle, S.; Schwarz, J.; Schmidt, G.; Neumann, T.; Hamon, C. Tandem Mass Tags: A Novel Quantification Strategy for Comparative Analysis of Complex Protein Mixtures by MS/MS. *Anal. Chem.* **2003**, *75* (8), 1895–1904. https://doi.org/10.1021/ac0262560.

[54]Savitski, M. M.; Reinhard, F. B. M.; Franken, H.; Werner, T.; Savitski, M. F.; Eberhard, D.; Molina, D. M.; Jafari, R.; Dovega, R. B.; Klaeger, S.; Kuster, B.; Nordlund, P.; Bantscheff, M.; Drewes, G. Tracking Cancer Drugs in Living Cells by Thermal Profiling of the Proteome. *Science (80-.).* **2014**, *346* (6205). https://doi.org/10.1126/science.1255784.

[55]Martinez Molina, D.; Nordlund, P. The Cellular Thermal Shift Assay: A Novel Biophysical Assay for in Situ Drug Target Engagement and Mechanistic Biomarker Studies. *Annu. Rev. Pharmacol. Toxicol.* **2016**, *56*, 141–161. https://doi.org/10.1146/annurev-pharmtox-010715-103715.

[56]Sun, W.; Dai, L.; Yu, H.; Puspita, B.; Zhao, T.; Li, F.; Tan, J. L.; Lim, Y. T.; Chen, M. W.; Sobota, R. M.; Tenen, D. G.; Prabhu, N.; Nordlund, P. Monitoring Structural Modulation of Redox-Sensitive Proteins in Cells with MS-CETSA. *Redox Biol.* **2019**, *24* (January), 101168. https://doi.org/10.1016/j.redox.2019.101168.

[57]Martinez, N. J.; Asawa, R. R.; Cyr, M. G.; Zakharov, A.; Urban, D. J.; Roth, J. S.; Wallgren, E.; Klumpp-Thomas, C.; Coussens, N. P.; Rai, G.; Yang, S. M.; Hall, M. D.; Marugan, J. J.; Simeonov, A.; Henderson, M. J. A Widely-Applicable High-Throughput Cellular Thermal Shift Assay (CETSA) Using Split Nano Luciferase. *Sci. Rep.* **2018**, *8* (1), 1–16. https://doi.org/10.1038/s41598-018-27834-y.

[58]Strickland, E. C.; Geer, M. A.; Tran, D. T.; Adhikari, J.; West, G. M.; Dearmond, P. D.; Xu, Y.; Fitzgerald, M. C. Thermodynamic Analysis of Protein-Ligand Binding Interactions in Complex Biological Mixtures Using the Stability of Proteins from Rates of Oxidation. *Nat. Protoc.* **2013**, *8* (1), 148–161. https://doi.org/10.1038/nprot.2012.146.

[59]Jin, L.; Wang, D.; Gooden, D. M.; Ball, C. H.; Fitzgerald, M. C. Targeted Mass Spectrometry-Based Approach for Protein-Ligand Binding Analyses in Complex Biological Mixtures Using a Phenacyl Bromide Modification Strategy. *Anal. Chem.* **2016**, *88* (22), 10987–10993. https://doi.org/10.1021/acs.analchem.6b02658.

[60]Walker, E. J.; Bettinger, J. Q.; Welle, K. A.; Hryhorenko, J. R.; Ghaemmaghami, S. Global Analysis of Methionine Oxidation Provides a Census of Folding Stabilities for the Human Proteome. *Proc. Natl. Acad. Sci. U. S. A.* **2019**, *116* (13), 6081–6090. https://doi.org/10.1073/pnas.1819851116.

[61]Spicer, C. D.; Davis, B. G. Selective Chemical Protein Modification. *Nat. Commun.* **2014**, *5*. https://doi.org/10.1038/ncomms5740.

[62]del Monte, F.; Agnetti, G. Protein Post-Translational Modifications and Misfolding: New Concepts in Heart Failure. *Proteomics - Clin. Appl.* **2014**, *8* (7–8), 534–542. https://doi.org/10.1002/prca.201400037.

[63]Walter J., Haass C. (2000) Posttranslational Modifications of Amyloid Precursor Protein. In: Hooper N.M. (eds) Alzheimer's Disease. Methods in Molecular Medicine™, vol 32. Humana Press. https://doi.org/10.1385/1-59259-195-7:149

[64]Schaffert, L. N.; Carter, W. G. Do Post-Translational Modifications Influence Protein Aggregation in Neurodegenerative Diseases: A Systematic Review. *Brain Sci.* **2020**, *10* (4). https://doi.org/10.3390/brainsci10040232.

[65]Bateman, L. A.; Nguyen, T. B.; Roberts, A. M.; Miyamoto, D. K.; Ku, W. M.; Huffman, T. R.; Petri, Y.; Heslin, M. J.; Contreras, C. M.; Skibola, C. F.; Olzmann, J. A.; Nomura, D. K. Chemoproteomics-Enabled Covalent Ligand Screen Reveals a Cysteine Hotspot in Reticulon 4 That Impairs ER Morphology and Cancer Pathogenicity. *Chem. Commun.* **2017**, *53* (53), 7234–7237. https://doi.org/10.1039/c7cc01480e.

[66]Matthews, M. L.; He, L.; Horning, B. D.; Olson, E. J.; Correia, B. E.; Yates, J. R.; Dawson, P. E.; Cravatt, B. F. Chemoproteomic Profiling and Discovery of Protein Electrophiles in Human Cells. *Nat. Chem.* **2017**, *9* (3), 234–243. https://doi.org/10.1038/nchem.2645.

[67]Counihan, J. L.; Duckering, M.; Dalvie, E.; Ku, W.; Bateman, L. A.; Fisher, K. J.; Nomura, D. K. Chemoproteomic Profiling of Acetanilide Herbicides Reveals Their Role in Inhibiting Fatty Acid Oxidation. *ACS Chem. Biol.* **2019**, *12* (3), 635–642. https://doi.org/10.1021/acschembio.6b01001.Table.

[68]Backus, K. M.; Correia, B. E.; Lum, K. M.; Forli, S.; Horning, B. D.; González-Páez, G. E.; Chatterjee, S.; Lanning, B. R.; Teijaro, J. R.; Olson, A. J.; Wolan, D. W.; Cravatt, B. F. Proteome-Wide Covalent Ligand Discovery in Native Biological Systems. *Nature* **2016**, *534* (7608), 570–574. https://doi.org/10.1038/nature18002.

[69]Ahmad, N. N.; Kamarudin, N. H. A.; Leow, A. T. C.; Rahman, R. N. Z. R. A. The Role of Surface Exposed Lysine in Conformational Stability and Functional Properties of Lipase from Staphylococcus Family. *Molecules* **2020**, *25* (17), 1–19. https://doi.org/10.3390/molecules25173858.

[70]Shah, D.; Shaikh, A. R. Interaction of Arginine, Lysine, and Guanidine with Surface Residues of Lysozyme: Implication to Protein Stability. *J. Biomol. Struct. Dyn.* **2016**, *34* (1), 104–114. https://doi.org/10.1080/07391102.2015.1013158.

[71]Arndt, J. R.; Brown, R. J.; Burke, K. A.; Legleiter, J.; Valentine, S. J. Lysine Residues in the N-Terminal Huntingtin Amphipathic α-Helix Play a Key Role in Peptide Aggregation. *J. Mass Spectrom.* **2015**, *50* (1), 117–126. https://doi.org/10.1002/jms.3504.

[72]Bamberger, C.; Pankow, S.; Martínez-Bartolomé, S.; Ma, M.; Diedrich, J.; Rissman, R. A.; Yates, J. R. Protein Footprinting via Covalent Protein Painting Reveals Structural Changes of the Proteome in Alzheimer's Disease. *J. Proteome Res.* **2021**, *20* (5), 2762–2771. https://doi.org/10.1021/acs.jproteome.0c00912.

[73]Leuenberger, P.; Ganscha, S.; Kahraman, A.; Cappelletti, V.; Boersema, P. J.; Von Mering, C.; Claassen, M.; Picotti, P. Cell-Wide Analysis of Protein Thermal Unfolding Reveals Determinants of Thermostability. *Science (80-.).* **2017**, *355* (6327). https://doi.org/10.1126/science.aai7825.

[74]Schopper, S.; Kahraman, A.; Leuenberger, P.; Feng, Y.; Piazza, I.; Müller, O.; Boersema, P. J.; Picotti, P. Measuring Protein Structural Changes on a Proteome-Wide Scale Using Limited Proteolysis- Coupled Mass Spectrometry. *Nat. Protoc.* **2017**, *12* (11), 2391–2410. https://doi.org/10.1038/nprot.2017.100.

[75]Feng, Y.; De Franceschi, G.; Kahraman, A.; Soste, M.; Melnik, A.; Boersema, P. J.; De Laureto, P. P.; Nikolaev, Y.; Oliveira, A. P.; Picotti, P. Global Analysis of Protein Structural Changes in Complex Proteomes. *Nat. Biotechnol.* **2014**, *32* (10), 1036–1044. https://doi.org/10.1038/nbt.2999.

[76]Petrotchenko, E. V.; Serpa, J. J.; Hardie, D. B.; Berjanskii, M.; Suriyamongkol, B. P.; Wishart, D. S.; Borchers, C. H. Use of Proteinase K Nonspecific Digestion for Selective and Comprehensive Identification of Interpeptide Cross-Links: Application to Prion Proteins. *Mol. Cell. Proteomics* **2012**, *11* (7), M111.013524-1-M111.013524-13. https://doi.org/10.1074/mcp.M111.013524.

[77]Silva, C. J.; Vázquez-Fernández, E.; Onisko, B.; Requena, J. R. Proteinase K and the Structure of PrPSc: The Good, the Bad and the Ugly. *Virus Res.* **2015**, *207*, 120–126. https://doi.org/10.1016/j.virusres.2015.03.008.

[78]The, M.; Käll, L. Integrated Identification and Quantification Error Probabilities for Shotgun Proteomics. *Mol. Cell. Proteomics* **2019**, *18* (3), 561–570. https://doi.org/10.1074/mcp.RA118.001018.

[79]Karpievitch, Y.; Stanley, J.; Taverner, T.; Huang, J.; Adkins, J. N.; Ansong, C.; Heffron, F.; Metz, T. O.; Qian, W. J.; Yoon, H.; Smith, R. D.; Dabney, A. R. A Statistical Framework for Protein Quantitation in Bottom-up MS-Based Proteomics. *Bioinformatics* **2009**, *25* (16), 2028–2034. https://doi.org/10.1093/bioinformatics/btp362.

[80]Hipp, M. S.; Kasturi, P.; Hartl, F. U. The Proteostasis Network and Its Decline in Ageing. *Nat. Rev. Mol. Cell Biol.* **2019**, *20* (7), 421–435. https://doi.org/10.1038/s41580-019-0101-y.

[81]Jayaraj, G. G.; Hipp, M. S.; Ulrich Hartl, F. Functional Modules of the Proteostasis Network. *Cold Spring Harb. Perspect. Biol.* **2020**, *12* (1). https://doi.org/10.1101/cshperspect.a033951.

[82]Santra, M.; Dill, K. A.; De Graff, A. M. R. Proteostasis Collapse Is a Driver of Cell Aging and Death. *Proc. Natl. Acad. Sci. U. S. A.* **2019**, *116* (44), 22173–22178. https://doi.org/10.1073/pnas.1906592116.

[83]Mardones, P.; Martínez, G.; Hetz, C. Control of Systemic Proteostasis by the Nervous System. *Trends Cell Biol.* **2015**, *25* (1), 1–10. https://doi.org/10.1016/j.tcb.2014.08.001.

[84]Klaips, C. L.; Jayaraj, G. G.; Hartl, F. U. Pathways of Cellular Proteostasis in Aging and Disease. *J. Cell Biol.* **2018**, *217* (1), 51–63. https://doi.org/10.1083/jcb.201709072.

[85]Barral, J. M.; Broadley, S. A.; Schaffar, G.; Hartl, F. U. Roles of Molecular Chaperones in Protein Misfolding Diseases. *Semin. Cell Dev. Biol.* **2004**, *15* (1), 17–29. https://doi.org/10.1016/j.semcdb.2003.12.010.

[86]Ciechanover, A.; Kwon, Y. T. Protein Quality Control by Molecular Chaperones in Neurodegeneration. *Front. Neurosci.* **2017**, *11* (APR), 1–18. https://doi.org/10.3389/fnins.2017.00185.

[87]Hartl, F. U.; Bracher, A.; Hayer-Hartl, M. Molecular Chaperones in Protein Folding and Proteostasis. *Nature* **2011**, *475* (7356), 324–332. https://doi.org/10.1038/nature10317.

[88]Amm, I.; Sommer, T.; Wolf, D. H. Protein Quality Control and Elimination of Protein Waste: The Role of the Ubiquitin-Proteasome System. *Biochim. Biophys. Acta - Mol. Cell Res.* **2014**, *1843* (1), 182–196. https://doi.org/10.1016/j.bbamcr.2013.06.031.

[89]Jackson, M. P.; Hewitt, E. W. Cellular Proteostasis: Degradation of Misfolded Proteins by Lysosomes. *Essays Biochem.* **2016**, *60* (2), 173–180. https://doi.org/10.1042/EBC20160005.

[90]Morris, J. H.; Knudsen, G. M.; Verschueren, E.; Johnson, J. R.; Cimermancic, P.; Greninger, A. L.; Pico, A. R. Affinity Purification-Mass Spectrometry and Network Analysis to Understand Protein-Protein Interactions. *Nat. Protoc.* **2014**, *9* (11), 2539–2554. https://doi.org/10.1038/nprot.2014.164.

[91]Meyer, K.; Selbach, M. Quantitative Affinity Purification Mass Spectrometry: A Versatile Technology to Study Protein-Protein Interactions. *Front. Genet.* **2015**, *6* (JUL), 1–7. https://doi.org/10.3389/fgene.2015.00237.

[92]Bessinger, M.; Buchner, J. How chaperones fold proteins. *Biol. Chem.* **1998,** 379(3), 245-259.

[93]Truman, A. W.; Kristjansdottir, K.; Wolfgeher, D.; Ricco, N.; Mayampurath, A.; Volchenboum, S. L.; Clotet, J.; Kron, S. J. ScienceDirect Quantitative Proteomics of the Yeast Hsp70 / Hsp90 Interactomes during DNA Damage Reveal Chaperone- Dependent Regulation of Ribonucleotide Reductase. *J. Proteomics* **2014**, *112*, 285–300. https://doi.org/10.1016/j.jprot.2014.09.028.

[94]Wu, Z.; Gholami, A. M.; Kuster, B. Systematic Identification of the HSP90 Candidate Regulated Proteome. *Mol. Cell. Proteomics* **2012**, *11* (6), M111.016675. https://doi.org/10.1074/mcp.M111.016675.

[95]Ryu, S. W.; Stewart, R.; Chase Pectol, D.; Ender, N. A.; Wimalarathne, O.; Lee, J. H.; Zanini, C. P.; Harvey, A.; Huibregtse, J. M.; Mueller, P.; Paull, T. T. Proteome-Wide Identification of HSP70/ HSC70 Chaperone Clients in Human Cells. *PLoS Biol.* **2020**, *18* (7), 1–27.

[96]Hwang, J.; Qi, L. Quality Control in the Endoplasmic Reticulum: Crosstalk between ERAD and UPR Pathways. *Trends Biochem. Sci.* **2018**, *43* (8), 593–605. https://doi.org/10.1016/j.tibs.2018.06.005.

[97]Read, A.; Schröder, M. The Unfolded Protein Response: An Overview. *Biology (Basel).* **2021**, *10* (5), 1–10. https://doi.org/10.3390/biology10050384.

[98]Singer-Krüger, B.; Fröhlich, T.; Franz-Wachtel, M.; Nalpas, N.; Macek, B.; Jansen, R. P. APEX2-Mediated Proximity Labeling Resolves Protein Networks in Saccharomyces Cerevisiae Cells. *FEBS J.* **2020**, *287* (2), 325–344. https://doi.org/10.1111/febs.15007.

[99]Chen, C. L.; Perrimon, N. Proximity-Dependent Labeling Methods for Proteomic Profiling in Living Cells. *Wiley Interdiscip. Rev. Dev. Biol.* **2017**, *6* (4), 1–10. https://doi.org/10.1002/wdev.272.

[100]Hung, V.; Udeshi, N. D.; Lam, S. S.; Loh, K. H.; Cox, K. J.; Pedram, K.; Carr, S. A.; Ting, A. Y. Spatially Resolved Proteomic Mapping in Living Cells with the Engineered Peroxidase APEX2. *Nat. Protoc.* **2016**, *11* (3), 456–475. https://doi.org/10.1038/nprot.2016.018.

[101]Kalocsay M. (2019) APEX Peroxidase-Catalyzed Proximity Labeling and Multiplexed Quantitative Proteomics. In: Sunbul M., Jäschke A. (eds) Proximity Labeling. Methods in Molecular Biology, vol 2008. Humana, New York, NY. https://doi.org/10.1007/978-1-4939-9537-0_4.

[102]Hung, V.; Lam, S. S.; Udeshi, N. D.; Svinkina, T.; Guzman, G.; Mootha, V. K.; Carr, S. A.; Ting, A. Y. Proteomic Mapping of Cytosol-Facing Outer Mitochondrial and ER Membranes in Living Human Cells by Proximity Biotinylation. *Elife* **2017**, *6*, 1–39. https://doi.org/10.7554/eLife.24463.

[103]Rajan, R.; Ahmed, S.; Sharma, N.; Kumar, N.; Debas, A.; Matsumura, K. Review of the Current State of Protein Aggregation Inhibition from a Materials Chemistry Perspective: Special Focus on Polymeric Materials. *Mater. Adv.* **2021**, *2* (4), 1139–1176. https://doi.org/10.1039/d0ma00760a.

[104]Chung, C. Y.; Khurana, V.; Yi, S.; Sahni, N.; Loh, K. H.; Auluck, P. K.; Baru, V.; Udeshi, N. D.; Freyzon, Y.; Carr, S. A.; Hill, D. E.; Vidal, M.; Ting, A. Y.; Lindquist, S. In Situ Peroxidase Labeling and Mass-Spectrometry Connects Alpha-Synuclein Directly to Endocytic Trafficking and MRNA Metabolism in Neurons. *Cell Syst.* **2017**, *4* (2), 242-250.e4. https://doi.org/10.1016/j.cels.2017.01.002.

[105]Kampinga, H. H.; Craig, E. A. The HSP70 Chaperone Machinery: J Proteins as Drivers of Functional Specificity. *Nat. Rev. Mol. Cell Biol.* **2010**, *11* (8), 579–592.

[106]Li, J., Qian, X., Sha, B. Heat Shock Protein 40: Structural Studies and Their Functional Implications. *Protein Pept.* **2009**, 16 (6), 606-612.

[107]Chen, K.; Qu, S.; Chowdhury, S.; Noxon, I. C.; Schonhoft, J. D.; Plate, L.; Powers, E. T.; Kelly, J. W.; Lander, G. C.; Wiseman, R. L. The Endoplasmic Reticulum HSP 40 Co-chaperone ER Dj3/ DNAJB 11 Assembles and Functions as a Tetramer . *EMBO J.* **2017**, *36* (15), 2296–2309. https://doi.org/10.15252/embj.201695616.

[108]Otero, J. H.; Lizák, B.; Feige, M. J.; Hendershot, L. M. Dissection of Structural and Functional Requirements That Underlie the Interaction of ERdj3 Protein with Substrates in the Endoplasmic Reticulum. *J. Biol. Chem.* **2014**, *289* (40), 27504–27512. https://doi.org/10.1074/jbc.M114.587147.

[109]Shen, Y.; Hendershot, L. M. ERdj3, a Stres-inducible Endoplasmic Reticulum DnaJ Homologue, Serves as a CoFactor for BiP's Interactions with Unfolded Substrates. *Mol. Biol. Cell* **2005**, *16*, 4-50.

[110]Hageman, J.; Rujano, M. A.; van Waarde, M. A. W. H.; Kakkar, V.; Dirks, R. P.; Govorukhina, N.; Oosterveld-Hut, H. M. J.; Lubsen, N. H.; Kampinga, H. H. A DNAJB Chaperone Subfamily with HDAC-Dependent Activities Suppresses Toxic Protein

Aggregation. *Mol. Cell* **2010**, *37* (3), 355–369. https://doi.org/10.1016/j.molcel.2010.01.001.

[111]Mei, L.; Montoya, M. R.; Quanrud, G. M.; Tran, M.; Villa-Sharma, A.; Huang, M.; Genereux, J. C. Bait Correlation Improves Interactor Identification by Tandem Mass Tag-Affinity Purification-Mass Spectrometry. *J. Proteome Res.* **2020**, *19* (4), 1565–1573. https://doi.org/10.1021/acs.jproteome.9b00825.

[112]Baron, D. M.; Kaushansky, L. J.; Ward, C. L.; Sama, R. R. K.; Chian, R. J.; Boggio, K. J.; Quaresma, A. J. C.; Nickerson, J. A.; Bosco, D. A. Amyotrophic Lateral Sclerosis-Linked FUS/TLS Alters Stress Granule Assembly and Dynamics. *Mol. Neurodegener.* **2013**, *8* (1), 1–18. https://doi.org/10.1186/1750-1326-8-30.

[113]Ratti, A.; Gumina, V.; Lenzi, P.; Bossolasco, P.; Fulceri, F.; Volpe, C.; Bardelli, D.; Pregnolato, F.; Maraschi, A. M.; Fornai, F.; Silani, V.; Colombrita, C. Chronic Stress Induces Formation of Stress Granules and Pathological TDP-43 Aggregates in Human ALS Fibroblasts and IPSC-Motoneurons. *Neurobiol. Dis.* **2020**, *145* (August), 105051. https://doi.org/10.1016/j.nbd.2020.105051.

[114]Quanrud, G. M.; Montoya, M. R.; Mei, L.; Awad, M. R.; Genereux, J. C. Hsp40 Affinity to Identify Proteins Destabilized by Cellular Toxicant Exposure. *Anal. Chem.* **2021**. https://doi.org/10.1021/acs.analchem.1c04230.

[115]Mohanty, S. S.; Jena, H. M. A Systemic Assessment of the Environmental Impacts and Remediation Strategies for Chloroacetanilide Herbicides. *J. Water Process Eng.* **2019**, *31* (March), 100860. https://doi.org/10.1016/j.jwpe.2019.100860.

[116]McCarroll, N. E.; Protzel, A.; Ioannou, Y.; Frank Stack, H.; Jackson, M. A.; Waters, M. D.; Dearfield, K. L. A Survey of EPA/OPP and Open Literature on Selected Pesticide Chemicals - III. Mutagenicity and Carcinogenicity of Benomyl and Carbendazim. *Mutat. Res. - Rev. Mutat. Res.* **2002**, *512* (1), 1–35. https://doi.org/10.1016/S1383-5742(02)00026-1.

[117]Peres, T. V.; Parmalee, N. L.; Martinez-Finley, E. J.; Aschner, M. Untangling the Manganese-α-Synuclein Web. *Front. Neurosci.* **2016**, *10* (AUG), 1–8. https://doi.org/10.3389/fnins.2016.00364.

Chapter 2: Hsp40 Affinity to Identify Proteins Destabilized by Cellular Toxicant Exposure

This chapter discusses the investigation into the effects of Arsenite and Cadmium in HEK293T cells. The work here was published in the Analytical Chemistry: *Anal. Chem. 2021, 93, 50, 16940-16946*.

2.1 Abstract

Environmental toxins and toxicants can damage proteins and threaten cellular proteostasis. Most current methodologies to identify misfolded proteins in cells survey the entire proteome for sites of changed reactivity. We describe and apply a quantitative proteomics methodology to identify destabilized proteins based on their binding to the human Hsp40 chaperone DNAJB8. These protein targets are validated by an orthogonal limited proteolysis assay using parallel reaction monitoring. We find that brief exposure of HEK293T cells to meta-arsenite increases the affinity of two dozen proteins to DNAJB8, including known arsenite-sensitive proteins. In particular, arsenite treatment destabilizes both the pyruvate dehydrogenase complex E1 subunit and several RNA-binding proteins. This platform can be used to explore how environmental toxins impact cellular proteostasis, and to identify the susceptible proteome.

2.2. Introduction

Exposure to environmental toxins threatens the structural integrity of proteins[1]. Structural changes due to oxidation, covalent modification, or non-covalent binding can

cause proteins to misfold, leading to aggregation or loss of function[2]. For example, the heavy metal arsenic (As) binds to protein sulfhydryl groups and generates reactive oxygen species (ROS)[3]. Consequent accumulation of misfolded proteins and oxidative stress activates the Heat Shock Response (HSR) to induce chaperones and restore protein homeostasis[4]. Activation of HSR or other similar misfolded protein stress responses is a common response to heavy metals, electrophilic pesticides/herbicides, and other environmental toxins. While measuring these responses indicates whether a given toxin is likely to be inducing protein misfolding, it does not indicate *which* proteins are misfolding, and hence which cellular pathways are being affected by the exposure.

Most current approaches to identify misfolded proteins measure proteome-wide solvent accessibility by mass spectrometry to infer conformational changes[5,6]. Stability of Proteins from Rates of Oxidation (SPROX) analyzes protein methionine oxidation in cellular lysates, with varying chaotrope concentrations to measure proteins' $\Delta G_{unfolding}$[7,8]. Fast Photochemical Oxidation of Proteins (FPOP) measures the exposure of protein sites in cells or organisms to in situ generated hydroxide radicals[9]. Limited Proteolysis (LiP) measures proteome-wide susceptibility to proteolytic cleavage[10]. Covalent protein painting measures differences in protein folding based on accessible lysine ε-amines after proteins are exposed to electrophilic reagents[11]. Cellular Thermal Shift Assay (CETSA) measures proteome-wide susceptibility to aggregation with increasing temperature[12]. Each technique offers a unique approach using quantitative proteomics to assess protein stability in a cell.

Alternatively, the cell identifies misfolded proteins through recognition by

chaperones. A highly promiscuous chaperone is Hsp70, which relies upon members of the Hsp40 family to identify and recruit misfolded protein clients for refolding; one third of the proteome relies on this cycle under basal conditions[13,14,15,16]. Release of clients from Hsp40 to Hsp70 can be blocked by an H-to-Q mutation in the Hsp40 J-domain, stabilizing misfolded protein binding[17].

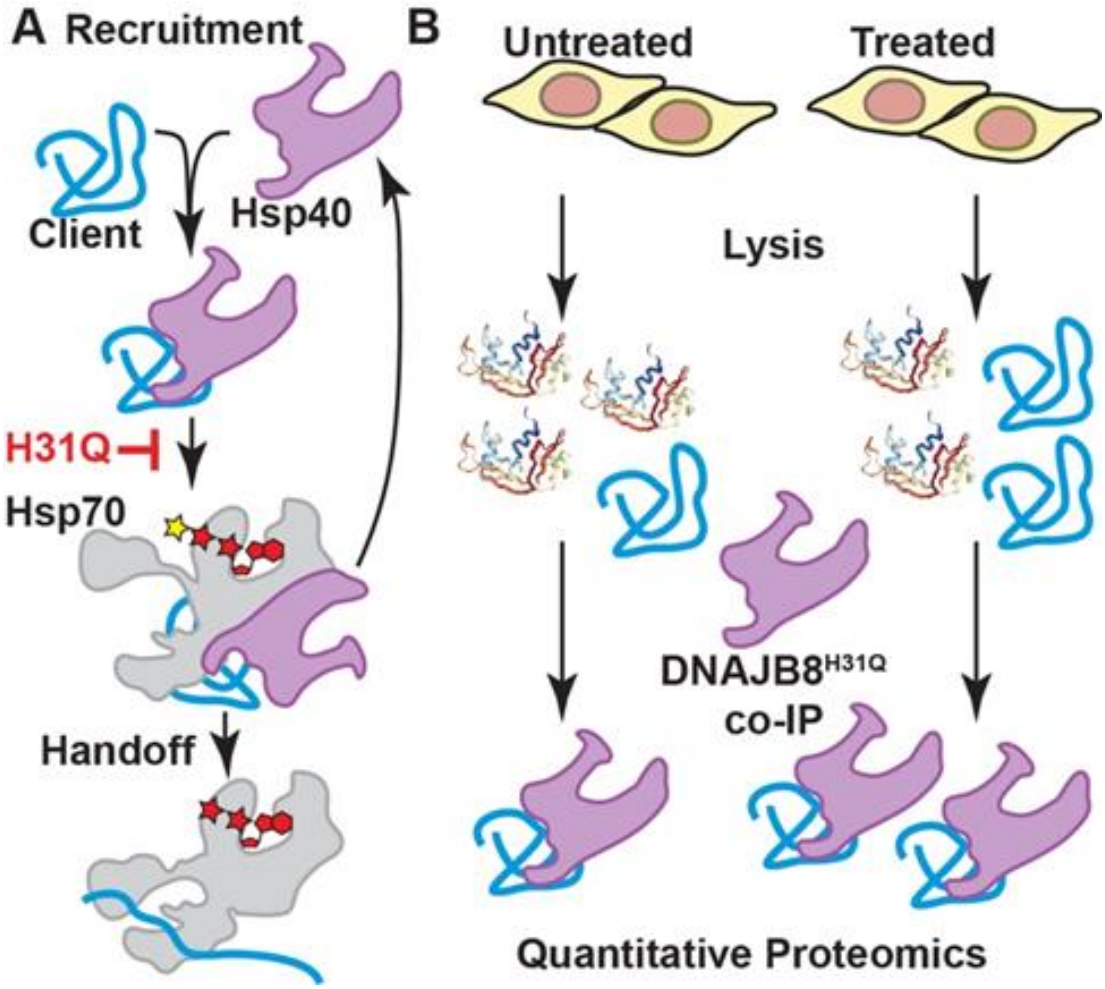

Figure 1. Design of the Hsp40 affinity assay for misfolded proteins. A) DNAJB8 binding and handoff to Hsp70 is interrupted by an H31Q mutation in the J-domain. B) If cellular treatment increases the misfolded population of a DNAJB8 client protein, then the apparent affinity of that protein for DNAJB8^{H31Q} will increase.

DNAJB8 is notable among human Hsp40s for its dual nuclear and cytosolic localization, formation of oligomers, and slow client release kinetics[18,19,20,21]. We previously used affinity purification and quantitative proteomics to identify hundreds of cellular protein clients of overexpressed human Hsp40 DNAJB8^{H31Q} with high reproducibility and statistical confidence[22]. Herein we exploit the ability of DNAJB8^{H31Q} to recognize misfolded protein clients to develop a platform for identifying proteins that are destabilized in response to exogenous stress (**Figure 1**). We demonstrate this approach in HEK293T cells treated with trivalent arsenic, a toxic metal that causes widespread damage to nucleic acids and proteins, leading to genomic and metabolic instability[23].

2.3 Materials and Methods

2.3.1 Materials:

Bovine Serum Albumin (BSA), Dulbecco's Modified Eagle Media (DMEM), Dulbecco's phosphate-buffered saline (DPBS), 10 cm plates, and 6 well plates were from VWR. Roche Protease Inhibitor cocktail w/o EDTA (PIC), 1,4-dithiothreitol (DTT), HEPES, sodium meta arsenite ($NaAsO_2$), $Cd(NO_3)_2•(H_2O)_4$ were from Sigma Aldrich. Sodium chloride (NaCl), Tris-Hydrochloride (Tris-HCl), Triton X-100, sodium deoxycholate, KCl, $MgCl_2$, $CaCl_2$, $Ag(NO_3)_2$, $Na_2S_2O_3$, urea, $Ca(O_2C_2H_3)_2$), glycerol, sodium dodecyl sulfate (SDS), poly D-lysine, and sequencing grade trypsin were from Thermo Fisher Scientific. Proteinase K (PK) was from Promega. Nanopure water was purified using a Millipore Milli-Q Laboratory lab 4 Chassis Reagent Water System. 5 μm

and 3 µm Aqua C18 resins were from Phenomenex. Sepharose-4B beads, anti-M2 Flag magnetic beads, tris (2-carboxyethyl)phosphine hydrochloride (TCEP), and iodoacetamide were from Millipore Sigma. 250 µm diameter fused silica columns were from Agilent. 100 µm diameter fused silica columns were from Polymicro. Strong cation exchange resin was from Partisphere, GE Healthcare. Rapigest was from Aobious (Gloucester, MA). TMT-6plex isotopic labels were from Pierce. Bradford reagent was purchased from Bio-rad.

2.3.2 AP-TMT-MudPIT:

TMT-AP-MS experiments were performed as previously described[22]. For each sixplex TMT-AP-MS, six 10 cm plates of HEK293T cells were transfected by the calcium phosphate method with 5 µg of plasmid DNA encoding ^{Flag}DNAJB8^{H31Q} in the pFLAG backbone. Plates were treated with heavy metal salts or vehicle at 40-46 hours post transfection. Cells were harvested by scraping in DPBS and lysed in 9 parts RIPA Buffer (150 mM NaCl, 50 mM Tris pH 7.5, 1% Triton X-100, 0.5% sodium deoxycholate, 0.1% SDS) and 1 part 10x PIC for 30 min on ice. Lysate was separated from cell debris by centrifugation at 21,000 x g for 15 minutes at 4 °C. Protein in the lysate was quantified by Bradford. Lysates were pre-cleared with 15 µL Sepharose-4B beads for 30 min at 4 °C, then centrifuged at 1,500 x g for 1 min to pellet beads. Lysate was then separated and incubated with 15 µL of M2 anti-Flag Magnetic Beads and rotated overnight at 4 °C. The anti-Flag beads were washed the next day four times with RIPA buffer. Each wash included rotation for 10 minutes at ambient temperature. Proteins

bound to the anti-Flag beads were eluted by boiling for 5 min at 100 °C in 30 µL of Laemmli concentrate (120 mM Tris pH 6.8, 60% glycerol, 12% SDS, brilliant phenol blue to color). 5 µL of the elutes were saved for silver stain analysis and the remainder was prepped for mass spectrometry and TMT-labeled.

Only MS quality organic solvents were used during sample preparation. The composition for buffer A is 5% acetonitrile, 0.1% formic acid in water. The composition for Buffer B is 80% acetonitrile, 0.1% formic acid. The composition for Buffer C is 500 mM ammonium acetate in Buffer A. The first arsenic exposure TMT-MS run was performed as one-dimensional LC/MS/MS on an Orbitrap Fusion Tribrid mass spectrometer (Thermo) interfaced with a nanoAquity UPLC (Waters) system. All other MS runs were performed with a two-dimensional LC/MS/MS setup on an LTQ Orbitrap Velos Pro hybrid mass spectrometer (Thermo) interfaced with an Easy-nLC 1000 (Thermo) according to standard MuDPIT protocols[24]. For each run, MS/MS spectra were extracted using MSConvert (version 3.0.21144) with Peak Picking Filtering. MS/MS spectra was then searched by FragPipe[25] against a Uniprot human proteome database (06/11/2021 release) containing 40858 human sequences (longest entry for each protein). MS/MS spectra were also searched against 20429 select decoys (e.g albumen, porcine trypsin, contaminants etc.). FragPipe searches allowed for static modification of cysteine residues (57.02146 Da, acetylation), and N-termini and lysine residues (229.1629 Da, TMT-tagging), half tryptic peptidolysis specificity, and mass tolerance of 20 ppm for precursor mass and 20 ppm for product ion masses. Spectra matches were assembled and filtered by MSFragger (version 3.2). Decoy proteins, common contaminants,

immunoglobulins and keratins were filtered from the final protein list. Quantitation in FragPipe was performed by averaging TMT reporter ion intensities for all spectra associated with an individual peptide.

2.3.2 Statistical Analysis:

Protein-level intensities were normalized to the intensity of bait (DNAJB8) in each TMT channel. To combine the multiple TMT runs, we used a version of the scaled reference approach[26]. A scaling factor was obtained from averaging the bait-normalized integrated TMT reporter ion intensities for each protein across the 3 control conditions in each AP-MS run. Each bait-normalized protein intensity was then divided by this scaling factor. Unadjusted p-values were converted to q-values (local false discovery rates) using Storey's modification to the method of Benjamini and Hochberg[27,28]. Unadjusted p-values were ranked in increasing order and the q-value for the *i*th protein determined from:

$$q_i = \pi \, min_{i \le j \le n} \frac{pn}{i}$$

Storey's modification is performed by determining the overrepresentation of low p-values to infer a global false discovery rate, and then scaling local false discovery rates accordingly. The π-factor for this scaling was 0.84 for the arsenic treatment TMT-AP-MS data set and 0.79 for the cadmium treatment.

2.3.4 Limited Proteolysis:

2.3.4.1 Limited Proteolysis Procedure:

The limited proteolysis procedure was optimized from standard protocols[29]. 1

mg/ml stocks were made from 25 mg of lyophilized Proteinase K (PK) dissolved in a storage buffer (50 mM Tris-HCl, 2 mM calcium acetate, pH 8.0) suitable for PK and stored at –70 °C. The following concentrations of PK were prepared from serial dilutions from 1mg/ml aliquot: 0.5 mg/ml, 0.2 mg/ml, 0.1 mg/ml, 0.05 mg/ml, 0.02 mg/ml, and added to lysate to yield 1:200, 1:500, 1:1000, 1:2000, and 1:5000 wt/wt protease: substrate protein ratios respectively. For each digestion, 2 µl PK was added to a 200 µg aliquot of protein lysate and incubated for 1 min at 25.0 °C. Samples were then boiled for 5 min to quench PK activity. Three separate digestions were performed for the no PK condition for each lysate sample. The sample set-up and the calculation of fraction remaining for each peptide is shown in **Figure S1**. Samples were prepared for mass spectrometry, spiked with an internal standard peptide NH_2-VFFAEDVGSNK-CO_2H to 83 nM and analyzed using LC-MS/MS and parallel reaction monitoring (PRM).

2.3.4.2 Limited Proteolysis: Peptide Selection and Analysis

Thirteen peptides were selected from PDHA1, TDP43, RACK1, HNRNPA0, RPS16, HNRNPK, and RPS3 for the initial LiP screen experiment. These proteins were chosen as having significantly increased interaction with DNAJB8 in response to arsenite. Our initial peptide identification searches, using a different software than FragPipe, did not identify NOSIP, CSDE1, MRPS28, and so we did not include these proteins in our LiP survey. Retention times for each peptide were determined by running unscheduled PRM runs from a trypsin digested lysate. Eleven peptides from PDHA1 and PDHB were selected for the E1 subunit LiP, and five peptides from TDP43 were chosen

for the TDP43 LiP experiment. Fragmentation patterns for all peptides were uploaded into Skyline software for analysis[30]. Samples were analyzed using two dimensional LC/MS/MS on an LTQ Orbitrap Velos hybrid mass spectrometer (Thermo) interfaced with an Easy-nLC 1000 (Thermo). 6 µg of protein were injected in each run onto a loading column packed with 2.5 cm of 5um Aqua C18 resin and washed prior to S-8 separation on the analytical column. Analytical columns were prepared by pulling 100 µm diameter fused silica columns with a P-2000 laser tip puller (Sutter Instrument Co., Novato, CA), followed by packing of 23 cm of reversed-phased 3 µm Aqua C18 Resin.

Peptides injected were scanned over scheduled 10 min windows centered around average retention time, and isolated with a 2.0 m/z isolation window. Peptides were fragmented with CID with a normalized energy of 35, activation Q of 0.25 and activation time of 10 msec. MS2 were acquired in the Orbitrap at 7500 resolving power and saved in profile mode. Peptide separations by LC-MS proceeded between Buffer A (5% acetonitrile: 95% water: 0.1% formic acid) and Buffer B (80% acetonitrile: 20% water: 0.1% formic acid) over a 100 min gradient with the following segments: 1-5 min: 1-6% Buffer B. 5-75 min: 6-29% Buffer B. 75-80 min: 29- 100% Buffer B. 80-85 min: 100% Buffer B. 85-90 min: 100-1% Buffer B. 90-100 min: 1% Buffer B. Flow rate was 500 nl/min.

2.2.4.3 Limited Proteolysis: Data Analysis

Three technical runs were run for each biological replicate, except only a single technical replicate was ran when using the method analyzing five TDP-43 peptides. For

each control (no PK) run, three separate digestions were prepared. Integrated fragment intensities were calculated in Skyline. Integrated fragment intensities were normalized to the integrated fragment intensity of the internal standard for method optimization. However, we did not use internal standard normalization for the digested samples, as we found unacceptable interference in the digested samples for this peptide. The integrated fragment intensities for each set of three technical replicates are averaged and normalized to the averages of the three no-PK controls (which themselves were run in technical triplicate) (**Figure S1**). Proteolytic susceptibility curves were made from graphs that plotted relative fragment intensity against increasing PK concentration. Differences between curves are assessed based on the summed fractions remaining across data points from 2000:1 to 100:1, and the significance of these sums determined by one-tailed Student's t test (**Table S8**). Coefficient of Variation S-9 (CV) were calculated from ten technical replicates of a Trypsin control and CV of biological replicates were calculated among three biological replicates for both LiP experiments. We should note that because our analysis does not assume linearity between integrated peptide response and actual peptide levels, no effort was made to establish whether the peptides observed are in the linear quantitative regime[31].

2.3.5 ^{Flag}PDHA1 co-IP Method:

Immunoprecipitations were performed similarly to those of ^{Flag}DNJAB8^{H31Q} with the exception that cells were crosslinked prior to lysis with 1 mM DSP/1% DMSO/DPBS for 30 mins while rotating at ambient temperature. DSP was quenched with 100 mM Tris

pH 8 (final concentration) with rotating for 15 minutes at room temperature

For each two plex, four 10 cm plates of HEK293T cells were transfected by the calcium phosphate method with 5 µg of plasmid DNA S-10 encoding ^{Flag}PDHA1 in the pFLAG backbone. Briefly, 5 µg of DNA in 1 mL 250 µM CaCl2 is vortexed while adding dropwise 1 mL HBS 2X for 10 seconds at ambient temperature, the transfection solution is promptly (≤ 15 min) added dropwise to cells, and the cell media is changed between 12 and 16 h. A positive transfection control is performed with GFP alongside each transfection. Plates were treated with heavy metal salts or vehicle at 40-46 hours post transfection. Cells were harvested by scraping in DPBS. Cells were diluted to 1ml of DPBS and incubated and rotated with 1 mM DSP (dithiobis(succinimyidyl propionate) in 1% DMSO vehicle for 30 mins at ambient temperature. DSP was quenched with 100 mM Tris pH 8 (final concentration) and rotated for 15 minutes at room temperature. Cells were then lysed in 9 parts RIPA Buffer (150 mM NaCl, 50 mM Tris pH 7.5, 1% Triton X-100, 0.5% sodium deoxycholate, 0.1% SDS) and 1 part 10x PIC for 30 min on ice. Lysate was separated from cell debris by centrifugation at 21,000 x g for 15 min at 4 °C. Protein in the lysate was quantified by Bradford. Each sample had protein content normalized to same amount and diluted to 3 µg/µl. Lysates were pre-cleared with 15 µL Sepharose-4B beads for 30 min at 4 °C, then centrifuged at 1,500 x g for 1 min to pellet beads. Lysate was then separated and incubated with 15 µL of M2 anti-Flag Magnetic Beads and rotated overnight at 4 °C. The anti-Flag beads were washed the next day four times with RIPA buffer. Each wash included rotation for 10 minutes at ambient temperature. Proteins bound to the antiFlag beads were eluted by boiling for 5 min at 100 °C in 25 µL of

Laemmli concentrate (120 mM Tris pH 6.8, 60% glycerol, 12% SDS, brilliant phenol blue to color). Eluates were blotted for Western Blot on 10% SDS-PAGE Gel with 1.0 mm thickness. Western blots were first probed to observe E1-E2 interaction: 1. Rabbit polyclonal anti-DLAT, 2. Rabbit polyclonal anti-PDHB, 3. Rabbit polyclonal anti-PDHA1. Blots were then probed with mouse monoclonal M2 anti-Flag (Sigma), mouse monoclonal anti-Beta Actin (7D2C10), and rabbit polyclonal anti-GFP using near-IR secondary antibodies (Li-COR). Bands corresponded to each antibody were visualized and quantified by densitometry on a Li-Cor Biosciences Fc Imager using Image Studio. DLAT and PDHB band intensities were normalized to band intensities from the bait, PDHA1.

2.3.6 Cell Culture:

HEK239T cells were obtained from the ATCC and maintained in DMEM with 10% FBS. Cell transfection was performed by the calcium phosphate method. Briefly, 5 µg of DNA in 1 mL 250 µM $CaCl_2$ is vortexed while adding dropwise 1 mL HBS 2X for 10 seconds at ambient temperature, the transfection solution is promptly (≤ 15 min) added dropwise to cells at about 50% confluency, and the cell media is changed between 12 and 16 h. A positive transfection control is performed with GFP alongside each transfection. These transfection amounts were used for 10 cm dishes; proportional amounts of reagents were used for transfection of different sized plates. Silver Stain. Silver stain was used to assess the amount of the ^{Flag}DNAJB8^{H31Q} in eluates after the immunoprecipitation and potential differences in the co-immunoprecipitated protein

levels between conditions[32]. DTT was added to a final concentration of 170 mM, and eluates boiled for 5 min at 100 °C prior to SDS-PAGE separation. Gels were fixed overnight in 30% ethanol/10% acetic acid or for a few hours with 50% methanol/12% acetic acid. Gels were washed in 35% ethanol three times for 20 minutes each, sensitized for 2 minutes (0.02% $Na_2S_2O_3$ in H_2O), washed three times for 1 minute each in H_2O, and stained for 30 minutes to overnight in Ag staining solution (0.2% $AgNO_3$, 0.076% formalin). After two one minute rinses in H_2O, gels were developed with 6% $NaCO_3$/0.05% formalin/0.0004% $Na_2S_2O_3$. Development was stopped with 5% acetic acid. Gels were imaged on a white-light transilluminator (UVP).

2.3.7 Activation after Applied Metal Stress:

Two 10 cm plates seeded with HEK293T cells were transfected at 40-60% confluency. One plate was transfected with 5 µg of DNA encoding ^{FLAG}DNABJ8^{H31Q} and the other plate was transfected with 5 µg of DNA encoding GFP. Both plates were split into 6-well plates or three separate 6 cm plates that were previously coated with Poly-D-Lysine. Each individual well was incubated with an increasing concentration (0 µM, 25 µM, 50 µM, 100 µM, 200 µM, 500 µM) of a metal for 15 min at 37 °C. Toxic metal media was replaced with fresh media and plates were incubated for 16 h at 37 °C to recover. Plates were then harvested by scraping in DPBS and then lysed in 9:1 RIPA:10x PIC in ice for 30 min. Lysates were separated from cell debris by centrifugation at 21,000 x g for 15 minutes at 4 °C. Bradford assay was used to quantify protein concentration in each lysate. 2 µg/µl of protein samples were prepared for western blot analysis after

addition of 9:1 Laemlli:1 M DTT (17% of solution). 15 µg of each sample were separated on a 12% SDS-PAGE Gel with 1.0 mm thickness. Western blots were probed for Flag (Sigma M2 monoclonal anti-Flag antibody), HSPA1A (rabbit polyclonal), Beta-actin (mouse monoclonal 7D2C10), and GFP (rabbit polyclonal) primary antibodies, near-IR secondary antibodies (Li-COR) and visualized on a Li-Cor Biosciences Fc Imager.

2.4 Results and Discussion

Protein misfolding stresses leads to extensive transcriptional, translational, and post-translational remodeling of the cell[33]. To isolate stress-induced protein misfolding from these pleiotropic effects, we limited cellular exposure to brief 15 min treatments. We validated that 15 min. 500 µM sodium meta-arsenite ($NaAsO_2$) induces expression of the HSR target HSPA1A in HEK293T cells (**Figure S2**). Because HSR is activated by misfolded protein accumulation, this suggests that 500 µM arsenite treatment causes protein misfolding in only 15 min. This response is not suppressed by overexpression of $^{Flag}DNAJB8^{H31Q}$ (**Figure S2**), indicating that our recognition element for misfolded protein does not prevent protein destabilization.

We used the experimental approach illustrated in **Figure 2A** to determine proteins that misfold in response to arsenite exposure. $^{Flag}DNAJB8^{H31Q}$ was transiently overexpressed in HEK293T cells, followed by 15 min. $NaAsO_2$ treatment and immediate Flag immunoprecipitation from cellular lysate. Co-immunoprecipitated proteins were identified and quantified by LC/LC-MS/MS in concert with TMT isobaric tagging[34]. Overall, 24 biological replicates (12 treated and 12 controls) were analyzed through four

6-plex TMT runs. Most observed protein clients slightly increase affinity to DNAJB8 following arsenite treatment, likely because peptides from proteins with increased DNAJB8 binding following arsenite treatment are more represented in the pooled peptide mixture, and thus have higher chances of identification during shotgun proteomics. However, the bulk DNAJB8 associated proteome does not change (**Figure 2B**). 24 proteins have significantly greater affinity for ^{Flag}DNAJB8^{H31Q} in response to the arsenite treatment. These proteins include PDHA1 and 17 ribosomal RNA-binding proteins, including HNRNPA0, TDP-43, RACK1, and RPS16 (**Figure 2C** and **Table S1**). Arsenite generally induces misfolding and aggregation of RNA-binding proteins into stress granules[35,36]. However, canonical stress granule markers[37] G3BP1 and EIF4G1 are not enriched in DNAJB8^{H31Q} pull-downs from arsenite-treated cells, indicating that DNAJB8^{H31Q} is not co-precipitating intact stress granules (**Table S1**).

TDP-43 is a ribonuclear protein that forms aggregates in ALS and other proteinopathies[*38*]. It accumulates in cytoplasmic and nuclear condensates in response to arsenite treatment, due to displacement from RNA and post-translational modification[39]. Yeast RACK1 migrates to stress granules in response to arsenite[40]. It is particularly interesting that PDHA1, the alpha subunit of the pyruvate dehydrogenase complex (PDC)[41], is destabilized by arsenite. Inhibition of PDC is a major contributor to arsenite-induced metabolic disfunction[42]. We are encouraged that our assay primarily finds proteins that are known to be arsenite-sensitive. The Hsp40 Affinity mass spectrometry experiments are comparisons between two sets of twelve AP-MS preparations, analyzed as four individual multiplexed injections of six samples each. The Hsp40 Affinity mass

spectrometry experiments are comparisons between two sets of twelve AP-MS preparations, analyzed as four individual multiplexed injections of six samples each.

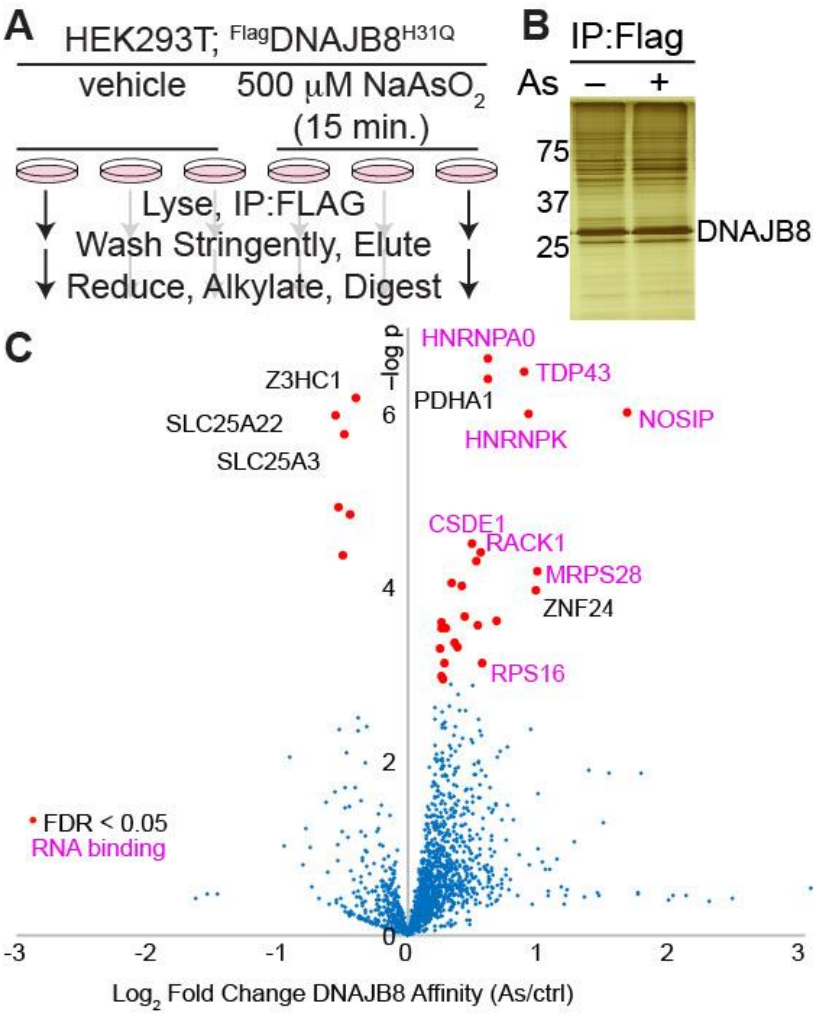

Figure 2. Arsenite treatment increases the affinity of a select subset of proteins with DNAJB8^{H31Q}. A) Experimental protocol. B) Representative silver stain for proteins co-immunoprecipitated with DNAJB8^{H31Q}. C) Volcano plot illustrating the effect of cellular As treatment on protein interactions with DNAJB8^{H31Q}. Red dots represent proteins with significantly increased interaction with DNAJB8^{H31Q}, using a false discovery rate threshold (FDR) of 5% (n = 12 biological replicates in 4 TMT-AP-MS runs). Protein names in purple are RNA-binding proteins.

To indicate the robustness of hits from this assay, the Strictly Standardized Mean Differences (SSMD) were compared between each multiplexed injection (**Figure S3**).

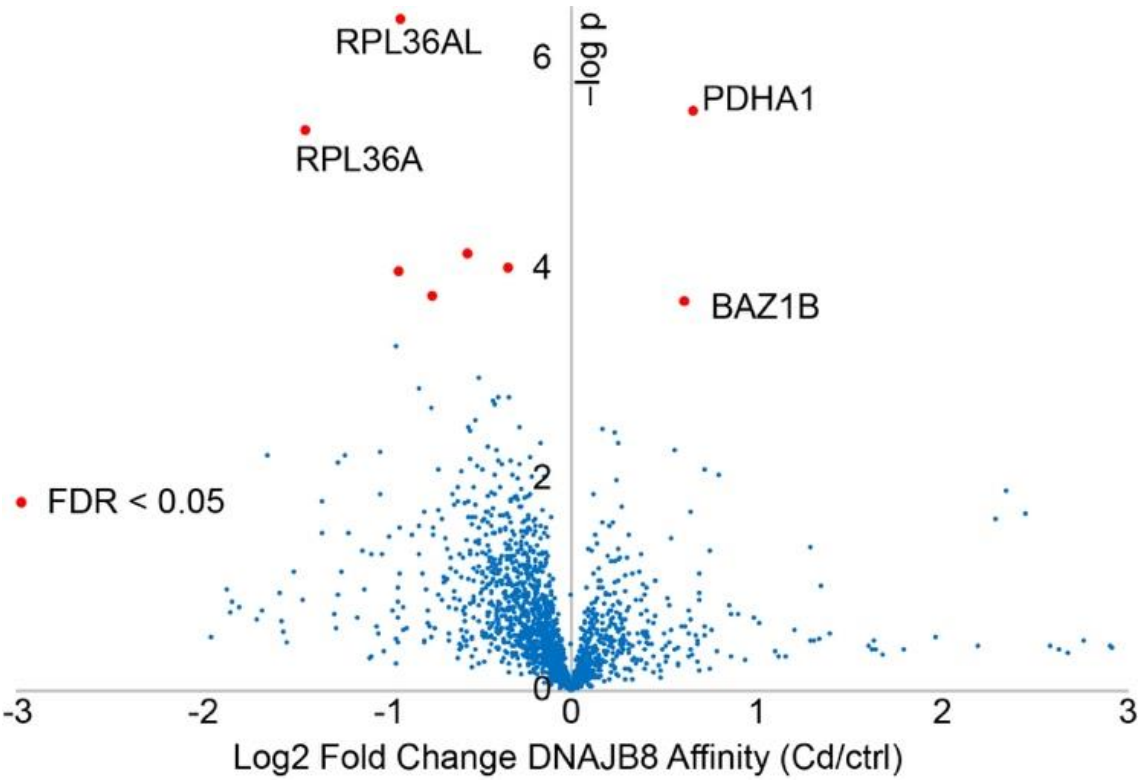

Figure 3. Cadmium treatment (200 µM $Cd(NO_3)_2$ for 15 min.) only affects the $DNAJB8^{H31Q}$ affinity of a few proteins. The experimental protocol is similar to Figure 1A. n = 12 biological replicates in 4 TMT-AP-MS runs.

SSMDs represent the mean differences between the treated and untreated populations, normalized by root-mean-square standard deviations. The most affected proteins reproduce well across each replicate. It is worth noting that arsenite treatment does not affect the bulk proteome of eluted $DNAJB8^{H31Q}$ co-IPs by silver stain of the eluate (**Figure S4**). The arsenite pulldowns collectively identified and quantified 1696 unique proteins, not including 28 keratin/immunoglobulin proteins that were excluded

from the set, and 24 proteins that were identified but whose TMT reporter ions could not be quantified. We previously characterized 562 high confidence DNAJB8^{H31Q} interactors from AP-MS in unstressed HEK293T cells[22]. Those included 379 of the proteins found in this study, and 21/30 of our high confidence arsenite-sensitive proteins.

It is possible that stress conditions, by increasing the affinity and thus recovery of a select proteome, also increase the likelihood of identifying those proteins from data-dependent analysis. Piette *et al* recently[43] reported comprehensive interactomes of human Hsp40 and Hsp70 family proteins (unlike our work, these all had active J-domains), finding 37 high confidence interactors of DNAJB8 and another 479 proteins that could not be reliably distinguished from background. We find 22/37 of their high-confidence interactors in our data set, with most of the missing proteins being either Hsp70s (which bind through the J-domain) or Hsp70 binding proteins (Hsp40s, CHIP, FKBP8 etc.), consistent with expected differences in recovery between the wild-type protein and a J-inactive variant. Conversely, 11/31 of our high confidence arsenite-sensitive proteins are found in their study, and none are among their high confidence interactors.

To determine whether the arsenite response is specific, we treated cells with Cd^{2+}, another heavy metal that induces cellular apoptosis through generation of ROS[44]. 15 min. treatment with 200 μM $Cd(NO_3)_2$ induces HSR in HEK293T cells (**Figure S5**). Cells were treated with Cd or vehicle for 15 min. and then immediately lysed, and the DNAJB8^{H31Q} interacting proteome quantified by TMT-AP-MS (**Figure 3** and **Table S2**). As with arsenite-treated cells, the bulk DNAB8^{H31Q} interacting proteome is unaffected (**Figure S6**). Unlike with arsenite, the only proteins destabilized by acute Cd treatment

are PDHA1 and BAZ1B (**Figure 3** and **Figure S7**). Rather, many proteins slightly lose affinity for DNAJB8 following treatment, perhaps due to direct binding to Cd. As with arsenite, Cd exposure inhibits pyruvate dehydrogenase activity[45]. TDP-43 association with DNAJB8 is unchanged, despite reports that Cd^{2+} treatment (100 μM, 2 h) promotes TDP-43 aggregation in Cos7 cells[38]. The difference in proteome destabilization between the two heavy metals suggests that ROS generation is not adequate to explain their effects on protein stability following acute arsenite exposure.

Protein sequences are optimized for a native conformational landscape, and hence damage that modulates charge, sterics, or binding partners has the potential to induce misfolding. However, binding to the native state will generally stabilize that state, decreasing the propensity to access misfolded states. This is the basis of ligand target discovery through stabilization as widely employed in CETSA[12]. Because our assay enriches Hsp40 clients, it will enrich proteins with enhanced destabilization in response to treatment and should be inherently disadvantaged for discovery of stabilized protein targets. However, we would still expect to see proteins that are stabilized, such as are observed on the left in **Figure 2C** and **Figure 3** if, for example, direct metal binding increases $\Delta G_{unfolding}$.

Although our short treatments and immediate processing avoid many pleiotropic effects (e.g. altered transcription, translation, trafficking, and degradation, etc.), unforeseen variables besides protein stability could impact DNAJB8-client affinity. Hence we applied an orthogonal assay, LiP, to validate and prioritize proteins with arsenite-induced binding to DNAJB8 (**Figure 4A**). LiP as a discovery technology is

challenged by the need to identify and quantify peptides in a proteome that has been rendered complex by the use of two orthogonal proteases; for example, hit overlap with SPROX from the same samples is about ~20%[46,47]. We targeted select peptides from our hit proteins to alleviate this challenge. The PK concentration gradient was optimized to bracket the full range of changes in observable protein on a Coomassie-stained SDS-PAGE gel (**Figure S8**). Bulk protein band intensity decreases at a PK:protein ratio of 1:1000 and little intact protein is observable at 1:100 PK:protein. These values are somewhat lower than commonly reported conditions, which range from 1:33 to 1:100[48,49]. Peptides for monitoring were chosen in the Picky software[50], based on chemical properties amenable to PRM and to maximize distribution across the chromatographic gradient. The PRM method had a median CV of 20%, with all but one peptide below 30% (**Table S3**). Biological replicates showed similar CV values (**Table S4**). Precision was unaffected by choice of MS2 resolving power (**Table S5**), consistent with a recent report on the dispensability of high resolution for PRM[51], so 7500 was used.

We treated cells with arsenite or vehicle for 15 min., followed by immediate lysis. Lysates were treated with varying concentration of proteinase K for 1 min, heat-quenched, tryptically digested, and peptides from candidate proteins quantified by Parallel Reaction Monitoring (PRM)[52]. If a cellular treatment increases the PK proteolysis yield of a peptide, that implies that the protein is destabilized in the vicinity of that sequence[48]. Limited proteolysis is a local measure of protein conformation and thus is subject to false negatives at the protein level. Hence, a given peptide being equally sensitive to proteolysis with or without cellular treatment does not imply that the entire

protein is unaffected.

We determined the proteolytic susceptibility with and without 15 min. cellular arsenite treatment for 13 peptides from PDHA1, RSP16, RPS3, TDP-43, HNRNPK, RACK1, and HNRNPA0. Although RPS3 was a lower significance protein from our screen, we included it in these targeted LiP experiments because arsenite causes release of RPS3 from RNA[53], which could affect protein stability. Peptides from PDHA1 and RPS16 are more susceptible to proteolysis upon arsenite treatment, implying that arsenite destabilizes these proteins (**Figures 4B** and **S9A**).

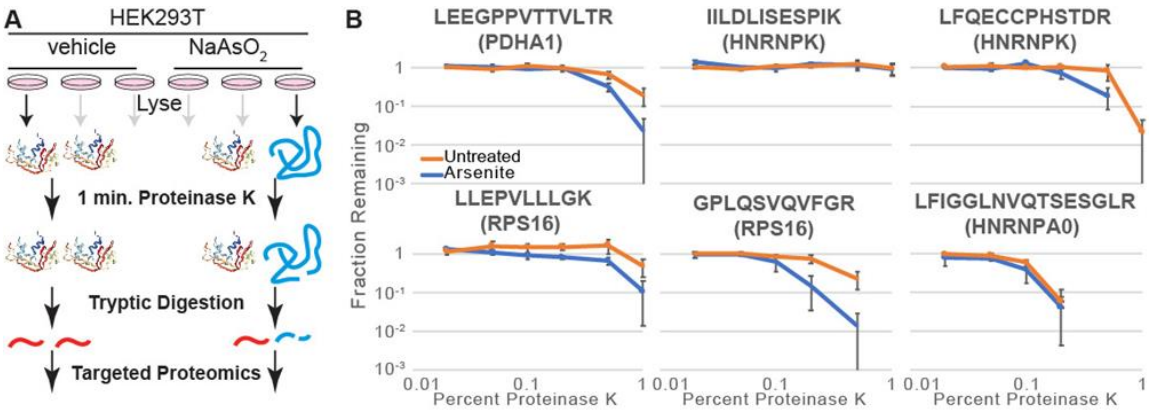

Figure 4. A) Schematic illustrating how limited proteolysis differentiates between different conformations of a protein. B) Proteinase K susceptibility curves for four peptides as monitored by LiP-PRM. Error bars represent standard error (n = 3).

The peptides chosen for TDP-43, HNRNPA0, RACK1 and RPS3 do not show a clear increase in proteolytic sensitivity; those proteins might still be destabilized by arsenite in unsampled regions of the protein. HNRNPK increases sensitivity at two peptides, but not at three others. No peptide became less sensitive to PK following cellular arsenite treatment. We expanded the TDP-43 evaluation to four additional

peptides, of which three showed arsenic sensitivity (**Figure S9B** and **Table S6**).

Surprisingly, all three peptides come from structured regions within the RNA-binding domains of the protein[54].

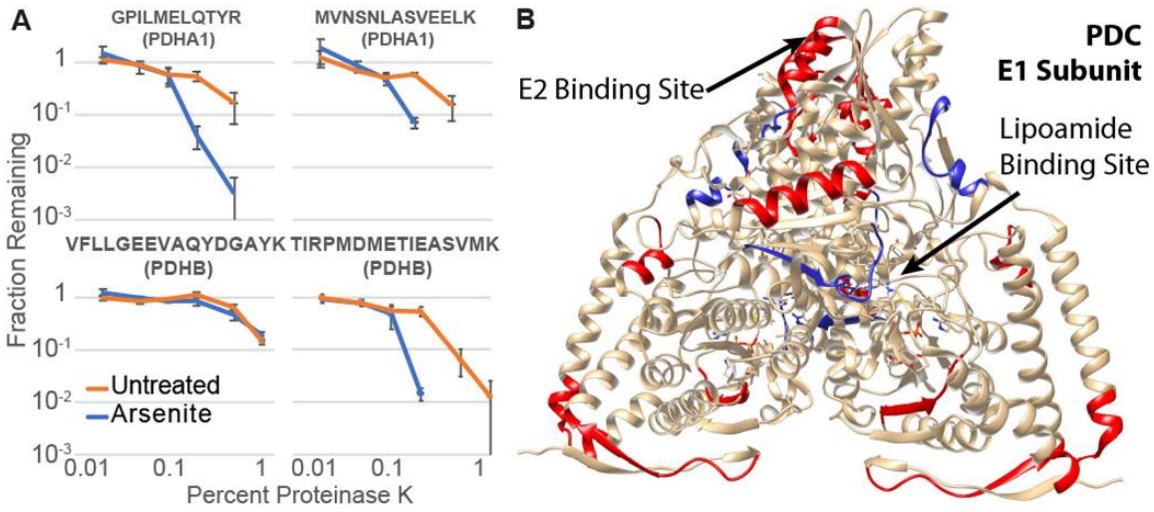

Figure 5. A) Proteinase K susceptibility curves for four peptides from the E1 subunit of PDC as monitored by LiP-PRM. Error bars represent standard error (n = 3). B) Crystal structure of the dimeric PDC E1 subunit (PDB: 1NI4)[55,56 55,56] with As destabilized peptides are colored red, and the two peptides that are not As-sensitive are blue. The arrow indicates the location of the lipoamide co-factor.

The two peptides that do not have increased proteolytic susceptibility in response to cellular arsenic exposure are in intrinsically disordered regions; one is in the linker between the RNA binding domains and the other is in the unstructured C-terminus. The general validation of protein destabilization by an orthogonal method demonstrates that DNAJB8^{H31Q} affinity successfully identified proteins that are destabilized by arsenite treatment.

The sensitivity of PDHA1 to arsenite is surprising. PDC inhibition by arsenite is

generally ascribed to arsenite coordination to vicinal thiols in the lipoamide cofactor[3], though other evidence strongly points to lipoamide binding being unnecessary for inhibition by arsenic[57]. PDC is composed of three subunits, including an E1 heterotetramer containing two PDHB and two PDHA1 proteins[41].

Lipoamide is anchored covalently to DLAT in the E2 subunit, but reacts in the groove of PDHB in the E1 subunit. We considered the hypothesis that arsenite destabilizes the rest of the E1 subunit. PDHB did show increased affinity to DNAJB8^{H31Q} in our initial screen, but with low significance (FC = 1.3 ± 0.3, q = 0.06). The binding of DLAT to DNAJB8^{H31Q} was not meaningfully unaffected by arsenite exposure (FC = 0.93 ± 0.48, q = 0.69). Because LiP measures local proteolytic sensitivity[47], we used targeted LiP to determine whether PDHA1 and PDHB are globally destabilized. Eleven peptides from PDHA1 and PDHB were selected, covering most of the protein sequences (**Figure 5A, Figure S9C,** and **Table S7**). Most locations on both proteins are destabilized by cellular arsenite treatment (**Figure 5B**), indicating that the proteins undergo an extensive conformational change with arsenite treatment. In particular, cellular arsenite increases proteolytic susceptibility at the E1-E2 interface (IMEGPAFNFLDAPAVR and TIRPMDMETIEASVMK peptides). The peptide at the lipoamide binding site (VFLLGEEVAQYDGAYK), however, is not affected. That lead us to explore the hypothesis that perhaps cellular inactivation of PDC is caused by complex destabilization and disassembly of E1. We cloned affinity tagged ^{Flag}PDHA1 and expressed by transfecting in HEK293T cells. As expected for a dynamic complex, ^{Flag}PDHA1 requires intracellular crosslinking to co-immunoprecipitate PDHB and DLAT (**Figure S10**).

However, neither 15 min. nor 4 h cellular arsenite treatment (500 μM) decreases the yield of PDHB and DLAT recovery with ^{Flag}PDHA1. Hence, despite complex destabilization by arsenite, the complex does not significantly dissociate (**Figures S11-S14** and **Supplemental Discussion**).

2.5 Supplemental Discussion on Limited Proteolysis

We determined assay precision across technical and biological replicates. To determine the reproducibility of the scheduled PRM assay itself, ten consecutive injections of a lysate tryptic digest were performed, and CVs calculated for the integrated fragment intensities of the 13 targeted peptides from a trypsin only digested lysate. Each targeted run included a 6 μg injection, a 10 minute retention time window for each peptide, and chromatograms that were scanned at 7500 nominal resolving power. The low resolving power was chosen to minimize cycle time. Lower cycles times allow more scans across peaks, increasing robustness of quantification[58]. The MS2 intensities of transitions from a precursor ion were integrated by Skyline for quantification of each peptide. The median CV for the summed transitions MS2 among the 13 targeted peptides was 20%. The median CV for the summed MS2 transitions normalized to internal standard was only slightly improved to 14% (**Table S2**). These CVs are typical for PRM[59]. TDYNASVSVPDSSGPER (HNRNPK) had a CV greater than 30%, possibly due to their hydrophilic character as they eluted early from the reversed-phase C18 column[52].

To determine whether 7500 nominal resolving power was too low to avoid matrix interference[31], we performed 6 more technical replicate PRM experiments on a HEK239T

tryptic digest using 60,000 nominal resolving power and scheduling only three select peptides and the internal standard. The four peptides selected had 10 minute retention time windows that did not overlap with each other to minimize cycle times. The calculated CV from the six runs were compared with the quantification of the previous measurements that were run at 7500 resolution.

The median CV for the summed transitions MS2 among the 4 targeted peptides was 18. The median CV for the summed MS2 transitions normalized to internal standard among the 4 peptides was 9% (**Table S5**). Higher resolving power hence did not meaningfully increase the precision of the method. S-12 The CV between biological replicates was addressed during the LiP mass spec runs. The LiP mass spec samples included three zero PK controls and the following Protein: PK samples: 5000:1, 2000:1, 1000:1, 500:1, 200:1, and 100:1.

Peptides were scanned in 10 minute retention time windows at 7500 resolution after a 6 μg HEK293T tryptic digest injection. The CV was calculated among the three Zero PK samples for both arsenite exposed and control cellular conditions. Across these biological replicates, median CV values were below 20% with only 1 peptide having a CV greater than 25% (**Table S3**). The median CV for LiP method targeting TDP-43 peptides was below 17%. (**Table S6**). The E1 subunit LiP experiment that looked at 11 peptides between PDHA1 and PDHB found CV below 20% for all peptides (**Table S7**). In summary, the peptide CVs in our PRM assay for biological replicates were relatively similar to the CVs calculated for technical replicates.

2.6 Supplemental Discussion on Investigation into PDC Complex

Both AP-MS and LiP experiments reveal that PDHA1 and PDHB proteins misfold after arsenite treatment. Both PDHA1 (fold change = 1.5 ± 0.4, q = 2 x 10-4) and PDHB (fold change = 1.3 ± 0.3, q = 0.06) increase their affinity to ^{FLAG}DNAJB8^{H31Q} after cellular treatment with 500 μM sodium meta arsenite ($NaAsO_2$) for 15 min. Seven peptides in the PDHA1 and PDHB proteins have increased susceptibility to proteinase K after this arsenite treatment (**Figure S9C**). The evidence of protein misfolding for both these proteins by AP-MS and LiP prompted further investigation of understanding the effects of arsenite on the Pyruvate Dehydrogenase Complex (PDC), particularly understanding the role of a destabilized E1 subunit. PDC consists of an icosahedral core of E2 subunits peripherally decorated with E1 and E3 subunits. Two PDHB and two PDHA1 proteins comprise each heterotetrameric E1 subunit, which decarboxylates pyruvate to acetylate a lipoamide cofactor[41]. The lipoamide cofactor is covalently bound to the core E2 subunit, which consists of several dozen copies of DLAT along with regulatory proteins. DLAT catalyzes transfer of the acetyl group from S-13 lipoamide to synthesize acetyl-CoA, the primary feedstock for cellular respiration. Destabilization of E1 activity is consistent with impaired PDC activity and consequently impaired mitochondrial ATP production, a major consequence of cellular arsenic exposure[60]. Direct arsenite binding to lipoamide could affect E1 stability if it impaired lipoamide interactions with the E1 active site[61]. However, we did not see any change in PK susceptibility near the lipoamide binding site of E1 (**Figure S9C**). An alternative mechanism for E1 misfolding is that arsenite treatment affects the salt bridges that bind

E1 to the peripheral subunit binding domain (PSBD) of E2[62].

The peptide located at the C-terminus of PDHB, which participates in PSBD binding, is more sensitive to Proteinase K after arsenite treatment (**Figure S9C**). Loss of interaction at the PSBD domain could lead to DLAT dissociating from the E1 subunit as a result of arsenite treatment, the PDC. We evaluated PDC stability by co-IP of E2 with E1[63]. ^{Flag}PDHA1 was overexpressed in HEK293T cells, which were then treated with either arsenite (500 μM for 15 min) or with water (control), lysed, and immunoprecipated with anti-Flag beads. Eluates were analyzed by SDS-PAGE and immunoblotting. Crosslinking with 1 mM DSP crosslinking following cell harvest provided optimal recovery of PDHB and DLAT (**Figure S10**). No significant differences in DLAT binding to E1 were observed (**Figures S11 and S13**). Literature reports achieve stoichiometric inhibition of purified pyruvate dehydrogenase with lower concentrations of trivalent arsenite and longer times[64]. We treated HEK293T cells overexpressing ^{Flag}PDHA1 with 2 μM arsenic for four hours. No discernable differences were seen in DLAT binding (**Figures S12 and S14**). Hence, even though the E1 complex is destabilized by arsenite exposure, the destabilization does not induce complex disassembly.

2.7 Conclusion

In conclusion, we have developed a platform to identify proteins that are destabilized in response to cellular stress. The DNAJB8^{H31Q} immunoprecipitation assay identifies destabilized proteins using the same criterion as the cell: increased binding to a chaperone. Identification of likely destabilized proteins in the screening step enables

targeted LiP-PRM as a mechanistically orthogonal, and technically straightforward, validation step. Using this technology, we identified proteins that are destabilized by just a brief 15 min. cellular arsenite exposure. Most of these proteins are known to be functionally perturbed by arsenite, with changes in post-translational modifications and even aggregation. However, it has not previously been demonstrated that these proteins are destabilized, nor that arsenite can induce conformational changes inside living cells within 15 min. of treatment. Furthermore, we have found that arsenite destabilizes both members of the E1 subunit of PDC. This platform will be useful in further understanding how environmental toxins and toxicants perturb proteome integrity.

DNAJB8 is localized to the nucleus and cytosol[65], consistent with the lack of genetically encoded localization sequences, suggesting that this approach might be limited to those two environments. Nevertheless, 13% and 1% of high-confidence DNAJB8^{H31Q} interactors are mitochondrial and secretory proteins respectively[22]. Given the high affinity of DNAJB8^{H31Q} for its clients, it is possible that the protein can engage substrates after lysis. If this is the case, then DNAJB8^{H31Q} could be used to profile across cellular environments, and suggests that cellular expression of DNAJB8^{H31Q} may be dispensable for the assay. Alternatively, another way to assay for protein misfolding in the ER may be to append the distinctive C-terminus of DNJAB8 onto the native ER Hsp40 DNAJB11, with the H53Q mutation to block handoff to the ER Hsp70 BiP. Similarly to DNAJB8, secreted DNAJB11 has irreversible client binding in the absence of Hsp70[66]. Mammalian mitochondria do not have Type II (DNAJB) Hsp40 chaperones[13]. For that environment, it would be necessary to evaluate whether DNAJB8^{H31Q} with mitochondrial

matrix or IMS localization sequences a) perturb mitochondrial proteostasis and b) are able to reach, fold, and function in those environments. Further investigation will establish what fraction of the proteome can be assayed by this approach.

2.8 Supplementary Figures

2.8.1 Limited Proteolysis Scheme:

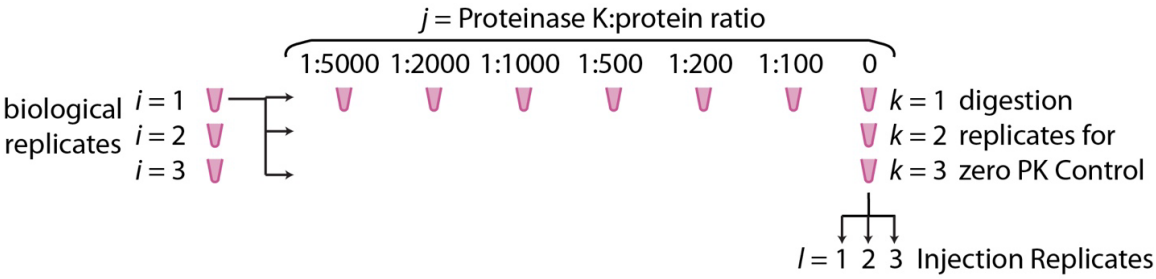

$$\text{fraction remaining } (i) = \frac{\frac{1}{3}\sum_{l=1}^{3}(I_{i,l})}{\frac{1}{9}\sum_{k=1}^{3}\sum_{l=1}^{3}(I_{i,0,k,l})}$$

Figure S1: Sample set-up for limited proteolysis experiments.

2.8.2 Western Blot Analysis of HSR Induction by Arsenite:

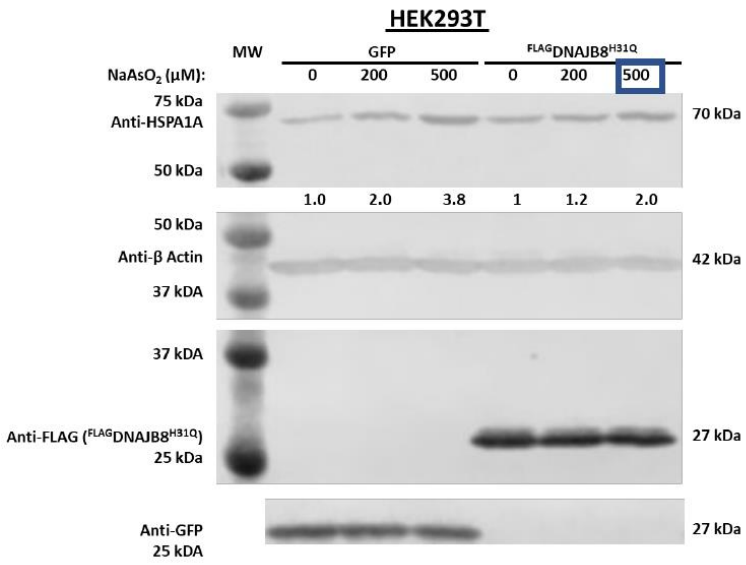

Figure S2: Western Blot analysis of HSR induction by arsenite on HEK293T Cells. Cells were treated for 15 min. with the indicated concentration of $NaAsO_2$ and then allowed to recover for 16 h to allow for accumulation of stress-induced proteins. 500 μM $NaAsO_2$ was chosen for AP-MS experiments and limited proteolysis experiments. Predicted weights for antibodies are shown on the right. Numerical values below Anti-HSPA1A slice are band intensities normalized to the 0 μM condition. Antibody for GFP is shown on 800 channel only.

2.8.3 Comparison between Replicates (Arsenite):

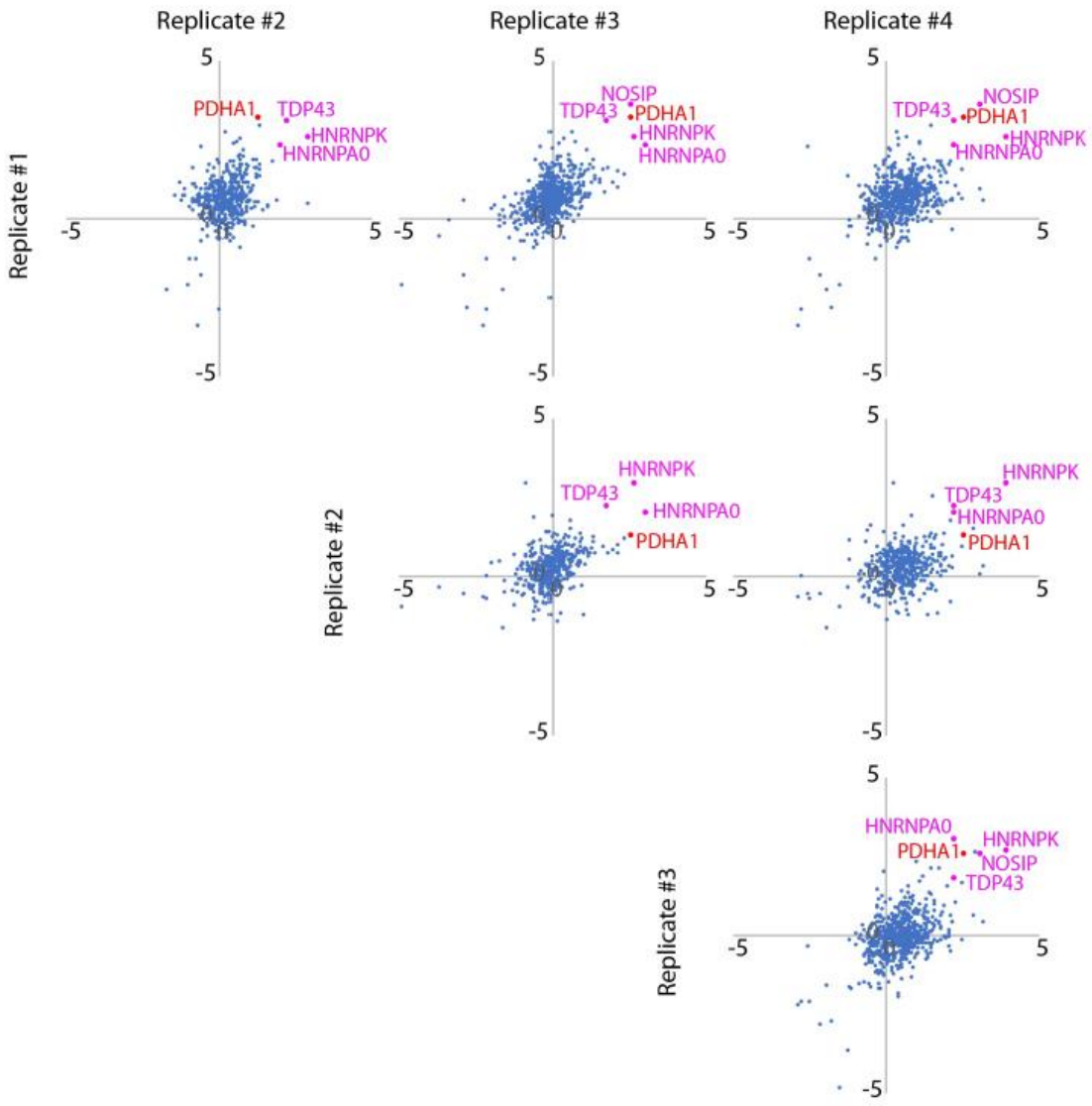

Figure S3: Strictly Standardized Mean Differences of individual TMT-AP-MS experiments involving cellular treatment by arsenite (500 μM, 15 minutes). Each plot compares separate runs (each run includes three arsenite-treated biological replicates and three vehicle-treated biological replicates) and includes fold changes that reflect the ratios between DNAJB8-normalized integrated TMT reporter ion intensities for the control (vehicle) and arsenite-treated cells. TDP43 and PDHA1 are labeled as pink and red and consistently increase in affinity to DNAJB8^{H31Q} after arsenite treatment.

2.8.4 Representative Silver Stain for an Arsenite AP-MS:

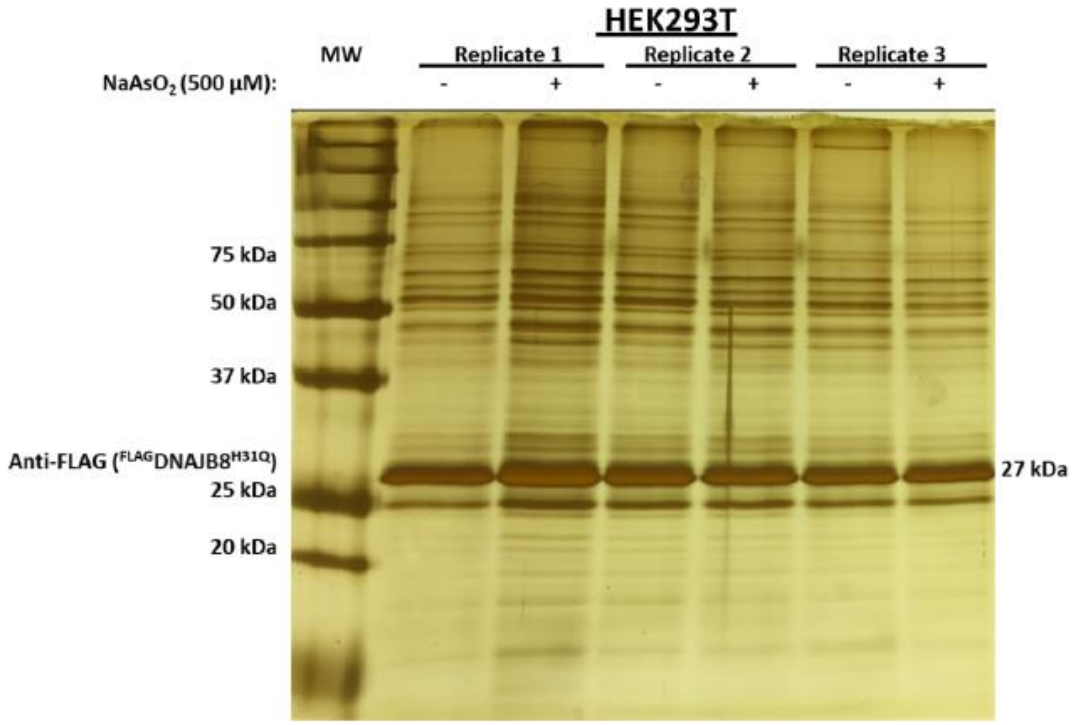

Figure S4: Representative Silver Stain for an Arsenite AP-MS. Each replicate contained two transfected ^{FLAG}DNAJB8^{H31Q} 10 cm plates treated with either 500 µM $NaAsO_2$ or water (control). Three replicates are stained to show bait and visually show differences in prey after each respective pulldown. ^{Flag}DNAJB8^{H31Q} is the most abundant protein in each replicate after the immunoprecipitation. Other bands represent proteins recovered with DNAJB8.

2.8.5 Western Blot Analysis for HSR induction by Cadmium:

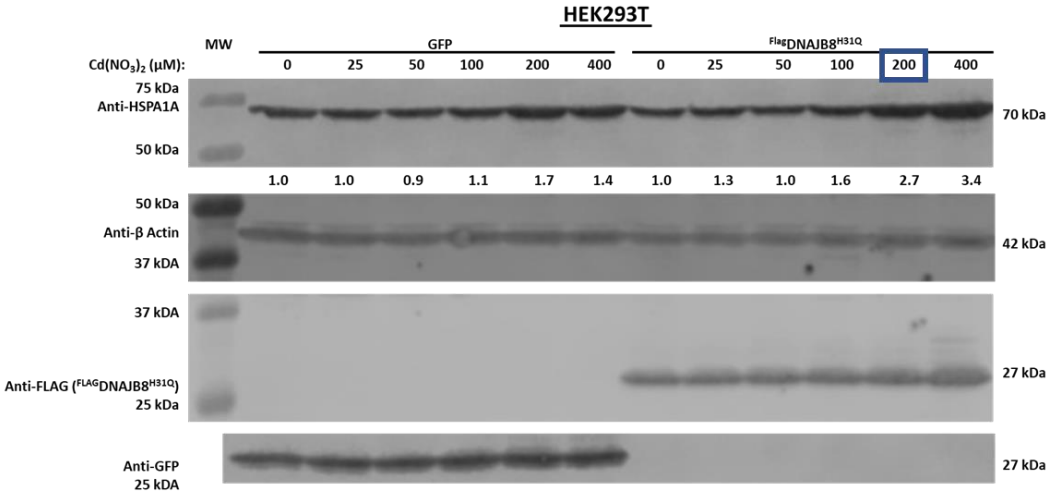

Figure S5: Western Blot analysis of HSR induction by cadmium on HEK293T Cells. Cells were treated for 15 min. with the indicated concentration of $Cd(NO3)_2$ and then allowed to recover for 16 h to allow for accumulation of stress-induced proteins. 200 μM $Cd(NO3)_2$ was chosen for AP-MS Experiments. Predicted weights for antibodies are shown on the right. Numerical values below Anti-HSPA1A slice are band intensities normalized to the 0 μM Cd condition. Antibody for GFP is shown on 800 channel only.

2.8.6 Representative Silver Stain for a Cadmium AP-MS:

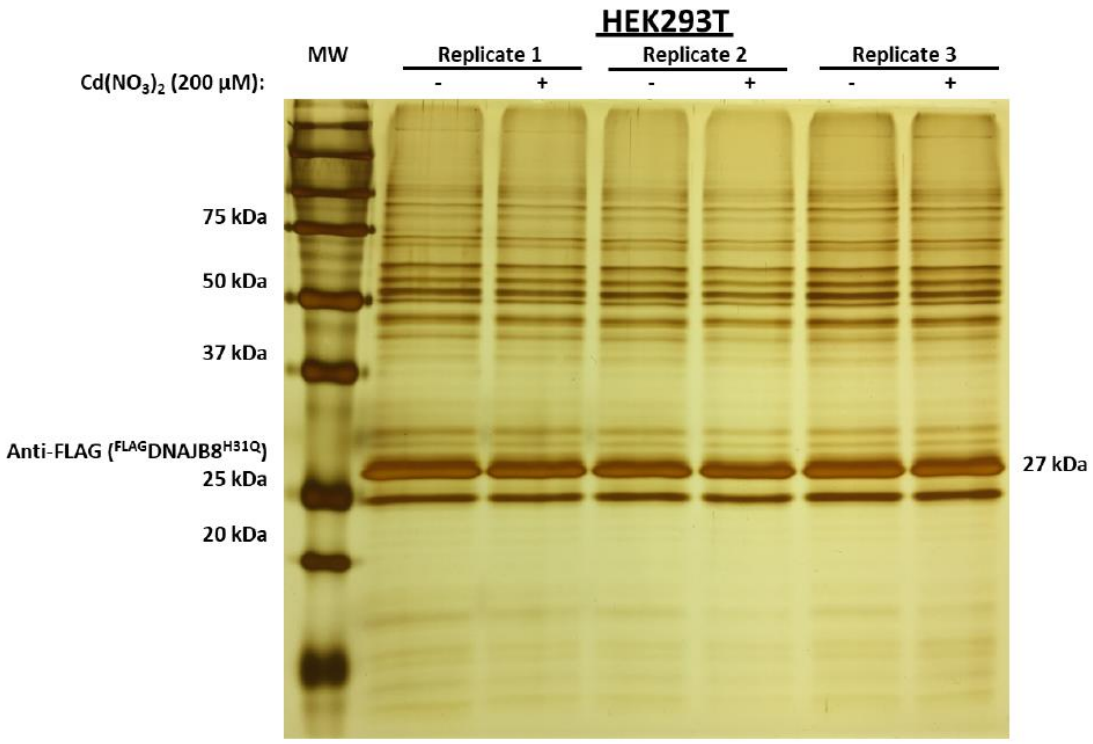

Figure S6: Representative Silver Stain for a Cadmium AP-MS. Each replicate contained two transfected ^{FLAG}DNAJB8^{H31Q} 10cm plates treated with either 200 µM $Cd(NO_3)_2$ or water (control). Three replicates are stained to show bait and visually show differences in prey after each respective pulldown. ^{Flag}DNAJB8^{H31Q} is the most abundant protein in each replicate after the immunoprecipitation. Other bands represent proteins recovered with DNAJB8.

2.8.7 Comparisons between Replicates (Cadmium):

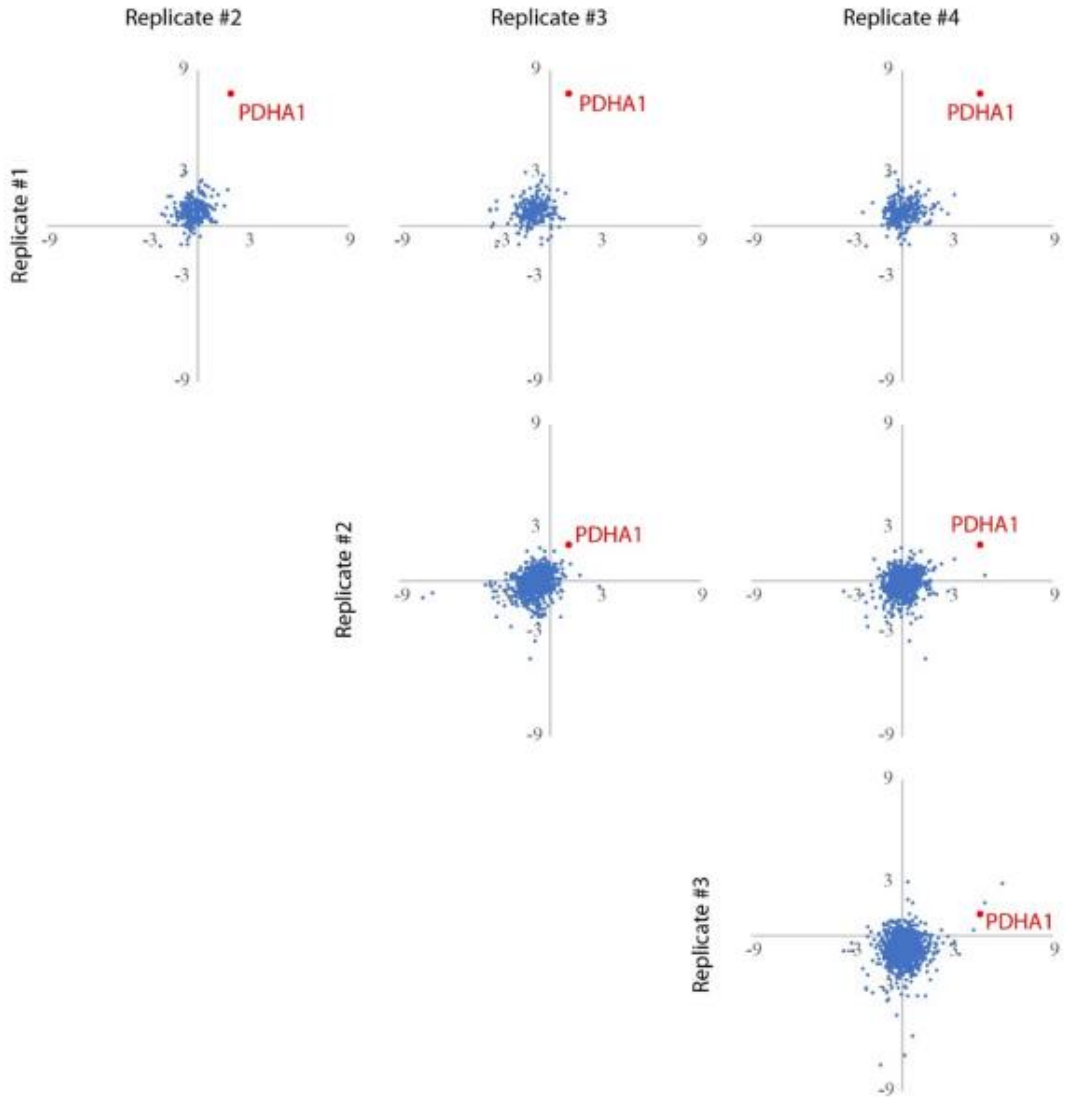

Figure S7: Strictly Standardized Mean Differences of individual TMT-AP-MS experiments involving cellular treatment by cadmium (200 µM, 15 minutes). Each plot compares separate runs (each run includes three cadmium-treated biological replicates and three vehicle-treated biological replicates) and includes fold changes that reflect the ratios between DNAJB8-normalized integrated TMT reporter ion intensities for the control (vehicle) and cadmium-treated cells. PDHA1 is labeled as red and consistently increase in affinity to DNAJB8H^{31Q} after cadmium treatment.

2.8.8 Coomassie Stain of Proteinase K Optimization:

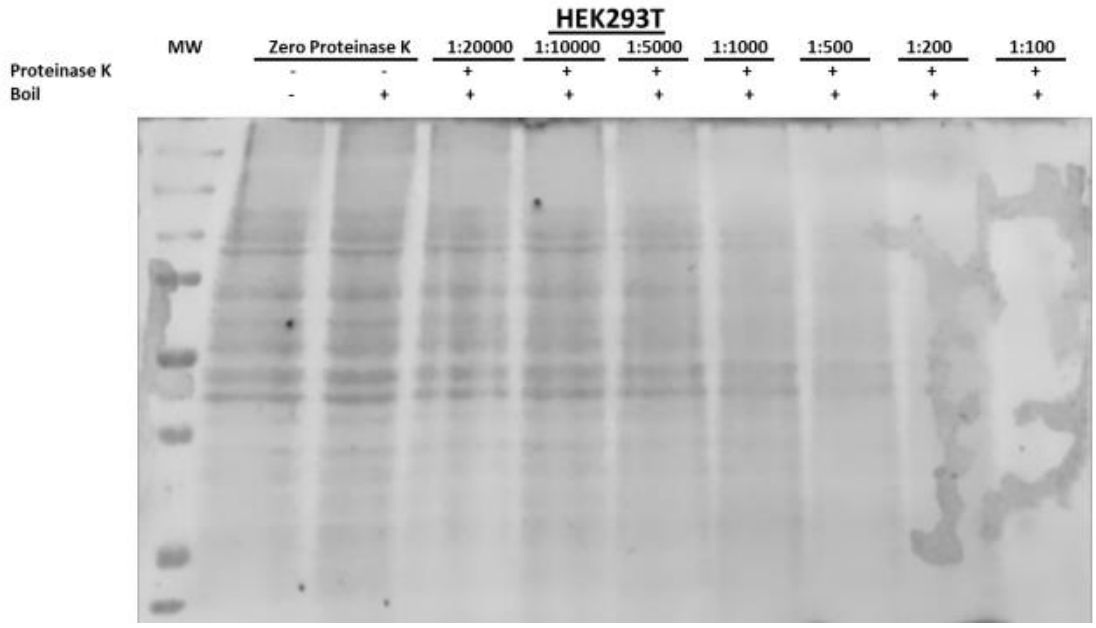

Figure S8: Coomassie Stain of Proteinase K Optimization. Each lane represents a different Proteinase K to Protein ratios. Samples of lysates were incubated with an amount of proteinase K for 1 minute at 25 degrees and then boiled for 5 minutes. Protein bands are no longer visible in the 1:100 Proteinase K: Protein sample. 25 μg of each lysate was used.

2.8.9 Proteinase K Susceptibility Curves for 13 peptides:

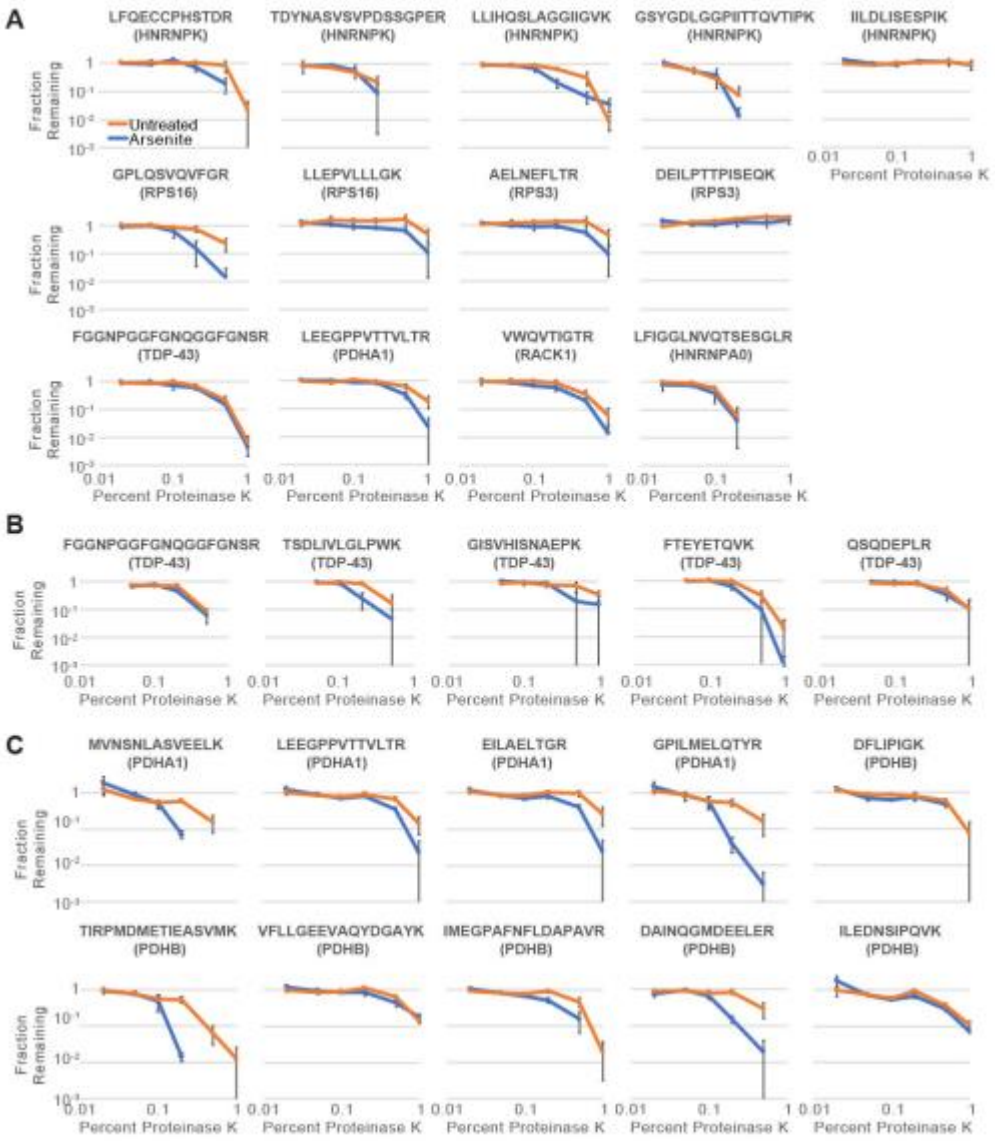

Figure S9: A) Proteinase K susceptibility curves for 13 peptides for several protein targets from the Hsp40 affinity assay. B) Proteinase K susceptibility curves for TDP-43 peptides. C) Proteinase K susceptibility curves for PDHA1 and PDHB peptides. Samples from untreated cells are in orange and samples from arsenite-treated cells are in blue (500 µM, 15 min). (n = 3 biological replicates). LC-PRM runs were performed in technical triplicate for set A,B and averaged. Error bars represents standard error across biological replicates. Representative chromatographic traces from Skyline are presented in the appendix.

2.8.10 DSP Crosslinking for Pulldown of E1 and E2 Subunit:

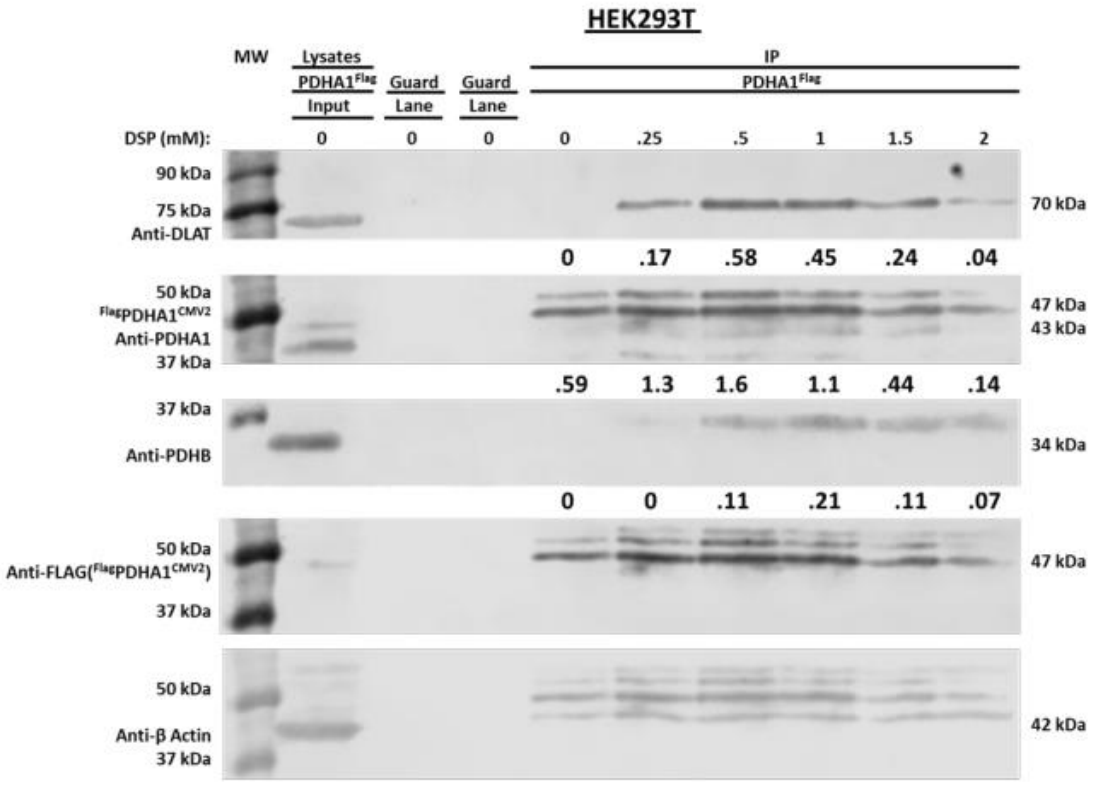

Figure S10: Western Blot Analysis for effects of DSP crosslinking on pulldown of E1 and E2 subunit. 1 mM of DSP crosslinker was chosen as conditions for the immunoprecipitation of ^{Flag}PDHA1. Transfected HEK293T cells were incubated with DSP crosslinking during cell harvest. Predicted weights are shown on the right. Numerical values shown below Anti-DLAT slice, Anti-PDHA1 and Anti-PDHB are densitometric intensities determined using Li-COR Biosciences Image Studio.

2.8.11 Shorter Treatment of Arsenite on E1 Subunit:

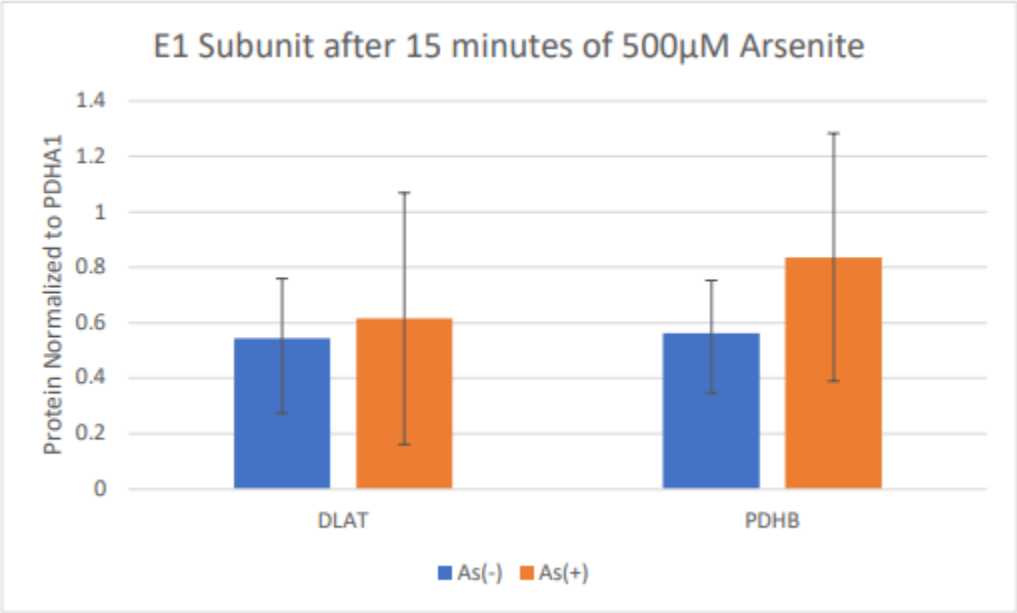

Figure S11: 15 minutes of 500 µM $NaAsO_2$ did not show evidence of E1 dissociating from E2 subunit. HEK293T cells transfected with ^{Flag}PDHA1 were treated with 500 µM of arsenite for 15 minutes prior to lysis. Protein eluates obtained after immunoprecipitation of ^{Flag}PDHA1 were blotted on SDS-Page gels. Band intensities of PDHB and DLAT were normalized to ^{Flag}PDHA1 (bait). Average of normalized PDHB and DLAT among all four replicates are shown above. No significant changes in amount of DLAT binding and PDHB binding to ^{Flag}PDHA1 after arsenite treatment was observed (from n = 4 biological replicates). Error bars represent standard deviation. A representative Western blot is shown in **Figure S13**.

2.8.12 Longer Treatment of Arsenite on E1 Subunit:

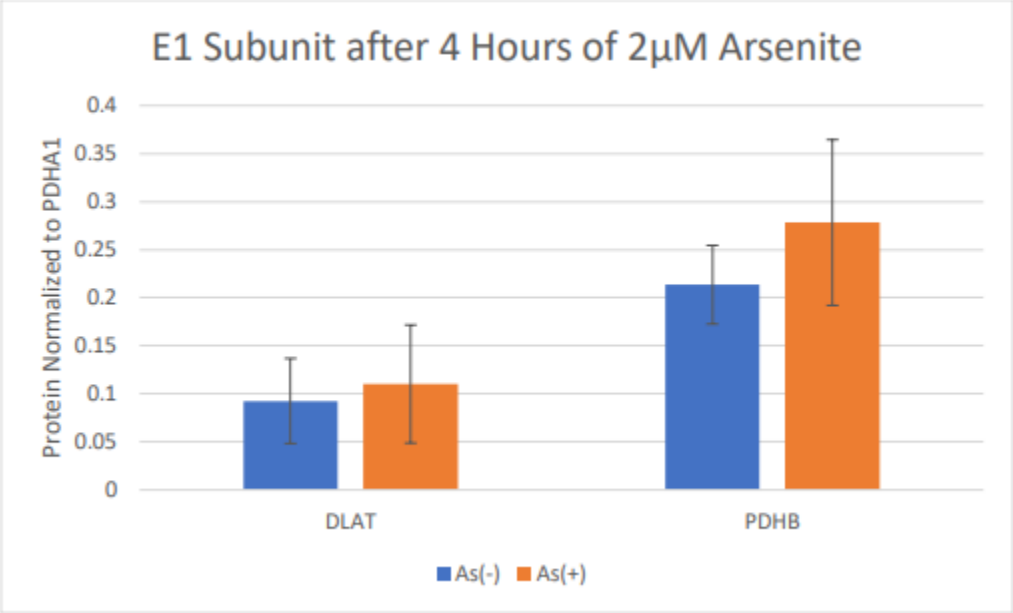

Figure S12: 4 hours of 2 µM $NaAsO_2$ did not lead to DLAT dissociating from E2 subunit. HEK293T cells transfected with ^{Flag}PDHA1 were treated with 2µM of arsenite for 4 hours prior to lysis. Protein eluates obtained after immunoprecipitation of ^{Flag}PDHA1 were blotted on SDS-Page gels. Band intensities of PDHB and DLAT were normalized to ^{Flag}PDHA1 (bait). Average of normalized PDHB and DLAT among all four replicates are shown above. No significant change in amount of DLAT binding and PDHB binding to ^{Flag}PDHA1 after arsenite treatment was observed (from n = 4 biological replicates). A representative Western blot is shown in **Figure S14.**

2.8.13 Representative Western Blot of E1 Subunit After Short Term Exposure of Arsenite:

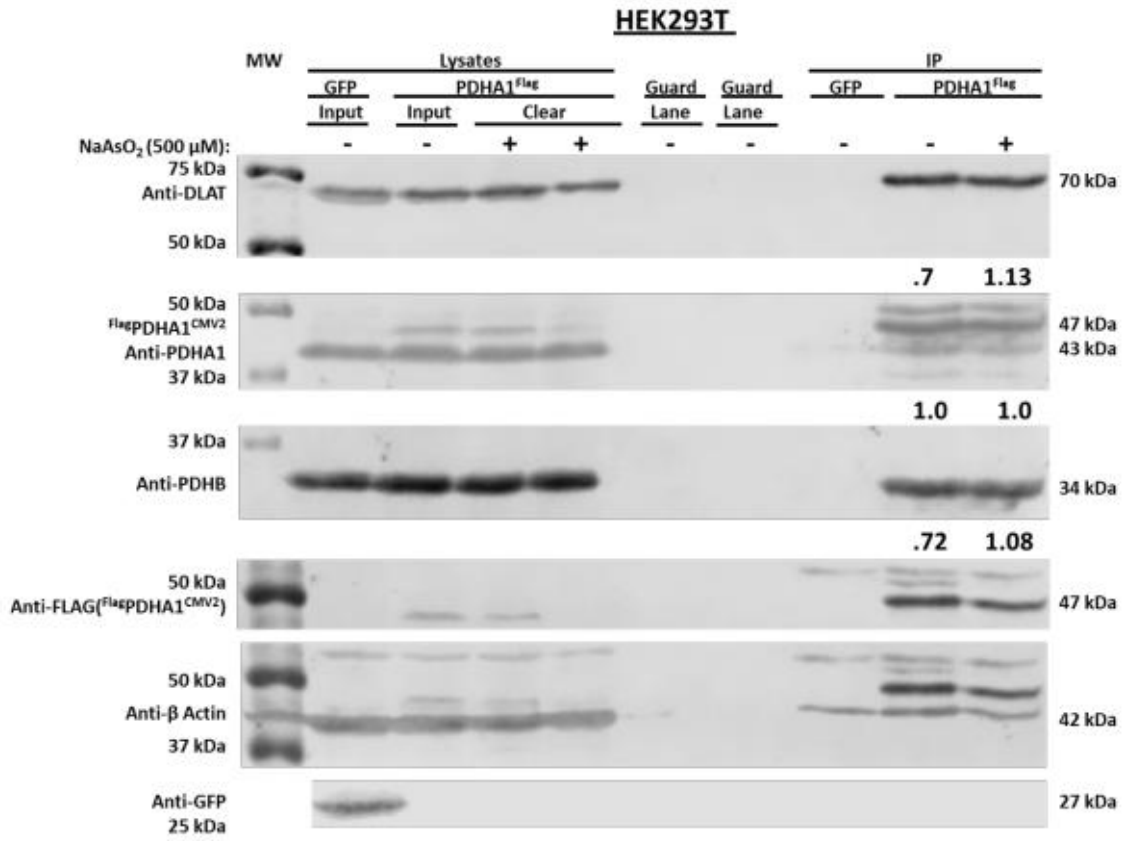

Figure S13: Representative western blot analysis for the effects of Arsenite on E1 and E2 subunit interaction after 15 minutes of treatment. One of four biological replicates is shown above. Transfected HEK293T cells were incubated with 500 µM $NaAsO_2$ for 15 minutes at 37 ^oC. Predicted weights for antibodies are shown on the right. Numerical values below Anti-DLAT, Anti-PDHA1, and Anti-PDHB slice are band intensities normalized to the intensity of PDHA1. Antibody for GFP is shown on 800 channel only.

2.8.14 Representative Western Blot of E1 Subunit after Longer Term Exposure of Arsenite:

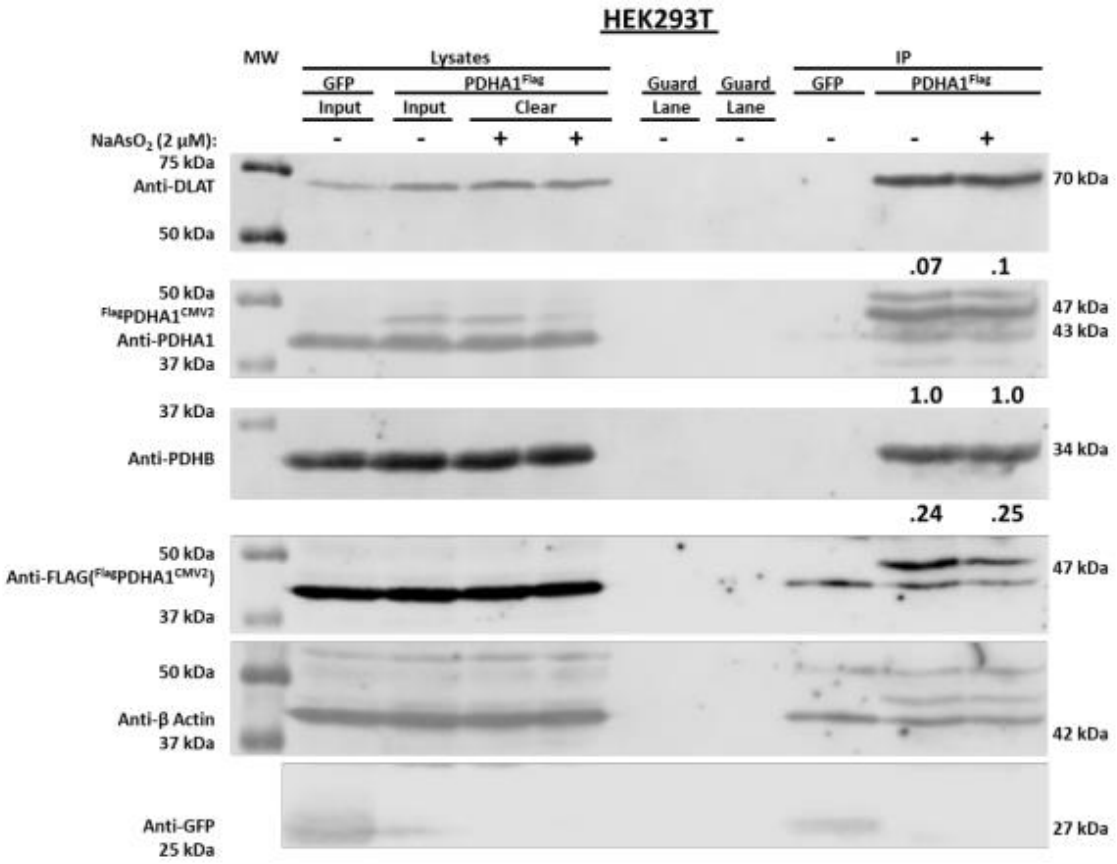

Figure S14: Representative Western Blot analysis for Arsenite effects on E1 and E2 subunit interaction after 4 hours of treatment. One of four replicates is shown above. Transfected HEK293T cells were incubated with 2 µM $NaAsO_2$ for 4 hours at 37 ºC. Predicted weights for antibodies are shown on the right. Numerical values below Anti-DLAT, Anti-PDHA1, and Anti-PDHB slice are band intensities normalized to the intensity of PDHA1. Antibody for GFP is shown on 800 channel only.

2.9 Supplementary Tables

2.9.1 Discussed DNAJB8^{H31Q} Interactors after Arsenite Treatment:

Gene	Combined ttest	Combined Fold Change	Combined Standard Deviation	log2 Combined Fold Change	-log p	rank	qvalue BH	qvalue Storey
HNRNPA0	2.376E-07	1.532560767	0.3057577	0.615944279	6.624173381	1	0.000223542	0.000181496
TARDBP	3.306E-07	1.856480195	0.611885159	0.892569925	6.480683642	2	0.000223542	0.000181496
PDHA1	4.117E-07	1.532073505	0.392878489	0.615485516	6.385440406	3	0.000223542	0.000181496
ZC3HC1	6.65E-07	0.761709492	0.116884352	-0.39268722	6.17720811	4	0.000253805	0.000206067
NOSIP	9.934E-07	3.209436598	1.862628714	1.682320061	6.002866111	5	0.000253805	0.000206067
HNRNPK	1.031E-06	1.908154498	0.546558031	0.932177987	5.986717893	6	0.000253805	0.000206067
SLC25A22	1.091E-06	0.683525497	0.134720053	-0.54893294	5.962322138	7	0.000253805	0.000206067
SLC25A3	1.754E-06	0.718746303	0.141645515	-0.476445465	5.755973914	8	0.000357155	0.000289978
CSDE1	3.222E-05	1.406375029	0.303212008	0.491981359	4.491881807	11	0.004771408	0.00387395
RACK1	4.021E-05	1.47464333	0.427561716	0.560366054	4.395659069	12	0.005431259	0.004409689
MRPS28	6.715E-05	1.994526171	0.423437827	0.996046054	4.172963379	15	0.007292332	0.005920711
ZNF24	0.0001124	1.976062976	0.835514811	0.982628925	3.949245346	18	0.010171927	0.00825868
RPS16	0.0007735	1.490484747	0.551311906	0.575781612	3.111514467	29	0.043451885	0.03527898
PDHB	0.0013142	1.258895988	0.275151804	0.33215909	2.881330414	32	0.066902245	0.05431854
RPS3	0.0066123	1.247714713	0.331145394	0.319288103	2.179647614	59	0.181159084	0.147084704
ETFA	0.0495394	1.16596745	0.25575923	0.221527514	1.305048822	193	0.355649274	0.288754872
G3BP1	0.275813	1.139492507	0.322270843	0.188391438	0.559385275	639	0.507720998	0.412223285
EIF4G1	0.3256408	1.140379939	0.494227063	0.189514565	0.487261137	745	0.594925666	0.483025546
DLAT	0.6163627	0.931542083	0.478576935	-0.10230715	0.210163641	1192	0.649791105	0.527571294

Table S1: DNAJB8^{H13Q} Interactors after Arsenite Treatment. Selected Proteins interacting with DNAJB8^{H31Q} after arsenite treatment are highlighted. The complete comprehensive list and definitions is available online in the supporting information[67].

2.9.2 Discussed DNAJB8^{H31Q} Interactors after Cadmium Treatment:

Gene	Combined ttest	Combined Fold Change	Combined Standard Deviation	log2 Combined Fold Change	-log p	rank	qvalue BH	qvalue Storey
RPL36AL	4.253E-07	0.528724394	0.186831097	-0.919412205	6.371314365	1	0.000692798	0.000544567
PDHA1	3.186E-06	1.576998155	0.442093297	0.657180972	5.496752193	2	0.002589081	0.00203512
RPL36A	4.768E-06	0.372275506	0.174620891	-1.4255574	5.321654142	3	0.002589081	0.00203512
BAZ1B	0.000205	1.53221753	0.102450877	0.615621132	3.688293897	8	0.041738535	0.032808135

Table S2: DNAJB8^{H13Q} Interactors after Cadmium Treatment. Selected Proteins from DNAJB8^{H31Q} are shown. The complete comprehensive list and definitions is available online in the supporting information[67].

2.9.3 Coefficient of Variance of Ten Technical Replicates at 7500 Resolution:

Protein Gene	Peptide Sequence	Precursor Mass m/z	Activation Energy	Retention Time Average	Avg. Intensity	CV	Avg. Intensity Normalized	CV Normalized
PDHA1	LEEGPPVTTVLTR	706.3932	35	42.1	7.24E+03	10.4	1.1	14.2
TARDBP	FGGNPGGFGNQGGFGNSR	863.8877	35	37.6	7.67E+03	11.7	1.2	18.3
RACK1	VWQVTIGTR	530.3009	35	41.8	4.41E+03	32	0.7	19.8
HNRNPA0	LFIGGLNVQTSESGLR	845.9598	35	54.4	5.19E+03	17.4	0.8	8.3
RPS16	GPLQSVQVFGR	594.3302	35	46	1.96E+04	16	3	9.7
RPS16	LLEPVLLLGK	547.8628	35	62	1.75E+04	36.5	2.6	30.1
HNRNPK	LFQECCPHSTDR	517.2223	35	45	4.41E+03	14.6	0.7	11.4
HNRNPK	TDYNASVSVPDSSGPER	890.9028	35	30.3	6.92E+04	34.9	10.8	32.3
HNRNPK	LLIHQSLAGGIIGVK	759.972	35	48.3	1.96E+04	14.9	3.1	16.5
HNRNPK	GSYGDLGGPIITTQVTIPK	959.02	35	53.2	4.81E+04	14	7.5	10.9
HNRNPK	IILDLISESPIK	670.9054	35	62.4	7.45E+04	19.9	11.5	11.5
RPS3	AELNEFLTR	546.7878	35	44.8	5.99E+03	23.6	0.9	10.8
RPS3	DEILPTTPISEQK	735.888	35	39.1	8.91E+03	13.7	1.4	16.6
Int. STD	VFFAEDVGSNK	606.7987	35	39.4	6.53E+03	19.9	1	0
					Median CV	16.7	**Median Norm CV**	14.2
					Average CV	20	**Average Norm CV**	15

Table S3: Coefficient of Variance (CV) of Ten Technical Replicates at 7500 Resolution. Calculated CV of targeted peptides are shown. Definitions can be found online in the supporting information[67].

Protein Gene	Peptide Sequence	Precursor Mass m/z	Activation Energy	Retention Time Average	CV Zero PK controls #1 (No As) Norm.	CV Zero PK controls #2 (No As) Norm.	CV Zero PK controls #3 (No As) Norm.		CV Zero PK controls #1 (As) Norm.	CV Zero PK controls #2 (As) Norm.	CV Zero PK controls #3 (As) Norm.
PDHA1	LEEGPPVTTVLTR	706.3932	35	40.9	14.25	8.11	9.14		14.25	8.11	9.14
TARDBP	FGGNPGGFGNQGGFGNSR	863.88767	35	35.5	11.86	13.57	3.72		20.27	9.5	4.9
RACK1	VWQVTIGTR	530.30092	35	40.2	11.97	9.16	13.85		10.2	3.44	10.74
HNRNPA0	LFIGGLNVQTSESGLR	845.95977	35	55.8	3.07	21.34	3.36		22.5	23.88	6.42
RPS16	GPLQSVQVFGR	594.3302	35	45.3	6.76	12.94	3.45		14.02	15.51	19.2
RPS16	LLEPVLLLGK	547.86282	35	64.6	14.59	17.18	8.82		1.51	23.95	9.31
HNRNPK	LFQECCPHSTDR	517.22226	35	43.7	14.81	14.35	3.3		21.2	11.87	16.07
HNRNPK	TDYNASVSVPDSSGPER	890.90284	35	27	12.18	10.06	4.18		14.98	31.29	4.72
HNRNPK	LLIHQSLAGGIIGVK	759.97195	35	47.9	12.14	8.44	0.79		15.71	13.51	9.84
HNRNPK	GSYGDLGGPIITTQVTIPK	959.02002	35	54.4	13.2	18.76	9.04		17.16	18.44	19.4
HNRNPK	IILDLISESPIK	670.90541	35	65.3	10.91	21.66	11.07		15.35	22.07	6.88
RPS3	AELNEFLTR	546.78784	35	43.6	13.64	14.76	9.41		10.95	12.09	3.86
RPS3	DEILPTTPISEQK	735.88795	35	37.3	6.84	7.07	14.08		19.3	15.21	7.65
Int. STD	VFFAEDVGSNK	606.79868	35	37.3	0	0	0		0	0	0
				Median CV	12.14	13.57	8.82	**Median CV**	15.35	15.21	9.14
				Combined Average Median CV (No As)	11.51			**Combined Average Median CV (As)**	13.23		
				Average CV	11.25	13.65	7.25	**Average CV**	15.18	16.07	9.86
				Combined Average CV (No As)	10.71			**Combined Average CV (As)**	13.7		

Table S4: Coefficient of Variance (CV) between Three Biological Replicates, Initial LiP Screen. CV are calculated among three biological replicates during the initial LiP Experiment. Definitions and more information can be found on supporting information online[67].

2.9.5 Coefficient of Variance after 6 Technical Replicates at 60000 Resolution:

Protein Gene	Peptide Sequence	Precursor Mass m/z	Activation Energy	Retention Time Average	Avg. Intensity	CV	Avg. Intensity Normalized	CV Normalized
HNRNPK	TDYNASVSVPDSSGPER	890.90284	35	29.8	2.23E+05	15.7	25.7	8.4
HNRNPK	GSYGDLGGPIITTQVTIPK	959.02002	35	53.1	1.66E+05	25.5	19.3	30.1
HNRNPK	IILDLISESPIK	670.90541	35	62.2	2.72E+05	13.8	31.4	9.3
Internal Standard	VFFAEDVGSNK	606.79868	35	38.8	9.22E+03	21.1	1	0
					Median CV	18.4	**Median CV**	9.3
					Average CV	19	**Average CV**	15.9

Table S5: Coefficient of Variance (CV) after 6 Technical Replicates at 60000 Resolution. CV of targeted peptides are shown. Definitions can be found on Supporting Information online[67].

Protein Gene	Peptide Sequence	Precursor Mass m/z	Activation Energy	Retention Time Average	CV Zero PK controls #1 (No As) Norm.	CV Zero PK controls #2 (No As) Norm.	CV Zero PK controls #3 (No As) Norm.		CV Zero PK controls #1 (As) Norm.	CV Zero PK controls #2 (As) Norm.	CV Zero PK controls #3 (As) Norm.
TDP43	FGGNPGGFGNQGGFGNSR	863.8877	35	35.68	1.49	20.34	2.62		16.02	24.86	14.38
TDP43	TSDLIVLGLPWK	671.3924	35	44.93	4.99	5.15	3.12		1.7	3.24	7.79
TDP43	GISVHISNAEPK	626.3382	35	39.34	20.2	5.83	8.04		20.46	15.68	12.33
TDP43	FTEYETQVK	572.7797	35	48.08	0.86	0.91	2.09		0.82	3.03	2.31
TDP43	QSQDEPLR	486.7409	35	37.21	25.82	9.44	9.71		18.18	25.69	7.49
				Median CV	4.99	5.83	3.12	**Median CV**	16.02	15.68	7.79
				Combined Average Median CV (No As)	4.65			**Combined Average Median CV (As)**	13.16		
				Average CV	10.67	8.33	5.12	**Average CV**	11.44	14.5	8.86
				Combined Average CV (No As)	8.04			**Combined Average CV (As)**	11.6		

Table S6: Coefficient of Variance (CV) between Three Biological Replicates, TARDBP LiP. CV of targeted peptides are shown. Definitions and more information can be found on Supporting Information online[67].

Protein Gene	Peptide Sequence	Precursor Mass m/z	Activation Energy	Retention Time Average	CV Zero PK controls #1 (No As) Norm.	CV Zero PK controls #2 (No As) Norm.	CV Zero PK controls #3 (No As) Norm.		CV Zero PK controls #1 (As) Norm.	CV Zero PK controls #2 (As) Norm.	CV Zero PK controls #3 (As) Norm.
PDHB	TIRPMDMETIEASVMK	926.4543	35	59.2	12.6	9.9	9.9		14.9	3.9	10.4
PDHB	VFLLGEEVAQYDGAYK	901.454	35	68.5	6.2	10	10.2		3.1	19.5	6.3
PDHB	IMEGPAFNFLDAPAVR	874.4454	35	71.9	9.9	4.6	16.9		8.3	14.5	17.9
PDHB	DAINQGMDEELER	760.3383	35	32.1	9.2	9.5	7.4		11.1	2.4	9.1
PDHB	ILEDNSIPQVK	628.3482	35	48.7	7.4	3.2	5.5		8.9	4.7	4.1
PDHB	DFLIPIGK	451.7709	35	55.5	14.2	10.1	2.9		29.8	12.8	9.8
PDHA1	MVNSNLASVEELK	717.3688	35	38.1	2.4	10.5	10.9		1.8	10	5.3
PDHA1	LEEGPPVTTVLTR	706.3932	35	38.9	3.1	7.2	18.9		4.2	3	6
PDHA1	EILAELTGR	501.2849	35	43.3	14.9	21	3.7		19.3	15.7	6.6
PDHA1	GPILMELQTYR	660.8526	35	57.2	2.6	9	4.5		5.2	11.6	13.5
Int. STD	VFFAEDVGSNK	606.7987	35	35	0	0	0		0	0	0
				Median CV	8.3	9.7	8.65	**Median CV**	8.6	10.8	7.85
				Combined Average Median CV (No As)	8.88			**Combined Average Median CV (As)**	9.08		
				Average CV	8.3	9.5	9.1	**Average CV**	10.7	9.8	8.9
				Combined Average CV (No As)	8.9			**Combined Average CV (As)**	9.8		

Table S7: Coefficient of Variance (CV) between Three Biological Replicates, E1 Subunit LiP. CV of targeted peptides are shown. Definitions and more information can be found on Supporting Information online[67].

2.9.8 Measurement of Significance in Proteolytic Susceptibility Curves:

Protein Gene	Peptide Sequence	Precursor Mass m/z	Experiment	P value
PDHA1	LEEGPPVTTVLTR	706.3932	Initial LiP Screen	0.29
TARDBP	FGGNPGGFGNQGGFGNSR	863.88767	Initial LiP Screen	0.15
RACK1	VWQVTIGTR	530.30092	Initial LiP Screen	0.19
HNRNPA0	LFIGGLNVQTSESGLR	845.95977	Initial LiP Screen	0.17
RPS16	GPLQSVQVFGR	594.3302	Initial LiP Screen	0.05
RPS16	LLEPVLLLGK	547.86282	Initial LiP Screen	0.09
HNRNPK	LFQECCPHSTDR	517.22226	Initial LiP Screen	0.31
HNRNPK	TDYNASVSVPDSSGPER	890.90284	Initial LiP Screen	0.42
HNRNPK	LLIHQSLAGGIIGVK	759.97195	Initial LiP Screen	0.04
HNRNPK	GSYGDLGGPIITTQVTIPK	959.02002	Initial LiP Screen	0.31
HNRNPK	IILDLISESPIK	670.90541	Initial LiP Screen	0.48
RPS3	AELNEFLTR	546.78784	Initial LiP Screen	0.13
RPS3	DEILPTTPISEQK	735.88795	Initial LiP Screen	0.25
TDP43	FGGNPGGFGNQGGFGNSR	863.8877	TDP43 LiP	0.27
TDP43	TSDLIVLGLPWK	671.3924	TDP43 LiP	0.10
TDP43	GISVHISNAEPK	626.3382	TDP43 LiP	0.27
TDP43	FTEYETQVK	572.7797	TDP43 LiP	0.06
TDP43	QSQDEPLR	486.7409	TDP43 LiP	0.44
PDHB	TIRPMDMETIEASVMK	926.4543	E1 LiP	0.08
PDHB	VFLLGEEVAQYDGAYK	901.454	E1 LiP	0.32
PDHB	IMEGPAFNFLDAPAVR	874.4454	E1 LiP	0.08
PDHB	DAINQGMDEELER	760.3383	E1 LiP	0.06
PDHB	ILEDNSIPQVK	628.3482	E1 LiP	0.28
PDHB	DFLIPIGK	451.7709	E1 LiP	0.17
PDHA1	MVNSNLASVEELK	717.3688	E1 LiP	0.46
PDHA1	LEEGPPVTTVLTR	706.3932	E1 LiP	0.23
PDHA1	EILAELTGR	501.2849	E1 LiP	0.14
PDHA1	GPILMELQTYR	660.8526	E1 LiP	0.28

Table S8: Measurement of Significance of all Proteolytic Susceptibility curves from all LiP experiments. P values are calculated by comparing the area under each proteolytic susceptibility curve among each condition.

References

[1]Tamás, M.; Sharma, S.;, Jacobsen, T.;, Christen, P. Heavy Metals and Metalloids As a Cause for Protein Misfolding and Aggregation. *Biomolecules*. **2014**, *4*, 252-267.

[2]Petrov, D.;, Zagrovic, B.;. Microscopic Analysis of Protein Oxidative Damage: Effect of Carbonylation on Structure, Dynamics, and Aggregability of Villin Headpiece. *J. Am. Chem. Soc*. **2011**, *133*, 7016-7024.

[3]Shen, S.; Li, X.;, Cullen, W. R.; Weinfield, M.; Lee, X. C. Arsenic Binding to Proteins. *Chem. Rev*. **2013**, *113*, 7769-7792.

[4]Alford, B. D.;, Brandman, O. Quantification of Hsp90 availability reveals differential coupling to the heat shock response. *J. Cell. Biol.* **2018**, *217*, 3809-3816.

[5]Kaur, U.;, Meng, H.;, Lui, F.; Ma, R.;, Ogburn, R. N.; Johnson, J. H. R.; Fitzgerald, M. C.; Jones, M. L.. Proteome-Wide Structural Biology: An Emerging Field for the Structural Analysis of Proteins on the Proteomic Scale. *J. Proteome Res.* **2018**, *17*, 3614-3627.

[6]Genereux, J. C.; Mass spectrometric approaches for profiling protein folding and stability. *Adv Protein Chem Struct Biol.*, **2019**, *118*, 111-144.

[7]Adhikari, J.; West, G. M.; Fitzgerald, M. C.. Global Analysis of Protein Folding Thermodynamics for Disease State Characterization. *J. Proteome Res*. **2015**, *14*, 2287-2297.

[8]Zhang, T.; Wolfe, C.; Pierle, A.; Welle, K. A.; Hryhoernko, J. R.; Ghaemmaghami, S.. Proteome-wide modulation of degradation dynamics in response to growth arrest *PNAS*, **2017**, *114*, DOI: 10.1073/pnas.1710238114.

[9]Chea, E. E.; Jones, L. M. Modifications generated by fast photochemical oxidation of proteins reflect the native conformations of proteins. *Protein Sci.*, **2018**, *27*, 1047-1056.

[10]Leuenberger, P.; Ganscha, S.; Kahraman, A.; Cappelletti, V.; Boersema, P. J.; Von Mering, C.; Classen, M.; Picotti, P.. Cell-wide analysis of protein thermal unfolding reveals determinants of thermostability. *Science* **2017**, 355.

[11]Bamberger, C.; Pankow, S.; Martínez-Bartolomé, S.; Ma, M.; Diedrich, J.; Rissman, R. A.; Yates, J. R.;. Protein Footprinting via Covalent Protein Painting Reveals Structural Changes of the Proteome in Alzheimer's Disease. *J. Proteome Res.* **2021**, DOI 10.1021/acs.jproteome.0c00912.

[12]Savitski, M. M.; Reinhard, F. B. M.; Franken, H.; Werner, T.; Savitski, M. F.;

Eberhard, D.;, Molina, D. M.; afari, R.; Dovega, R. B.; Klaeger, S.; Kuster, B.; Nordlund, P.; Bantscheff, M.;, Drewes, G.. Tracking cancer drugs in living cells by thermal profiling of the proteome. *Science* **2014**, *346*, 1255784 DOI: 10.1126/science.1255784.

[13]Kampinga, H. H.; Craig, E. A. The HSP70 chaperone machinery: J proteins as drivers of functional specificity. *Nat. Rev.* **2010**, *11*, 570-592.

[14]Bukau, B.; Weissman, J.; Horwich, A.. Molecular Chaperones and Protein Quality Control. *Cell.* **2006**, *125*, 443-451.

[15]Kim, Y. E.; Hipp, M. S.; Bracher, A.; Hayer-Hartl, M.; Hartl, F. U. Molecular chaperone functions in protein folding and proteostasis *Annu. Rev. Biochem.* **2013**, *82*, 323-355.

[16]Labbadia, J.; Morimoto, R. I. The Biology of Proteostasis in Aging and Disease. *Annu. Rev. Biohem*. **2015**, *84*, 435-464.

[17]Otero, J. H.; Lizak, B.; Feige, M. J.; Hendershot, L. M. Dissection of Structural and Functional Requirements That Underlie the Interaction of ERdj3 Protein with Substrates in the Endoplasmic Reticulum. *J. Biol. Chem*. **2014**, *289*, 27504-27512.

[18]Yamashita, M.; Hirohashi, Y.; Torigoe, T.; Kusumoto, H.; Murai, A.; Imagawa, T.; Sato, N. Dnajb8, a Member of the Heat Shock Protein 40 Family Has a Role in the Tumor Initiation and Resistance to Docetaxel but Is Dispensable for Stress Response. *PLoS One.* **2016**, DOI:10.1371/journal.pone.0146501.

[19]Hageman, J.; Rujano, M. A.; van Waarde, M. A. W. H.; Kakkar, V.; Dirks, R. P.; Govorukhina, N.; Oosterveld-Hut, H. M. J.; Lubsen, N. H.; Kampinga. H. H. A DNAJB Chaperone Subfamily with HDAC-Dependent Activities Suppresses Toxic Protein Aggregation. *Mol. Cell.* **2010**, *37*, 355-369

[20]Kakkar, V.; Månsson, C.; de Mattos, E. P.; Bergink, S.; van der Zwaag, M.; M. van Waarde, M. A. W. H.; Kloosterhuis, N. J.; Melki, R.; van Cruchten, R. T.P.; Al-Karadaghi, S.; Arosio, P.; Dobson, C. M.; Knowles, T. P. J.; Bates, G. P.; van Deursen, J. M.; Linse, S.; van de Sluis, B.; Emanuelsson, C.; Kampinga. H. H. The S/T-Rich Motif in the DNAJB6 Chaperone Delays Polyglutamine Aggregation and the Onset of Disease in a Mouse Model. . *Mol. Cell.* **2016**, *62*, 272-283.

[21]Gillis, J.; Schipper-Krom, S.; Juenemann, K.; Gruber, A.; Coolen, S.; van den Nieuwendijk, R.; van Veen, H.; Overkleeft, H.; Goedhart, J.; Kampinga, H. H.; Reits, E. A. The DNAJB6 and DNAJB8 Protein Chaperones Prevent Intracellular Aggregation of Polyglutamine Peptides. *J. Biol.* **2013**, *288*, 17225-17237.

[22]Mei, L.; Montoya, M. R.; Quanrud, G. M.; Tran, M.; Villa-Sharma, A.; Huang, H.;

Genereux, J. C.. Bait Correlation Improves Interactor Identification by Tandem Mass Tag-Affinity Purification-Mass Spectrometry. *J. Proteome. Res.* **2020**, *19*, 1565-1573.

[23]Naujokas, M. F.; Anderson, B.; Ahsan, H.; Aposhian, H. V.; Graziano, J. H.; Thompson, C.; Suk, W. A.. The broad scope of health effects from chronic arsenic exposure: update on a worldwide public health problem *Environ. Health. Perspect*. **2013**, *121*, 295-302.

[24]Washburn, M. P.; Wolters, D.; Yates, J. R. Large-scale analysis of the yeast proteome by multidimensional protein identification technology. *Nat. Biotechnol*. **2001**, *19*, 242-247.

[25]Kong, A. T.; Leprevost, F. V.; Avtonomov, D. M.; Mellacheruvu, D.; Nesvizhskii, A. I. MSFragger: ultrafast and comprehensive peptide identification in shotgun proteomics. *Nat. Meth.* **2017**, *14*, 513-520.

[26]Plubell, D. L.; Wilmarth, P. A.; Zhao, Y.; Fenton, A. M.; Minnier, J.; Reddy, A. P.; Klimek, J.; Yang, X.; David, L. L.; Pamir, N. Extended Multiplexing of Tandem Mass Tags (TMT) Labeling Reveals Age and High Fat Diet Specific Proteome Changes in Mouse Epididymal Adipose Tissue. *Mol. Cell. Proteomics* **2017**, *16*, 873–890.

[27]Yekutieli, D.; Benjamini.Y.; Resampling-based false discovery rate controlling multiple test procedures for correlated test statistics. *J. Stat. Plan. Inference* **1999**, *82*, 171–196.

[28]Storey, J. D.; Tibshirani. R. Statistical significance for genomewide studies. *Proc. Natl. Acad. Sci.* USA **2003,** *100*, 9440–9445.

[29]Schopper, S.; Kahraman, A.; Leunberger, P.; Feng, Y.; Piazza, I.; Muller, O.; Boersema, P. J.; Picotti, P. Measuring protein structural changes on a proteome-wide scale using limited proteolysis-coupled mass spectrometry. *Nat. Protocol.* **2017**, *1*, 2391-2410.

[30]Maclean, B.; Tomazela, D.M.; Shulman, N.; Chambers, M.; Finney, G.L.; Frewen, B.; Kern, R. Tabb, D.L.; Liebler, D.C.; MacCoss, M.J. Skyline: an open source document editor for creating and analyzing targeted proteomics experiments. *Bioinformatics.* **2010**, 26, 966-968.

[31]Pino, L.K.; Searle, B.C.; Yang, H.Y.; Hoofnagle, A.N.; Noble, W.S.; MacCoss, M.J. Matrix-Matched Calibration Curves for Assessing Analytical Figures of Merit in Quantitative Proteomics. *J. Proteome Res.* **2020**, *19*, 1147–1153.

[32]Guo, R.; Xu D.; Wang. W. Identification and analysis of new proteins involved in the DNA damage response network of Fanconi anemia and Bloom syndrome. *Methods*. **2009**, 48. 72-79.

[33]Cao, S. S.; Kaufman. R. J. Endoplasmic reticulum stress and oxidative stress in cell fate decision and human disease. *Antioxid. Redox Signal*. **2014**, *21*, 396-413.

[34]Rauniyar, N.; Yates. J. R.; Isobaric labeling-based relative quantification in shotgun proteomics. *J. Proteome Res*. **2014**, *13*, 5293–5309.

[35]Turakhiya, A.; Meyer, S. R.; Marincola, G.; Schlosser, A.; Hofmann, K.. ZFAND1 Recruits p97 and the 26S Proteasome to Promote the Clearance of Arsenite-Induced Stress Granules. *Mol. Cell* **2018**, 906–919.

[36]Tam, S.; Geller, R.; Spiess, C.; Frydman. J. The chaperonin TRiC controls polyglutamine aggregation and toxicity through subunit-specific interactions. *Nat. Cell Biol*. **2006**, *8*, DOI 10.1038/ncb1477.

[37]Wheeler, J. R.; Matheny, T.; Jain, S.; Abrisch, R.; Parker, R. Distinct stages in stress granule assembly and disassembly. *Elife* **2016**, 1–25.

[38]Hergesheimer, R. C.; Chami, A. A.; De Assis, D. R.; Vourc, P.; Andres, C. R.; Corcia. P. A role for SUMOylation in the Formation and Cellular Localization of TDP-43 Aggregates in Amyotrophic Lateral Sclerosis. *Brain* **2019**, 1176–1194.

[39]Cohen, T. J.; Hwang, A. W.; Restrepo, C. R.; Yuan, C.; Trojanowski, J. Q.; Lee. Y. M. Y. An acetylation switch controls TDP-43 function and aggregation propensity. *Nat. Commun*. **2015**, DOI: 10.1038/ncomms6845.

[40]Satoh, R.; Tanaka, A.; Kita, A.; Morita, T.; Matsumura, Y.; Umeda, N.; Takada, M.; Hayashi, S.; Tani, T.; Shinmyozu, K.; Sugiura. R. Role of the RNA-Binding Protein Nrd1 in Stress Granule Formation and Its Implication in the Stress Response in Fission Yeast.*PLoS One*. **2012**, *7*, DOI: 10.1371/journal.pone.0029683.

[41]Patel, M. S.; Nemeria, N. S.; Furey, W.; Jordan, F. The pyruvate dehydrogenase complexes: structure-based function and regulation. *J. Biol. Chem.* **2014**, *289*, 16615-23.

[42]Petrick, J. S.; Jagadish, B.; Mash, E. A.; Aposhian, H. V. Monomethylarsonous acid (MMA(III)) and arsenite: LD(50) in hamsters and in vitro inhibition of pyruvate dehydrogenase. *Chem. Res. Toxicol.* **2001**, *14*, 651-656.

[43]Piette, B. L.; Alerasool, N.; Lin, Z.; Lacoste, J.; Hiu, M.; Lam, Y.; Qian, W. Tran, S.; Larsen, B.; Campos, E.; Peng, J.; Gingras, A. C.; Taipale, M. Comprehensive interactome profiling of the human Hsp70 network highlights functional differentiation of J domains. *Mol. Cell* **2021**, *81*, 2549-2565.

[44]Gobe, G.; Crane, D.;. Mitochondria, reactive oxygen species and cadmium toxicity in the kidney. *Toxicology. Letters*. **2010**, *198*, 49-55.

[45]Tynecka, Z.; Malm, A. Substrate-dependent cadmium toxicity affecting energy-linked K+/86Rb transport inStaphylococcus aureus. *J. Basic Microbiol*. 1998, 36, 447-452.

[46]Meng, H.; Fitzgerald., M. C. Proteome-Wide Characterization of Phosphorylation-Induced Conformational Changes in Breast Cancer. *J. Proteome Res.* **2018**, *17*, 1129–1137.

[47]Liu, F.; Fitzgerald, M. C. Large-Scale Analysis of Breast Cancer-Related Conformational Changes in Proteins using Limited Proteolysis. *J. Proteome Res*. **2016**, *15*, 4666–4674.

[48]Feng, Y.; De Franceschi, G.; Kahraman, A.; Soste, M.; Melnik, A.; Boersema, P.J.; Polverino de Laureto, P.; Nikolaev, Y.;, Oliveira, A. P.; Picotti, P.. Global analysis of protein structural changes in complex proteomes. *Nat. Biotech.* **2014**, *32*, 1036-1044.

[49]To, P.; Whitehead, B.; Tarbox, H. E.; Fried. S.D. Nonrefoldability is Pervasive Across the E. coli Proteome. *J. Am. Chem. Soc.* **2021**, *143*, 11435-11448.

[50]Zauber, H.; Kirchner, M.; Selbach, M. Picky: a simple online PRM and SRM method designer for targeted proteomics *Nat. Meth.* **2018**, *15*, 156-157.

[51]Heil, L. R.; Remes, P. M.; Maccoss, M. J. Comparison of unit resolution versus high-resolution accurate mass for parallel reaction monitoring. *BioRxiv* **2021**, 2021.05.04.442680.

[52]Peterson, A.C.; Russell, J. D.; Bailey, D. J.; Westphall, M. S.; Coon, J. J.. Parallel reaction monitoring for high resolution and high mass accuracy quantitative, targeted proteomics. *Mol. Cell. Proteomics*. **2012**, *11*, 1475-1488.

[53]Trendel, J.; Schwarzl, T.; Horos, R.; Prakash, A.; Bateman, A.; Hentze, M.W.; Krigsveld. J. The Human RNA-Binding Proteome and Its Dynamics during Translational Arrest. *Cell*. 2019, 176, 391-403.

[54]Johnson, B. S.; McCaffery, J. M.; Lindquist, S.; Gitler. A.D. A yeast TDP-43 proteinopathy model: Exploring the molecular determinants of TDP-43 aggregation and cellular toxicity. *PNAS.* **2008**, *105*, 6439–6444.

[55]Ciszak, E. M.; Korotchkina, L. G.; Dominiak, P. M.; Sidhu, S.;Patel. M. S.; Structural Basis for Flip-Flop Action of Thiamin Pyrophosphate-dependent Enzymes Revealed by Human Pyruvate Dehydrogenase. *J. Biol. Chem.* **2003**, *278*, 21240-21246.

[56]Pettersen, E.F.; Goddard, T. D.; Huang, C. C.; Couch, G. S.; Greenblatt, D. M.; Meng, E.C.; Ferrin. T.E.; UCSF Chimera--a visualization system for exploratory research and analysis. *J Comput Chem.* **2004**, *25*, 1605-12.

[57]Samikkannu, T.; Chen, C.;Yih, L.; Wang, A. S. S.; Lin, S.; Chen, T.; Jan, K.. Reactive oxygen species are involved in arsenic trioxide inhibition of pyruvate dehydrogenase activity. *Chem. Res. Toxicol*. **2003**, 409–414.

[58]Gallien, S.; Bourmaud, A.; Kim, S.Y.; Domon. B. Technical considerations for large-scale parallel reaction monitoring analysis. *J. Proteomics.* **2014,** *100,* 147-159.

[59]Ronsein, G.E.; Pamir, N.; Von Haller, P.D.; Kim, D.S.; Oda, M.N.; Jarvik, G.P.; Vaisar, T.; Heinecke, J.W. Parallel reaction monitoring (PRM) and selected reaction monitoring (SRM) exhibit comparable linearity, dynamic range and precision for targeted quantitative HDL proteomics. *J. Proteomics.* **2015**, *113,* 388-399.

[60]Tseng, C. The potential biological mechanisms of arsenic-induced diabetes mellitus. *Toxicol. Appl. Pharmacol.* **2004**, *197*, 67–83.

[61]Kato, M.; Wynn, R.M.; Chuang, J.L.; Tso, S.C.; Machius, M.; Li, J.; Chuang, D.T. Structural Basis for Inactivation of the Human Pyruvate Dehydrogenase Complex by Phosphorylation: Role of Disordered Phosphorylation Loops. *Structure* **2008**, *16,* 1849–1859.

[62]Frank, R.A.W.; Pratap, J.V.; Pei, X.Y.; Perham, R.N.; Luisi, B.F. The molecular origins of specificity in the assembly of a multienzyme complex. *Structure* **2005**, *13,* 1119–1130.

[63]Yonashiro, R.; Eguchi, K.; Wake, M.; Takeda, N.; Nakayama, K. Pyruvate Dehydrogenase PDH-E1β Controls Tumor Progression by Altering the Metabolic Status of Cancer Cells. *Cancer Res.* **2018**, *78,* 1592-1603.

[64]Bergquist, E.R.; Fischer, R.J.; Sugden, K.D.; Martin, B.D. Inhibition by methylated organo-arsenicals of the respiratory 2-oxo-acid dehydrogenases. *J. Organomet. Chem.* **2009**, *694*, 973–980.

[65]Hageman, J.; Van Waarde, M. A. W. H.;. Zylicz, A.; Walerych, D.; Kampinga. H. H. The diverse members of the mammalian HSP70 machine show distinct chaperone-like activities. *Biochem. J.* **2011**, *435*, 127-142.

[66]Genereux, J. C.; Qu, S.; Zhou, M.; Ryno, L.M.; Wang, S.; Shoulders, M.D.; Kaufman, R.J.; Lasmézas, C.I.; Kelly, J.W.; Wiseman, R. L. Unfolded protein response-induced ERdj3 secretion links ER stress to extracellular proteostasis. *EMBO J.* **2015**, *34*, 4-19.

[67]Quanrud, G. M.; Montoya, M. R.; Mei, L.; Awad, M. R.; Genereux, J. C. Hsp40 Affinity to Identify Proteins Destabilized by Cellular Toxicant Exposure. *Anal. Chem.* **2021**, *93,* 16940–16946. https://doi.org/10.1021/acs.analchem.1c04230.

Chapter 3: Hsp40 Affinity Profiling Identifies Unique Cellular Protein Destabilization Profiles Induced by Exposure to Chloroacetanilide Herbicides

This chapter discusses the investigation into the effects of propachlor, alachlor, and acetochlor in HEK293T cells.

3.1 Abstract

The popular chloroacetanilide class of herbicides harbor a potent electrophilic moiety, which can damage proteins by nucleophilic substitution. Modified proteins are subject to misfolding, and accumulation of misfolded proteins compromises cell integrity by disrupting cellular proteostasis networks, which can further destabilize the cellular proteome. While direct conjugation targets can be discovered through affinity-based protein profiling, there are few approaches to probe how cellular exposure to toxicants impacts the stability of the proteome. We apply a quantitative proteomics methodology to identify chloroacetanilide-destabilized proteins in HEK293T cells based on their binding to the H31Q variant of the human Hsp40 chaperone DNAJB8. We find that brief cellular exposure to the chloroacetanilides acetochlor, alachlor, and propachlor induces distinct but overlapping profiles of protein destabilization, highly concentrated in proteins with reactive cysteine residues. Propachlor induces a general increase in protein aggregation, and selectively targets GAPDH and PARK7, leading to a decrease in their cellular activities. The Hsp40 affinity strategy is an effective technique to profile cellular proteins that are destabilized by cellular toxin exposure, and can elucidate the affected biological pathways.

3.2. Introduction

Proteins are generally considered to be nucleophilic, particularly at the cysteine thiol, the lysine ε-amine, and the N-terminus. While the reactivity of these sites enables post-translational modifications that play central roles in cellular signaling and function, they are also subject to modification by environmental and metabolic electrophiles. This damage can deprive the cell of protein function[1], interfere with binding interactions, or promote protein misfolding and toxic aggregation[2]. Despite the clear threat that electrophilic exposure agents present to the cellular proteome and protein homeotasis, protein conjugation is not nearly as well investigated as nucleic acid conjugation. This likely stems from the larger variability in protein reactivity compared to nucleic acids; nucleic acid reactivities vary far less than protein reactivities, and the mutagenic potential of nucleic acid adducts can be readily determined through well-established mutagenicity assays such as the Ames test. Assays that allow broader interrogation of how the complete proteome responds to electrophilic agents are necessary to understand their molecular mechanisms of toxicity.

One of the most popular herbicide classes over the past 50 years is the chloroacetanilides, which feature a highly electrophilic haloacetamide motif. These herbicides are N-alkoxy alkyl-N-chloroacetyl substituted derivatives of aniline and commonly used to minimize weed control for agricultural goods such as corn, maize, and rice[3]. The once common application of chloroacetanilides has significantly decreased in the United States due to its carcinogenic effects[4,5] and potential to accumulate in soil and wetlands[6]. Although the reported carcinogenicity is presumably through the formation of

DNA and protein adducts[7,8,9], other studies have found that chloroacetamides are not genotoxic and do not damage DNA *in vivo*[10]. In both soil and in groundwater, microbial metabolism of chloroacetanilides by N-dealkylation or glutathione conjugation creates further toxic products, including 2,6-diethylaniline (DEA) or 2-methyl-6-ethylaniline (MEA)[11]. These products can also modify proteins, and could also be involved in chloroacetamide toxicity and carcinogenicity. However, little work has been performed to identify which proteins are most susceptible to chloroacetanilide conjugation, and none at all to determine how this modification impacts protein stability (**Scheme 1A**).

Most of our knowledge regarding protein targets of chloroacetanilides come from activity-based protein profiling (ABPP) experiments. Mass spectrometry-based methods that profile proteome-wide reactivity to herbicides can help profile the damaged proteins and pathways affected by these herbicides. Activity-based protein profiling (ABPP) was used to identify acetochlor and metachlor targets and screen for covalent ligands that can react with cysteines[12,13]. Variations of ABPP such as Fragment-Based Ligand Discovery (FBLD) and Reversible Polarity Activity (RP)-ABPP expanded the proteome wide screening to account for proteins with electrophilic post translational modifications (PTM) or proteins prone to react with a binding handle rather than undergo covalent nucleophilic substitution[14,15]. Electrophilic modifications of proteins often are associated with oxidative stress and thus covalent of modifications of proteins could be quantitatively measured by SPROX and FPOP to account for additional oxidative modifications[16,17]. Covalent Protein Painting (CPP) can address modifications of lysines

after electrophilic exposure[18]. Each technique can address proteomic and structural changes of proteins after covalent modifications.

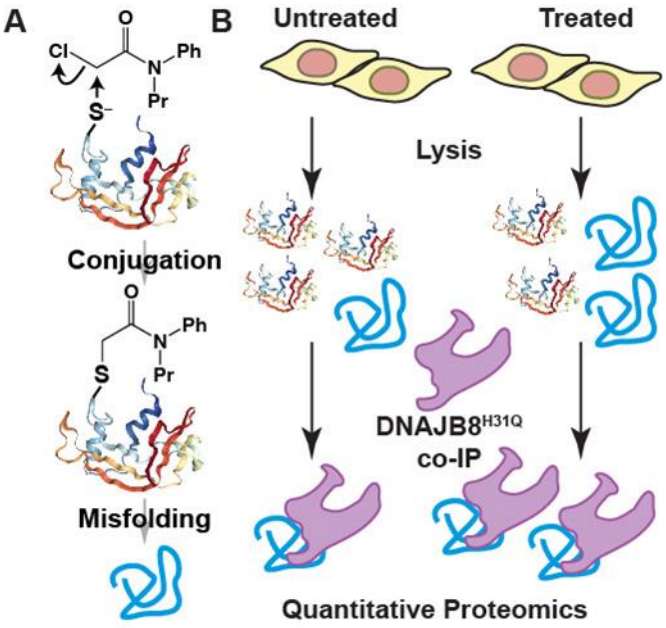

Scheme 1 Overview of Electrophilic Stress: A) Propachlor can conjugate to cysteine. This type of protein damage could induce protein misfolding. B) Description of our assay to identify changes in protein stability based on affinity to the Hsp40 DNAJB8^{H31Q}.

We previously developed an affinity purification mass spectrometry approach to profile misfolded proteome using human Hsp40 ^{Flag}DNAJB8^{H31Q} [19]. This assay combines affinity purification of overexpressed ^{Flag}DNAJB8^{H31Q} with quantitative proteomics to identify hundreds of co-isolating cellular proteins with reproducibility and statistical confidence[19]. The H31Q mutation blocks the release of misfolded protein clients from DNAJB8, allowing immunoprecipitates to be stringently washed. We further applied this

strategy and incorporated limited proteolysis to identify several misfolded ribosomal proteins such as TDP43 and PDHA1 from an arsenite-effected proteome[20].

We believed that heat shock proteins, particularly DNAJB8, can also profile proteome reactivity toward electrophiles. Pesticides can induce reactive oxygen species (ROS) inside the cell and heat shock factors are in turn activated to refold proteins and prevent downstream effects such as apoptosis[21]. Molecular chaperones induced by stress responsive transcriptional remodeling, such as that downstream of HSF1 activation, can in principle address the toxicological mechanism of a herbicide by recognizing and identifying an electrophilically-exposed misfolded client.

We utilize the ability of DNAJB8^{H31Q} to identify proteins that are destabilized in response to exposure from chloroacetanilide herbicides. We profiled the effects of acetochlor, alachlor, and propachlor on the HEK293T proteome and discovered distinct destabilized proteins for each condition and protein targets for propachlor stress.

3.3 Materials and Methods

3.3.1 Materials:

We purchased the 1,4-dithiothreitol (DTT), Roche Protease Inhibitor cocktail w/o EDTA (PIC), HEPES, Propachlor, Acetochlor, Alachlor, and GAPDH Activity assay Kit from Sigma Aldrich. We purchased the Bovine Serum Albumin (BSA), Dulbecco's Modified Eagle Media (DMEM), Dulbecco's phosphate-buffered saline (DPBS), 10 cm plates, and 6 well plates from VWR. We purchased the KCl, $MgCl_2$, $CaCl_2$, $Ag(NO_3)_2$, $Na_2S_2O_3$, sodium chloride (NaCl), Tris-Hydrochloride (Tris-HCl), Triton X-100, sodium

deoxycholate, urea, $Ca(O_2C_2H_3)_2$), glycerol, sodium dodecyl sulfate (SDS), poly D-lysine, and sequencing grade trypsin from Thermo Fisher Scientific. Proteinase K (PK) was purchased from Promega. Nanopure water was purified We using a Millipore Milli-Q Laboratory lab 4 Chassis Reagent Water System. 5 µm and 3 µm Aqua C18 resins were purchased from Phenomenex. Tris (2-carboxyethyl)phosphine hydrochloride (TCEP), Sepharose-4B beads, anti-M2 Flag magnetic beads, and iodoacetamide were purchased from Millipore Sigma. 250 µm diameter fused silica columns were from Agilent. 100 µm diameter fused silica columns were from Polymicro. Strong cation exchange resin was from Partisphere, GE Healthcare. Rapigest was purchased from Aobious (Gloucester, MA). TMT-6plex isotopic labels were from Pierce. Bradford reagent was purchased from Bio-rad.

3.3.2 AP-TMT-MudPIT:

TMT-AP-MS experiments were performed as described previously[20]. Six 10 cm plates of HEK293T cells were transfected by the calcium phosphate method with 5 µg of plasmid DNA encoding ^{Flag}DNAJB8^{H31Q} in the pFLAG backbone. Plates were treated with 1mM chloroacetanilide at 40-46 hours post transfection for 30 minutes in serum free media. Cells were harvested by scraping in DPBS. Cells were then lysed in 9 parts RIPA Buffer (150 mM NaCl, 50 mM Tris pH 7.5, 1% Triton X-100, 0.5% sodium deoxycholate, 0.1% SDS) and 1 part 10x PIC on ice for 30 minutes. Samples were placed in centrifugation and spun 21,000 x g for 15 minutes at 4 °C to separate lysate from cell debris. Bradford was used to quantify protein in each lysate was quantified. Lysates were

incubated with 15 µL Sepharose-4B beads for 30 min at 4 °C, then centrifuged at 1,500 x g for 1 min to pellet beads. Lysate was then separated and then incubated with 15 µL of M2 anti-Flag Magnetic Beads and rotated overnight at 4 °C. The anti-Flag beads were washed the next day four times with RIPA buffer. Each wash included rotation for 10 minutes at ambient temperature. Proteins bound to the anti-Flag beads were eluted by boiling for 5 min at 100 °C in 30 µL of Laemmli concentrate (120 mM Tris pH 6.8, 60% glycerol, 12% SDS, brilliant phenol blue to color). 5 µL of the elutes were saved for silver stain analysis and the remainder was prepped for mass spectrometry and TMT-labeled from a sixplex TMT set.

Only MS quality organic solvents were used during sample preparation. The composition for buffer A is 0.1% formic acid, 5% acetotrile in water. The composition for Buffer B is 0.1% formic acid, 80% acetonitrile. The composition for Buffer C is 500 mM ammonium acetate in Buffer A. MS runs were performed by using a two-dimensional LC/MS/MS setup on an LTQ Orbitrap Velos Pro hybrid mass spectrometer (Thermo) interfaced with an Easy-nLC 1000 (Thermo) according to standard MuDPIT protocols[22]. For each run, MS/MS spectra were extracted using MSConvert (version 3.0.21144) with Peak Picking Filtering. FragPipe was used to search MS/MS spectra against a Uniprot human proteome database (06/11/2021 release) containing 40858 human sequences (longest entry for each protein)[23]. MS/MS spectra were also searched against 20429 select decoys (e.g albumen, porcine trypsin, contaminants etc.). FragPipe searches allowed for static modification of cysteine residues (57.02146 Da, acetylation), modifications of herbicide adducts (176.1075 for propachlor adducts, 234.1494 for

acetochlor and alachlor adducts), and N-termini and lysine residues (229.1629 Da, TMT-tagging), and half tryptic peptidolysis specificity. Fragpipe also selected amass tolerance of 20 ppm for precursor mass and 20 ppm for product ion masses. MSFragger (Version 3.2) was used to match and filter spectra. Decoy proteins, common contaminants, immunoglobulins, and keratins were filtered from the final protein list. Quantitation in FragPipe was performed by averaging TMT reporter ion intensities for all spectra associated with an individual peptide.

All MS runs were performed using the same two-dimensional LC/MS/MS setup on an LTQ Orbitrap Velos Pro hybrid mass spectrometer (Thermo) interfaced with an Easy-nLC 1000 (Thermo) as completed in the above TMT-Mudpit runs. Samples were loaded onto a triphasic loading column for analysis. Triphasic loading columns were made by polymerizing a Kasil 1624 frit into a 250 µm diameter fused silica capillary. The column was then packed with 2.5 cm of reversed-phase 5 µm Aqua C18 resin, followed by 2.5 cm of 5 µm strong cation exchange resin, and again with 2.5 cm of reversed-phase 5 µm Aqua C18 resin. Analytical columns were prepared by pulling 100 µm diameter fused silica columns with a P-2000 laser tip puller (Sutter Instrument Co., Novato, CA), followed by packing with at least 20 cm reversed-phase 3 µm Aqua C18 resin. Analysis was performed using a 11-cycle chromatographic run, with progressively increasing concentrations of ammonium acetate salt bumps injected prior to each cycle (0% C, 1% C, 2.5% C, 5% C, 7.5% C, 10% C, 20% C, 30% C, 40% C, 50% C, 60%C, 80%C, 100%C, 90% C+ 10% B; balance of each buffer A), followed by acetonitrile gradient (5 min from 1% B to 7% B, 60 min to 36% B, 15 min to 100% B, 5 min at 100% B, 5 min to 1% B; 500 nL/min flow rate). Eluted peptides were ionized by electrospray (3.0 kV) and scanned from 110 to 2000 m/z in the Orbitrap with resolution 30,000 in data dependent acquisition mode. The top ten peaks with

charge states of 2+, 3+, or 4+ from each full scan were fragmented by HCD using a stepped collision energy of 36%, 42%, and 48%, a 100 milliseconds activation time, and a resolution of 7500. Dynamic exclusion parameters were 1 repeat count, 30 milliseconds repeat duration, 500 exclusion list size, 120 seconds exclusion duration, and 2.00 Da exclusion width.

3.3.3 Statistical Analysis:

All statistical analysis were performed according to previous experiments[19,20]. Initially, protein-level intensities were normalized to the intensity of bait (DNAJB8) in each TMT channel. We then used a version of the scaled reference approach combine multiple TMT runs[24]. The bait-normalized integrated TMT reporter ion intensities were averaged for each protein across the three control conditions in each AP-MS run providing a scaling factor. Each bait-normalized protein intensity was then divided by this scaling factor. Storey's modification and the method of Benjamini and Hochberg was used to convert unadjusted p-values to q-values (local false discovery rates)[25,26]. Unadjusted p-values were ranked in increasing order and the q-value for the *i*th protein determined from:

$$q_i = \pi \, min_{i \leq j \leq n} \frac{pn}{i}$$

Storey's modification is performed by determining the overrepresentation of low p-values to infer a global false discovery rate, and then scaling local false discovery rates accordingly. The π-factor for this scaling was 0.54 for the acetochlor treatment, 0.5 for alachlor treatment, 0.3 for propachlor treatment.

3.3.4 Limited Proteolysis and PRM:

3.3.4.1 Limited Proteolysis Procedure and PRM:

The limited proteolysis procedure was optimized from standard protocols and previous experiments[20, 27]. 1 mg/ml stocks were prepared from 25 mg of lyophilized Proteinase K (PK) dissolved in a storage buffer (50 mM Tris-HCl, 2 mM calcium acetate, pH 8.0) suitable for PK and stored at –70 °C. The following concentrations of PK were prepared from serial dilutions from 1 mg/ml aliquot: 0.5 mg/ml, 0.2 mg/ml, 0.1 mg/ml, 0.05 mg/ml, , and added to lysate to yield 1:200, 1:500, 1:1000, 1:2000, wt/wt protease: substrate protein ratios respectively. 2 µl PK was added to a 200-µg aliquot of protein lysate and incubated for 1 min at 25.0 °C for each digestion. Samples were then boiled for 5 min to quench PK activity. Three separate digestions were performed for the no PK condition for each lysate sample. Samples were prepared for mass spectrometry were analyzed using LC-MS/MS and parallel reaction monitoring (PRM). Peptide separations by LC-MS proceeded between Buffer A (5% acetonitrile:95 % water: 0.1% formic acid) and Buffer B (80% acetonitrile: 20% water: 0.1% formic acid) over a 100 min gradient with the following segments: 1-5 min: 1-6% Buffer B. 5-75 min: 6-31% Buffer B. 75-80 min: 29-100% Buffer B. 80-85 min: 100% Buffer B. 85-90 min: 100-1% Buffer B. 90-100 min: 1% Buffer B. Flow rate was 500 nl/min. Chromatograms and product ions were quantified by skyline[28]. Skyline chromatograms can be seen in the appendix.

PRM was also used to search for propachlor modified peptides in GAPDH. A list of peptides with cysteines modified by propachlor in GAPDH were compiled in skyline[28]. One injection from a propachlor treated lysate was compared to the one

injection of DMSO treated lysate looking for those modifications. Data Analysis was performed from previous experiments[20].

3.3.5 GAPDH Activity Assay:

Enzymatic activity of GAPDH was measured after propachlor treatment and protocol was modified from standard GAPDH activity assay from Sigma Aldrich[29]. Three 10 cm plates of HEK293T cells were treated with 1 mM Propachlor for 30 minutes in serum free media and three 10 cm plates of HEK293T cells were treated with DMSO in serum free media for 30 minutes. Each plate was then harvested by scraping with DPBS and pellets were frozen in -80 ºC for future use. Each pellet was lysed in GAPDH Assay buffer and 8 µl from each plate were aliquoted into a separate row for 4 wells where each well had 42 µl of GAPDH assay buffer including GAPDH Developer. There were 6 rows used in the plate. 2 wells were treated with GAPDH substrate, and 2 wells were treated without substrate. Measurements were recorded on Bio-tek Synergy H1 microplate reader at 0 minutes and then cycles of 10 minutes for a total of 60 minutes. Absorbance measurements were recorded at 450nm and normalized to protein concentration measured by Bradford.

3.3.6 DJ-1 Deglycase Activity Assay:

DJ-1 (PARK7) Deglycase Assay was modified from Tsumoto et al.[30]. Four 6 cm plates of HEK293T cells were at 80% confluency. One 6 cm plate was treated with control (DMSO) for 30 minutes in serum free media and then control (water) in media for

8 hours. The second 6 cm plate was treated with 1mM Propachlor 30 minutes in serum free media and then 8 hours of control (water) in media for 8 hours. The third 6 cm plate was treated with control (DMSO) for 30 minutes in serum free media and then 2 mM Glyoxal in media for 8 hours. The fourth 6 cm plate was treated with control (DMSO) for 30 minutes in serum free media and then 2 mM glyoxal in media. Each plate after treatment was immediately harvested by scraping with DPBS and lysed in 9 parts RIPA Buffer (150 mM NaCl, 50 mM Tris pH 7.5, 1% Triton X-100, 0.5% sodium deoxycholate, 0.1% SDS) and 1 part 10x PIC for 30 min on ice. Cell lysates were quantified by Bradford on loaded on 10% SDS page gels for western blotting analysis. Western blots were probed to measured to determine amount of Carboxy-Methyl Lysine (CML) proteins. Blots were first probed for CML (rabbit polyclonal) and then Beta-actin (mouse monoclonal 7D2C10), near IR-secondary antibodies (Li-Core) and visualized on a Li-Core Biosciences Fc imager. Experiments exploring 4 mM glyoxal were performed the same way except for the concentration of glyoxal.

3.3.7 Propachlor Aggregation Studies:

Three out of six 10 cm plates of HEK293T cells were treated with 1 mM Propachlor for 30 minutes. The other three 10 cm plates were treated with DMSO for 30 min. Media was then changed for recovery for 6 hours. Cells were harvested by scraping in DPBS and lysed in 9 parts RIPA Buffer (150 mM NaCl, 50 mM Tris pH 7.5, 1% Triton X-100, 0.5% sodium deoxycholate, 0.1% SDS) and 1 6part 10x PIC for 30 min on ice. Lysate was separated from cell debris by centrifugation at 21,000 x g for 15 minutes at 4

°C. Protein in the lysate was quantified by Bradford. Protein samples were normalized and balanced to 2mg in 1ml of RIPA. The rest left is a representative of total (T) sample. Samples were placed in TLA-SS rotor and spun in a Beckman Opti-MAX at 77,000g for four hours. Soluble fraction was separated from insoluble fraction. The insoluble fraction was washed four times with RIPA buffer. Each wash included gentle resuspension for 1 minute. The insoluble fraction (P) was resolubilized in 8 M Urea in 50 mM Tris overnight at 4 ºC. Aliquots from initial lysis, soluble fraction, and insoluble fraction was taken for western blot analysis.

Two separate TMT experiments were used to quantify changes in aggregation between propachlor and control treated samples. TMT sample prep was adapted from labeling procedure from AP-TMT-MudPIT experiments. Only MS quality organic solvents were used during sample preparation. Aliquots of 20 µg were taken from each T sample. Samples were precipitated by methanol/chloroform precipitation. Pellets were then air-dried and resuspended in 1% rapigest in water. Resuspended protein solutions were then diluted to 50 µL in 100 mM HEPES, pH 8.0, and reduced with 10 mM TCEP for 30 min at 37 °C. Protein solutions were then alkylated with 5 mM iodoacetamide for 30 min in the dark at ambient temperature. 0.5 µg sequencing grade trypsin was added to the protein solution for digestion overnight at 37 °C with agitation (600 rpm). TMT isotopic labels were resuspended (100 ug/80 µL acetonitrile) and 40 µL of label was added to each 60 µL sample of digested peptides. Samples were labeled for 1 h at ambient temperature. Labeling was quenched with 0.4% ammonium bicarbonate at ambient temperature for 1 h. Samples were pooled, acidified, centrifuged for 30 min at

21,100 x g to remove any insoluble debris. Samples were then dried by centrifugal evaporation to 10 µL. Solutions were then brought to 200 µL in Buffer A, incubated at 37 °C for 1 h, and centrifuged for 30 minutes at 21,100 x g. Solutions were transferred to new low-binding tubes (Eppendorf) and the process of heat-spinning was repeated three more times to complete elimination of Rapigest.

Pellet (P) fractions were quantified by Bradford. The amount of sample required to make 20 µg of protein was averaged among the 6 samples. That average aliquot was then taken from each sample and precipitated by methanol/chloroform precipitation. The sample was then labeled as shown above for the T fractions. All MS runs were performed in same fashion as AP-TMT-MudPIT runs. P-values were moderated to compare samples treated with propachlor versus control[31].

3.3.8 Resazurin Assay:

Resazurin sodium salt was purchased from Acros Organic. Resazurin assay was adapted from Abcam[32]. For cell viability experiments exploring propachlor treatments, 50,000 cells were plated in 64 wells in a Poly-D-Lysine coated 96 well plate. Each row was treated with an increasing amount of Propachlor for 30 minutes starting with 0 mM to 1 mM propachlor in serum free media. The media was then changed and allowed to recover for 24 hours. Two mg of resazurin sodium salt was resuspended in 1ml of DPBS. 5 µl of resazurin solution was added to each well. Fluorescence measurements were recorded on the Bio-tek Synergy H1 microplate reader at 550 nm excitation and 590 nm emission.

3.3.9 Assessing HSF1 Activation after Applied Chloroacetanilide Stress:

Cellular experiments were performed based on previous experiments[20]. Two 10 cm plates seeded with HEK293T cells were transfected at 40-60% confluency by calcium phosphate method. One plate was transfected with 5 µg of GFP and the other plate was transfected with DNA encoding ^{FLAG}DNABJ8^{H31Q}. Both plates were split into 6-well plates coated with Poly-D-Lysine. Each individual well was incubated with an increasing concentration (0 µM, 25 µM, 50 µM, 100 µM, 500 µM, 1 mM) of a chloroacetanilide for 15 min at 37 °C. Chloroacetanilide treated media was replaced with fresh media. Plates were then incubated for 16 h at 37 °C to recover. Plates were then harvested by scraping in DPBS. Pellets were then lysed in 9:1 RIPA:10x PIC in ice for 30 min. Lysates were separated from cell debris by centrifugation at 21,000 x g for 15 minutes at 4 °C. Bradford assay was used to quantify protein concentration in each lysate. 2 µg/µl of protein samples were prepared for western blot analysis after addition of 9:1 Laemlli:1 M DTT (17% of solution).

15 µg of each sample were separated on a 12% SDS-PAGE Gel with 1.0 mm thickness. Western blots were probed for HSPA1A (rabbit polyclonal), Flag (Sigma M2 monoclonal anti-Flag antibody), GFP (rabbit polyclonal) primary antibodies, and Beta-actin (mouse monoclonal 7D2C10). Near-IR secondary antibodies (Li-COR) were used and blots were visualized on a Li-Cor Biosciences Fc Imager.

3.3.10 Cell Culture and Silver Stain:

HEK239T cells were obtained from the ATCC and maintained in DMEM with

10% FBS. Cell transfection was conducted by the calcium phosphate method. 5 µg of DNA in 1 mL 250 µM $CaCl_2$ is vortexed while adding dropwise 1 mL HBS 2X for 10 seconds at room temperature. The transfection solution is promptly (≤ 15 min) added dropwise to cells at around 50% confluency. The cell media is changed between 12 and 16 h. A positive transfection control is performed with GFP alongside each transfection. These transfection amounts were used for 10 cm dishes; proportional amounts of reagents were used for transfection of different sized plates.

Silver stain was used to assess the amount of the ^{Flag}DNAJB8^{H31Q} in eluates after the immunoprecipitation and potential differences in the co-immunoprecipitated protein levels between conditions[33] (**Figure S12**). Eluents were diluted in DTT to a final concentration of 170 mM DTT. Eluates were boiled for 5 min at 100 °C prior to SDS-PAGE separation. Gels were fixed overnight in 30% ethanol/10% acetic acid or for a few hours with 50% methanol/12% acetic acid. Gels were washed in 35% ethanol three times for 20 minutes each. Gels were then sensitized for 2 minutes (0.02% $Na_2S_2O_3$ in H_2O). Gels were then washed three times for 1 minute each in H_2O. Gels were finally stained for 30 minutes to overnight in Ag staining solution (0.2% $AgNO_3$, 0.076% formalin). Gels were developed with 6% $NaCO_3$/0.05% formalin/0.0004% $Na_2S_2O_3$ After two one minute rinses in water. Development was stopped with addition 5% acetic acid. Gels were imaged on a white-light transilluminator (UVP).

3.4 Results and Discussion

Short acute treatments of each chloroacetanilide on HEK293T cells were

optimized to limit the possibilities of transcriptional, translational, and post-translational remodeling of the cell[34], while still inducing protein misfolding. The primary misfolded protein stress response in the cell is the Heat Shock Response (HSR), in which the presence of nuclear or cytosolic misfolded proteins activates the transcription factor HSF1, leading to increased transcription and translation of chaperones and degradation factors and consequent restoration of cellular protein homeostasis[35]. A primary chaperone target of HSF1 is the cytosolic Hsp70 HSPA1A. We validated that 30 min 1 mM of acetochlor in serum free media induces HSR target HSPA1A in HEK293T cells and that overexpression of ^{Flag}DNAJB8^{H31Q}, the bait, does not suppress its response (**Figure 1**).

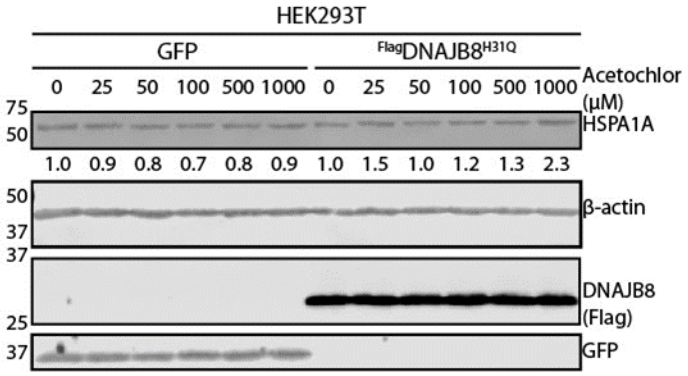

Figure 1: Representative immunoblot after Acetochlor exposure. SDS-PAGE separated lysates from HEK293T cells expressing the indicated proteins and treated with acetochlor in serum-free media for 30 min., followed by a 16 h recovery in complete media. Induction of the HSR target HSPA1A in response to acetochlor treatment is a proxy for the level of HSR activation. HSPA1A density is below the blot slice. Molecular weight markers are indicated on the left. Antigens targeted by immunoblotting are listed to the right of the slice.

Rather, ^{Flag}DNAJB8^{H31Q} sensitizes the cells to a slightly stronger response, possibly due to its strong holdase function[36]. Treatment of 1 mM of acetochlor for 30 minutes in serum media was thus chosen for profiling using our AP-MS strategy. Serum-

free media is necessary to avoid small molecule scavenging and is a standard incubation condition for cellular exposure to acetochlor[13,37]. Indeed, the use of complete media ablated HSR activation by acetochlor. 1 mM propachlor and 1 mM alachlor in serum-free media for 30 minutes were chosen to be consistent with the acetochlor conditions despite neither herbicide upregulating HSPA1A (**Figure S1A and S1B)**. Using the same conditions for each herbicide treatment allows us to relate effects on the proteome to structural characteristics rather than to incubation time and concentration[38]. Even in the absence of adequate proteostatic stress for HSF1 activation, propachlor and alachlor could still induce misfolding of specific protein targets with consequent cellular toxicity[39,40]. Consistent with this possibility, we found that 30 min. incubation with 1 mM propachlor inhibited viability of HEK293T cells by resazurin assay (**Figure S2**).

We utilized the Hsp40 affinity approach **(Scheme 1)** to profile the chloroacetanilide-dependent misfolded proteomes. ^{Flag}DNAJB8^{H31Q} was transiently overexpressed in HEK293T cells, followed by 30 min of chloroacetanilide herbicide, and immediate Flag immunoprecipitation from cellular lysate. Co-immunoprecipitated proteins were labeled by TMT isobaric tagging[41] and then identified and quantified by LC/LC-MS/MS. Each herbicide treatment (acetochlor, alachlor, and propachlor) was performed over 24 biological replicates (12 treated and 12 controls) and analyzed by four 6-plex TMT runs.

The Hsp40 affinity profile for each chloroacetanilide exposure provides a distinct fingerprint. Acetochlor treatment increases DNAJB8 affinity for most (82%) of DNAJB8 clients identified across the mass spectrometry runs (**See Figure 2, Figure S3-5, Supp.**

Tables 1-3), with 2% of clients demonstrating a greater than 2 fold increase in affinity. We further compared to a previously reported liver ABPP of mice exposed to acetochlor[13]. Out of 338 common quantified proteins, there is no correlation (**Figure S6**, $R^2 < 0.01$) between proteins that are destabilized by the Hsp40 assay and those that lose iodoacetamide reactivity following acetochlor exposure, indicating that our assay is distinct from measuring conjugation. Of the 28 mouse liver proteins that lost iodoacetamide reactivity or alkynylated acetochlor reactivity following mouse acetochlor treatment, 20 were identified in our Hsp40 affinity runs, with 6 demonstrating significantly (q-value < 0.05) increased Hsp40 affinity (SCP2, ACAT1, PDIA3, NNT, HSPD1, and DLD). Given the differences in model system (intraperitoneal injection of mice followed by ex vivo liver excision vs. human tissue culture) and in the assays, it is encouraging that several of the same targets are found in both studies.

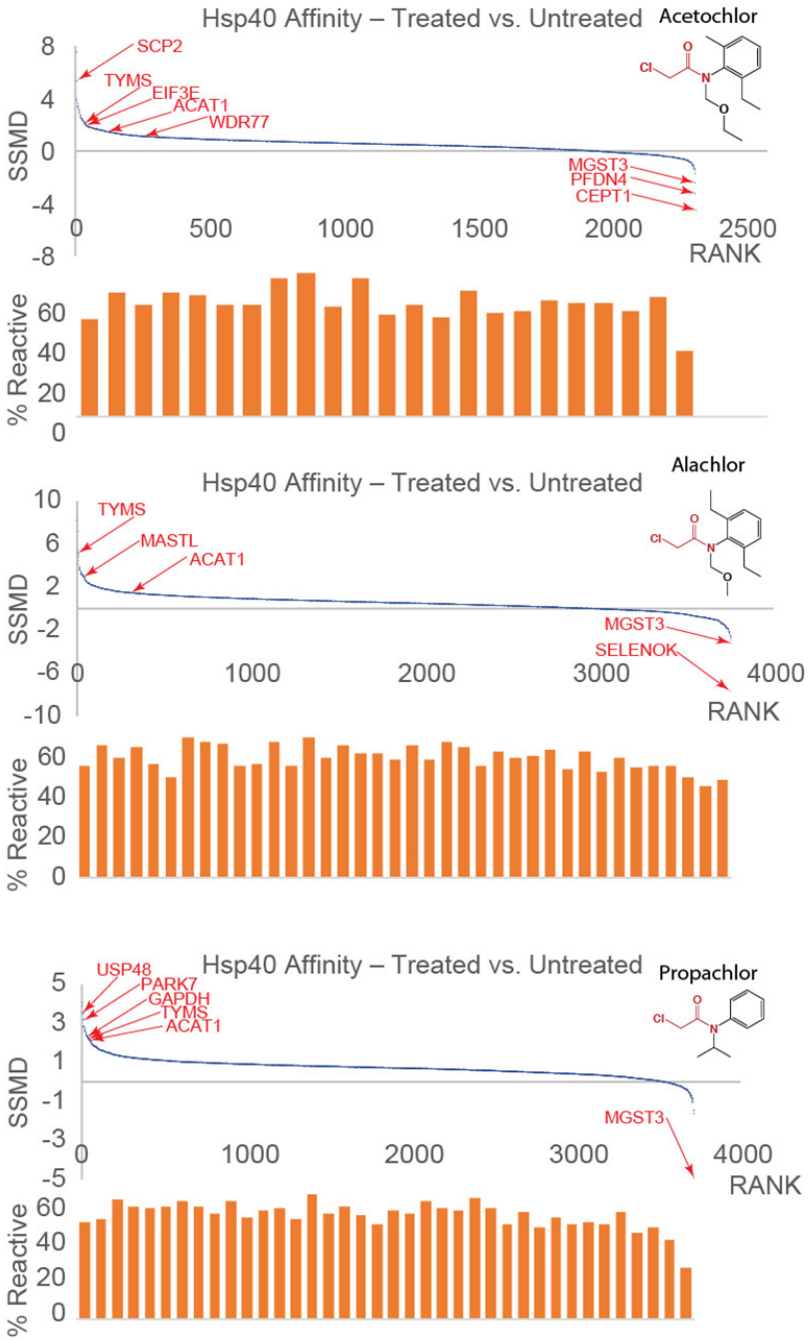

Figure 2: Differential Hsp40 affinity of proteins in response to treatment (1 mM, 30 min. in serum-free media, n = 4 biological replicates) of HEK293T cells with the indicated herbicides. The DNAJB8^{H31Q}-interacting proteins are ranked by Strictly Standardized Mean Differences (SSMDs, variance-normalized differences between control and treatment). Notable proteins are indicated by red arrows. The bar plots represent the percent of proteins (binned by 100) that were reported as iodoacetamide reactive in Kuljanin et al.[42]. Volcano plots can be found in **Figures S3-5**.

Several enzymes with active cysteines prone to electrophilic modification had significantly greater affinity for DNAJB8^{H31Q} after acetochlor exposure. Thymidylate Synthase (TYMS) (Fold Change = 3, q value = .003), an enzyme essential for production of thymidine nucleotides[43], has an active site cysteine that is specifically targeted by electrophilic chemotherapeutic drug)[44]. Another protein with significantly increased Hsp40 affinity following acetochlor treatment is eukaryotic translation initiation factor 3 subunit E (eIF3e) (Fold Change = 1.96, q value = .0004) which plays a role in tumor growth[45] and the hypoxia response[46]. Some enzymes such as Acetyl-CoaA acetyltransferase 1 (ACAT1, Fold change = 2.91, q value = .02) were logically more significantly destabilized since it has multiple cysteines and multiple active sites[46,47].

By contrast, another strongly destabilized acetochlor target WDR77 (FC = 2.25, q value = 0.01) lacks known reactive cysteines. However, it shares a complex with the arginine methylase PRMT5 (FC = 1.88, q value = 0.05), which does contain a pK-perturbed cysteine in its active site[48,49]. Choline /ethanolaminephosphotransferase 1 (CEPT1) and microsomal glutathionine S-transferase 3 (MGST3) on the other hand bind less to DNAJB8^{H31Q} after treatment, indicating stabilization. These two enzymes both contain active site cysteines that interact with substrates (glutathione and ethanolamine phosphate respectively)[50,51]. Nevertheless, the unusual increase in stability against all three conditions makes them possible protein targets for dysregulation as a treatment to suppress the toxic effects from each herbicide[52].

Despite its lack of HSR induction, alachlor exposure increases DNAJB8 affinity of many more proteins than acetochlor exposure (**Figure 2 and Figure S4)**. 764 proteins

show significantly (q-value < 0.05) increased DNAJB8 affinity following alachlor exposure, as opposed to 81 proteins following acetochlor exposure. Selectively targeted proteins included Microtubule Associated Serine/Threonine Kinase Like (MASTL) (fold change = 2.02, q value = 5 x 10^{-5}), a kinase involved in mitosis[53], and Zinc Finger Protein 24 (ZNF24), a tumor suppressor[54]. The higher impact of alachlor as opposed to acetachlor is in some ways surprising, as the two molecules are isomers differing only by a methyl group. However, regioisomers can have substantially different lipophilicities and cellular uptake[55]. Alachlor has a log K_{ow} of 3.5, as opposed to 3.0 for acetachlor. Small structural differences were found to have substantial effects on aryl halide reactivity towards cysteines[56]. The higher reactivity for acetachlor isn't surprising considering how they are digested metabolically. Metabolites digest Acetochlor faster than Alachlor to 2-chloro-N-(2,6-diethylphenyl)acetamide (CMEMPA) and 2-methyl-6-ethylaniline (MEA), two toxic precursors that can damage the proteome by forming DNA adducts during transcription[57,58].

Propachlor treatment has the strongest effect on the DNAJB8^{H31Q}-associated proteome (**Figure 2** and **Figure S5**) Glyceraldehyde-3-phosphate dehydrogenase (GAPDH) (Fold change = 5.97, Q value = 6.09 x10^{-5}), an enzyme that uses a susceptible active-site cysteine to bind and reduce nicotinamide adenine dinucleotide (NAD) in glycolysis, has more affinity to DNAJB8^{H31Q} after propachlor treatment[59]. GAPDH when inhibited by 3,4-dihydroxyphenylacetaldehyde (DOPAL), a metabolite of dopamine, can aggregate and thus is a target for Parkinson's Disease (PD) pathology[60]. Parkinson disease protein 7 (PARK7) (Fold change = 3.8, q value = 5.56 x 10^{-6}) was another

significantly destabilized protein after propachlor treatment. PARK7 can deglycase and repair active cysteines, but can be inhibited at the cysteine 106 position, making it also another biomarker for PD[61]. These two misfolded targets highlight the overall greater change in dynamic range of the misfolded proteome after propachlor treatment (**Figure 2**). Comparing proteins between the three herbicides with fold changes greater than 2 and a p value which measures binding to DNAJB8^{H31Q} less than 0.1, propachlor has 76 proteins that fit that classification (**Figure 3**). That number of misfolded clients more than doubles the combined number of proteins destabilized under the same criteria after alachlor and acetochlor treatments. The higher susceptibility of the proteome to propachlor could be based on substitution reaction reactivity. Kinetic studies between propachlor and alachlor reactivity found a 2-fold increase in the substitution of propachlor against several nucleophiles and a lower Gibbs free energy required for substitution reactions of propachlor with nucleophilic thiols[62].

There are similar destabilized proteins shared among the three chloroacetanilide herbicides (**Figure 3**). Strictly standardized mean differences (SSMD) were compared between different treatments. SSMDs are the mean differences between the herbicide-treated and untreated populations and then normalized by root-mean-square standard deviations. Several interactors that bind more to DNAJB8 after treatment such as ACAT1 and TYMS are commonly destabilized. GAPDH and PARK7 are not significantly destabilized after acetochlor and alachlor treatment.

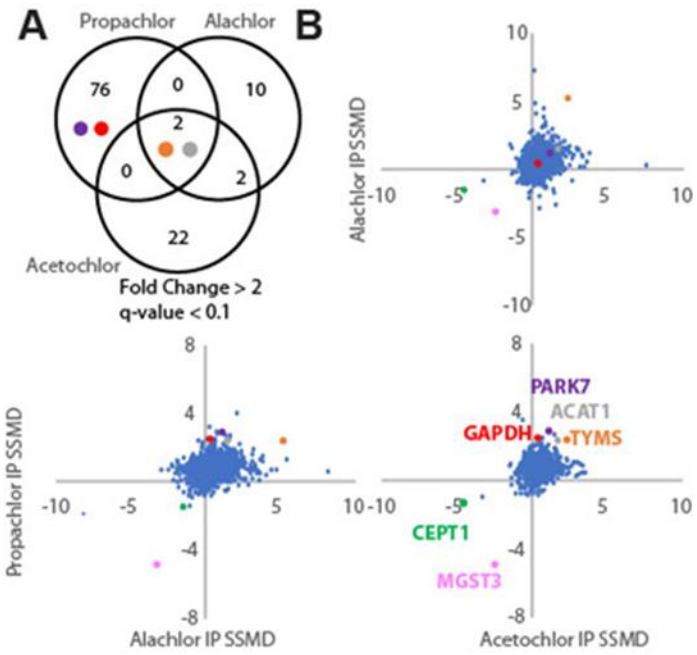

Figure 3: Comparison of proteome-wide Hsp40 affinity changes from the three chloroacetanilide herbicide treatments. **A.** Comparison of the most impacted proteins and **B.** Comparison of Strictly Standardized Mean Differences (SSMDs; treatment vs. control).

Choline /ethanolaminephosphotransferase 1 (CEPT1) and microsomal glutathionine S-transferase 3 (MGST3) on the other hand bind less to DNAJB8^{H31Q} after treatment with each herbicide. These two enzymes would appear to be susceptible to electrophilic modification as both proteins utilize cysteines to bind to a unique substrate such as glutathione for MGST3 and ethanolamine phosphate for CEPT1[63,64]. Nevertheless, the unusual increase in stability against all three conditions makes them possible protein targets for dysregulation as a treatment to suppress the toxic effects from each herbicide[65].

Each DNAJB8^{H31Q} profile was additionally enriched with proteins prone to covalent modification from electrophiles. Streamlined Cysteine Activity-Based Protein

Profiling (SLC-ABPP) was used to profile large electrophilic libraries against HEK293T cells and thus provided a reference of proteins with cysteines prone to modification[66]. High amounts of reactive proteins predicted to be modified by electrophiles were recognized by DNAJB8^{H31Q} (**Figure S6**). About 60% of DNAJB8^{H31Q} interactors for each herbicide-stressed proteome were demonstrated to form electrophilic adducts. During each IP analyzed, 50% of the FASTA database were selected as decoys, indicating that an even higher number of proteins may be prone to modification[23]. Within each herbicide-affected proteome, few proteins with herbicide adducts were discovered (**Figure 2**). Low numbers of proteins with herbicide adducts identified in previous DDA runs could be due to the method not selecting or missing different subsets of modified proteins for detection[67].

Protein misfolding is a necessary intermediate step for protein aggregation[68,69], and all misfolded proteins have the potential to aggregate[70]. The increase in protein misfolding following propachlor exposure could also lead to an increase in aggregation. We used ultracentrifugation to isolate the insoluble proteome following cellular propachlor exposure (**Figure 4, Supplementary Table 4**). Cells were allowed to recover 6 h post-treatment to allow misfolded proteins time to partition towards an aggregated state. Nearly all detected proteins aggregate more in response to cellular propachlor exposure (**Figure 4** and **Figure S7**). Propachlor treatment has no significant effect on the total protein abundances, suggesting that the cellular proteome is not meaningfully remodeled over this time-scale (**Figure S8**).

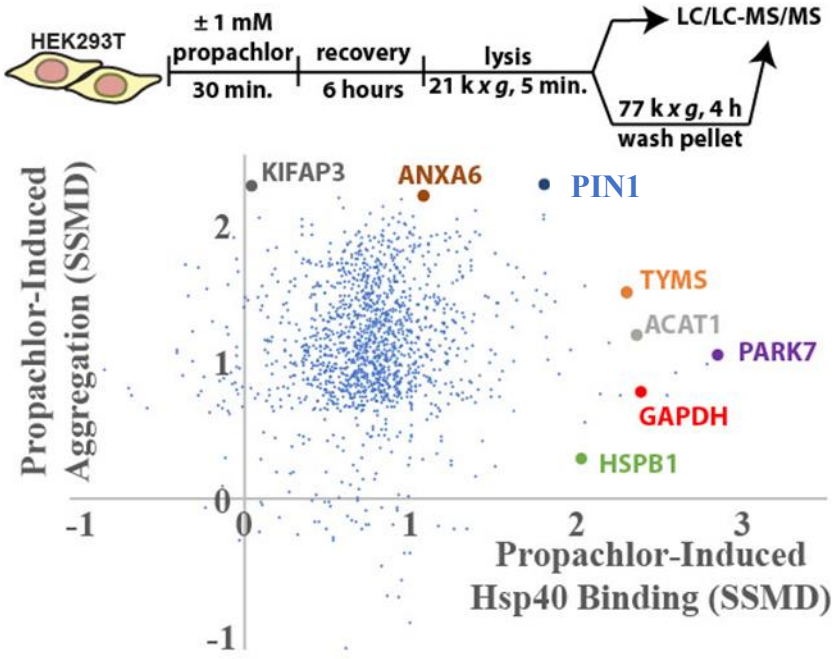

Figure 4: Aggregation of cellular proteins in response to propachlor exposure. HEK293T cells were treated as indicated, lysed, pre-clarified by centrifugation, and the lysates normalized to total protein. Protein aggregates were further prepared by ultracentrifugation (6 biological replicates for each treatment condition). The plot compares the change in aggregate levels for each protein to the change in Hsp40 binding (from **Figure 2**) for proteins identified in both sets of experiments (1477 proteins). Volcano plots for both propachlor-dependent changes in the total and aggregated proteome are in **Figures S7 and S8**.

Despite both aggregation and Hsp40 affinity increasing across a majority of the observed proteome after cellular propachlor exposure, there is no meaningful correlation between these two factors. This is consistent with a previous study that found that stress-dependent protein aggregation does not correlate with solubility across diverse stresses[71]. The vesicular trafficking proteins[72,73]: SMAP2, GAK, CLTA, CLTB, CLTC, CLTC1, AP1B1, AP1M1, EPS15, and CLINT1 all substantially lose solubility in response to propachlor treatment, but this network only modestly increases its DNAJB8 affinity. These proteins rely on Hsp70 for clathrin disaggregation, but GAK serves as a dedicated

Hsp40 co-chaperone (except in the brain, where DNAJC6 is expressed)[74,75]. Hence, these proteins may not be particularly surveilled by promiscuous Hsp40 such as DNAJB8. These proteins may have lower thresholds for aggregations in comparison to the most significant DNAJB8 interactors that wouldn't be overcome in thirty minutes of propachlor treatment[76].

The susceptibility of GAPDH to propachlor modification prompted further investigation into its pathway as a mechanism for propachlor toxicity. GAPDH is highly abundant in the human proteome and multifaceted in many roles including glycolysis[77]. The abundance and interactome of GAPDH could make the enzyme a dangerous precursor to propachlor toxicity similar to how known misfolded proteins can aggregate in known neurodegenerative diseases[78,79]. GAPDH was more bound to DNAJB8^{H31Q} possibly because it was recognized by the bait as misfolded protein and thus could follow as similar pathology.

Direct modification of GAPDH at its active site and evidence of destabilization around peptides used for reduction of NAD for propachlor can provide structural credence for the protein to be recognized by DNAJB8. GAPDH has been found to be covalently modified at its active cysteine by electrophiles such as 4-hydroxynonal and methylglyoxal as confirmed by mass spectrometry[80,81]. We used PRM to search for the modified cysteine in propachlor treated lysate (**Figure 5**).

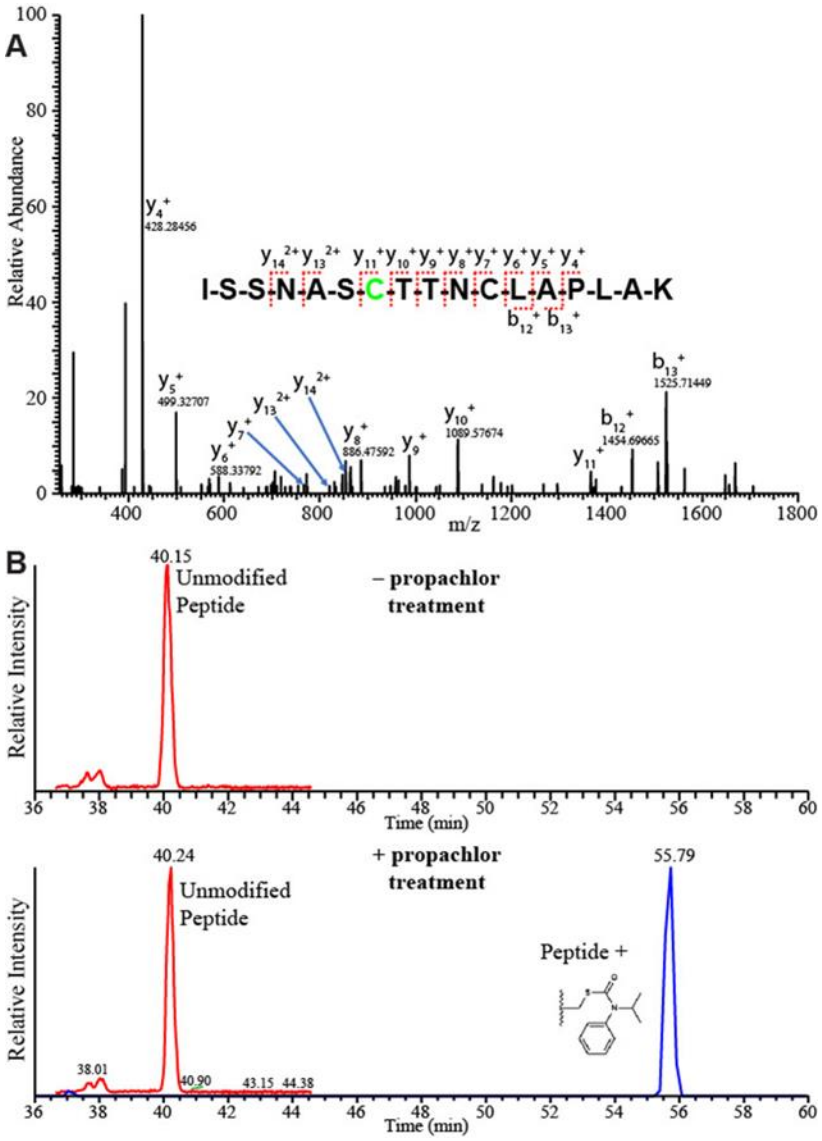

Figure 5: Propachlor modifies a catalytic cysteine in the active site. A) MS2 fragmentation spectrum obtained from LC-MS/MS shotgun proteomics analysis of lysate collected from propachlor treated (1 mM, 30 min., serum-free media) HEK293T cells. This peptide is modified at the C152 position with an adduct that corresponds to propachlor thiocarbamate. B) PRM chromatograms demonstrating the dependence of the adduct on propachlor treatment.

We did not find evidence for propachlor adducts on C156.The propachlor adduct at cysteine 152 was found in only propachlor-treated lysate compared to the control and

thus provides evidence of direct covalent modification of GAPDH (**Figure 5**). However, the integration of the unmodified peptide IISNASCTTNCLAPLAK does not substantially decrease with propachlor treatment; the abundance fold change (treated/untreated) by PRM is 1.09 ± 0.07 s.e.m (n = 3). Thus the stoichiometric yield of GAPDH modification at C152 is not enough to meaningfully deprive the cell of GAPDH function.

Peptides around the active cysteine of GAPDH could change its orientation as part of an overall change in conformation after propachlor treatment. Several peptides around the active site utilize hydrogen bonding to help NAD bind to GAPDH and an inhibited active site can make them inactive as well[82]. We previously used limited proteolysis an orthogonal assay to validate and characterize stress-induced misfolded proteins to DNAJB8[20]. We selected peptides from GAPDH for LiP to assess structural changes after propachlor treatment. If propachlor treatment decreases the amount of a targeted peptide recovered after Proteinase K (PK) proteolysis, then the treatment destabilized the protein in vicinity of the peptide[83]. We found several GAPDH peptides to be more proteolytically sensitive to proteinase K after propachlor treatment (**Figure 6 and Figure S9**), including the active site peptides LVINGNPITIFQER, LISWYDNEFGYSNR, VGVNGFGR. Hence, propachlor induces a more extended conformation in GAPDH, consistent with destabilization. Destabilization of GAPDH could also decrease likelihood of protein-protein interactions.

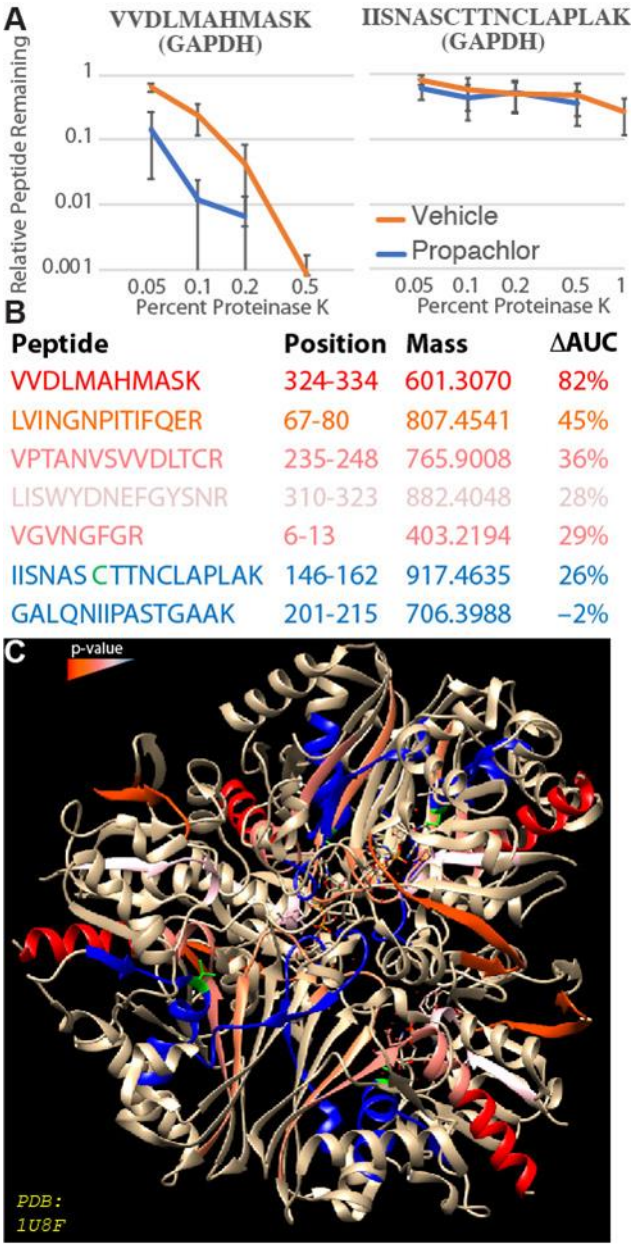

Figure 6: Propachlor destabilization of GAPDH peptides measured by limited proteolysis (LiP). A) LiP-PRM traces illustrating the proteolytic susceptibility of two GAPDH peptides following cellular treatment with propachlor (blue) or vehicle (orange) as indicated. B) Characteristics of the analyzed GAPDH peptides are described. ΔAUC refers to the decrease in the area under the curve for the proteolytic susceptibility curves. C) The GAPDH peptides are colored according to the significance of the effect of propachlor treatment on proteolytic susceptibility. C152 is indicated in green. The structure (PDB: 1U8F) is taken from Jenkins et al.[84] PRM chromatograms are in the Appendix.

Misfolding in the vicinity of the LVINGNPITIFQER peptide in GAPDH may prevent the enzyme from interacting with extracellular vesicles (EV) such as such as phosphatidylserine (PS)[85,86]. Lack of interaction from GAPDH could lead decrease in EV activity such as regulating immune response and metastasis of cancer cells[87].

Propachlor treatment may impair the GAPDH ability to reduce NAD and ability to assist and regulate other proteins. Propachlor treatment could also compromise the GAPDH tetrameric structure and ability to interact with other proteins. VPTANVSVVDLTCR, a peptide involved in the dimer interface of GAPDH, was found to be destabilized after propachlor treatment[88]. Mutations in this peptide are associated with conformational changes at the dimeric interface[82] and a loss of tetrameric stability[87]. Evidence of destabilization of VPTANVSVVDLTCR in GAPDH may show that propachlor treatment may inhibit formation of its active conformation.

We used also used limited proteolysis to explore for PARK7. We were only able to find three peptides in PARK7 that gave robust PRM signals; each is far from the active site[89] and none show evidence of differential stability (**Figure S9**), nor did we find evidence for modification of the catalytic cysteine 106 from PRM analysis. It is possible that PARK7 undergoes conformational changes in regions that we could not profile by LiP.

Protein destabilization can lead to both gain-of-function (toxic conformations) and loss-of-function. GAPDH activity has previously been shown to decrease in response to methylglyoxal and copper exposures, presumably due to conjugate and oxidation respectively[90,91]. We evaluated GAPDH activity in cells treated with propachlor. GAPDH

activity in lysates was measured using a colorimetric assay for NAD^+ reduction in the presence of substrate.

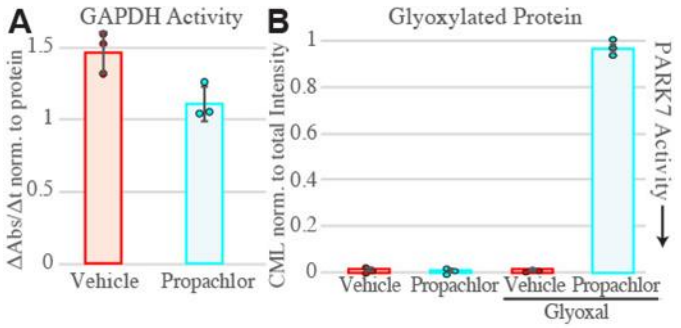

Figure 7: A) Activity of GAPDH from cells treated with propachlor or vehicle. Activity was determined from the NADH production rate in lysates, as measured by colorimetry at 450 nm over the linear range, and normalized to total protein (g/mL) as determined by Bradford assay. $p < 0.05$ by Student's t-test, $n = 3$). Kinetic traces are in **Figure S10**. B) Inactivation of PARK7 determined by total anti-carboxymethyllysine (CML) densitometry of SDS-PAGE separated lysates. HEK293T cells were treated for 30 min. with vehicle or propachlor (1 mM in serum-free media), followed by 2 h treatment with vehicle or glyoxal (4 mM) and immediate lysis ($n = 3$). 2-way ANOVA yields $F = 1909 > F_{crit} = 4.07$, and Tukey's HSD finds propachlor + glyoxal condition mean differences compared to all other conditions exceeds the q_{crit} for 0.001.

Treating HEK293T cells with 1 mM propachlor for 30 minutes decreased GAPDH activity by 25% (**Figure 7A**). It is surprising that we see substantial inhibition, as we do not see a clear decrease in the levels of unmodified GAPDH. The two catalytic sites of GAPDH exhibit strong negative cooperativity[92]. If modification at a single site is sufficient to inactivate the tetramer, 25% inhibition requires modification of 7% of the monomers. A more likely scenario is that other modifications to GAPDH are driving the loss of activity, that GAPDH is aggregating, or that other damaged proteins lead to pleiotropic loss of GAPDH activity. Aggregation of misfolded GAPDH can thus be a downstream effect of propachlor stress on the cell[93,94]. Our proteomic characterization of

propachlor-induced aggregation found an increase in GAPDH aggregation induced by propachlor treatment (FC in aggregates = 4.9, q = 0.008; **Figure S7**). Similar results were obtained from Western Blot analysis assessing the levels of GAPDH in the pellet fraction after ultracentrifugation (**Figure S11A**), however there is no significant depletion of total GAPDH (**Figure S11B**).

Alternatively, PARK7 is a chaperone-like peptidase that can repair methylglyoxal and glyoxal-glycated amino acids, including the cysteines of GAPDH[95]. PARK7 was also significantly destabilized after propachlor treatment and thus could be inactive. If propachlor inhibits PARK7 deglycase activity, that could lower the activity and promote the misfolding of cysteine-containing proteins such as GAPDH. A cellular assay designed to quantify PARK7 ability to deglaciate glyoxal modified proteins in HEK293T cells had been previously established[30].

We measured PARK7 ability to degylcase glyoxal-modified proteins after incubation with 1 mM propachlor for 30 minutes (**Figure 7B, Figure S10 B,C**). In the presence of propachlor, the intensity of proteins converted to carboxy-methyl-lysine after glyoxal treatment increased significantly in comparison with the control experiment (DMSO). Propachlor was thus proposed to inhibit the activity of PARK7 glycation of proteins as seen in other inhibitor treatments[30]. Cellular exposure of propachlor thus inhibits PARK7's ability to deglycate damaged proteins offering an alternative mechanism by which propachlor exposure can induce protein misfolding beyond direct modification.

3.5 Supplemental Discussion on Limited Proteolysis

We measured assay precision across technical and biological replicates according to previous experiment[20]. To determine the reproducibility of the scheduled PRM assay itself, ten consecutive injections of a lysate tryptic digest were performed to determine the reproducibility of the scheduled PRM assay. CVs calculated for the integrated fragment intensities of the 10 targeted peptides from a trypsin only digested lysate. Each targeted run included a 6 µg injection, a 8 minute retention time window for each peptide, and chromatograms that were scanned at 7500 nominal resolving power. The low resolving power was chosen to minimize cycle time. Lower cycles times allow more scans across peaks, increasing robustness of quantification[96]. The MS2 intensities of transitions from a precursor ion were integrated by Skyline for quantification of each peptide. The median CV for the summed transitions MS2 among the 10 targeted peptides was 20%. The median CV for the summed MS2 transitions was 12% (**Supp. Table 5**). These CVs are typical for PRM[20,97].

PRM runs at 60,000 nominal resolving power were run to compare to the runs at 7500 nominal resolving power. We performed 6 more technical replicate PRM experiments on a HEK239T tryptic digest using 60,000 nominal resolving power and scheduled only three select peptides. The three selected peptides had 10 minute retention time windows that did not overlap with each other to minimize cycle times. The calculated CV from the six runs were compared with the quantification of the previous measurements that were run at 7500 resolution. The median CV for the summed

transitions MS2 among the 3 targeted peptides was 7 (**Supp. Table 6**). Higher resolving power hence did not meaningfully improve the precision of the method.

The CV between biological replicates was addressed during the LiP mass spec runs. The LiP mass spec samples included three zero PK controls and the following Protein: PK samples: 2000:1, 1000:1, 500:1, 200:1, and 100:1. Peptides were scanned in 10 minute retention time windows at 7500 resolution after a 6 μg HEK293T tryptic digest injection. The CV was calculated among the three Zero PK samples for both propachlor exposed and control cellular conditions. Across these biological replicates, median CV values were below 15% (**Supp. Table 7**). CV values were comparable compared to previous experiments[20].

3.6 Conclusion

In summary, we present profiles of destabilized proteomes in response to different herbicide stresses. The DNAJB8^{H31Q} assay identified destabilized proteins based on cellular recognition and increased binding to the molecular chaperone. Proteins susceptible to covalent modifications such as TYMS and ACAT1 were commonly destabilized after exposure from all three herbicides and several proteins such as GAPDH and PARK7 were significantly destabilized depending on the type of stress. We believe our AP-MS strategy can be comparable to other proteome wide electrophilic modification assays as DNAJB8^{H31Q} pulled down significant amounts of predicted reactive proteins. Furthermore, we incorporated limited proteolysis and protein activity assays to profile a propachlor effected pathway through GAPDH. Although the exact connection between

misfolded GAPDH and propachlor toxicity is unknown, we believe that our platform can highlight possible protein candidates of cellular stresses. Therefore, we believe our platform is viable for the initial screening of a damaged proteome as part of an overall workflow to identifying protein targets from the effects of environmental toxins and toxicants. We also believe that our platform can be effective in identifying proteins that are damaged and modified after electrophilic exposure.

3.7 Supplementary Figures

3.7.1 Representative Immunoblots after Propachlor and Alachlor Exposure:

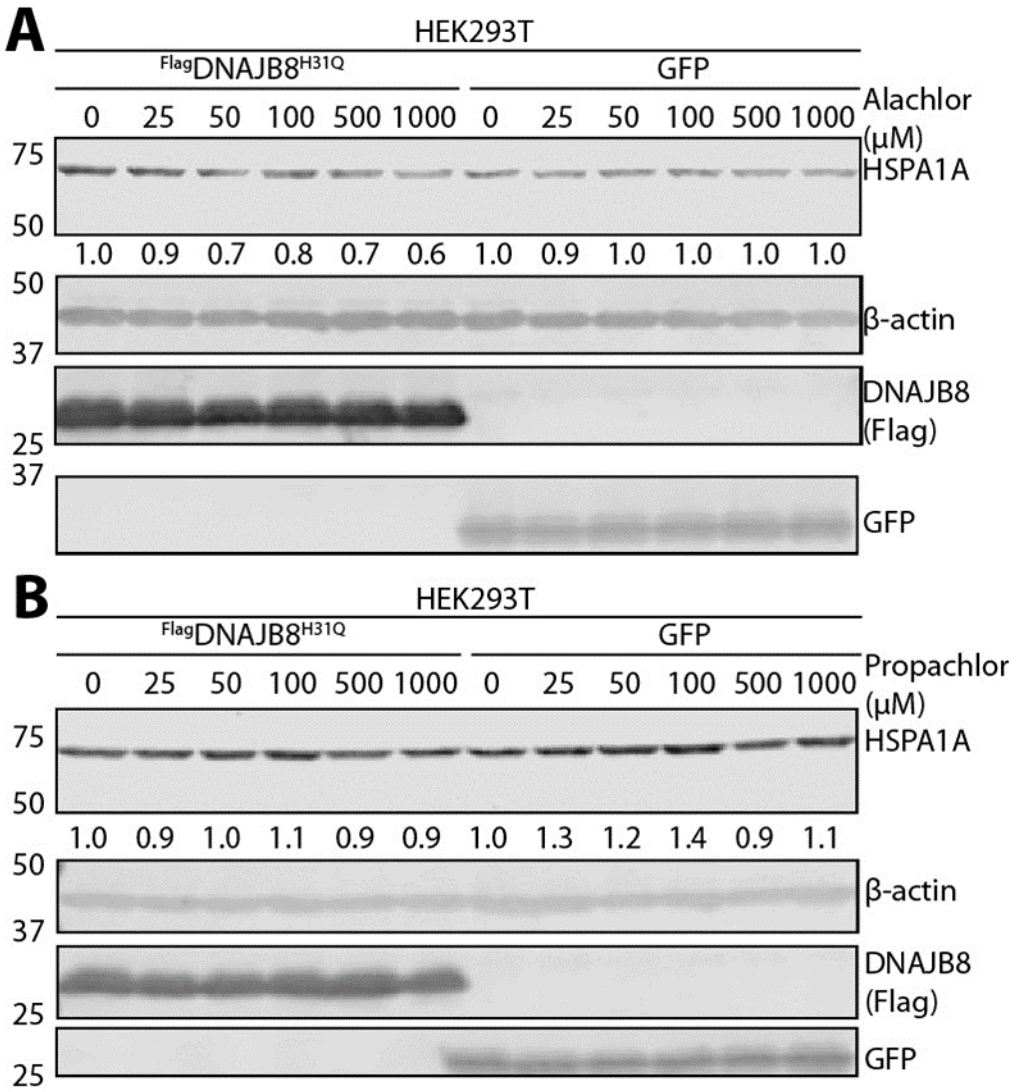

Figure S1: Representative immunoblots after Propachlor or Alachlor Exposure. SDS-PAGE separated lysates from HEK293T cells expressing the indicated proteins and treated with alachlor (A) or propachlor (B) in serum-free media for 30 min., followed by a 16 h recovery. Induction of the HSR target HSPA1A in response to acetochlor treatment is a proxy for the level of HSR activation. HSPA1A density is below the blot slice. Molecular weight markers are indicated on the left. Antigens targeted by immunoblotting are listed to the right of the slice.

3.7.2 Resazurin Assay after Propachlor Exposure:

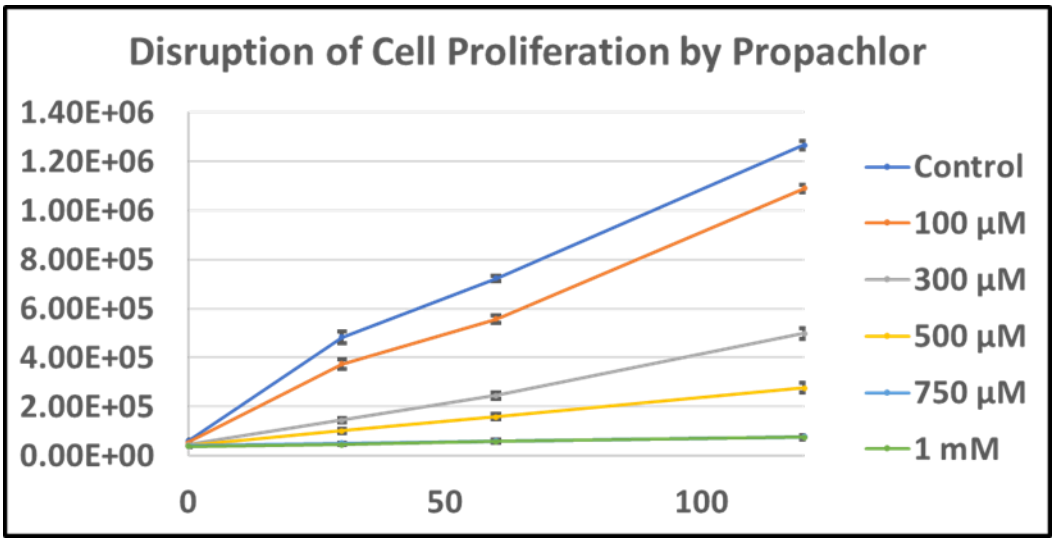

Figure S2: Effect of propachlor on cell growth in HEK293T Cells. HEK293T cells were seeded in 64 wells of a 96 well plate. Each well had 50,000 cells and eight wells were treated with each condition respectively. Standard error is shown as error bars. Each row was treated with the indicated concentration of propachlor in serum-free media for 30 min., followed by a 16 h recovery. Resazurin dye was added to each well and measurements were taken at 0, 1, and 2 h post-recovery. Propachlor disrupts cell proliferation of HEK293T cells.

3.7.3 Volcano Plot for Profiling DNAJB8^{H31Q} Affinity After Acetochlor Exposure:

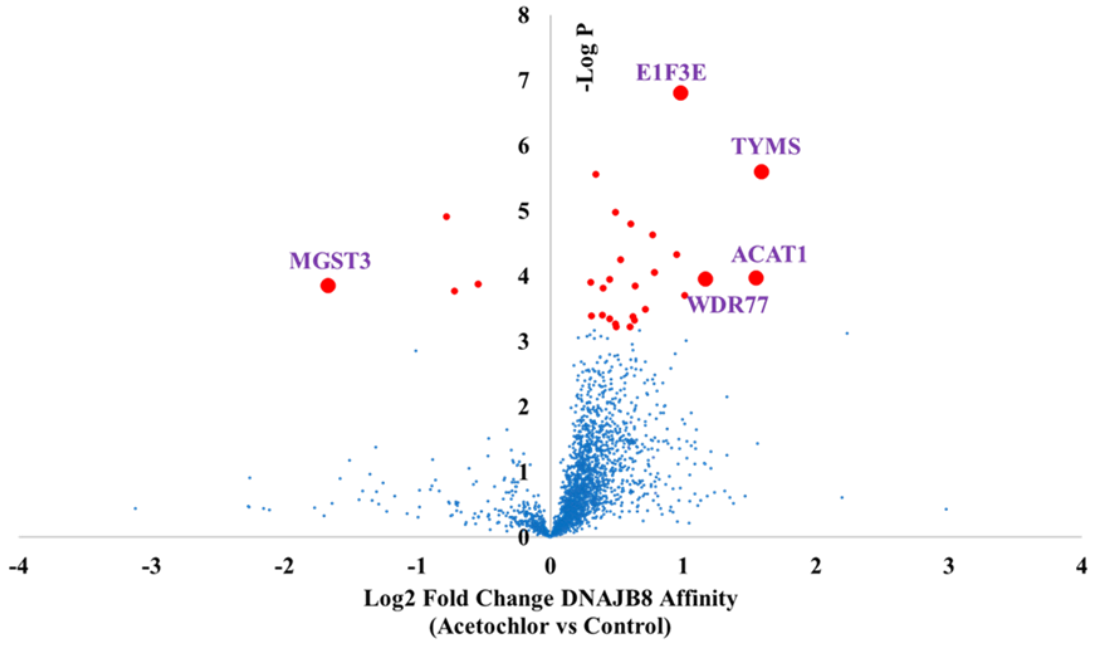

Figure S3: Volcano plot for profiling DNJAB8^{H31Q} affinity in response to cellular acetochlor exposure. 1 mM acetochlor treatment for 30 min increases the affinity of a subset of proteins with DNAJB8^{H31Q}. A DNAJB8^{H31Q} pulldown experiment consists of three transfected HEK293T cells treated with 1 mM acetochlor for 30 min in serum-free media and three plates treated with vehicle (DMSO), followed by immediate lysis. Red dots represent proteins with significantly increased interaction with DNAJB8^{H31Q}, using a false discovery rate threshold (FDR) of 0.05 (n = 12 biological replicates in 4 TMT-AP-MS runs).

3.7.4 Volcano Plot for Profiling DNAJB8^{H31Q} Affinity After Alachlor Exposure:

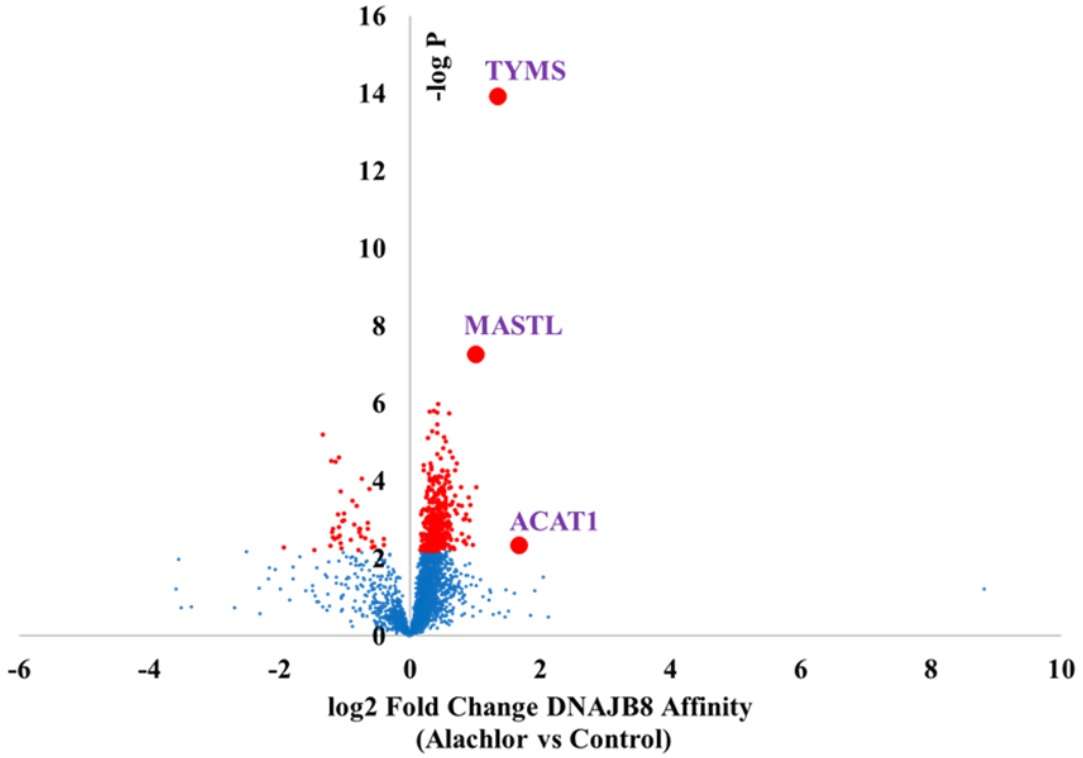

Figure S4: Volcano plot for profiling DNJAB8^{H31Q} affinity in response to cellular alachlor exposure. 1 mM alachlor treatment for 30 min increases the affinity of a subset of proteins with DNAJB8^{H31Q}. A DNAJB8^{H31Q} pulldown experiment consists of three transfected HEK293T cells treated with 1 mM alachlor for 30 min in serum-free media and three plates treated with vehicle (DMSO), followed by immediate lysis. Red dots represent proteins with significantly increased interaction with DNAJB8^{H31Q}, using a false discovery rate threshold (FDR) of 0.05 (n = 12 biological replicates in 4 TMT-AP-MS runs).

3.7.5 Volcano Plot for Profiling DNAJB8^{H31Q} Affinity after Propachlor Exposure:

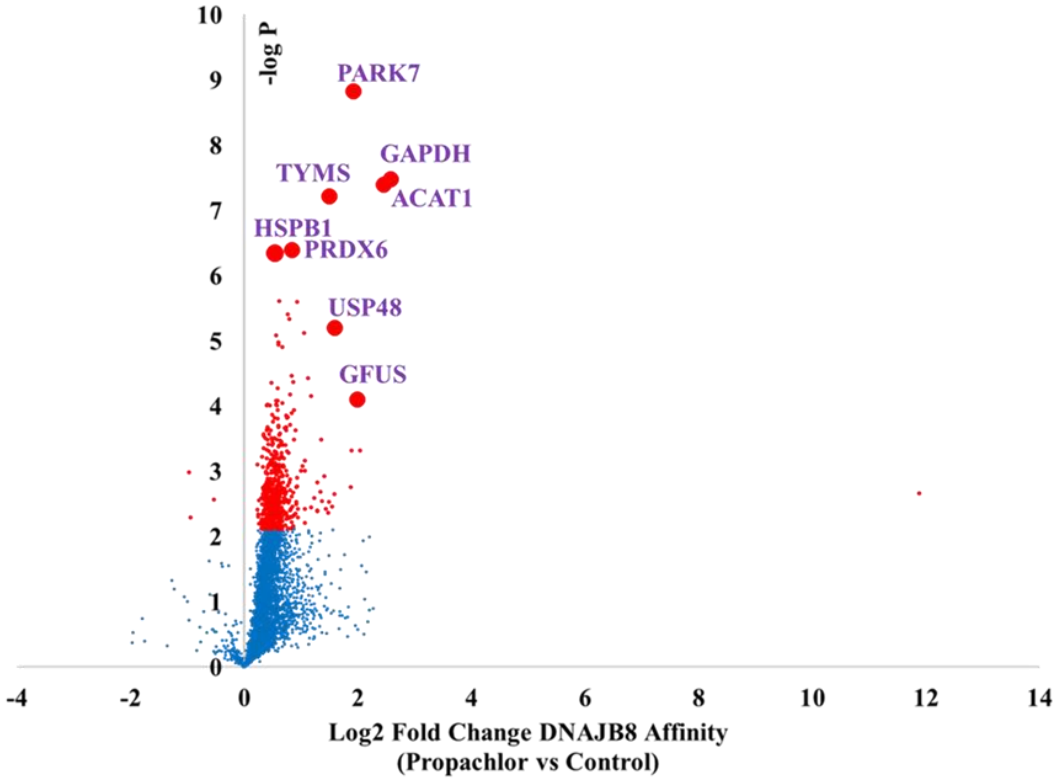

Figure S5: Volcano plot for profiling DNJAB8^{H31Q} affinity in response to cellular propachlor exposure. 1 mM propachlor treatment for 30 min increases the affinity of a subset of proteins with DNAJB8^{H31Q}. A DNAJB8^{H31Q} pulldown experiment consists of three transfected HEK293T cells treated with 1 mM propachlor for 30 min in serum-free media and three plates treated with vehicle (DMSO), followed by immediate lysis. Red dots represent proteins with significantly increased interaction with DNAJB8^{H31Q}, using a false discovery rate threshold (FDR) of 0.05 (n = 12 biological replicates in 4 TMT-AP-MS runs).

3.7.6 Volcano Plots Comparing iodoacetamide-reactive vs. non-reactive proteins:

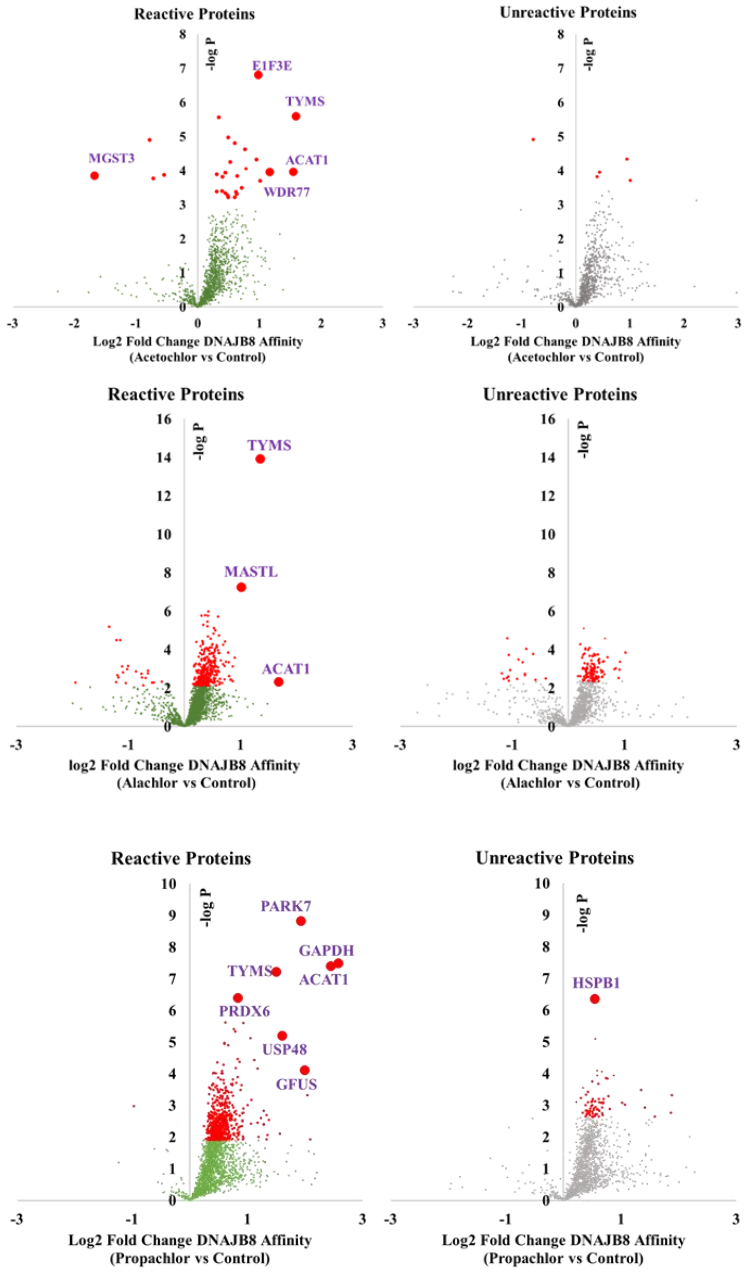

Figure S6: DNAJB8 affinity profiles for iodoacetamide-reactive vs. non-reactive proteins. Iodoacetamide reactivity is based on the electrophilic reactivity library of Kuljanin et al.[42]. Iodoacetamide-reactive proteins are on the left; the remaining proteins are on the right. Red dots represent proteins with significantly increased interaction with DNAJB8^{H31Q}, using a false discovery rate threshold (FDR) of 0.05 (n = 12 biological replicates in 4 TMT-AP-MS runs).

3.7.7 Volcano Plot for Pellet fraction after Propachlor Exposure:

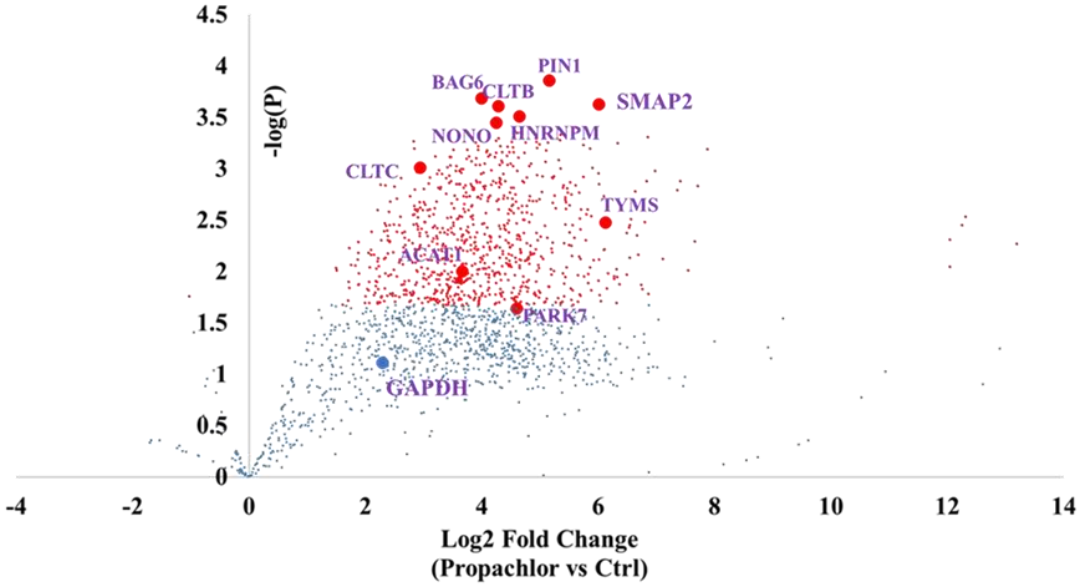

Figure S7: TMT analysis of Pellet Fractions. 10cm plates of HEK293T cells were treated with either 1mM propachlor or vehicle (DMSO) for 30 minutes. After 6 hours of recovery and ultracentrifugation, 12 Insoluble fractions were labeled and analyzed with TMT. P values were moderated from R calculations[31]. 826 Proteins were found to significantly aggregate according to Benjamini-Hochberg analysis including previously identified DNAJB8^{H31Q} interactors such as ACAT1, PARK7, and TYMS. SMAP2 is involved in vesicular trafficking with Clarathin Heavy chain (CLTB) and both significantly more abundant in the insoluble fraction of propachlor-treated lysate[98]. GAPDH was not the most significant protein aggregating into the pellet fraction (n=6 biological replicates).

3.7.8 Volcano Plot for Total Fraction after Propachlor Exposure:

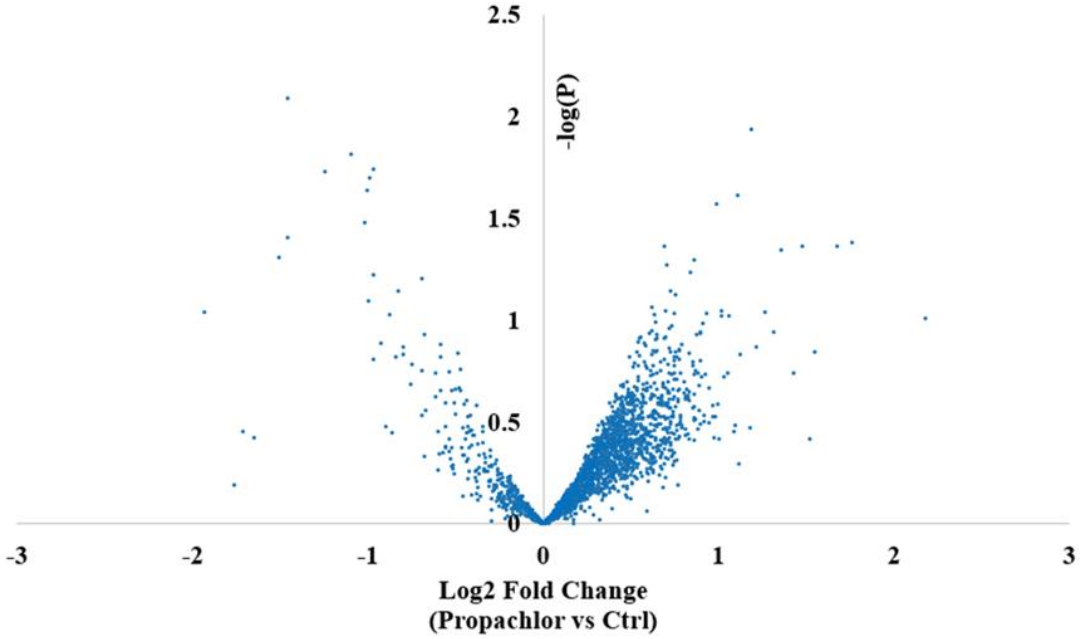

Figure S8: Initial TMT analysis of ultracentrifugation data. Ten cm plates of HEK293T cells were treated with either 1mM propachlor or vehicle (DMSO) for 30 minutes. Samples were lysed after 6 hours of recovery and aliquots were taken out and labeled with Tandem Mass Tags (TMT) and run by MUDpit. P values were moderated from using Kammer's algorithm on R[31]. No proteins were found to be significantly aggregating in the total protein fraction (n=6 biological replicates).

3.7.9 Limited Proteolysis Scheme and Susceptibility Curve:

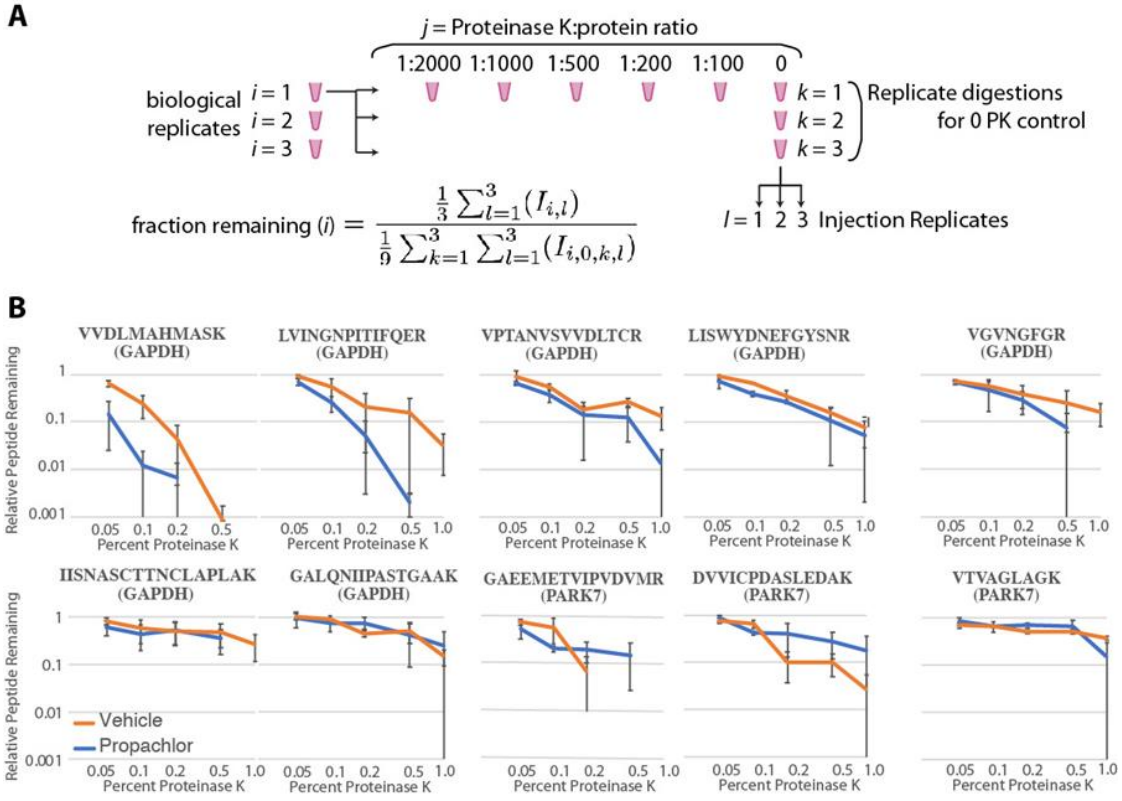

Figure S9: Sample Set up for Limited Proteolysis and Protease Susceptibility Curves. A) Schematic set-up for limited proteolysis experiments. B) Proteinase K susceptibility curves for 10 peptides from GAPDH and PARK7.

3.7.10 Activity Assays for GAPDH and PARK7 Function in propachlor treated cells:

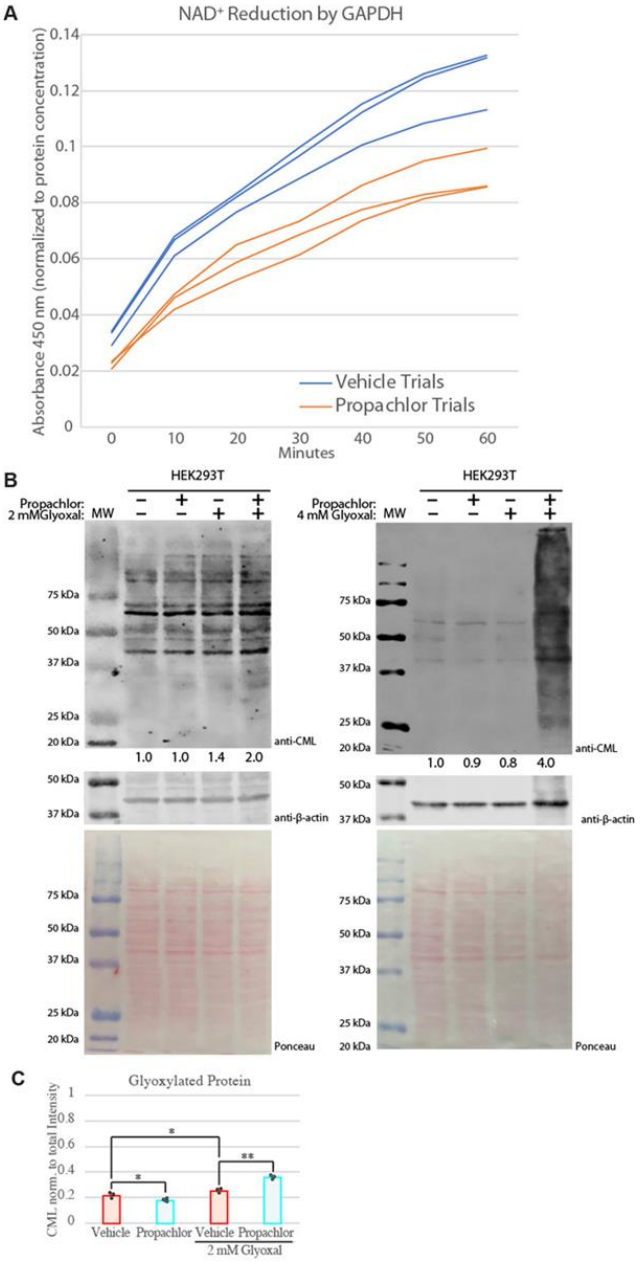

Figure S10: Representative Results for GAPDH and PARK7 Activity Assays. A) Kinetic Traces of GAPDH activity assay are shown. B) Two Representative western blots of PARK7's degylcase activity are shown. Corresponding ponceau stains can be seen below each blot. Predicted weights for antibodies are shown on the right. Protein modified by carboxy methyl lysine (CML) are shown on the top slice. Numerical values below anti CML are band intensities normalized to untreated sample. C) Effects of 2 mM glyoxal treatment after 1 mM propachlor treatment on degylcase activity are shown.

3.7.11 Representative Western Blots for analysis of GAPDH:

A

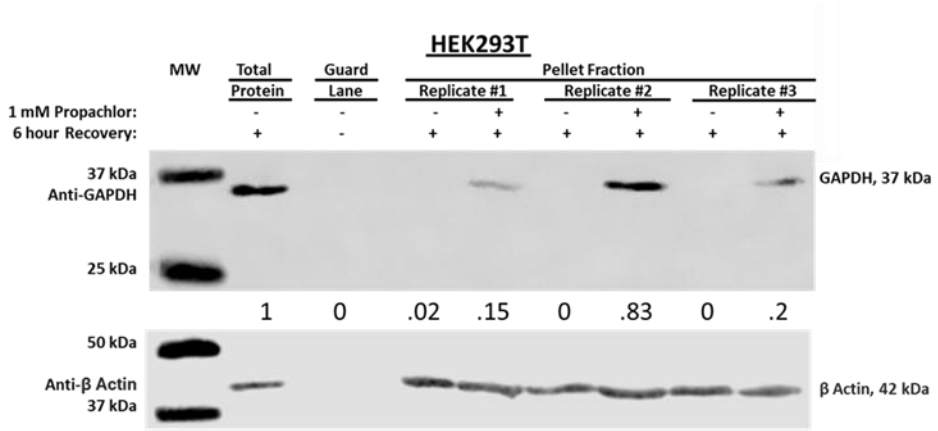

B

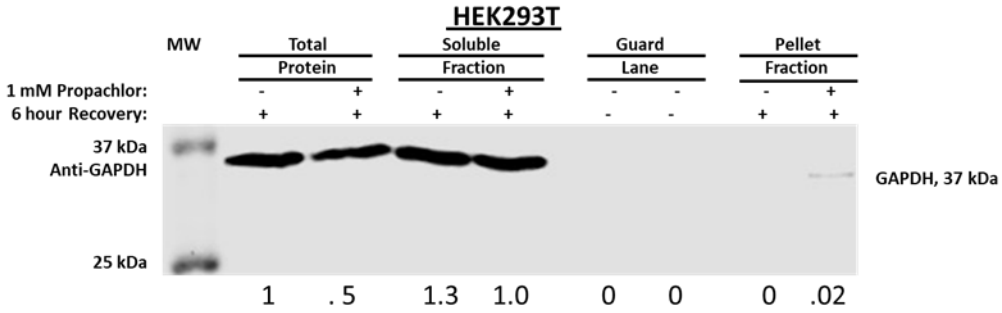

Figure S11: Representative Western Blots Comparing Different Fractions after Ultracentrifugation. A. Representative Western Blot analysis of GAPDH among three biological replicates looking at 30% of the pellet fraction. 30% of each insoluble fraction from three biological replicates was loaded and ran on 10% SDS page gels. Western Blots were blotted for GAPDH and β-Actin. Predicted weights for antibodies are shown on the right. Numerical values below anti-GAPDH slice are band intensities normalized to the total fraction. GAPDH is significantly more present in propachlor treated insoluble fractions. B. **Representative Western Blot comparing 1.6 % of initial total protein, soluble fraction, and insoluble fraction in one biological replicate**. 1.6% of each fraction was loaded into each lane. Predicted weights for antibodies are shown on the right. GAPDH bands were normalized to the total protein band in untreated sample. The amount of GAPDH does not significantly decrease from total protein to soluble fraction after ultracentrifugation. Small amounts of GAPDH can be seen in the pellet fraction for propachlor-treated sample.

3.7.12 Representative Silver Stains for each Herbicide IP

3.7.12.1 Representative Silver Stain for an Acetochlor IP:

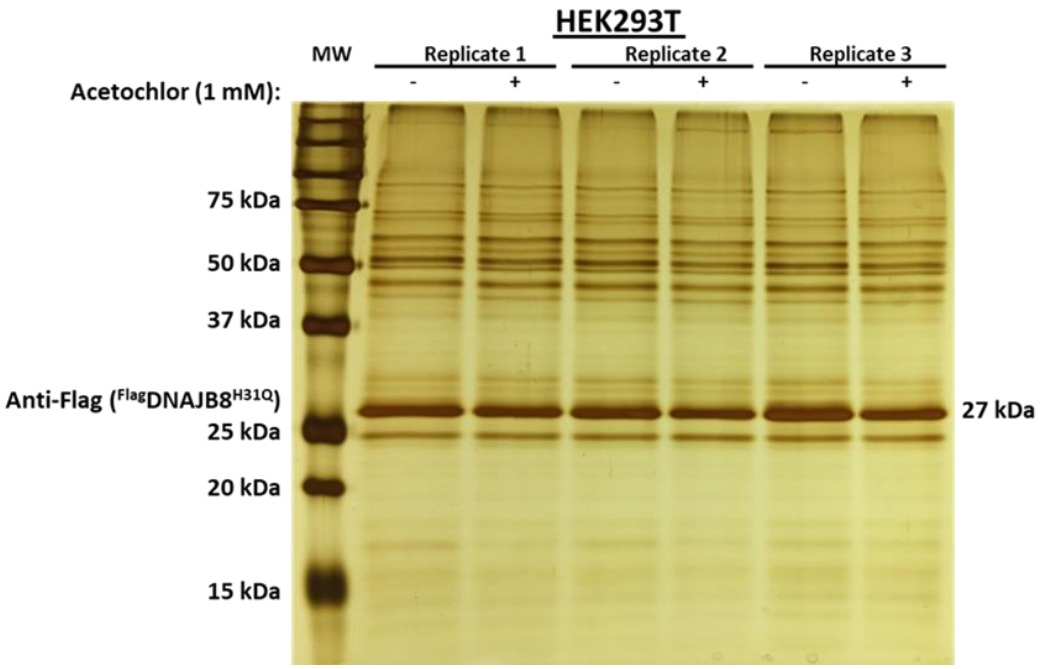

Figure S12A: Representative Silver Stain for an Acetochlor AP-MS. Each replicate contained two transfected ^{FLAG}DNAJB8^{H31Q} 10 cm plates treated with either 1 mM Acetochlor or DMSO (control) for thirty minutes. Three replicates are stained to show bait and visually show differences in prey after each respective pulldown. ^{Flag}DNAJB8^{H31Q} is the most abundant protein in each replicate after the immunoprecipitation. Other bands represent proteins recovered with DNAJB8.

3.7.12.2 Representative Silver Stain for an Alachlor IP:

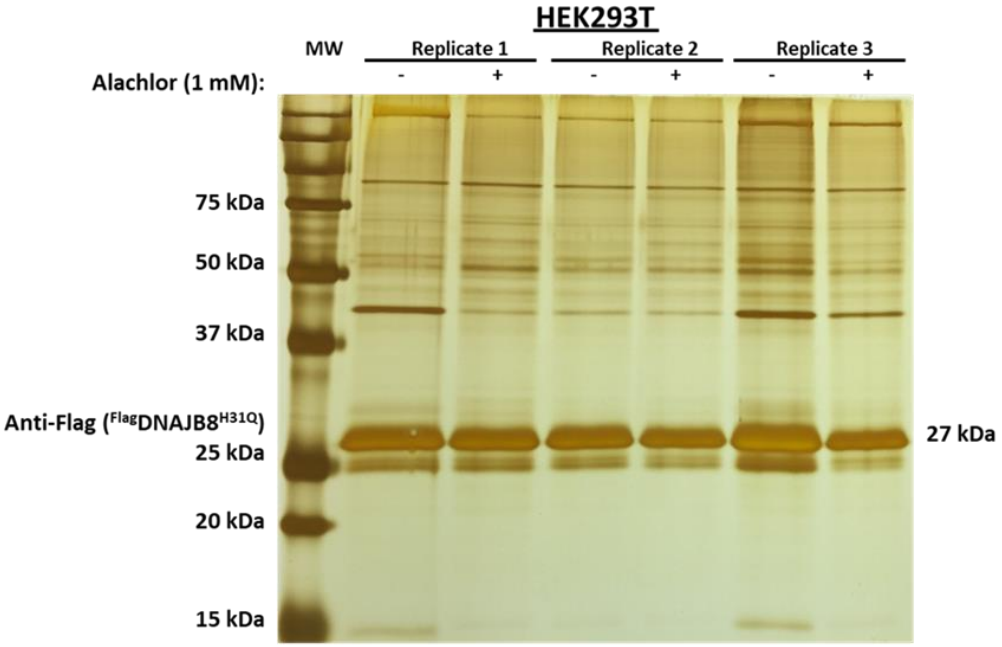

Figure S12B: Representative Silver Stain for an Alachlor AP-MS. Each replicate contained two transfected ^{FLAG}DNAJB8^{H31Q} 10 cm plates treated with either 1 mM Alachlor or DMSO (control) for thirty minutes. Three replicates are stained to show bait and visually show differences in prey after each respective pulldown. ^{Flag}DNAJB8^{H31Q} is the most abundant protein in each replicate after the immunoprecipitation. Other bands represent proteins recovered with DNAJB8.

3.7.12.2 Representative Silver Stain for a Propachlor IP:

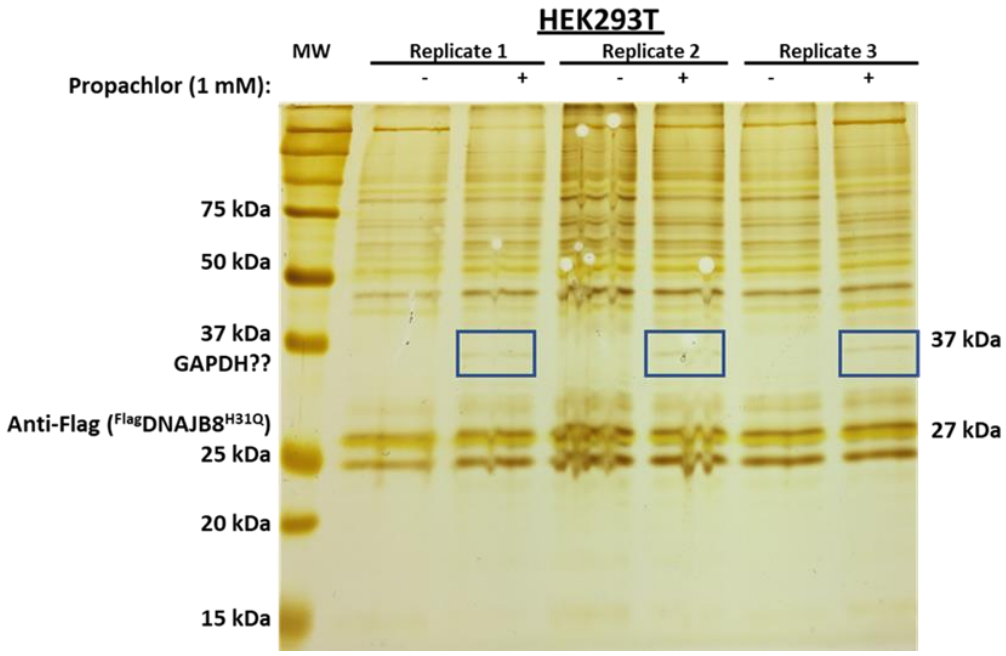

Supporting Figure 12C: Representative Silver Stain for a Propachlor AP-MS. Each replicate contained two transfected $^{Flag}DNAJB8^{H31Q}$ 10 cm plates treated with either 1 mM Propachlor or DMSO (control). Three replicates are stained to show bait and visually show differences in prey after each respective pulldown. $^{Flag}DNAJB8^{H31Q}$ is the most abundant protein in each replicate after the immunoprecipitation. Other bands represent proteins recovered with DNAJB8. A protein around 37 kDa is more abundant in propachlor treated samples and could be GAPDH.

3.8 Supplementary Tables

3.8.1 Discussed DNAJB8^{H31Q} Interactors after Acetochlor Treatment:

Gene	Combined ttest	Combined Fold Change	Standard Deviation	Combined Fold Change	-log p	rank	qvalue BH	qvalue BH	qvalue Storey	SSMD
EIF3E	1.552E-07	1.9668278	0.74199549	0.975870652	6.809003	1	0.000353	0.000353	0.000194	2.176861
TYMS	2.513E-06	3.00285878	2.21225288	1.586336629	5.599821	2	0.002856	0.002856	0.001573	2.366883
PFDN4	1.236E-05	0.580973167	0.09611352	-0.78345656	4.907883	4	0.007025	0.007025	0.00387	-3.24786
ACAT1	0.0001053	2.917263659	1.42709816	1.544615781	3.977388	10	0.023945	0.020229	0.011142	1.702633
WDR77	0.0001101	2.245430485	1.32958564	1.166992059	3.958112	11	0.022756	0.020229	0.011142	1.35577
MGST3	0.000139	0.313127068	0.19093836	-1.67517987	3.857139	15	0.021056	0.020229	0.011142	-2.43406
SCP2	0.0007541	4.710052009	1.4474387	2.23574299	3.122593	31	0.05529	0.05529	0.030454	5.350315
CEPT1	0.0014346	0.496859041	0.0796429	-1.00909148	2.84327	40	0.081521	0.081521	0.044903	-4.5222
PRMT5	0.0026496	1.87677483	0.9946954	0.90825557	2.576816	60	0.100376	0.093321	0.051402	0.977865

Table S1: DNAJB8^{H13Q} Interactors after Acetochlor Treatment. Selected Proteins interacting with DNAJB8^{H31Q} after acetochlor treatment are highlighted. The complete comprehensive list and definitions can be available with permission.

3.8.2 Discussed DNAJB8^{H31Q} Interactors after Alachlor Treatment:

Gene	Combined ttest	Combined Fold Change	Combined Standard Deviation	log2 Combined Fold Change	-log p	rank	qvalue BH	min qvalue BH	qvalue Storey	SSMD
TYMS	1.1788E-14	2.552003151	1.08507251	1.35163011	13.92856619	1	4.5E-11	4.4888E-11	2.341E-11	5.198596
MASTL	5.5125E-08	2.019558208	0.353586237	1.014039728	7.258651971	2	0.0001	0.00010496	5.474E-05	3.169501
SELENOK	0.00018597	0.477505984	0.055236744	-1.066409282	3.730567458	72	0.0097	0.00969604	0.0048868	-7.6658
CEPT1	0.00032706	0.540050241	0.204757796	-0.888834466	3.485378572	93	0.0132	0.01320179	0.0066536	-1.51707
ACAT1	0.00472993	3.204022412	1.679999868	1.679884239	2.325144866	399	0.0445	0.04438743	0.0223711	1.475754
MGST3	0.00516292	0.259713697	0.063093568	-1.945005995	2.28710447	424	0.04571	0.04571134	0.0230383	-3.20324
ZNF24	0.01377737	1.892716304	0.771913735	0.920458184	1.860833598	677	0.0775	0.07749518	0.0404163	1.217105

Table S2: DNAJB8^{H13Q} Interactors after Alachlor Treatment. Selected Proteins interacting with DNAJB8^{H31Q} after acetochlor treatment are highlighted. The complete comprehensive list and definitions can be available with permission.

3.8.3 Discussed DNAJB8^{H31Q} Interactors after Propachlor Treatment:

Gene	Combined ttest	Combined Fold Change	Combined Standard Deviation	log2 Combined Fold Change	-log p	rank	qvalue BH	min qvalue BH	qvalue Storey	SSMD
PARK7	1.49608E-09	3.799189753	3.056469612	1.92569177	8.825045963	1	5.56391E-06	5.56391E-06	1.67261E-06	2.85284
GAPDH	3.27595E-08	5.973457901	7.343872595	2.578566317	7.484662217	2	6.09164E-05	5.56391E-06	1.67261E-06	2.392085
ACAT1	3.96166E-08	5.461065283	6.444789736	2.449182403	7.402123113	3	4.91113E-05	5.56391E-06	1.67261E-06	2.365232
TYMS	5.97614E-08	2.826939149	1.518711597	1.499240829	7.223579312	4	5.55632E-05	5.56391E-06	1.67261E-06	2.307694
HSPB1	4.47607E-07	1.458249669	0.26401072	0.544237746	6.349103479	6	0.000277442	4.91113E-05	1.47638E-05	2.03593
USP48	6.21598E-06	3.028206617	2.168127388	1.598463645	5.206490517	11	0.002101566	0.001160331	0.000348817	3.51092
MGST3	0.001033027	0.511097049	0.169838062	-0.968330835	2.985888287	142	0.027055125	0.026857534	0.00807387	-4.92914
CEPT1	0.005030253	0.520758565	0.275756868	-0.941313431	2.298410165	441	0.04242066	0.04231434	0.012720471	-1.46062

Table S3: DNAJB8^{H13Q} Interactors after Propachlor Treatment. Selected Proteins interacting with DNAJB8^{H31Q} after acetochlor treatment are highlighted. The complete comprehensive list and definitions can be available with permission.

3.8.4 Discussed Aggregated Proteins after Propachlor Treatment:

Gene	Moderated Pvalue	Neg Log Pvalue	Rank	Fold Change	Log2Fold	SSMD
KIFAP3	0.12494614	0.903277147	1566	59.32991	5.890688	2.270783
ANXA6	0.00070132	3.154084996	45	26.59885	4.733292	2.19311
PIN1	0.00013829	3.859195014	1	35.8587	5.164251	2.280901
GAPDH	0.07765113	1.109852196	1406	4.915972	2.297477	0.764424
ACAT1	0.01214196	1.915711177	613	12.23766	3.613256	1.181592
PARK7	0.02298318	1.638589819	858	24.37351	4.607242	1.03845
TYMS	0.00329248	2.482476775	265	69.59919	6.120999	1.489719
HSPB1	0.49142427	0.308543395	1712	1.696637	0.762678	0.279355
GAK	0.00170901	2.767256329	158	51.21811	5.678582	1.697271
SMAP2	0.00023353	3.631663189	3	64.45806	6.010289	2.170364
CLTA	0.00171704	2.765220673	160	22.4562	4.489042	1.620885
CLTB	0.00024396	3.612675624	4	19.46954	4.283147	2.101491
AP1B1	0.05822704	1.234875295	1274	24.81059	4.632884	0.87482
CLTC	0.00121395	2.915798603	99	8.642908	3.111517	1.702379
CLTCL1	0.00654629	2.184004759	437	10.42533	3.382022	1.47271
AP1M1	0.00385477	2.41400189	303	12.45471	3.63862	1.482254
EPS15	0.00393388	2.405178797	307	10.7607	3.4277	2.139384
CLINT1	0.00063636	3.196294516	32	**7.154927**	**2.838937**	1.860164

Table S4: Aggregated Proteins after propachlor treatment. Selected proteins present in the aggregate fraction are highlighted. The complete comprehensive list and definitions can be available with permission.

3.8.5 Coefficient of Variance of Ten Technical Replicates at 7500 Resolution:

Protein Gene	Peptide Sequence	Precursor Mass m/z	Activation Energy	Retention Time Average	Avg. Intensity	CV
GAPDH	LISWYDNEFGYSNR	882.4048	35	53.79	8.51E+05	6
GAPDH	IISNASCTTNCLAPLAK	917.4635	35	39.83	1.15E+05	5
GAPDH	LVINGNPITIFQER	807.4541	35	58.77	1.38E+06	3
GAPDH	VPTANVSVVDLTCR	765.9008	35	39.17	3.62E+05	34
GAPDH	GALQNIIPASTGAAK	706.3988	35	36.82	4.80E+05	9
GAPDH	VVDLMAHMASK	601.307	35	30.3	6.72E+05	14
GAPDH	VGVNGFGR	403.2194	35	22.86	7.49E+04	14
PARK7	GAEEMETVIPVDVMR	838.4051	35	52.76	7.01E+04	13
PARK7	DVVICPDASLEDAK	766.369	35	52.32	2.01E+05	16
PARK7	VTVAGLAGK	408.2529	35	30.87	8.53E+04	10
					Median CV	11.5
					Average CV	12.4

Table S5: Coefficient of Variance (CV) of Ten Technical Replicates at 7500 Resolution. Calculated CV of targeted peptides are shown. Definitions can be provided with permission.

3.8.6 Coefficient of Variance after 6 Technical Replicates at 60000 Resolution:

Protein Gene	Peptide Sequence	Precursor Mass m/z	Activation Energy	Retention Time Average	Avg. Intensity	CV
GAPDH	LISWYDNEFGYSNR	882.4048	35	54.16	1.82E+06	3
GAPDH	VVDLMAHMASK	601.307	35	34.04	2.99E+06	6.7
GAPDH	VGVNGFGR	403.2194	35	22.84	3.73E+06	19.9
					Median CV	6.7
					Average CV	9.9

Table S6: Coefficient of Variance (CV) after 6 Technical Replicates at 60000 Resolution. CV of targeted peptides are shown. Definitions can be provided with permission.

3.8.7 Coefficient of Variance for GAPDH and PARK7 LiP:

Protein Gene	Peptide Sequence	Precursor Mass m/z	Activation Energy	Retention Time Average	CV Zero PK controls #1 (No Propachlor)	CV Zero PK controls #2 (No Propachlor)	CV Zero PK controls #3 (No Propachlor)		CV Zero PK controls #1 (Propachlor)	CV Zero PK controls #2 (Propachlor)	CV Zero PK controls #3 (Propachlor)
GAPDH	LISWYDNEFGYSNR	882.4048	35	51.85	2.7	3	4.2		1.9	10.3	6.7
GAPDH	IISNASCTTNCLAPLAK	917.4635	35	40.74	12.6	6.1	6		9.1	9.8	9.1
GAPDH	LVINGNPITIFQER	807.4541	35	56.45	4.2	8.2	7.1		7.1	13.7	3.1
GAPDH	VPTANVSVVDLTCR	765.9008	35	42.03	9.4	24.6	10.3		27.6	32.8	22.5
GAPDH	GALQNIIPASTGAAK	706.3988	35	35.49	21.7	2.3	6.1		13.5	3	16.8
GAPDH	VVDLMAHMASK	601.307	35	29.33	16.7	13.3	12.4		20.7	31.5	8.6
GAPDH	VGVNGFGR	403.2194	35	20.2	17.4	8.9	7.7		7.6	28	17
PARK7	GAEEMETVIPVDVMR	838.4051	35	50.57	3.2	25.1	8.4		5.3	14	3.8
PARK7	DVVICPDASLEDAK	766.369	35	41.91	4.5	20.2	4.9		17.1	25.8	3.7
PARK7	VTVAGLAGK	408.2529	35	30.07	18.2	11.5	18.2		20.4	25.7	21.3
				Median CV	11	10.2	7.4	**Median CV**	11.3	19.85	8.85
				Median CV (No Propachlor)	9.5			**Combined Average Median CV (Propachlor)**	13.3		
				Average CV	11.06	12.32	8.53	**Average CV**	13.03	19.46	11.26
				Combined Average CV (No Propachlor)	10.6			**Combined Average CV (Propachlor)**	14.6		

Table S7: Coefficient of Variance (CV) between Three Biological Replicates, Initial LiP Screen. CV are calculated among three biological replicates during the initial LiP Experiment. Definitions and more information can be provided with permission.

References

[1]A. K. Ghosh, I. Samanta, A. Mondal, W. Ray, *Chem Med Chem Rev.* **2019**, *14*, 889–906.

[2]Allaman, I.; Bélanger, M.; Magistretti, P. J. Methylglyoxal, the Dark Side of Glycolysis. *Front. Neurosci.* **2015**, *9* (FEB), 1–12. https://doi.org/10.3389/fnins.2015.00023.

[3]S. S. Mohanty, H. M. Jena, *J. Water Process Eng.* **2019**, *31*, 100860.

[4]Dearfield, K. L.; Mccarroll, N. E.; Protzel, A.; Stack, H. F.; Jackson, M. A.; Waters, M. D. A Survey of EPA r OPP and Open Literature on Selected Pesticide Chemicals II . Mutagenicity and Carcinogenicity of Selected Chloroacetanilides and Related Compounds 1. *Mutat. Res.* **1999**, *443*, 183–221.

[5]Lerro, C. C.; Koutros, S.; Andreotti, G.; Hines, C. J.; Blair, A.; Lubin, J.; Ma, X.; Zhang, Y.; Beane Freeman, L. E. Use of Acetochlor and Cancer Incidence in the Agricultural Health Study. *Int. J. Cancer* **2015**, *137* (5), 1167–1175. https://doi.org/10.1002/ijc.29416.

[6]Gideon, J.; Mulligan, J.; Hui, C.; Cheng, S. Heliyon UV and Temperature Effects on Chloroacetanilide and Triazine Herbicides Degradation and Cytotoxicity. *Heliyon* **2021**, *7* (April), e08010. https://doi.org/10.1016/j.heliyon.2021.e08010.

[7]Ã, B. A.; Farah, M. A.; Ahmad, W. Detection of DNA Damage by Alkaline Single Cell Gel Electrophoresis Erythrocytes of Clarias Batrachus. *Ecotoxicol. Environ. Saf.* **2005**, *62*, 348–354. https://doi.org/10.1016/j.ecoenv.2004.12.011.

[8]Hill, A. B.; Jefferies, P. R.; Quistad, G. B.; Casida, J. E. Dialkylquinoneimine Metabolites of Chloroacetanilide Herbicides Induce Sister Chromatid Exchanges in Cultured Human Lymphocytes. *Mutat. Res.* **1997**, *395*, 159–171.

[9]Green, T.; Lee, R.; Moore, R. B.; Ashby, J.; Willis, G. A.; Lund, V. J.; Clapp, M. J. L. Acetochlor-Induced Rat Nasal Tumors : Further Studies on the Mode of Action and Relevance to Humans. *Regul. Toxicol. Pharmacol.* **2000**, *133*, 127–133. https://doi.org/10.1006/rtph.2000.1413.

[10]Ashby, J.; Kier, L.; Wilson, A.; Green, T.; Lefevre, P. A.; Tinwell, H.; Willis, G. A.; Heydens, W. F.; Clapp, M. J. L. Evaluation of the Potential Carcinogenicity and Genetic Toxicity to Humans of the Herbicide Acetochlor. *Hum. Exp. Toxicol.* **1996**, *15* (9), 702–735. https://doi.org/10.1177/096032719601500902.

[11]Q. Chen, C.-H. Wang, S.-K. Deng, Y.-D. Wu, Y. Li, Y. Li, J.-D. Jiang, X. Yan, J. He, L. Shun-Peng, *Appl. Environ. Microbiol.* **2014**, *80*, 5078–5085.

[12]L. A. Bateman, T. B. Nguyen, A. M. Roberts, D. K. Miyamoto, W. Ku, T. R. Huffman, Y. Petri, M. J. Heslin, C. M. Contreras, C. F. Skibola, J. A. Olzmann, D. K. Nomura, *Chem. Commun.* **2017**, *53*, 7234–7237.

[13]J. L. Counihan, M. Duckering, E. Dalvie, W. Ku, L. A. Bateman, K. J. Fisher, D. K. Nomura, *ACS Chem. Biol.* **2017**, *12*, 635–642.

[14]Matthews, M. L.; He, L.; Horning, B. D.; Olson, E. J.; Correia, B. E.; Yates, J. R.; Dawson, P. E.; Cravatt, B. F. Chemoproteomic Profiling and Discovery of Protein Electrophiles in Human Cells. *Nat. Chem.* **2017**, *9* (3), 234–243. https://doi.org/10.1038/nchem.2645.

[15]Backus, K. M.; Correia, B. E.; Lum, K. M.; Forli, S.; Horning, B. D.; LuGonzález-páez, G. E.; Chatterjee, S.; Lanning, B. R.; Teijaro, J. R.; Olson, A. J.; Wolan, D. W.; Cravatt, B. F. Proteome-Wide Covalent Ligand Discovery in Native Biological Systems. *Nature* **2016**, *534* (7608), 570–574. https://doi.org/10.1038/nature18002.Proteome-wide.

[16]West, G. M.; Tang, L.; Fitzgerald, M. C. Thermodynamic Analysis of Protein Stability and Ligand Binding Using a Chemical Modification- and Mass Spectrometry-Based Strategy. *Anal. Chem.* **2008**, *80* (11), 4175–4185. https://doi.org/10.1021/ac702610a.

[17]Chea, E. E.; Jones, L. M. Modifications Generated by Fast Photochemical Oxidation of Proteins Reflect the Native Conformations of Proteins. *Protein Sci.* **2018**, *27* (6), 1047–1056. https://doi.org/10.1002/pro.3408.

[18]Bamberger, C.; Pankow, S.; Martínez-Bartolomé, S.; Ma, M.; Diedrich, J.; Rissman, R. A.; Yates, J. R. Protein Footprinting via Covalent Protein Painting Reveals Structural Changes of the Proteome in Alzheimer's Disease. *J. Proteome Res.* **2021**, *20*, 2762–2771. https://doi.org/10.1021/acs.jproteome.0c00912.

[19]L. Mei, M. R. Montoya, G. M. Quanrud, M. Tran, A. Villa-Sharma, M. Huang, J. C. Genereux, *J. Proteome Res.* **2020**, *19*, 1565–1573.

[20]Quanrud, G. M.; Montoya, M. R.; Mei, L.; Awad, M. R.; Genereux, J. C. Hsp40 Affinity to Identify Proteins Destabilized by Cellular Toxicant Exposure. *Anal. Chem.* **2021**, *93*, 16940–16946. https://doi.org/10.1021/acs.analchem.1c04230.

[21]A. A. A. Asea, P. Kaur, Eds. , *Regulation of Heat Shock Protein Responses*, Springer US, **2018**.

[22]M.P. Washburn, D. Wolters, J.R. Yates. *Nat. Biotechnol*. **2001**, *19*, 242-247.

[23]A.T. Kong, F.V. Leprevost, D.M. Avtonomov, D. Mellacheruvu, A.I. Nesvizhskii. Nat. Meth. **2017**, 14, 513-520.

[24]D. L. Plubell, P. A. Wilmarth, Y. Zhao, A. M. Fenton, J. Minnier, A. P. Reddy, J. Klimek, X. Yang, L. L. David, N. Pamir, Mol. Cell. Proteomics **2017**, 16, 873–890.

[25]D. Yekutieli, Y. Benjamini. J. Stat. Plan. Inference **1999**, 82, 171–196.

[26]J.D. Storey, R. Tibshirani. *Proc. Natl. Acad. Sci.* USA **2003,** *100*, 9440–9445.

[27]S. Schopper, A. Kahraman, P. Leunberger, Y. Feng, I. Piazza, O. Muller, P. J. Boersema, P. Picotti. Nat. Protocol. **2017**, 1, 2391-2410.

[28]B. Maclean, D.M Tomazela, N. Shulman, M. Chambers, G.L. Finney, B. Frewen, R. Kern, D. L. Tabb, D. C. Liebler, M. J. MacCoss. *Bioinformatics.* **2010**, 26, 966-968.

[29]GAPDH Activity Assay Kit, **2015**. https://assets.thermofisher.com/TFS-Assets/LSG/manuals/1639M.pdf

[30]S. Tashiro, J. M. M. Caaveiro, M. Nakakido, A. Tanabe, S. Nagatoishi, Y. Tamura, N. Matsuda, D. Liu, Q. Q. Hoang, K. Tsumoto, ACS Chem. Biol. **2018**, 13, 2783–2793.

[31]K. Kammers, R. N. Cole, C. Tiengwe, I. Ruczinski, *EuPA Open Proteomics* **2015**, *7*, 11–19.

[32]Ab129732-Resazurin Cell Viability Assay, **2019**. https://www.abcam.com/ps/products/129/ab129732/documents/ab129732_Resazurin%20Cell%20Viability%20Assay_20190715_ACW%20(website).pdf

[33]Guo, R.; Xu D.; Wang. W. Identification and analysis of new proteins involved in the DNA damage response network of Fanconi anemia and Bloom syndrome. *Methods*. **2009**, 48. 72-79.

[34]S. S. Cao, R. J. Kaufman. *Antioxid. Redox Signal*. **2014**, *21*, 396-413.

[35]Anckar, J.; Sistonen, L. Regulation of HSF1 Function in the Heat Stress Response: Implications in Aging and Disease. *Annu. Rev. Biochem.* **2011**, *80*, 1089–1115. https://doi.org/10.1146/annurev-biochem-060809-095203.

[36]Chatterjee, S.; Burns, T. F. Targeting Heat Shock Proteins in Cancer: A Promising Therapeutic Approach. *Int. J. Mol. Sci.* **2017**, *18* (9). https://doi.org/10.3390/ijms18091978.

[37]Kumar, S.; Acharya, S. K. 2,6-Dichloro-Phenol Indophenol Prevents Switch-over of Electrons between the Cyanide-Sensitive and -Insensitive Pathway of the Mitochondrial Electron Transport Chain in the Presence of Inhibitors. *Anal. Biochem.* **1999**, *268* (1), 89–93. https://doi.org/10.1006/abio.1998.3009.

[38]A. Gautier, M. J. Hinner, Eds. , *Site-Specfic Protein Labeling: Methods and Protocols*, Springer Protocols, **2015**.

[39]Powers, E. T.; Gierasch, L. M. The Proteome Folding Problem and Cellular Proteostasis. *J. Mol. Biol.* **2021**, *433* (20), 167197. https://doi.org/10.1016/j.jmb.2021.167197.

[40]Jacquin, H.; Gilson, A.; Shakhnovich, E.; Cocco, S.; Monasson, R. Benchmarking Inverse Statistical Approaches for Protein Structure and Design with Exactly Solvable Models. *PLOS Comput. Biol.* **2016**, 1–18. https://doi.org/10.1371/journal.pcbi.1004889.

[41]N. Rauniyar, J. R. Yates, *J. Proteome Res.* **2014**, *13*, 5293–5309.

[42]M. Kuljanin, D. C. Mitchell, D. K. Schweppe, A. S. Gikandi, D. P. Nusinow, N. J. Bulloch, E. V Vinogradova, D. L. Wilson, E. T. Kool, J. D. Mancias, B. F. Cravatt, S. P. Gygi, *Nat. Biotechnol.* **2021**, *39*, DOI 10.1038/s41587-020-00778-3.

[43] Carreras, C. W.; Santi, D. V. Quick Links to Online Content THE CATALYTIC MECHANISM AND STRUCTURE OF. *Annu. Rev. Biochem.* **1995**, *64*, 721–762.

[44] Hyatt, D. C.; Maley, F.; Montfort, W. R. Use of Strain in a Stereospecific Catalytic Mechanism: Crystal Structures of Escherichia Coli Thymidylate Synthase Bound to FdUMP and Methylenetetrahydrofolate. *Biochemistry* **1997**, *36* (15), 4585–4594. https://doi.org/10.1021/bi962936j.

[45]J. Sesen, A. Cammas, S. J. Scotland, B. Elefterion, A. Lemarié, S. Millevoi, L. K. Mathew, C. Seva, C. Toulas, E. C. J. Moyal, N. Skuli, *Int. J. Mol. Sci.* **2014**, *15*, 2172–2190.

[46]Weerapana, E.; Wang, C.; Simon, G. M.; Richter, F.; Khare, S.; Dillon, M. B. D.; Bachovchin, D. A.; Mowen, K.; Baker, D.; Cravatt, B. F. Quantitative Reactivity Profiling Predicts Functional Cysteines in Proteomes. *Nature* **2010**, *468* (7325), 790–797. https://doi.org/10.1038/nature09472.

[47]Z. Y. Guo, C. C. Y. Chang, T. Y. Chang, *Biochemistry* **2007**, *46*, 10063–10071.

[48]Lin, H.; Wang, M.; Zhang, Y. W.; Tong, S.; Leal, R. A.; Shetty, R.; Vaddi, K.; Luengo, J. I. Discovery of Potent and Selective Covalent Protein Arginine Methyltransferase 5 (PRMT5) Inhibitors. *ACS Med. Chem. Lett.* **2019**, *10* (7), 1033–1038. https://doi.org/10.1021/acsmedchemlett.9b00074.

[49]Friesen, W. J.; Wyce, A.; Paushkin, S.; Abel, L.; Rappsilber, J.; Mann, M.; Dreyfuss, G. A Novel WD Repeat Protein Component of the Methylosome Binds Sm Proteins *. *J. Biol. Chem.* **2002**, *277* (10), 8243–8247. https://doi.org/10.1074/jbc.M109984200.\

[50]Q. Kuang, P. Purhonen, J. Ålander, R. Svensson, V. Hoogland, J. Winerdal, L. Spahiu, A. Ottosson-Wadlund, C. Jegerschöld, R. Morgenstern, H. Hebert, *Sci. Rep*. **2017**, 7, 1–10.

[51] Y. Horibata, H. Ando, H. Sugimoto, *J. Lipid Res.* **2020**, *61*, 1221–1231.

[52] R. Y. Ebright, S. Lee, B. S. Wittner, K. L. Niederhoffer, B. T. Nicholson, A. Bardia, S. Truesdell, D. F. Wiley, B. Wesley, S. Li, A. Mai, N. Aceto, N. Vincent-Jordan, A. Szabolcs, B. Chirn, J. Kreuzer, V. Comaills, M. Kalinich, W. Haas, D. T. Ting, M. Toner, S. Vasudevan, D. A. Haber, S. Maheswaran, D. S. Micalizzi, *Science.* **2020**, *367*, 1468–1473. DOI: 10.1126/science.aay0939.

[53]K. Marzec, A. Burgess, *Front. Cell Dev. Biol.* **2018**, *6*, 1–9.

[54]Jia, D.; Hasso, S. M.; Chan, J.; Filingeri, D.; D'Amore, P. A.; Rice, L.; Pampo, C.; Siemann, D. W.; Zurakowski, D.; Rodig, S. J.; Moses, M. A. Transcriptional Repression of VEGF by ZNF24: Mechanistic Studies and Vascular Consequences in Vivo. *Blood* **2013**, *121* (4), 707–715. https://doi.org/10.1182/blood-2012-05-433045.

[55]M. A. S. Anwair, L. Károlyházy, D. Szabó, B. Balogh, I. Kövesdi, V. Harmat, J. Krenyácz, Á. Gellért, K. Takács-Novák, P. Mátyus, *J. Agric. Food Chem.* **2003**, *51*, 5262–5270.

[56]Shannon, D. A.; Banerjee, R.; Webster, E. R.; Bak, D. W.; Wang, C.; Weerapana, E. Investigating the Proteome Reactivity and Selectivity of Aryl Halides. *J. Am. Chem. Soc.* **2014**, *136* (9), 3330–3333. https://doi.org/10.1021/ja4116204.

[57]S. Coleman, R. Linderman, E. Hodgson, R. L. Rose, *Environ. Health Perspect.* **2000**, *108*, 11511157.

[58]Bonfanti, M.; Taverna, P.; Chiappetta, L.; Villa, P.; D'Incalci, M.; Bagnati, R.; Fanelli, R. DNA Damage Induced by Alachlor after in Vitro Activation by Rat Hepatocytes. *Toxicology* **1992**, *72* (2), 207–219. https://doi.org/10.1016/0300-483X(92)90113-S.

[59]C. Nicholls, H. Li, J. Liu, Clin. *Exp. Pharmacol. Physiol*. **2012**, 674–679.

[60]B. C. Vanle, V. R. Florang, D. J. Murry, A. L. Aguirre, J. A. Doorn, *Biochem. Biophys. Res. Commun.* **2017**, *492*, 275–281.

[61]M. Repici, F. Giorgini, *J. Clin. Med.* **2019**, *8*, 1–11. doi:10.3390/jcm8091377.

[62]K. A. Lippa, S. Demel, I. H. Lau, A. L. Roberts, *J. Agric. Food Chem.* **2004**, *52*, 3010–3021.

[63]Q. Kuang, P. Purhonen, J. Ålander, R. Svensson, V. Hoogland, J. Winerdal, L. Spahiu, A. Ottosson-Wadlund, C. Jegerschöld, R. Morgenstern, H. Hebert, *Sci. Rep.* **2017**, *7*, 1–10.

[64]Y. Horibata, H. Ando, H. Sugimoto, *J. Lipid Res.* **2020**, *61*, 1221–1231.

[65]R. Y. Ebright, S. Lee, B. S. Wittner, K. L. Niederhoffer, B. T. Nicholson, A. Bardia, S. Truesdell, D. F. Wiley, B. Wesley, S. Li, A. Mai, N. Aceto, N. Vincent-Jordan, A. Szabolcs, B. Chirn, J. Kreuzer, V. Comaills, M. Kalinich, W. Haas, D. T. Ting, M. Toner, S. Vasudevan, D. A. Haber, S. Maheswaran, D. S. Micalizzi, *Science.* **2020**, *367*, 1468–1473. DOI: 10.1126/science.aay0939.

[66]M. Kuljanin, D. C. Mitchell, D. K. Schweppe, A. S. Gikandi, D. P. Nusinow, N. J. Bulloch, E. V Vinogradova, D. L. Wilson, E. T. Kool, J. D. Mancias, B. F. Cravatt, S. P. Gygi, *Nat. Biotechnol.* **2021**, *39*, DOI 10.1038/s41587-020-00778-3.

[67]J. Fert-Bober, C. I. Murray, S. J. Parker, J. E. Van Eyk, *Circ. Res.* **2018**, *122*, 1221–1237.

[68]Colon, W.; Kelly, J. W. Partial Denaturation of Transthyretin Is Sufficient for Amyloid Fibril Formation in Vitro. *Biochemistry* **1992**, *31* (36), 8654–8660. https://doi.org/10.1021/bi00151a036.

[69]Radford, S. E.; Dobson, C. M.; Evanst, P. A. The Folding of Hen Lysozyme Involves Partially Structured Intermediates and Multiple Pathways. **1992**, *358* (July).

[70]Baldwin, A. J.; Knowles, T. P. J.; Tartaglia, G. G.; Fitzpatrick, A. W.; Devlin, G. L.; Shammas, S. L.; Waudby, C. A.; Mossuto, M. F.; Meehan, S.; Gras, S. L.; Christodoulou, J.; Anthony-cahill, S. J.; Barker, P. D.; Vendruscolo, M.; Dobson, C. M. Metastability of Native Proteins and the Phenomenon of Amyloid Formation. **2011**, 14160–14163.

[71]Sui, X.; Pires, D. E. V; Ormsby, A. R.; Cox, D.; Nie, S.; Vecchi, G. Widespread Remodeling of Proteome Solubility in Response to Different Protein Homeostasis Stresses. *PNAS* **2020**, *117* (5). https://doi.org/10.1073/pnas.1912897117.

[72]Waka Natsume, Kenji Tanabe, Shunsuke Kon, Naomi Yoshia, Toshio Watanabe, Tetsuo Torii, M. S. SMAP2, a Novel ARF GTPase-Activating Protein, Interacts with Clathrin and Clathrin Assembly Protein and Functions on the AP-1-Positive Early Endosome/Trans-Golgi Network. *Mol. Biol. Cell* **2006**, *17* (June), 2592–2603. https://doi.org/10.1091/mbc.E05.

[73]Kaksonen, M.; Roux, A. Mechanisms of Clathrin-Mediated Endocytosis. *Nat. Publ. Gr.* **2018**, *19* (5), 313–326. https://doi.org/10.1038/nrm.2017.132.

[74]Yu, A.; Shibata, Y.; Shah, B.; Calamini, B.; Lo, D. C.; Morimoto, R. I. Protein Aggregation Can Inhibit Clathrin-Mediated Endocytosis by Chaperone Competition. *Proc. Natl. Acad. Sci. U. S. A.* **2014**, *111* (15). https://doi.org/10.1073/pnas.1321811111.

[75]He, K.; Song, E.; Upadhyayula, S.; Dang, S.; Gaudin, R.; Skillern, W.; Bu, K.; Capraro, B. R. Dynamics of Auxilin 1 and GAK in Clathrin-Mediated Traffic. *J. Cell Biol.* **2020**.

[76] Weids, A. J.; Ibstedt, S.; Tamás, M. J.; Grant, C. M. Distinct Stress Conditions Result in Aggregation of Proteins with Similar Properties. *Nat. Publ. Gr.* **2016**, No. February, 1–12. https://doi.org/10.1038/srep24554.

[77]N. W. Seidler, *GAPDH: Biological Properties and Diversity*, Springer US, New York, **2014**.

[78]D. J. Irwin, V. M. Y. Lee, J. Q. Trojanowski, *Nat. Rev. Neurosci.* **2013**, *14*, 626–636.

[79]J. Schulte, J. T. Littleton, *Curr. Trends Neurol.* **2011**, *5*, 65–78.

[80]K. Uchidas, E. R. Stadtmant, *J. Biol. Chem.* **1993**, *268*, 6388–6393.

[81]H. J. Lee, S. K. Howell, R. J. Sanford, P. J. Beisswenger, *Ann. N. Y. Acad. Sci.* **2005**, *1043*, 135–145.

[82]E. Duée, L. Olivier-Deyris, E. Fanchon, C. Corbier, G. Branlant, O. Dideberg, *J. Mol. Biol.* **1996**, *257*, 814–838.

[83]P. Leuenberger, S. Ganscha, A. Kahraman, V. Cappelletti, P. J. Boersema, C. Von Mering, M. Claassen, P. Picotti, *Science.* **2017**, *355*, DOI 10.1126/science.aai7825.

[84]Jenkins, J. L.; Tanner, J. J. High-resolution structure of human D-glyceraldehyde-3-phosphate dehydrogenase. *Acta Cryst.* **2006**, D62, 290-301, https://doi.org/10.1107/S0907444905042289

[85]Sirover, M. A. Structural Analysis of Glyceraldehyde-3-Phosphate Dehydrogenase Functional Diversity. *Int. J. Biochem. Cell Biol.* **2014**, *57*, 20–26. https://doi.org/10.1016/j.biocel.2014.09.026.

[86]Dar, G. H.; Mendes, C. C.; Kuan, W. L.; Speciale, A. A.; Conceição, M.; Görgens, A.; Uliyakina, I.; Lobo, M. J.; Lim, W. F.; EL Andaloussi, S.; Mäger, I.; Roberts, T. C.; Barker, R. A.; Goberdhan, D. C. I.; Wilson, C.; Wood, M. J. A. GAPDH Controls Extracellular Vesicle Biogenesis and Enhances the Therapeutic Potential of EV Mediated SiRNA Delivery to the Brain. *Nat. Commun.* **2021**, *12* (1). https://doi.org/10.1038/s41467-021-27056-3.

[87]Qvit, N.; Joshi, A. U.; Cunningham, A. D.; Ferreira, J. C. B.; Mochly-Rosen, D. Glyceraldehyde-3-Phosphate Dehydrogenase (GAPDH) Protein-Protein Interaction Inhibitor Reveals a Non-Catalytic Role for GAPDH Oligomerization in Cell Death. *J. Biol. Chem.* **2016**,

[88]White, M. R.; Khan, M. M.; Deredge, D.; Ross, C. R.; Quintyn, R.; Zucconi, B. E.; Wysocki, V. H.; Wintrode, P. L.; Wilson, G. M.; Garcin, E. D. A Dimer Interface Mutation in Glyceraldehyde-3-Phosphate Dehydrogenase Regulates Its Binding to AU-Rich RNA. *J. Biol. Chem.* **2015**, *290* (3), 1770–1785. https://doi.org/10.1074/jbc.M114.618165.

[89]Wilson, M. A.; Collins, J. L.; Hod, Y.; Ringe, D.; Petsko, G. A. The 1.1-Å Resolution Crystal Structure of DJ-1, the Protein Mutated in Autosomal Recessive Early Onset Parkinson's Disease. *Proc. Natl. Acad. Sci. U. S. A.* **2003**, *100* (16), 9256–9261. https://doi.org/10.1073/pnas.1133288100.

[90]H. J. Lee, S. K. Howell, R. J. Sanford, P. J. Beisswenger, *Ann. N. Y. Acad. Sci.* **2005**, *1043*, 135–145.

[91]N. Wiebelhaus, J. M. Zaengle-Barone, K. K. Hwang, K. J. Franz, M. C. Fitzgerald, *ACS Chem. Biol.* **2021**, *16*, 214–224.

[92]Henis, Y. I.; Levitzki, A. Mechanism of Negative Cooperativity in Glyceraldehyde-3-Phosphate Dehydrogenase Deduced from Ligand Competition Experiments. *Proc. Natl. Acad. Sci. U. S. A.* **1980**, *77* (9), 5055–5059. https://doi.org/10.1073/pnas.77.9.5055.

[93]Gerszon, J.; Rodacka, A. Oxidatively Modified Glyceraldehyde-3-Phosphate Dehydrogenase in Neurodegenerative Processes and the Role of Low Molecular Weight Compounds in Counteracting Its Aggregation and Nuclear Translocation. *Ageing Res. Rev.* **2018**, *48* (July), 21–31. https://doi.org/10.1016/j.arr.2018.09.003.

[94]Zaffagnini, M.; Fermani, S.; Costa, A.; Lemaire, S. D.; Trost, P. Plant Cytoplasmic GAPDH: Redox Post-Translational Modifications and Moonlighting Properties. *Front. Plant Sci.* **2013**, *4* (NOV), 1–18. https://doi.org/10.3389/fpls.2013.00450.

[95]G. Richarme, M. Mihoub, J. Dairou, L. C. Bui, T. Leger, A. Lamouri, *J. Biol. Chem.* **2015**, *290*, 1885–1897.
[96]S. Gallefi, A. Bourmaud, S. Y. Kim, B. Domon. *J. Proteomics.* **2014,** 147-159.

[97]G. E. Ronsein, N. Pamir, P. D. Von Haller, D. S. Kim, M. N. Oda, G. P. Jarvik, T. Vaisar, J. W. Heinecke. *J. Proteomics.* **2015**, 3899.

[98]M. S. Waka Natsume, Kenji Tanabe, Shunsuke Kon, Naomi Yoshia, Toshio Watanabe, Tetsuo Torii, *Mol. Biol. Cell* **2006**, *17*, 2592–2603.

Chapter 4: Hsp40 Affinity to Identify Proteins Destabilized by Manganese

This chapter discusses the investigation into the effects of Manganese in HEK293T cells.

4.1 Abstract

Heavy metals in groundwater are a growing threat to cellular health and proteostasis. Manganese, an abundant and toxic heavy metal, has been increasingly contaminating groundwater sources. High exposure to manganese can cause a catastrophic series of cellular toxicity even ranging from immediate protein misfolding to long term symptoms resembling neurological diseases such as Parkinson's Disease (PD). We describe an approach to identify the destabilized proteome in HEK293T cells after manganese exposure. We used DNAJB8, a Hsp40 chaperone to quantitatively identify destabilized proteins after manganese treatment. We validated NKRF as a significantly destabilized protein by Limited Proteolysis (LiP). Several proteins from HEK293T cells increased affinity to DNAJB8 after manganese exposure. The destabilization of NKRF signifies a potential manganese toxicity in the nucleus. In total, the destabilized proteins identified by DNAJB8 provide further credence and relevance to regulating manganese levels in groundwater.

4.2. Introduction

The contamination of groundwater by heavy metals is a growing health concern[1,2,3]. Heavy metals in the presence of cells, can undergo several toxic mechanisms

such as producing reactive oxygen species (ROS) and interfering with cell signaling, which are all relevant in neurological diseases[4,5,6]. The increase in exposure to heavy metals can come from anthropogenic and geogenic sources such as waste disposal sites[7], septic systems[8], and pollutants seeping into and contaminating groundwater[9]. Several efforts in detoxifying heavy metals from groundwater include using adsorption instrumentation or adding more protective barriers to remove or prevent contaminants[10,11]. These groundwater technologies, though, are not completely effective without better help from groundwater governance and environmental policies[12]. Thus, these contamination sources make demands for healthy groundwater for watering crops or for drinking increasingly difficult to achieve[13,14]. To better understand the troubling reality of the current groundwater situation, more investigations are being conducted into learning the effects of heavy metals in groundwater on human health. Heavy metals can be specific in their targets on the proteome level and understanding which proteins are most sensitive to heavy metal can help elucidate their toxic individual mechanisms.

An emerging heavy metal contaminant in groundwater is Manganese (Mn). Mn, a highly abundant element in the earth, has been found to be more concentrated in groundwater sources well above its recommended level of 0.05 mg/L[1]. Thousands of wells in the U.S have been found to be contaminated from land surface-soil-aquifier connections with Mn concentrations measuring at least 0.3 mg/L[14]. One of the consequences of the elevated amounts of Mn in groundwater are the resulting effects of the toxin as an oxidant. Mn can be oxidized from Mn^{2+} to Mn^{3+} when metabolized and these states can penetrate across cellular membranes, form complexes with proteins, or

penetrate the blood-brain barrier (BBB)[15,16]. If cells are more exposed to these oxidative states of Mn, the increased amount of oxidative stress can be harmful for cellular survival.

The long-term effects of cellular damage and distinct mechanisms of Mn exposure are a bit unexplored despite ongoing investigation. Several studies of Mn exposure suggest that the heavy metal can cause neurodegeneration. Recurring exposure to divalent Mn has been found to promote α-syn aggregation and other symptoms of Parkinson's disease[17,18]. Mn can also bind to prion proteins to make them toxic in Creutzfeldt-Jakob Disease (CJD)[19,20]. Cellular exposure to Mn has also been found to disrupt proteostasis. Mn treatment in cells has been found to induce heat shock response which means that the oxidative stress can cause protein misfolding[21,22]. The oxidative havoc that Mn exposure can bring to the cells in the short term and the long term brings opportunity to explore the destabilized proteome. Proteins that are most sensitive to the toxic mechanisms can be deduced to help understand how cells can adapt to the presence of Mn.

Several high throughput assays by mass spectrometry can measure misfolded proteins after Mn treatment. Limited proteolysis (LiP) can measure differences in protein stability by analyzing proteome-wide susceptibility to enzymatic digestion[23]. Stability of Proteins from Rates of Oxidation (SPROX) can be used to analyze methionine oxidation or proteins in cellular lysates through $\Delta G_{unfolding}$[24,25]. Cellular Thermal Shift Assay (CETSA) measures misfolded proteins by using proteome-wide susceptibility to aggregation with increasing temperatures[26]. Each of these proteomic approaches can use

quantitative proteomics to assess the effects of Mn on the proteome.

We recently used a chaperone-based approach to profile the effects of arsenite and cadmium on proteomes in HEK293T cells[27]. DNAJB8, an hsp40 localized in the nucleus and cytosol, can be mutated to DNAJB8^{H31Q} to identify hundreds of clients with high reproducibility and statistical confidence[28]. We combined this mutated chaperone with limited proteolysis to identify several ribosomal destabilized proteins such as TDP43 and PDHA1 after arsenite exposure[27]. Here, we used DNAJB8^{H31Q} to recognize misfolded proteins after treatment with divalent Mn. We found that Mn in HEK293T overall damages the proteome and may significantly target RNA binding proteins such as NKRF.

4.3 Materials and Methods

4.3.1 Materials:

Dulbecco's phosphate-buffered saline (DPBS), 6 well plates, 10 cm plates, and Eagle Media (DMEM) were from VWR. Manganese Chloride hexahydrate ($MnCl_2$) •$(H_2O)_6$, Roche Protease Inhibitor cocktail w/o EDTA (PIC), HEPES, 1,4-dithiothreitol (DTT), were from Sigma Aldrich. Urea, glycerol, poly D-lysine, Sodium chloride (NaCl), sequencing grade trypsin, Tris-Hydrochloride (Tris-HCl), Triton X-100, sodium deoxycholate, KCl, $CaCl_2$, $Ag(NO_3)_2$, $MgCl_2$, $Na_2S_2O_3$, $Ca(O_2C_2H_3)_2$), sodium dodecyl sulfate (SDS), and poly D-lysine were from Thermo Fisher Scientific. Proteinase K (PK) was obtained from Promega. Millipore Milli-Q Laboratory lab 4 Chassis Reagent Water System was used to purify nanopure water. 3 µm and 5 µm Aqua C18 resins were from Phenomenex. Anti-M2 Flag magnetic beads, Sepharose-4B beads, iodoacetamide, and

tris (2-carboxyethyl)phosphine hydrochloride (TCEP) were from Millipore Sigma. 250 µm diameter fused silica columns were obtained from Agilent. 100 µm diameter fused silica columns were obtained from Polymicro. Strong cation exchange resin was obtained from Partisphere, GE Healthcare. Rapigest was obtained from Aobious (Gloucester, MA). TMT-6plex isotopic labels were from Pierce. Bradford reagent was purchased from Bio-rad.

4.3.2 AP-TMT-MudPIT:

TMT-AP-MS experiments were adapted from previous experiments[27]. Each sixplex TMT-AP-MS comprised of six 10 cm plates of HEK293T cells. Each plate was transfected with 5 µg of plasmid DNA encoding ^{Flag}DNAJB8^{H31Q} in the pFLAG backbone by the calcium phosphate method. Plates were treated with Manganese or vehicle at 40-46 hours post transfection. Cells were harvested in DPBS by scraping. Cell pellets were lysed in 1 part 10x PIC and 9 parts RIPA Buffer (50 mM Tris pH 7.5, 150 mM NaCl, 0.1% SDS, 1% Triton X-100, and 0.5% sodium deoxycholate) for 30 min on ice. Cells were then centrifuged at 21,000 x g for 15 minutes at 4 °C. Lysate was separated from cell debris and protein in the lysate was quantified by Bradford Assay. Lysates were then pre-cleared with 15 µL Sepharose-4B beads for 30 min at 4 °C. Lysates were then centrifuged at 1,500 x g for 1 min to pellet beads. Lysate was then separated and incubated with 15 µL of M2 anti-Flag Magnetic Beads. Each sample was rotated with M2 beads overnight at 4 °C. The anti-Flag beads were separated the next day and washed the four times with RIPA buffer. Each sample was rotated for 10 minutes at ambient

temperature during each wash. 30 μL of Laemmli concentrate (60% glycerol, 12% SDS, 120 mM Tris pH 6.8, brilliant phenol blue to color) was added to each sample. Proteins were eluted by boiling for 5 min at 100 °C. 5 μL of the elutes were saved for silver stain analysis. The remainder was used for mass spectrometry and TMT-labeled.

MS quality organic solvents were only used during sample preparation. Buffer A is composed of 5% acetonitrile, 0.1% formic acid in water. Buffer B is composed of 80% acetonitrile, 0.1% formic acid. Buffer C is composed of 500 mM ammonium acetate in Buffer A. All MS runs were performed with a two-dimensional LC/MS/MS setup. This setup was an LTQ Orbitrap Velos Pro hybrid mass spectrometer (Thermo) interfaced with an Easy-nLC 1000 (Thermo) according to standard MuDPIT protocols[29]. MS/MS spectra from each run were extracted using MSConvert (version 3.0.21144) with Peak Picking Filtering. FragPipe[30] was used to analyze MS/MS spectra against a Uniprot human proteome database (06/11/2021 release) containing 40858 human sequences (longest entry for each protein). The MS/MS spectra were searched against 20429 select decoys (e.g porcine trypsin, albumen, contaminants etc.). FragPipe searches allowed for static modification N-termini and lysine residues (229.1629 Da, TMT-tagging), modification of cysteine residues (57.02146 Da, acetylation), and half tryptic peptidolysis specificity.

Peptides were searched with mass tolerance of 20 ppm for precursor mass and 20 ppm for product ion masses. MSFragger were used to assemble and filter spectra matches. Keratins, decoy proteins, immunoglobulins, and common contaminants were filtered from the final protein list. Quantitation in FragPipe was performed by averaging TMT reporter ion intensities for all spectra associated with an individual peptide.

4.3.3 Statistical Analysis:

Destabilized proteins were performed from previous experiment[27]. The intensity of bait (DNAJB8) in each TMT channel was used to normalized protein-level intensities. We used a version of the scaled reference approach to combined the multiple TMT runs[31]. Averaging the bait-normalized integrated TMT reporter ion intensities for each protein across the 3 control conditions in each AP-MS run created a scaling factor. This scaling factor was used to divide each bait-normalized protein intensity. The method of Benjamini and Hochberg and Storey's modification was used to convert unadjusted p-values to q values (local discovery rates)[32,33]. Unadjusted p-values were ranked in increasing order. Q-value for the *i*th protein determined from:

$$q_i = \pi \, min_{i \leq j \leq n} \frac{pn}{i}$$

Storey's modification works by determining the overrepresentation of low p-values. This is used to infer a global false discovery rate and then scaling local false discovery rates accordingly. The π-factor for this scaling was 0.49 for the manganese treatment TMT-AP-MS data set.

4.3.4 Limited Proteolysis:

4.3.4.1 Limited Proteolysis Procedure:

The limited proteolysis procedure was adapted and optimized previous procedures [27]. Six 10 cm plates seeded with HEK293T cells prepared. Three plates were incubated with 100 μm Mn and 3 plates were incubated with water for 30 minutes at 37 °C. Plates were immediately harvested by scraping in DPBS. Cell pellets were then lysed with 9:1

Native Lysis Buffer (20 mM HEPES, 150 mM KCl, 10 mM $MgCl_2$, 0.3% Triton, pH 7.5): 10x PIC for 30 minutes in ice. Lysates were separated from cell debris by centrifugation at 21,000 x g for 15 minutes at 4 °C. Lysates were quantified using Bradford assay and 200 µg aliquots were prepared for limited proteolysis.
1 mg/ml stocks of Proteinase K (PK) were made from 25 mg of lyophilized PK dissolved in a storage buffer (50 mM Tris-HCl, 2 mM calcium acetate, pH 8.0). These aliquots are stored at –70 °C. Serial dilutions from 1mg/ml stocks were made to prepare the following concentrations of PK: 0.5 mg/ml, 0.2 mg/ml, 0.1 mg/ml, 0.05 mg/ml. Thus 2 µl PK are added to lysate to yield 1:200, 1:500, 1:1000, 1:2000, wt/wt protease: substrate protein ratios respectively. The following samples were thus prepared for each condition: 3 each of the Trypsin control (No PK), 1:2000 PK:protein, 1:1000 PK:protein, 1:500 PK:protein, 1:200 PK:protein, and 1:100 PK:protein. Three biological replicates were prepared for Mn treatment and for untreated, yielding a total of 102 samples.

The sample set-up and the calculation of fraction remaining for each peptide is shown in **Figure S1**. Samples were prepared for mass spectrometry and analyzed using LC-MS/MS and parallel reaction monitoring (PRM). Three peptides from NKRF were chosen. Samples were run according to previous protocol and one the same setup[27].

4.3.4.2 Limited Proteolysis Data Analysis:

Data analysis was performed according to previous experiments[27]. One technical replicate was run for each biological replicate. Skyline was used to calculate integrated fragment intensities. The integrated fragment intensities for each sample and normalized

to the averages of the three no-PK controls (which themselves were run in technical triplicate) (**Schematic S1**). Proteolytic susceptibility curves were made by plotting the relative fragment intensity against the increasing PK concentration. Differences between curves are assessed based on the summed fractions remaining across data points from 2000:1 to 100:1 (**see Supp. Table 2**). Coefficient of Variation (CV) were calculated from ten technical replicates of a Trypsin control. The CV of biological replicates were calculated among three biological replicates. We should note that because our analysis does not assume linearity between integrated peptide response and actual peptide levels. Therefore, no effort was made to establish whether the peptides observed are in the linear quantitative regime[34].

4.3.5 XRN2 and NKRF RNA Blotting:

RNA blotting measuring effects of Manganese on NKRF and XRN2 was adapted from Coccia et al.[35] In a single gel, eight 10 cm plates of HEK293T were analyzed. Three plates were treated with 24 hours of 100 μM of Manganese at 37 ^{o}C and three plates were treated with vehicle for 24 hours at 37 ^{o}C. The last two plates were treated with vehicle but were heated at different incubations. One plate (positive control) was heated at 43 ^{o}C for 40 minutes and the other plate was heat at 37 ^{o}C for 40 minutes. Plates were immediately lysed using TRIzol following RNA extraction protocols and total RNA was quantified by using a NanoDrop^{TM} One/One^{C} Microvolume UV-Vis Spectrophotometer[36]. 1% Agarose gel was prepared with formaldehyde and samples were run at 100V for 45 minutes following protocols from Hansour et al.[37] Gels were

transferred to Nylon membranes for and blotted by ITS1. Sequence for ITS1 can be found below:

Probe	Source	Sequence
ITS1	35	5′-AGGGGTCTTTAAACCTCCGCGCCGGAACGCGCTAGGTAC-3'

ITS1 sequence was additionally conjugated to IR 700 Dye. Blots were visualized on a Li-Core Biosciences Fc Imager.

4.3.6 Cell Culture and Silver Stain:

The ATCC provided HEK293T cells and cells were maintained in DMEM with 10% FBS. The calcium phosphate method was used for cell transfection. 1ml HBS 2x was added dropwise to a 1 mL solution of 250 µM $CaCl_2$ containing 5 µg of DNA while the solution was vortexed for 10 seconds at room temperature. The transfection solution is then quickly (≤ 15 minutes) added dropwise to cells are about 50% confluent. The cell media is changed between 12 and 16 hours. GFP is used as a positive transfection control alongside each transfection. These transfection amounts were used for 10 cm dishes. Reagents are proportionally adjusted for transfection of different sized plates.

Silver stain was used to assess the amount of the ^{Flag}DNAJB8^{H31Q} in eluates after the immunoprecipitation and potential differences in the co-immunoprecipitated protein levels between conditions (**Figure S4**)[38]. Each eluate was diluted with DTT was added to a final concentration of 170 mM. Eluates were boiled for 5 minutes at 100 °C prior. Eluates were then loaded into SDS-PAGE gels and run for separation. Gels were either fixed overnight in 30% ethanol/10% acetic acid or gels were fixed for a few hours with

50% methanol/12% acetic acid. After gels were fixed, they were washed in 35% ethanol three times for 20 minutes each. Gels were then sensitized for 2 minutes (0.02% $Na_2S_2O_3$ in H_2O) and washed three times for 1 minute each in H_2O. Each gel was then stained for 30 minutes to overnight in Ag staining solution (0.2% $AgNO_3$, 0.076% formalin). Gels were developed with 6% $NaCO_3$/0.05% formalin/0.0004% $Na_2S_2O_3$ after two one-minute rinses in H_2O. 5% acetic acid was added stop development of the stain. Gels were imaged on a white-light transilluminator (UVP).

4.3.7 Assessing HSF1 Activation after Applied Manganese Stress:

Cellular experiments were performed according to previous experiments[27]. Two separate experiments were attempted to evaluate HSF1 activation after Mn treatment. Two 10 cm plates seeded with HEK293T cells were transfected at 40-60% confluency by calcium phosphate method. One 10 cm plate was transfected with 5 µg of GFP. The other 10 cm plate was transfected with DNA encoding ^{FLAG}DNABJ8^{H31Q}. Both plates were split into 6-well plates coated with Poly-D-Lysine.

The first experiment incubated each well with an increasing concentration (0 µM, 50 µM, 100 µM, 200 µM, 500 µM, 1 mM) of Mn for 15 minutes at 37 °C. The second experiment incubated each well with an increasing concentration (0 µM, 0.5 µM, 10 µM, 100 µM, 200 µM) of Mn for 24 hours at 37 °C. Mn treated media was replaced with fresh media. Plates were then incubated for 16 h at 37 °C to recover. Plates were then immediately harvested by scraping in DPBS. Pellets were then lysed in 9:1 RIPA:10x PIC in ice for 30 minutes. Samples were then spun in centrifugation at 21,000 x g for 15

minutes at 4 °C. Lysates were separated from cellular debris. Lysates were quantified by Bradford assay to determine amount of protein. 2 µg/µl of protein samples were prepared for western blot analysis after addition of 9:1 Laemlli:1 M DTT (17% of solution).

15 µg of each sample were separated on a 12% SDS-PAGE Gel. The gel was 1.0 mm thickness. Western blots were probed for Flag (Sigma M2 monoclonal anti-Flag antibody), GFP (rabbit polyclonal) primary antibodies, HSPA1A (rabbit polyclonal), and Beta-actin (mouse monoclonal 7D2C10). Near-IR secondary antibodies (Li-COR) were used. Blots were visualized on a Li-Cor Biosciences Fc Imager.

4.4. Results and Discussion

DNAJB8^{H31Q} can be effective in analyzing destabilized proteins if heat shock factors are activated. Protein misfolding stress can lead to large transcription, translational, and post-translational changes in the cell that can be recognized by activated quality control factors[39,40]. We first attempted to limit cellular exposure by exposing HEK293T cells with short acute treatments of Mn to active HSF1 in the cytosol (**Figure S2**). Short treatments of Mn did not cause protein misfolding as indicated by the lack of overexpression for HSPA1A and HSPBD1.

Longer treatments of less concentrated Mn treatment did not activate heat shock factor in the cytosol as well (**Figure S3**). We determined that DNAJB8^{H31Q} would assess the HEK293T proteome after 24 hours of treatment of 100 µM of manganese. This concentration is within the pathophysiological and physiological levels of Mn in brain cells and thus ideal for studying their toxic mechanisms and protein targets for

destabilization[41]. We used the same approach as performed in previous experiments[27]. ^{Flag}DNAJB8^{H31Q} was transiently overexpressed in HEK293T cells and then treated with 100 μM of manganese for 24 hours.

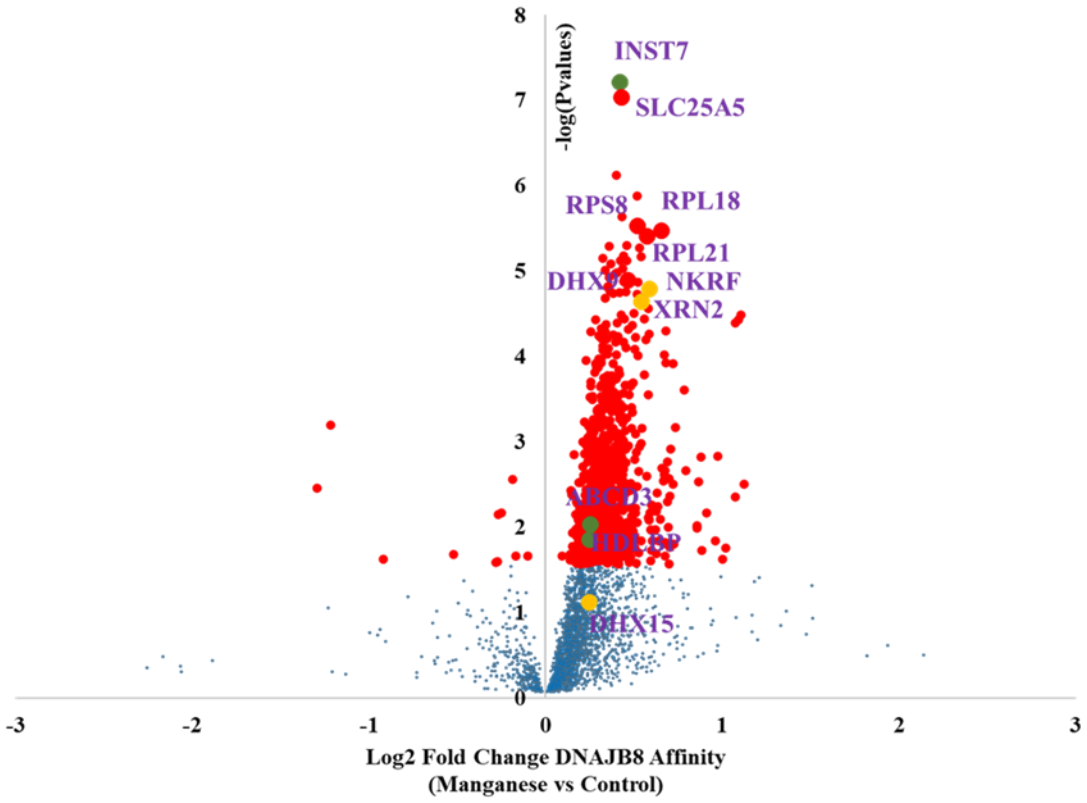

Figure 1. Manganese treatment increases the affinity of a subset of proteins with DNAJB8^{H31Q}. A DNAJB8^{H31Q} pulldown experiment consists of three transfected HEK293T cells treated with 100 μM Manganese for 24 hours and the other three plates were treated with control (water) prior to lysis. Red dots represent proteins with significantly increased interaction with DNAJB8^{H31Q}, using a false discovery rate threshold (FDR) of 0.05 (n = 15 biological replicates in 5 TMT-AP-MS runs). Most of the proteome appears destabilized as indicated by large amount of proteins > 1. XRN2, NKRF, and DHX15 are highlighted in yellow. INST7, ABCD3, and HDLBP are highlighted in green.

Cells immediately then underwent Flag immunoprecipitation from the cellular lysate. Co-immunoprecipitated proteins were quantified and identified by LC/LS-MS/MS

after TMT isobaric labeling[42]. In total, 30 biological replicates (15 treated and 15 controls) were analyzed through five 6-plex TMT runs.

Most proteins appear to bind more to DNAJB8 after manganese treatment (**Figure 1**). A total of 898 proteins have significantly greater affinity for ^{Flag}DNAJB8^{H31Q} in response to the manganese treatment with Q value by Storey's modification < 0.05. Several of the most significant proteins are ribosomal proteins such as Ribosomal Protein S8 (RPS8) (FC = 1.43 $\pm$ .29, Q value = 0.0008), Ribosomal Protein RPL18A (FC = 1.58 $\pm$ 0.35, Q value = 0.0008) and Ribosomal Protein L21 (RPL21) (FC = 1.49 $\pm$ 0.28, Q value = 0.0008) that can be aggregated into stress granules in response to the manganese treatment[43,44]. The most significant interactors to DNAJB8 were Integrator Complex Subunit 7 (INST7) (FC = 1.34 $\pm$ 0.16, Q value = 7.6E-5) and Solute Carrier Family 25 (SLC25A5) (FC = 1.35 $\pm$ 0.19, Q value = 7.623E-05). In response to oxidative stress, INST7 can coordinate with ATP-binding Cassette Sub-Family D Member 3 (ABCD3) and High Density Lipoprotein Binding Protein (HDLBP) to help cells attempt to proliferate[45]. Consequently, ABDC3 (FC = 1.19 $\pm$ 0.27, Q value = 0.028) and HDLBP (FC = 1.19 $\pm$ 0.3, Q value = 0.035) both bind more to DNAJB8^{H31Q} after manganese treatment and thus these complexes could form in response to the presence of oxidant. SLC25A5 is a mitochondrial protein overexpressed in response to oxidative stress[46]. Metalloproteins that carry manganese in their structure such as DExH-Box Helicase 9 (DHX9) (FC = 1.38 $\pm$ 0.27, Q value = 0.0009) were also strongly destabilized.

One RNA binding process that appears destabilized after manganese treatment and of significant interest involves NF-Kappa-B-repressing Factor (NKRF) (FC = 1.45 $\pm$

0.34, Q value = 0.0001), 5'-3' Exoribonuclease 2 (XRN2) (FC = 1.50 $\pm$ 0.39, Q value = 0.0009), and DEAH-Box Helicase 15 (DHX15) (FC = 1.18 $\pm$ 0.24, Q value = 0.10). NKRF, as an RNA binding protein interacts with XRN2, a ribonuclease, and DHX15 to process RNA[47,48]. Loss of function from one of these proteins can lead to impairment of early pre-rRNA cleavage which could lead to cellular toxicity from the resulting uncleaved RNA[49,50]. NKRF could arguably be considered the most responsible binding partner for this process as it stimulates DHX15 catalytic activity and recruits XRN2 to this nucleosome for processing pre-RNA[49]. Interference of this biological process could be a toxic mechanism from Mn exposure if the heavy metal damages one of these proteins, specifically NKRF. We applied an orthogonal assay, LiP, to assess structural changes in NKRF after Mn treatment.

Mn treatment could misfold the protein and thus prevent it from interacting with DHX15 and NKRF. We targeted three peptides (TNPEYIYAPLK, SESHTDLTFSR, and MTVEYVYER) and followed LiP protocols from previously described experiments[27]. We treated HEK293T cells with 24 hours of either treatment of 100 μM Mn or vehicle and then immediately conducted lysis. Lysates were exposed to several concentrations of PK for 1 minute, quenched by boiling water, and digested by trypsin, and then peptides were quantified by Parallel Reaction Monitoring[51]. The Mn treatment could increase PK proteolysis yield of a peptide implying that NKRF could be destabilized near that sequence[27,52]. If LiP can show Mn treatment destabilized different regions of the NKRF, it also provides structural evidence the protein is misfolded and thus ready to be recognized for refolding by DNAJB8.

We determined that SESHTDLTFSR (P value = 0.03) and MTVEYVYER (P value = 0.03) in NKRF were destabilized after treatment of 100 µM Mn (**Figure 2, Figure S4**).

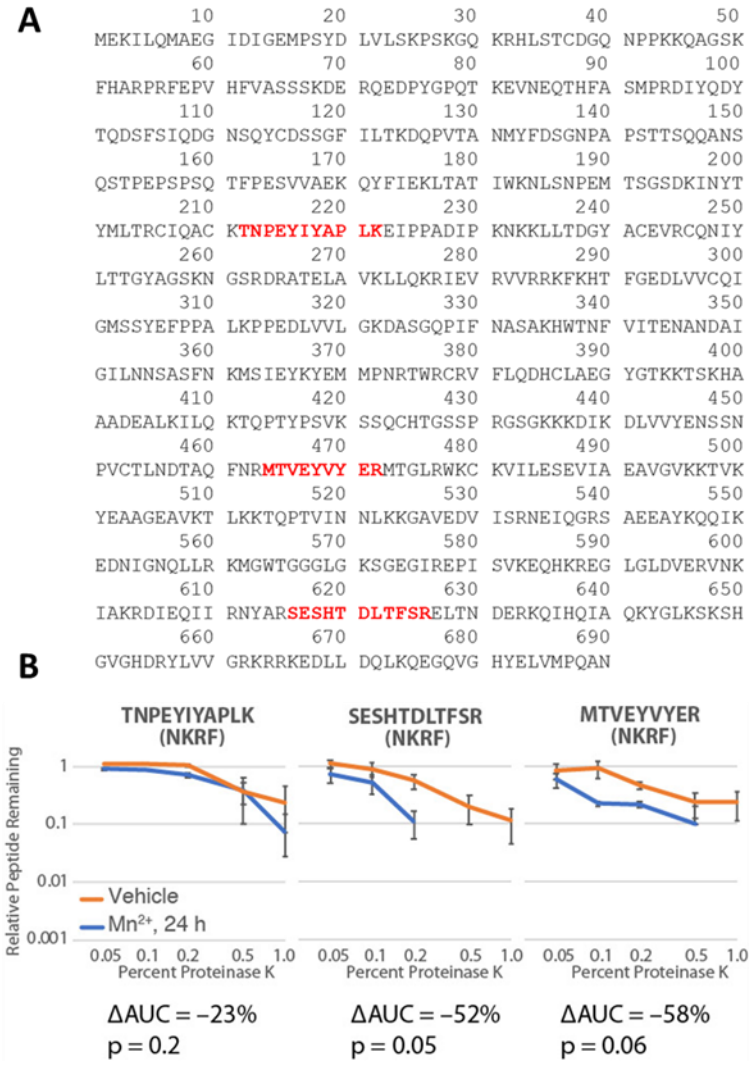

Figure 2. Protein K Susceptibility Curves for Peptides in NKRF. A) Full length amino acid sequence of NKRF is shown with peptides searched for bolded in Red. B) Samples from untreated cells are in orange and samples from Manganese-treated cells are in blue (100 µM, 24 hours). (n=3 biological replicates). B) LiP-PRM graphs show the proteolytic susceptibility of the three peptides. Error bars represents standard error across biological replicates. P values account for significance comparing total area under each condition are located under each graph. ΔAUC refers to the decrease in the area under the curve for the proteolytic susceptibility curves.

Without a crystal structure of NKRF, it's difficult to draw structural conclusions about the consequences of destabilization at these peptides. Both peptides are near a sequence of NKRF known to bind to domains of two different DHX15[48]. Both peptides are also close to the C-terminus compared to the N-terminus where NKRF could bind to XRN2 by the XTBD binding motif[47]. While it's unclear how destabilization of these peptides could inhibit binding to XRN2 and DHX15, increased sensitivity of these two peptides to pk does indicate a change in structure. A misfolded NKRF could lead to possible breakdown of the complex formation with XRN2 and DHX5, and thus not able to process RNA.

Evidence of Mn causing NKRF destabilization by DNAJB8^{H31Q} and LiP follow a similar study profiling the role of NKRF in heat-induced stress environments[35]. The presence of heat (43^{o}C for 40 minutes) induced NKRF is induced in HeLa cells indicating the protein expression as a response of NKRF[35]. NKRF interacts less with XRN2 in the nucleus as seen by confocal imaging[35]. The consequences of NKRF not interacting with XRN2 due to cellular heat can be seen by northern blotting in which blotting for Internal Transcribed Spacers 1 (ITS1) in 47S showed an increase in pre-ribosomal fragment 30SL[35]. Heat stress interfered with NKRF ability in assisting the processing of 47S by XRN2 leading to an overabundance of 30SL[35]. We followed the same experiment to determine if the effects of Mn were similar to effects of heat stress in the interaction between NKRF and XRN2. By using a sample heated to 43 ^{o}C for 40 minutes as a positive control, samples treated with either Mn treatment or water can be compared in particularly by the levels of 30SL. If Mn treatment leads to NKRF not binding to XRN2,

then 47S will only be cleaved into 30SL as indicated by blotting with ITS1. The levels of 30SL in Mn-treated samples should also be larger in comparison to the controls. 100 μM of Manganese did not significantly dissociate XRN2 from NKRF as indicated by the lack of change in the amount of 30SL (Figure S5). XRN2 appears able to process the preRNA into other fragments (21s, 26s, etc.) indicating that Mn treatment may effect NKRF differently in comparison to heat.

4.5 Supplemental Discussion on Limited Proteolysis

We measured assay precision across technical and biological replicates following previous experiments[27]. Ten consecutive injections of a lysate tryptic digest were performed to determine the reproducibility of the scheduled PRM assay. Each targeted run included a 6 μg injection. Each run also had 8 minute retention time window for each peptide, and chromatograms that were scanned at 7500 nominal resolving power. The low resolving power was chosen to minimize cycle time. Lower cycles times allow can increase robustness of quantification since it will allow for more scans across peaks[53]. CVs were calculated for the integrated fragment intensities of the 3 targeted peptides. Skyline was used to quantify the MS2 intensities of transitions from a precursor ion from each peptide. The median CV for the summed MS2 transitions among the 3 targeted peptides was 7.6% (**Table S3**). These CVs are typical for PRM[27,54].

PRM runs at 60,000 nominal resolving power were then run. These runs were compared to the runs at 7500 nominal resolving power. We performed 6 more technical replicate PRM experiments on a HEK239T tryptic digest using 60,000 nominal resolving

power and scheduled only two select peptides (**Table S4**). The two selected peptides had retention time windows that did not overlap with each other to minimize cycle times. The calculated CV from the six runs were compared with the quantification of the previous measurements that were run at 7500 resolution. The median CV for the summed transitions MS2 among the 2 targeted peptides was 12.6. Higher resolving power hence did not increase the precision of the method.

The CV between biological replicates was addressed during the LiP mass spec runs. The LiP mass spec samples included three zero PK controls and the following Protein: PK samples: 2000:1, 1000:1, 500:1, 200:1, and 100:1. Peptides were scanned in 8 minute retention time windows at 7500 resolution after a 6 µg HEK293T tryptic digest injection. The CV was calculated among the three Zero PK samples for both Mn exposed and control cellular conditions (**Table S5**). Across these biological replicates, median CV values were below 15%. CV values were comparable compared to previous experiments[27].

4.6 Conclusion

In conclusion, we utilized our platform to identify proteins that are destabilized in response to Mn stress. Several ribosomal proteins were destabilized in response to 24 hours of 100 µM of Mn treatment and one mechanism of Mn toxicity could be through destabilizing NKRF as indicated by limited proteolysis. We thus hope that our approach has provided a few mechanisms and targets for measuring the effects of groundwater polluted with manganese. More importantly, the evidence of destabilized proteins and

cellular toxicity of manganese should contribute to growing need for stricter regulation and more funding for lowering the amounts of manganese in groundwater.

4.7 Supplementary Figures

4.7.1 Limited Proteolysis Scheme:

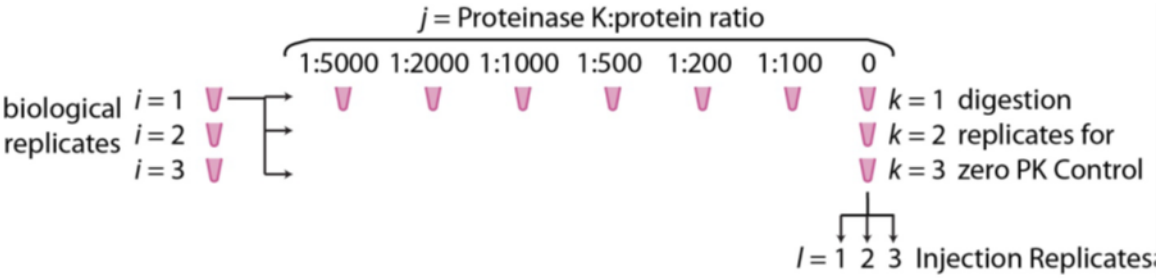

$$\text{fraction remaining } (i) = \frac{\frac{1}{3}\sum_{l=1}^{3}(I_{i,l})}{\frac{1}{9}\sum_{k=1}^{3}\sum_{l=1}^{3}(I_{i,0,k,l})}$$

Figure S1: Sample set-up for limited proteolysis experiments exploring Manganese treatment.

4.7.2 Western Blot Analysis of HSR induction by Manganese

4.7.2.1 Western Blot analysis of HSR induction after short treatment of Manganese:

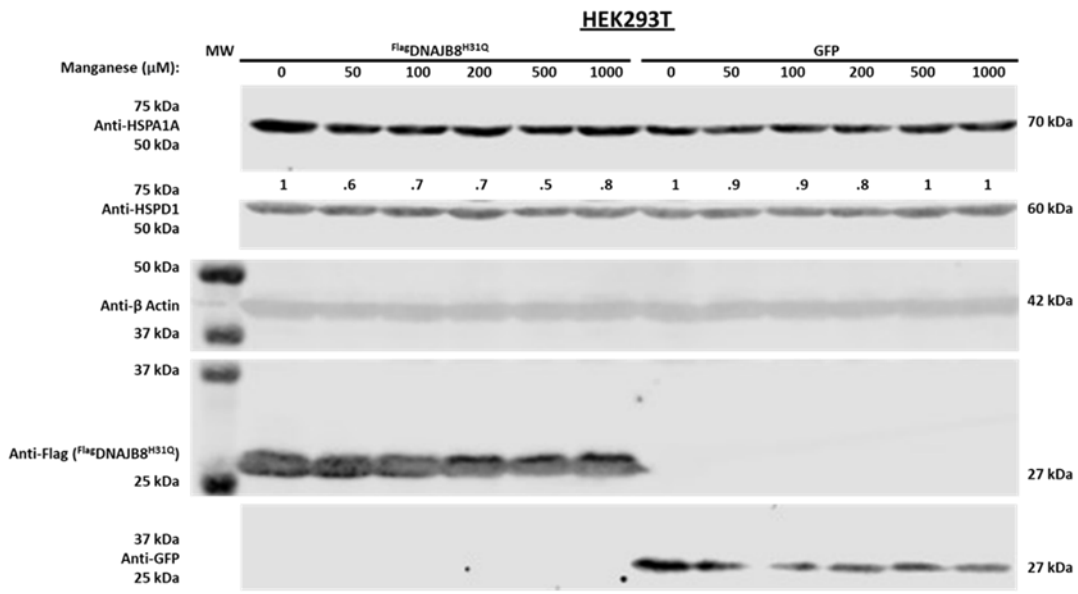

Figure S2: Western Blot analysis of HSR induction by Manganese on HEK293T Cells. Cells were treated for 1 hour with the indicated concentration of manganese ($(MnCl_2) \bullet (H2O)_6$). Cells were then allowed to recover for 16 hours to allow for induction and accumulation of stress response proteins. Predicted weights for antibodies are shown on the right. Numerical values below Anti-HSPA1A slice are band intensities normalized to the 0 μM condition. Antibody for GFP is shown on 800 channel only.

4.7.2.2 Western Blot analysis of HSR induction after longer treatment of Manganese:

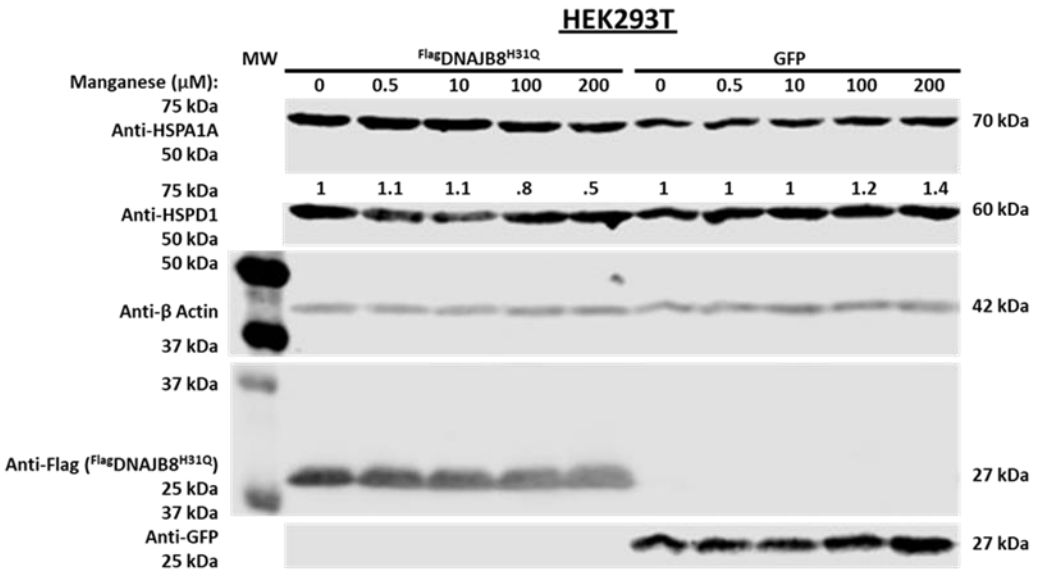

Figure S3: Western Blot analysis of HSR induction by Manganese on HEK293T Cells. Cells were treated for 24 hours with the indicated concentration of manganese ($(MnCl_2) \bullet (H2O)_6$). Cells were then allowed to recover for 16 hours to allow for induction and accumulation of stress response proteins. Predicted weights for antibodies are shown on the right. Numerical values below Anti-HSPA1A slice are band intensities normalized to the 0 μM condition. Antibody for GFP is shown on 800 channel only.

4.7.2.3 Representative Silver Stain for Mn Treatment:

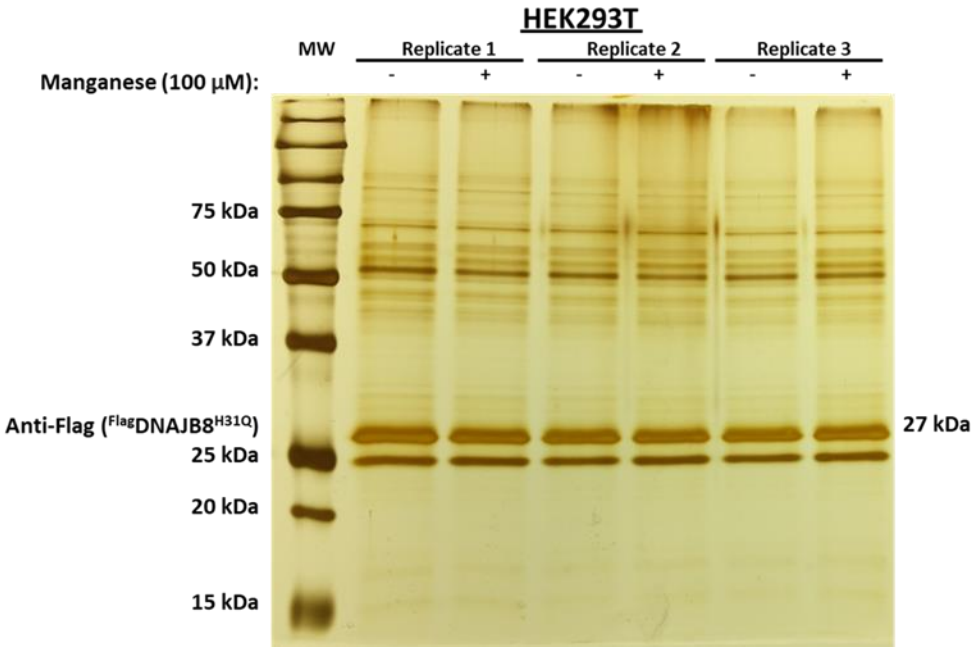

Figure S4: Representative Silver Stain for Mn Treatment. Each replicate contained two transfected ^{FLAG}DNAJB8^{H31Q} 10 cm plates treated with either 100 μM Manganese or water (control). Three replicates are stained to show bait and visually show differences in prey after each respective pulldown. ^{Flag}DNAJB8^{H31Q} is the most abundant protein in each replicate after the immunoprecipitation. Other bands represent proteins recovered with DNAJB8.

4.7.2.4 Representative Northern Blot after Manganese Treatment:

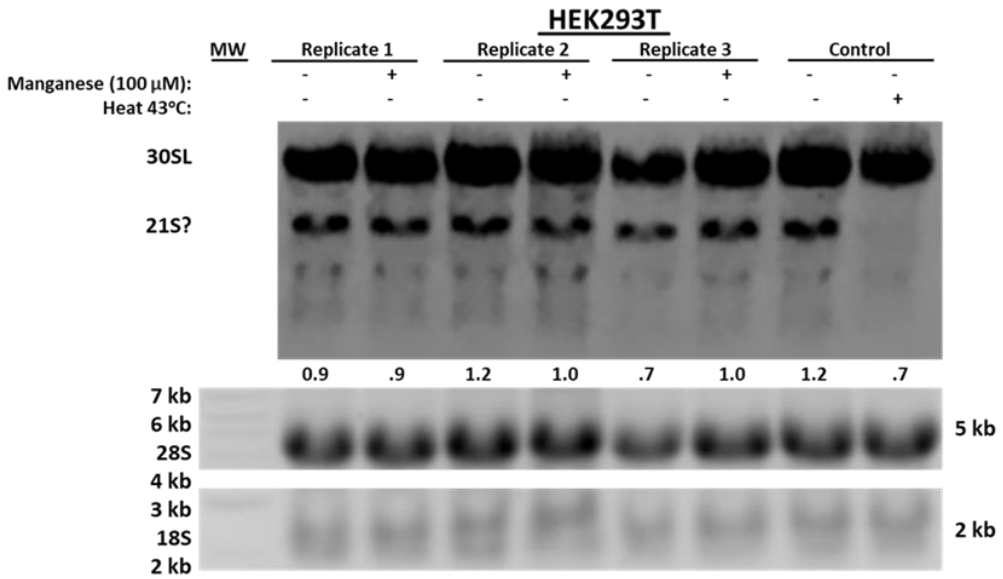

Figure S5: Representative Northern Blot after Manganese Treatment. Northern blot experiment consists of three plates treated with 100 μM Manganese for 24 hours compared to three plates treated with water for 24 hours. Gels were blotted with ITS-700 conjugated to 700-Dye. Samples were compared to a positive control that was heated at 43 ºC for 40 minutes. A secondary technical replicate was stained by Ethidium bromide to show 28S and 18S levels.

4.8 Supplementary Tables

4.8.1 Discussed DNAJB8^{H31Q} Interactors after Manganese Treatment:

Gene	Combined ttest	Combined Fold	Combined Standard Deviation	log2 Combined Fold Change	-log p	rank	qvalue BH	qvalue BH	qvalue Storey
INTS7	6.08601E-08	1.3405891	0.163064267	0.422867144	7.215668	1	0.000209	0.000157	7.35E-05
SLC25A5	9.14028E-08	1.3464507	0.188371019	0.429161361	7.03904	2	0.000157	0.000157	7.35E-05
RPS8	2.93182E-06	1.4337106	0.299380601	0.519753821	5.532863	6	0.00168	0.001611	0.000754
RPL18A	3.34842E-06	1.5778304	0.352845303	0.657942179	5.475161	7	0.001645	0.001611	0.000754
RPL21	3.87078E-06	1.4871304	0.282600848	0.572531134	5.412202	8	0.001663	0.001611	0.000754
DHX9	1.26313E-05	1.381924	0.27007729	0.466678276	4.89855	23	0.001888	0.001849	0.000865
XRN2	1.59896E-05	1.5038116	0.385066929	0.588623864	4.796163	28	0.001963	0.001941	0.000908
NKRF	2.25223E-05	1.4571542	0.339167218	0.543153571	4.647387	35	0.002212	0.002207	0.001032
ABCD3	0.009197367	1.191985	0.265371898	0.253366041	2.036337	542	0.05834	0.05834	0.027289
HDLBP	0.013791008	1.1903313	0.297418943	0.251363203	1.860404	666	0.071191	0.071191	0.0333
DHX15	0.073937645	1.1836036	0.240688458	0.243185979	1.131134	1289	0.197205	0.197205	0.092243

Table S1: DNAJB8^{H13Q} Interactors after Manganese Treatment. Selected Proteins interacting with DNAJB8^{H31Q} after manganese treatment are highlighted. The complete comprehensive list and definitions is available with permission.

4.8.2 Measurement of Significance in Proteolytic Susceptibility Curve:

Protein Gene	Peptide Sequence	Precursor Mass m/z	Experiment	P value
NKRF	TNPEYIYAPLK	654.8453	NKRF LiP	0.09
NKRF	SESHTDLTFSR	640.2993	NKRF LiP	0.05
NKRF	MTVEYVYER	595.2815	NKRF LiP	0.06

Table S2: Measurement of Significance of all Proteolytic Susceptibility curves from LiP Experiment. P values are determining by comparing the area under each proteolytic susceptibility curve.

4.8.3. Coefficient of Variance at 7500 Resolution:

Protein Gene	Peptide Sequence	Precursor Mass m/z	Activation Energy	Retention Time Average	Avg. Intensity	CV
NKRF	TNPEYIYAPLK	654.8453	35	32.3	2.27E+04	7.6
NKRF	SESHTDLTFSR	640.2993	35	33.49	2.65E+04	5.6
NKRF	MTVEYVYER	595.2815	35	24.53	6.48E+03	20.2
					Median CV	7.6
					Average CV	11.1

Table S3: Coefficient of Variance (CV) after Ten Technical Replicates at 7500 Resolution. CV were calculated for the three peptides at 7500 resolution.

4.8.4 Coefficient of Variance at 60,000 Resolution:

Protein Gene	Peptide Sequence	Precursor Mass m/z	Activation Energy	Retention Time Average	Avg. Intensity	CV
NKRF	SESHTDLTFSR	640.2993	35	32.1	1.82E+06	11.5
NKRF	MTVEYVYER	595.2815	35	22.8	2.99E+06	13.6
					Median CV	12.6
					Average CV	12.6

Table S4: Coefficient of Variance (CV) after Six Technical Replicates at 60,000 Resolution. CV were calculated for the three peptides at 60,000 resolution.

Protein Gene	Peptide Sequence	Precursor Mass m/z	Activation Energy	Retention Time Average	CV Zero PK controls #1 (No Manganese)	CV Zero PK controls #2 (No Manganese)	CV Zero PK controls #3 (No Manganese)		CV Zero PK controls #1 (Manganese)	CV Zero PK controls #2 (Manganese)	CV Zero PK controls #3 (Manganese)
NKRF	TNPEYIYAPLK	654.8453	35	31.1	12.1	4	2.1		10.1	3.3	6.2
NKRF	SESHTDLTFSR	640.2993	35	32.2	20.2	9	13.9		9.3	3.6	19.5
NKRF	MTVEYVYER	595.2815	35	23.1	16.5	14.1	26.4		15	26.1	13.9
				Median CV	16.5	9	13.9	**Median CV**	10.1	3.6	13.9
				Combined Average Median CV (No Manganese)	13.1			**Combined Average Median CV (Manganese)**	9.2		
				Average CV	16.3	9	14.1	**Average CV**	13.03	19.46	11.26
				Combined Average CV (No Manganese)	13.1			**Combined Average CV (Manganese)**	11.9		

Table S5: Coefficient of Variance (CV) between three biological replicates in NKRF LiP. CV of targeted peptides are shown. Definitions and more information can be provided with permission.

References

[1]Ramachandran, M.; Schwabe, K. A.; Ying, S. C. Shallow Groundwater Manganese Merits Deeper Consideration. *Environ. Sci. Technol.* **2021**, *55* (6), 3465–3466. https://doi.org/10.1021/acs.est.0c08065.

[2]Shaji, E.; Santosh, M.; Sarath, K. V.; Prakash, P.; Deepchand, V.; Divya, B. V. Arsenic Contamination of Groundwater: A Global Synopsis with Focus on the Indian Peninsula. *Geosci. Front.* **2021**, *12* (3), 101079. https://doi.org/10.1016/j.gsf.2020.08.015.

[3]Deda, A.; Alushllari, M.; Mico, S. Measurement of Heavy Metal Concentrations in Groundwater. *AIP Conf. Proc.* **2019**, *2109* (June 2019), 3–7. https://doi.org/10.1063/1.5110136.

[4]Tchounwou P.B., Yedjou C.G., Patlolla A.K., Sutton D.J. (2012) Heavy Metal Toxicity and the Environment. In: Luch A. (eds) Molecular, Clinical and Environmental Toxicology. Experientia Supplementum, vol 101. Springer, Basel. https://doi.org/10.1007/978-3-7643-8340-4_6.

[5]Balali-Mood, M.; Naseri, K.; Tahergorabi, Z.; Khazdair, M. R.; Sadeghi, M. Toxic Mechanisms of Five Heavy Metals: Mercury, Lead, Chromium, Cadmium, and Arsenic. *Front. Pharmacol.* **2021**, *12* (April), 1–19. https://doi.org/10.3389/fphar.2021.643972.

[6]Chin-Chan, M.; Navarro-Yepes, J.; Quintanilla-Vega, B. Environmental Pollutants as Risk Factors for Neurodegenerative Disorders: Alzheimer and Parkinson Diseases. *Front. Cell. Neurosci.* **2015**, *9* (APR), 1–22. https://doi.org/10.3389/fncel.2015.00124.

[7]Vasanthi, P.; Kaliappan, S.; Srinivasaraghavan, R. Impact of Poor Solid Waste Management on Ground Water. *Environ. Monit. Assess.* **2008**, *143* (1–3), 227–238. https://doi.org/10.1007/s10661-007-9971-0.

[8]Schaider, L. A.; Ackerman, J. M.; Rudel, R. A. Septic Systems as Sources of Organic Wastewater Compounds in Domestic Drinking Water Wells in a Shallow Sand and Gravel Aquifer. *Sci. Total Environ.* **2016**, *547*, 470–481. https://doi.org/10.1016/j.scitotenv.2015.12.081.

[9]Mohankumar, K.; Hariharan, V.; Rao, N. P. Heavy Metal Contamination in Groundwater around Industrial Estate vs Residential Areas in Coimbatore, India. *J. Clin. Diagnostic Res.* **2016**, *10* (4), BC05–BC07. https://doi.org/10.7860/JCDR/2016/15943.7527.

[10]Al-Hashimi, O.; Hashim, K.; Loffill, E.; Tina Marolt, C.; Nakouti, I.; Faisal, A. A. H.; Al-Ansari, N. A Comprehensive Review for Groundwater Contamination and

Remediation : Occurrence , Migration and Adsorption Modelling. *Molecules* **2021**, *26* (5913), 1–28.

[11]Selvi, A.; Rajasekar, A.; Theerthagiri, J.; Ananthaselvam, A.; Sathishkumar, K.; Madhavan, J.; Rahman, P. K. S. M. Integrated Remediation Processes toward Heavy Metal Removal/Recovery from Various Environments-A Review. *Front. Environ. Sci.* **2019**, *7* (May). https://doi.org/10.3389/fenvs.2019.00066.

[12]Petersen-Perlman, J. D.; Megdal, S. B.; Gerlak, A. K.; Wireman, M.; Zuniga-Teran, A. A.; Varady, R. G. Critical Issues Affecting Groundwater Quality Governance and Management in the United States. *Water (Switzerland)* **2018**, *10* (6), 1–17. https://doi.org/10.3390/w10060735.

[13]Madramootoo, C. A. Sustainable Groundwater Use in Agriculture. *Irrig. Drain.* **2012**, *61* (SUPPL.1), 26–33. https://doi.org/10.1002/ird.1658.

[14]Carrard, N.; Foster, T.; Willetts, J. Groundwater as a Source of Drinking Water in Southeast Asia and the Pacific: A Multi-Country Review of Current Reliance and Resource Concerns. *Water (Switzerland)* **2019**, *11* (8). https://doi.org/10.3390/w11081605.

[15]Sidoryk-Wegrzynowicz, M.; Aschner, M. Manganese Toxicity in the Central Nervous System: The Glutamine/Glutamate-γ-Aminobutyric Acid Cycle. *J. Intern. Med.* **2013**, *273* (5), 466–477. https://doi.org/10.1111/joim.12040.

[16]Chen, P.; Bornhorst, J.; Aschner, M. Manganese Metabolism in Humans. *Front. Biosci. - Landmark* **2018**, *23* (9), 1655–1679. https://doi.org/10.2741/4665.

[17]Peres, T. V.; Parmalee, N. L.; Martinez-Finley, E. J.; Aschner, M. Untangling the Manganese-α-Synuclein Web. *Front. Neurosci.* **2016**, *10* (AUG), 1–8. https://doi.org/10.3389/fnins.2016.00364.

[18]Kwakye, G. F.; Paoliello, M. M. B.; Mukhopadhyay, S.; Bowman, A. B.; Aschner, M. Manganese-Induced Parkinsonism and Parkinson's Disease: Shared and Distinguishable Features. *Int. J. Environ. Res. Public Health* **2015**, *12* (7), 7519–7540. https://doi.org/10.3390/ijerph120707519.

[19]Brazier, M. W.; Davies, P.; Player, E.; Marken, F.; Viles, J. H.; Brown, D. R. Manganese Binding to the Prion Protein. *J. Biol. Chem.* **2008**, *283* (19), 12831–12839. https://doi.org/10.1074/jbc.M709820200.

[20]Brown, D. R.; Hafiz, F.; Glasssmith, L. L.; Wong, B. S.; Jones, I. M.; Clive, C.; Haswell, S. J. Consequences of Manganese Replacement of Copper for Prion Protein Function and Proteinase Resistance. *EMBO J.* **2000**, *19* (6), 1180–1186.

https://doi.org/10.1093/emboj/19.6.1180.

[21]Wong, B. S.; Chen, S. G.; Colucci, M.; Xie, Z.; Pan, T.; Liu, T.; Li, R.; Gambetti, P.; Sy, M. S.; Brown, D. R. Aberrant Metal Binding by Prion Protein in Human Prion Disease. *J. Neurochem.* **2001**, *78* (6), 1400–1408. https://doi.org/10.1046/j.1471-4159.2001.00522.x.

[22]Zhu, Y., Lu, X., Wu, D. *et al.* The Effect of Manganese-induced Cytotoxicity on mRNA Expressions of HSP27, HSP40, HSP60, HSP70 and HSP90 in Chicken Spleen Lymphocytes in Vitro. *Biol Trace Elem Res* **156,** 144–152 (2013). https://doi.org/10.1007/s12011-013-9817-2

[23]Leuenberger, P.; Ganscha, S.; Kahraman, A.; Cappelletti, V.; Boersema, P. J.; Von Mering, C.; Claassen, M.; Picotti, P. Cell-Wide Analysis of Protein Thermal Unfolding Reveals Determinants of Thermostability. *Science (80).* **2017**, *355* (6327). https://doi.org/10.1126/science.aai7825.

[24]Adhikari, J.; West, G. M.; Fitzgerald, M. C. Global Analysis of Protein Folding Thermodynamics for Disease State Characterization. *J. Proteome Res.* **2015**, *14* (5), 2287–2297. https://doi.org/10.1021/acs.jproteome.5b00057.

[25] T. Zhang, C. Wolfe, A. Pierle, K. A. Welle, J. R. Hryhoernko, S. Ghaemmaghami. *PNAS*, **2017**, 114, DOI: 10.1073/pnas.1710238114.

[26] M. M. Savitski, F. B. M. Reinhard, H. Franken, T. Werner, M. F. Savitski, D. Eberhard, D. M. Molina, R. Jafari, R. B. Dovega, S. Klaeger, B. Kuster, P. Nordlund, M. Bantscheff, G. Drewes. Science 2014, 346, 1255784 DOI: 10.1126/science.1255784.

[27]Quanrud, G. M.; Montoya, M. R.; Mei, L.; Awad, M. R.; Genereux, J. C. Hsp40 Affinity to Identify Proteins Destabilized by Cellular Toxicant Exposure. *Anal. Chem.* **2021**. https://doi.org/10.1021/acs.analchem.1c04230.

[28]L. Mei, M. R. Montoya, G. M. Quanrud, M. Tran, A. Villa-Sharma, M. Huang, J. C. Genereux. *J. Proteome. Res.* **2020**, 19, 1565-1573.

[29]Washburn, M. P.; Wolters, D.; Yates, J. R. Large-Scale Analysis of the Yeast Proteome by Multidimensional Protein Identification Technology. *Nat. Biotechnol.* **2001**, *19* (3), 242–247. https://doi.org/10.1038/85686.

[30]A.T. Kong, F.V. Leprevost, D.M. Avtonomov, D. Mellacheruvu, A.I. Nesvizhskii. *Nat. Meth.* **2017**, *14*, 513-520.
[31]D. L. Plubell, P. A. Wilmarth, Y. Zhao, A. M. Fenton, J. Minnier, A. P. Reddy, J. Klimek, X. Yang, L. L. David, N. Pamir, *Mol. Cell. Proteomics* **2017**, *16*, 873–890.

[32]Washburn, M. P.; Wolters, D.; Yates, J. R. Large-Scale Analysis of the Yeast Proteome by Multidimensional Protein Identification Technology. *Nat. Biotechnol.* **2001**, *19* (3), 242–247. https://doi.org/10.1038/85686.

[33]Storey, J. D.; Tibshirani, R. Statistical Significance for Genomewide Studies. *Proc. Natl. Acad. Sci. U. S. A.* **2003**, *100* (16), 9440–9445. https://doi.org/10.1073/pnas.1530509100.

[34]L. K. Pino, B. C. Searle, H. Y. Yang, A. N. Hoofnagle, W. S. Noble, M. J. MacCoss, *J. Proteome Res.* **2020**, *19*, 1147–1153.

[35]Coccia, M.; Rossi, A.; Riccio, A.; Trotta, E.; Santoro, M. G. Human NF-KB Repressing Factor Acts as a Stress-Regulated Switch for Ribosomal RNA Processing and Nucleolar Homeostasis Surveillance. *Proc. Natl. Acad. Sci. U. S. A.* **2017**, *114* (5), 1045–1050. https://doi.org/10.1073/pnas.1616112114.

[36]Thermo Fisher Scientific. TRIzol Reagent User Guide - Pub. No. MAN0001271 - Rev. A.0. *Thermo Fish. Sci.* **2016**, 1–6.

[37]Mansour, F. H.; Pestov, D. G. Separation of Long RNA by Agarose-Formaldehyde Gel Electrophoresis. *Anal. Biochem.* **2013**, *441* (1), 18–20. https://doi.org/10.1016/j.ab.2013.06.008.

[38]Guo, R.; Xu D.; Wang. W. Identification and analysis of new proteins involved in the DNA damage response network of Fanconi anemia and Bloom syndrome. *Methods*. **2009**, 48. 72-79.

[39]S. S. Cao, R. J. Kaufman. *Antioxid. Redox Signal*. **2014**, *21*, 396-413.

[40]Klaips CL, Jayaraj GG, Hartl FU. Pathways of cellular proteostasis in aging and disease. *J Cell Biol* 2018;**217**:51–63. https://doi.org/10.1083/jcb.201709072.

[41]Bowman, A. B.; Aschner, M. Considerations on Manganese (Mn) Treatments for in Vitro Studies. *Neurotoxicology* **2014**, *41*, 141–142. https://doi.org/10.1016/j.neuro.2014.01.010.

[42]N. Rauniyar, J. R. Yates, *J. Proteome Res*. **2014**, *13*, 5293–5309.

[43]A. Turakhiya, S. R. Meyer, G. Marincola, A. Schlosser, K. Hof-mann, *Mol. Cell* **2018**, 906–919.

[44]S. Tam, R. Geller, C. Spiess, J. Frydman, *Nat. Cell Biol*. **2006**, *8*, DOI 10.1038/ncb1477.

[45]Liu, Y.; Yu, X.; Huang, A.; Zhang, X.; Wang, Y.; Geng, W.; Xu, R.; Li, S.; He, H.; Zheng, B.; Chen, G.; Xu, Y. INTS7–ABCD3 Interaction Stimulates the Proliferation and Osteoblastic Differentiation of Mouse Bone Marrow Mesenchymal Stem Cells by Suppressing Oxidative Stress. *Front. Physiol.* **2021**, *12* (November), 1–12. https://doi.org/10.3389/fphys.2021.758607.

[46]Lytovchenko, O.; Kunji, E. R. S. Expression and Putative Role of Mitochondrial Transport Proteins in Cancer. *Biochim. Biophys. Acta - Bioenerg.* **2017**, *1858* (8), 641–654. https://doi.org/10.1016/j.bbabio.2017.03.006.

[47]Alexandrova, J.; Piñeiro, D.; Jukes-Jones, R.; Mordue, R.; Stoneley, M.; Willis, A. E. Full-Length NF-KB Repressing Factor Contains an XRN2 Binding Domain. *Biochem. J.* **2020**, *477* (4), 773–786. https://doi.org/10.1042/BCJ20190733.https://portlandpress.com/biochemj/article/477/4/773/222031/Full-length-NF-B-repressing-factor-contains-an

[48]Studer, M. K.; Ivanovic, L.; Weber, M. E.; Marti, S.; Jonas, S. Structural Basis for DEAH-Helicase Activation by G-Patch Proteins. *Proc. Natl. Acad. Sci. U. S. A.* **2020**, *117* (13), 7159–7170. https://doi.org/10.1073/pnas.1913880117.

[49]Memet, I.; Doebele, C.; Sloan, K. E.; Bohnsack, M. T. The G-Patch Protein NF-KB-Repressing Factor Mediates the Recruitment of the Exonuclease XRN2 and Activation of the RNA Helicase DHX15 in Human Ribosome Biogenesis. *Nucleic Acids Res.* **2017**, *45* (9), 5359–5374. https://doi.org/10.1093/nar/gkx013.

[50]Sicot, G.; Gomes-Pereira, M. RNA Toxicity in Human Disease and Animal Models: From the Uncovering of a New Mechanism to the Development of Promising Therapies. *Biochim. Biophys. Acta - Mol. Basis Dis.* **2013**, *1832* (9), 1390–1409. https://doi.org/10.1016/j.bbadis.2013.03.002.

[51]A. C. Peterson, J. D. Russell, D. J. Bailey, M. S. Westphall, J. J. Coon. *Mol. Cell. Proteomics*. **2012**, *11*, 1475-1488.

[52]Y. Feng, G. De Franceschi, A. Kahraman, M. Soste, A. Melnik, P.J. Boersema, P. Polverino de Laureto, Y. Nikolaev, A. P. Oliveira, P. Picotti. *Nat. Biotech*. **2014**, *32*, 1036-1044.

[53]S. Gallefi, A. Bourmaud, S. Y. Kim, B. Domon. *J. Proteomics.* **2014,** 147-159.

[54]G. E. Ronsein, N. Pamir, P. D. Von Haller, D. S. Kim, M. N. Oda, G. P. Jarvik, T. Vaisar, J. W. Heinecke. *J. Proteomics.* **2015**, 3899.

Chapter 5 Conclusions and Outlook

5.1 Unique Assessments by DNAJB8^{H31Q} of Misfolded Proteins

Each environmental stress produced different significantly destabilized proteins based on their interactions with DNAJB8^{H31Q}. Oxidative stresses, depending on whether from arsenite, cadmium, or manganese, all targeted different proteins. TAR DNA-binding protein (TDP43), a known biomarker for Amyotrophic Lateral Sclerosis (ALS) was significantly destabilized only after arsenite treatment in comparison to exposure to other heavy metals tested[1,2]. While DNAJB8^{H31Q} interacting with TDP43 after arsenite treatment reaffirms its toxicity with metal, it also reaffirms the selective reactivity TDP43 can have toward some metals other than manganese and cadmium[3,4]. The misfolded proteins pulled down from each oxidative stress are thus unique to each environmental treatment despite all metals sharing similar oxidative mechanisms.

There were also differences in how the proteome responded to different types of stresses. Exposure to different electrophilic herbicides affected proteins differently. Structural isomers (alachlor and acetochlor) exhibited different proteome reactivity profiles. The smaller herbicide (propachlor) destabilized the proteome even more when more proteins interacted with DNAJB8^{H31Q} after treatment. Comparing the herbicide affected proteomes with the proteomes exposed to heavy metals, the proteins that were destabilized and significantly interacted with DNAJB8^{H31Q} were different. A subset of the destabilized proteome affected by arsenite or manganese were ribosomal proteins, possibly aggregating into stress granules[5,6,7]. Ribosomal proteins were also affected by

herbicides, but more significantly destabilized proteins were mostly enzymatic proteins such as TYMS, ACAT1, and GAPDH, all prone to covalent modification at active cysteines[8,9]. These enzymes appeared more destabilized after electrophilic modification despite having cysteines that can also be prone to oxidation[10,11]. These enzymes appeared to be more vulnerable to electrophilic exposure compared to oxidative exposure. These differences in protein reactivity to same and different types of stresses are shown based on the protein interaction with DNAJB8^{H31Q}.

The structural recognition of misfolded proteins from DNAJB8^{H31Q} was also validated by Limited Proteolysis (LiP) and other assays. LiP provided evidence that these proteins changed conformationally whether globular or regional after incubation of a stress due to their increased sensitivity to proteinase K (PK)[12]. LiP showed that several proteins such as PDHA1 and NKRF were indeed misfolded and thus likely to bind to DNAJ8^{H31Q} after treatment to be refolded. Enzymatic activity assays that explore the effects on herbicides on protein activities for GAPDH and PARK7 showed a loss of function indicating both proteins may misfold after propachlor treatment. The improved likelihood that DNAJB8^{H31Q} identified misfolded proteins after incubation of a stress provided further credibility in the assessment of the cellular effects from each environmental toxin.

5.2 More Insights into Investigating Environmental Stresses Using DNAJB8^{H31Q}

There are added possible benefits in utilizing DNAJB8^{H31Q} as a sensor for misfolded proteins. Cellular stresses can modify native and folding intermediates and

cause them to misfold and possibly aggregate together[13,14]. DNAJB8^{H31Q}, as part of the heat shock response, is prompted to recognize and bind to any level of a misfolded protein to determine which proteins are more sensitive to a cellular stress. The role and involvement that DNAJB8 has in the protein misfolding response can also provide additional insights based on the pulled down interactors. DNAJB8^{H31Q} can identify the essential protein quality control factors involved as part of the proteostasis response to a particular cellular stress. Coimmunoprecipitated proteins with DNAJB8^{H31Q} for example can be small Hsp (sHsps) proteins overexpressed in response to cellular stress, and thus these proteins cooperate with DNAJB8 to help target misfolded proteins[15]. HSPB1, a small heat shock protein, significantly interacted with DNAJB8 after propachlor treatment. Rather than misfolding, this protein quality control factor may be assisting DNAJB8 in refolding proteins. Proteins that also bind with DNAJB8^{H31Q} less after incubation with the cellular stress can be possible treatments against the stimulus. Proteins can be overexpressed to activate heat shock response or suppress aggregation, and DNAJB^{H31Q} can identify them by looking at proteins that bind significantly less with DNAJB8 after treatment of a cellular stress[16,17]. The interactors with DNAJB8^{H31Q} after incubation of a cellular stress can thus both provide the misfolded proteome and proteins involved in protein recognition and prevention of cellular stress. DNAJB8^{H31Q} can additionally highlight some of the proteostasis response to cellular stress.

The nature of the cellular stress in terms of the type of mechanisms can also be inferred based on the client list of interactors with DNAJB8^{H31Q}. Cellular stresses can be very specific in the type of damage and targeted region in the cell[18]. Genomic stress, a

type of cellular stress related to DNA damage, can specifically target DNA associated interactors in the nucleus and cytosol[19]. Reactive Oxygen Species (ROS) can initially target the Ubiquitin-Proteasome system and mitochondria before spreading oxidative stress into the cytosol in neurodegenerative diseases[20]. Proteins that significantly bind more to DNAJB8^{H31Q} can be considered the targets of the cellular stress. DNAJB8 thus can specify which proteins in the proteome and regions of the cell are most vulnerable to a cellular stress. It can determine if the effects of a cellular stress are more proteome specific than generally specific.

DNAJB8^{H31Q} thus has the capabilities of providing a large overview of cellular stress. The protein-protein interactions of DNAJB8^{H31Q} can determine which proteins are misfolded by cellular stresses, which proteins are activated to respond to the stress, and which proteins are targeted by the stresses. One constant cellular exposure that could use these evaluations from DNAJB8 is profiling the cellular effects of environmental toxins and toxicants. The everyday environment that people experience provides a broad range of different types of cellular exposures. Sunlight for example can shine toxicity into cells through ultraviolet radiation, visible light, and infra-red radiation[21,22]. The increase in dietary intake of toxic metals found in groundwater, food, and air can damage cellular activity[23,24,25,26]. The high amount of cellular exposure to the environment can use DNAJB8^{H31Q} to understand how proteins misfold after treatment, which proteins are specifically targeted by the toxin, and how can cells adapt and respond to them.

There was also strong evidence of protein misfolding after exposure to environmental stresses that can be recognized by DNAJB8^{H31Q}. Heavy metals such as

arsenite can disrupt protein activity by several means, such as by displacing native metals, inactivating catalytic nucleophiles, or oxidizing of certain residues[27,28,29,30]. The oxidizing nature of heavy metals can generate superoxide, hydroxy radicals, and singlet oxygen species that are all prevalent in several diseases[31,32]. Herbicides can damage proteins through covalent modification. Enzymatic function can be depleted after covalent conjugation, and carbonylation can promote protein aggregation[33,34,35]. These structural modifications can make them misfold and aggregate and thus ideal for DNAJB8^{H31Q} recognition. The identity of the misfolded proteins can also elucidate which part of the proteome is most vulnerable to the environmental stress.

The accumulation of misfolded proteins due to environmental stress has also been known to activate different stress responses. Exposure to heavy metals has been found to induce Heat Shock Response (HSR), the Unfolded Protein Response (UPR), and the mitochondrial Unfolded Protein Response (mtUPR)[36,37,38,39]. Incubation of pesticides and herbicides has also been found to activate HSR[40]. Activation of these stress responses indicates the presence of protein quality control factors that can assist DNABJ8^{H31Q} in protein misfolding. DNAJB8^{H31Q} can thus also help identify how the cell adapts to the cellular stress by identifying proteins involved in the protein refolding response.

The interactors pulled down by DNAJB8^{H31Q} can thus provide the mechanism and key proteins involved in how an environmental stress affects the cell. Misfolded clients and proteins involved in the folding response can be identified and quantified to elucidate proteins involved in response to the environmental stress. Most significant binding proteins to DNAJB8^{H31Q} targets can be deemed the proteins most vulnerable to the

environmental incubation. Investigations of arsenite, manganese, and propachlor exposure all utilized the interactors of DNAJB8^{H31Q} to determine possible biological mechanisms of toxicity. Thus continuing to profiling many environmental stresses by DNAJB8^{H31Q} can hopefully show distinct toxic mechanisms for each condition and provide compelling evidence of overall toxic cellular disruption.

5.3 Strategic Outcomes and Goals from DNAJB8^{H31Q}Assessments

DNAJB8^{H31Q} combined with LiP, can provide the effective first steps in protein screening. Proteins can be screened against a different cellular stress by interaction with DNAJB8^{H31Q}, and then enriched to be identified by LC-MS/MS. Secondary assays such as LiP can validate the most significant interactors as possibly misfolded and thus provide possible targets for combating the cellular stress. Immediate strategies could be to protect these stress-effected proteins by screening the proteins against small molecules similarly to CETSA[41,42]. Proteins that bind to ligand could be protected from the stress, less likely to misfold, and thus not recognized by DNAJB8^{H31Q}.

Other strategies could aim to strengthen the significance of a misfolded protein after incubation of a stress. RNA silencing (RNAi) can be used to interfere and reduce expression of a targeted protein as an effort to reduce the toxicity of the cellular stress[43,44]. RNA silencing could be used to reduce expression of PDHA1 in an attempt to minimize arsenite toxicity for example. Other gene editing alternatives to RNAi to alter expression of a targeted protein could be with CRISR/CAS9. CRISPR/CAS9 can be used to completely knockdown a misfolded protein and can also be used to overexpress a

protein that could be used to protect the cell against a cellular stress[45,46]. Several proteins identified to bind significantly less to DNAJ8^{H31Q} after propachlor treatment, for example, could be overexpressed by CRISPR/CAS9 to help the cell recover or survive the electrophilic stress better.

Competing or serial stress mechanisms can be worth exploring with DNAJB^{H31Q} by profiling how the misfolded proteome changes with successive exposure of different stresses. Proteins oxidized after exposure to a heavy metal could have different reactivity toward an electrophile. Proteins could also become more stable depending on the type of oxidative stress. For example, pulldowns from DNAJB8^{H31} showed that the cadmium-effected and arsenite-effected proteomes were almost opposite in terms of affinity for the bait based on comparing their fold changes. The arsenite-effected proteome can become more stable with addition of cadmium exposure and proteins may bind less to DNABJ8^{H31Q}. Thus, DNAJB8^{H31Q} could be used to track more conformational changes in a protein between different stresses.

A more readily and accessible use of using DNAJB8^{H31Q} is to keep exploring environment toxins. Here we profiled only a few heavy metals and electrophiles that we can be exposed to everyday and found success in identifying misfolded proteins and learning about how these toxins can influence the cell. DNAJB8^{H31Q} can be used to assess other heavy metals such as lead, chromium, mercury, or vanadium to investigate protein induced to misfold and their toxic mechanisms. The ultimate advantage of using these DNAJB8^{H31Q} profiles is that it can provide more evidence on how proteins fold and how individuals can better prepare themselves for treatments and possible prevention from

future cellular toxicity.

References

[1]Mackenzie, I. R. A.; Rademakers, R. The Role of Transactive Response DNA-Binding Protein-43 in Amyotrophic Lateral Sclerosis and Frontotemporal Dementia. *Curr. Opin. Neurol.* **2008**, *21* (6), 693–700. https://doi.org/10.1097/WCO.0b013e3283168d1d.

[2]Boyd, J. D.; Peter Lee-Armandt, J.; Feiler, M. S.; Zaarur, N.; Liu, M.; Kraemer, B.; Concannon, J. B.; Ebata, A.; Wolozin, B.; Glicksman, M. A. A High-Content Screen Identifies Novel Compounds That Inhibit Stress-Induced TDP-43 Cellular Aggregation and Associated Cytotoxicity. *J. Biomol. Screen.* **2014**, *19* (1), 44–56. https://doi.org/10.1177/1087057113501553.

[3]Koski, L.; Ronnevi, C.; Berntsson, E.; Wärmländer, S. K. T. S.; Roos, P. M. Metals in Als Tdp-43 Pathology. *Int. J. Mol. Sci.* **2021**, *22* (22), 1–16. https://doi.org/10.3390/ijms222212193.

[4]Ash, P. E. A.; Dhawan, U.; Boudeau, S.; Lei, S.; Carlomagno, Y.; Knobel, M.; Al Mohanna, L. F. A.; Boomhower, S. R.; Newland, M. C.; Sherr, D. H.; Wolozin, B. Heavy Metal Neurotoxicants Induce ALS-Linked TDP-43 Pathology. *Toxicol. Sci.* **2019**, *167* (1), 3–4. https://doi.org/10.1093/toxsci/kfy267.

[5]Wheeler, J. R.; Matheny, T.; Jain, S.; Abrisch, R.; Parker, R. Distinct Stages in Stress Granule Assembly and Disassembly. *Elife* **2016**, 1–25. https://doi.org/10.7554/eLife.18413.

[6]Zhang, K.; Daigle, J. G.; Cunningham, K. M.; Coyne, A. N.; Ruan, K.; Grima, J. C.; Bowen, K. E.; Wadhwa, H.; Yang, P.; Rigo, F.; Taylor, J. P.; Gitler, A. D.; Rothstein, J. D.; Lloyd, T. E. Stress Granule Assembly Disrupts Nucleocytoplasmic Transport. *Cell* **2018**, *173* (4), 958-971.e17. https://doi.org/10.1016/j.cell.2018.03.025.

[7]Campos-Melo, D.; Hawley, Z. C. E.; Droppelmann, C. A.; Strong, M. J. The Integral Role of RNA in Stress Granule Formation and Function. *Front. Cell Dev. Biol.* **2021**, *9* (May), 1–19. https://doi.org/10.3389/fcell.2021.621779.

[8]Tamura, T.; Hamachi, I. Chemistry for Covalent Modification of Endogenous/Native Proteins: From Test Tubes to Complex Biological Systems. *J. Am. Chem. Soc.* **2019**. https://doi.org/10.1021/jacs.8b11747.

[9]Phan, J.; Mahdavian, E.; Nivens, M. C.; Minor, W.; Berger, S.; Spencer, H. T.; Dunlap, R. B.; Lebioda, L. Catalytic Cysteine of Thymidylate Synthase Is Activated upon Substrate Binding. *Biochemistry* **2000**, *39* (23), 6969–6978. https://doi.org/10.1021/bi000367g.

[10]Chung, H. S.; Wang, S. B.; Venkatraman, V.; Murray, C. I.; Van Eyk, J. E. Cysteine Oxidative Posttranslational Modifications: Emerging Regulation in the Cardiovascular System. *Circ. Res.* **2013**, *112* (2), 382–392. https://doi.org/10.1161/CIRCRESAHA.112.268680.

[11]Alcock, L. J.; Perkins, M. V.; Chalker, J. M. Chemical Methods for Mapping Cysteine Oxidation. *Chem. Soc. Rev.* **2018**, *47* (1), 231–268. https://doi.org/10.1039/c7cs00607a.

[12]Schopper, S.; Kahraman, A.; Leuenberger, P.; Feng, Y.; Piazza, I.; Müller, O.; Boersema, P. J.; Picotti, P. Measuring Protein Structural Changes on a Proteome-Wide Scale Using Limited Proteolysis- Coupled Mass Spectrometry. *Nat. Protoc.* **2017**, *12* (11), 2391–2410. https://doi.org/10.1038/nprot.2017.100.

[13]Schramm, F. D.; Schroeder, K.; Jonas, K. Protein Aggregation in Bacteria. *FEMS Microbiol. Rev.* **2019**, *44* (1), 54–72. https://doi.org/10.1093/femsre/fuz026.

[14]Balchin, D.; Hayer-Hartl, M.; Hartl, F. U. In Vivo Aspects of Protein Folding and Quality Control. *Science (80-.).* **2016**, *353* (6294). https://doi.org/10.1126/science.aac4354.

[15]Sinnige T., Yu A., Morimoto R.I. **(2020)** Challenging Proteostasis: Role of the Chaperone Network to Control Aggregation-Prone Proteins in Human Disease. In: Mendillo M.L., Pincus D., Scherz-Shouval R. (eds) HSF1 and Molecular Chaperones in Biology and Cancer. Advances in Experimental Medicine and Biology, vol 1243. Springer, Cham. https://doi.org/10.1007/978-3-030-40204-4_4.

[16]Khodaparast, L.; Khodaparast, L.; Gallardo, R.; Louros, N. N.; Michiels, E.; Ramakrishnan, R.; Ramakers, M.; Claes, F.; Young, L.; Shahrooei, M.; Wilkinson, H.; Desager, M.; Mengistu Tadesse, W.; Nilsson, K. P. R.; Hammarström, P.; Aertsen, A.; Carpentier, S.; Van Eldere, J.; Rousseau, F.; Schymkowitz, J. Aggregating Sequences That Occur in Many Proteins Constitute Weak Spots of Bacterial Proteostasis. *Nat. Commun.* **2018**, *9* (1). https://doi.org/10.1038/s41467-018-03131-0.

[17]Jena, K. K.; Kolapalli, S. P.; Mehto, S.; Nath, P.; Das, B.; Sahoo, P. K.; Ahad, A.; Syed, G. H.; Raghav, S. K.; Senapati, S.; Chauhan, S.; Chauhan, S. TRIM16 Controls Assembly and Degradation of Protein Aggregates by Modulating the P62-NRF2 Axis and Autophagy. *EMBO J.* **2018**, *37* (18). https://doi.org/10.15252/embj.201798358.

[18]Abramowicz, A.; Widłak, P.; Pietrowska, M. Different Types of Cellular Stress Affect the Proteome Composition of Small Extracellular Vesicles: A Mini Review. *Proteomes* **2019**, *7* (2). https://doi.org/10.3390/proteomes7020023.

[19]Madlung, A.; Comai, L. The Effect of Stress on Genome Regulation and Structure. *Ann. Bot.* **2004**, *94* (4), 481–495. https://doi.org/10.1093/aob/mch172.

[20]Maharjan, S.; Oku, M.; Tsuda, M.; Hoseki, J.; Sakai, Y. Mitochondrial Impairment Triggers Cytosolic Oxidative Stress and Cell Death Following Proteasome Inhibition. *Sci. Rep.* **2014**, *4*, 1–11. https://doi.org/10.1038/srep05896.

[21]Parrado, C.; Mercado-Saenz, S.; Perez-Davo, A.; Gilaberte, Y.; Gonzalez, S.; Juarranz, A. Environmental Stressors on Skin Aging. Mechanistic Insights. *Front. Pharmacol.* **2019**, *10* (July), 1–17. https://doi.org/10.3389/fphar.2019.00759.

[22]Shih, B. B.; Farrar, M. D.; Vail, A.; Allan, D.; Chao, M. R.; Hu, C. W.; Jones, G. D. D.; Cooke, M. S.; Rhodes, L. E. Influence of Skin Melanisation and Ultraviolet Radiation on Biomarkers of Systemic Oxidative Stress. *Free Radic. Biol. Med.* **2020**, *160* (August), 40–46. https://doi.org/10.1016/j.freeradbiomed.2020.07.034.

[23]Balali-Mood, M.; Naseri, K.; Tahergorabi, Z.; Khazdair, M. R.; Sadeghi, M. Toxic Mechanisms of Five Heavy Metals: Mercury, Lead, Chromium, Cadmium, and Arsenic. *Front. Pharmacol.* **2021**, *12* (April), 1–19. https://doi.org/10.3389/fphar.2021.643972.

[24]Khairul, I.; Wang, Q. Q.; Jiang, Y. H.; Wang, C.; Naranmandura, H. Metabolism, Toxicity and Anticancer Activities of Arsenic Compounds. *Oncotarget* **2017**, *8* (14), 23905–23926. https://doi.org/10.18632/oncotarget.14733.

[25]Rice, K. M.; Walker, E. M.; Wu, M.; Gillette, C.; Blough, E. R. Environmental Mercury and Its Toxic Effects. *J. Prev. Med. Public Heal.* **2014**, *47* (2), 74–83. https://doi.org/10.3961/jpmph.2014.47.2.74.

[26]Briffa, J.; Sinagra, E.; Blundell, R. Heavy Metal Pollution in the Environment and Their Toxicological Effects on Humans. *Heliyon* **2020**, *6* (9), e04691. https://doi.org/10.1016/j.heliyon.2020.e04691.

[27]Tamás, M. J.; Sharma, S. K.; Ibstedt, S.; Jacobson, T.; Christen, P. Heavy Metals and Metalloids as a Cause for Protein Misfolding and Aggregation. *Biomolecules* **2014**, *4* (1), 252–267. https://doi.org/10.3390/biom4010252.

[28]Pochapsky, T. C. *Encyclopedia of Metalloproteins*; 2013; Vol. 150. https://doi.org/10.1007/978-1-4614-1533-6.

[29]Valko, M.; Morris, H.; Cronin T. D. Metals, Toxicity, and Oxidative Stress. *Curr. Med. Chem.* **2005**, *12* (10), 1161-1208.

[30]Jiang, J.; Bellani, M.; Li, L.; Wang, P.; Seidman, M. M.; Wang, Y. Arsenite Binds to the RING Finger Domain of FANCL E3 Ubiquitin Ligase and Inhibits DNA Interstrand Crosslink Repair. *ACS Chem. Biol.* **2017**, *12* (7), 1858–1866. https://doi.org/10.1021/acschembio.6b01135.

[31]Breydo, L.; Uversky, V. N. Role of Metal Ions in Aggregation of Intrinsically Disordered Proteins in Neurodegenerative Diseases. *Metallomics* **2011**, *3* (11), 1163–1180. https://doi.org/10.1039/c1mt00106j.

[32]Lee, S.; Liu, Y.; Lim, M. H. Untangling Amyloid- β , Tau, and Metals in Alzheimer ' s Disease. *ACS Chem. Biol.* **2013**, *8*, 856–865.

[33]Ghosh, A. K.; Samanta, I.; Mondal, A.; Liu, W. R. Covalent Inhibition in Drug Discovery. *ChemMedChem* **2019**, *14* (9), 889–906. https://doi.org/10.1002/cmdc.201900107.

[34]Petrov, D.; Zagrovic, B. Microscopic Analysis of Protein Oxidative Damage: Effect of Carbonylation on Structure, Dynamics, and Aggregability of Villin Headpiece. *J. Am. Chem. Soc.* **2011**, *133* (18), 7016–7024. https://doi.org/10.1021/ja110577e.

[35]Tanase, M.; Urbanska, A. M.; Zolla, V.; Clement, C. C.; Huang, L.; Morozova, K.; Follo, C.; Goldberg, M.; Roda, B.; Reschiglian, P.; Santambrogio, L. Role of Carbonyl Modifications on Aging-Associated Protein Aggregation. *Sci. Rep.* **2016**, *6* (December 2015), 1–14. https://doi.org/10.1038/srep19311.

[36]Kim, J.; Song, H.; Heo, H. R.; Kim, J. W.; Kim, H. R.; Hong, Y.; Yang, S. R.; Han, S. S.; Lee, S. J.; Kim, W. J.; Hong, S. H. Cadmium-Induced ER Stress and Inflammation Are Mediated through C/EBP-DDIT3 Signaling in Human Bronchial Epithelial Cells. *Exp. Mol. Med.* **2017**, *49* (9), e372. https://doi.org/10.1038/emm.2017.125.

[37]Shinkai, Y.; Yamamoto, C.; Kaji, T. Lead Induces the Expression of Endoplasmic Reticulum Chaperones GRP78 and GRP94 in Vascular Endothelial Cells via the JNK-AP-1 Pathway. *Toxicol. Sci.* **2010**, *114* (2), 378–386. https://doi.org/10.1093/toxsci/kfq008.

[38]Hiramatsu, N.; Kasai, A.; Du, S.; Takeda, M.; Hayakawa, K.; Okamura, M.; Yao, J.; Kitamura, M. Rapid, Transient Induction of ER Stress in the Liver and Kidney after Acute Exposure to Heavy Metal: Evidence from Transgenic Sensor Mice. *FEBS Lett.* **2007**, *581* (10), 2055–2059. https://doi.org/10.1016/j.febslet.2007.04.040.

[39]Steurer, C.; Eder, N.; Kerschbaum, S.; Wegrostek, C.; Gabriel, S.; Pardo, N.; Ortner, V.; Czerny, T.; Riegel, E. HSF1 Mediated Stress Response of Heavy Metals. *PLoS One* **2018**, *13* (12), 1–18. https://doi.org/10.1371/journal.pone.0209077.

[40]*Regulation of Heat Shock Protein Responses*; Asea, A. A. A., Kaur, P., Eds.; Springer US, **2018**; Vol. 13. https://doi.org/doi.org/10.1007/978 3 319 74715 6_2.

[41]Jafari, R.; Almqvist, H.; Axelsson, H.; Ignatushchenko, M.; Lundbäck, T.; Nordlund, P.; Molina, D. M. The Cellular Thermal Shift Assay for Evaluating Drug Target Interactions in Cells. *Nat. Protoc.* **2014**, *9* (9), 2100–2122. https://doi.org/10.1038/nprot.2014.138.

[42]Stevens R.C., Sancho J., Martinez A. (**2010**) Rescue of Misfolded Proteins and Stabilization by Small Molecules. In: Bross P., Gregersen N. (eds) Protein Misfolding and Cellular Stress in Disease and Aging. Methods in Molecular Biology (Methods and Protocols), vol 648. Humana Press, Totowa, NJ. https://doi.org/10.1007/978-1-60761-756-3_22

[43]Ghildiyal, M.; Zamore, P. D. Small Silencing RNAs: An Expanding Universe. *Nat. Rev. Genet.* **2009**, *10* (2), 94–108. https://doi.org/10.1038/nrg2504.

[44]Moazed, D. Small RNAs in Transcriptional Gene Silencing and Genome Defence. *Nature* **2009**, *457* (7228), 413–420. https://doi.org/10.1038/nature07756.

[45]Norouzi-Barough, L.; Sarookhani, M.; Salehi, R.; Sharifi, M.; Moghbelinejad, S. CRISPR/Cas9, a New Approach to Successful Knockdown of ABCB1/P-Glycoprotein and Reversal of Chemosensitivity in Human Epithelial Ovarian Cancer Cell Line. *Iran. J. Basic Med. Sci.* **2018**, *21* (2), 181–187. https://doi.org/10.22038/ijbms.2017.25145.6230.

[46]Fang, L.; Hung, S. S. C.; Yek, J.; El Wazan, L.; Nguyen, T.; Khan, S.; Lim, S. Y.; Hewitt, A. W.; Wong, R. C. B. A Simple Cloning-Free Method to Efficiently Induce Gene Expression Using CRISPR/Cas9. *Mol. Ther. - Nucleic Acids* **2019**, *14* (March), 184–191. https://doi.org/10.1016/j.omtn.2018.11.008.

APPENDIX: PRM Chromatograms were provided from Skyline.

RPS3, DEILPTTPISEQK, 735.888 2+:

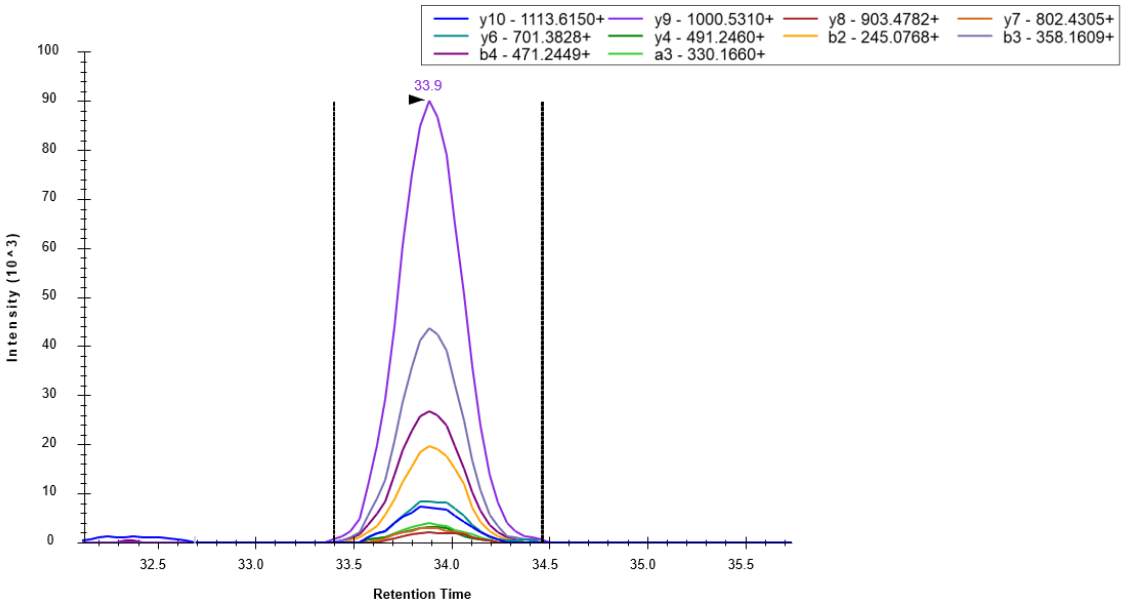

RPS3, AELNEFLTR, 546.78784 2+:

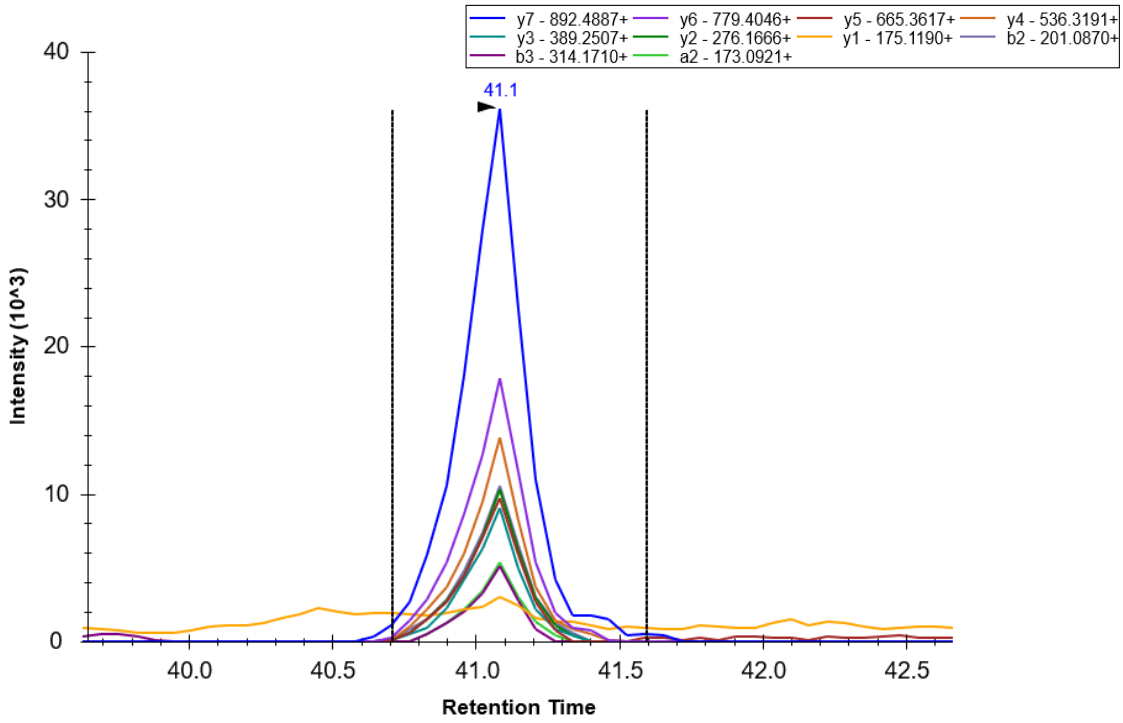

HNRNPK, IILDLISESPIK, 670.90541 2+:

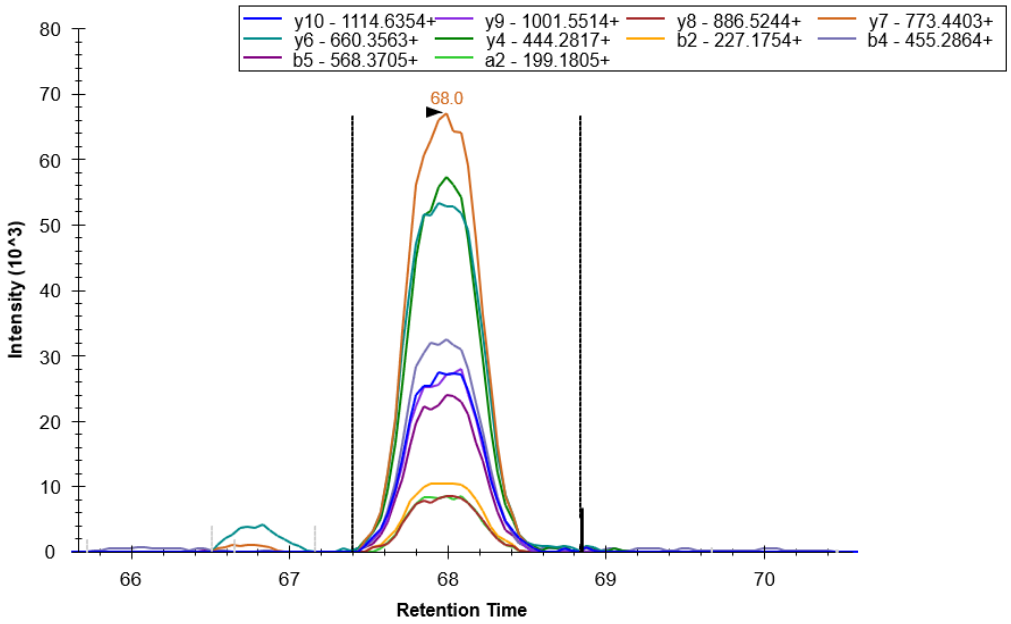

HNRNPK, GSYGDLGGPIITTQVTIPK, 959.02002 2+:

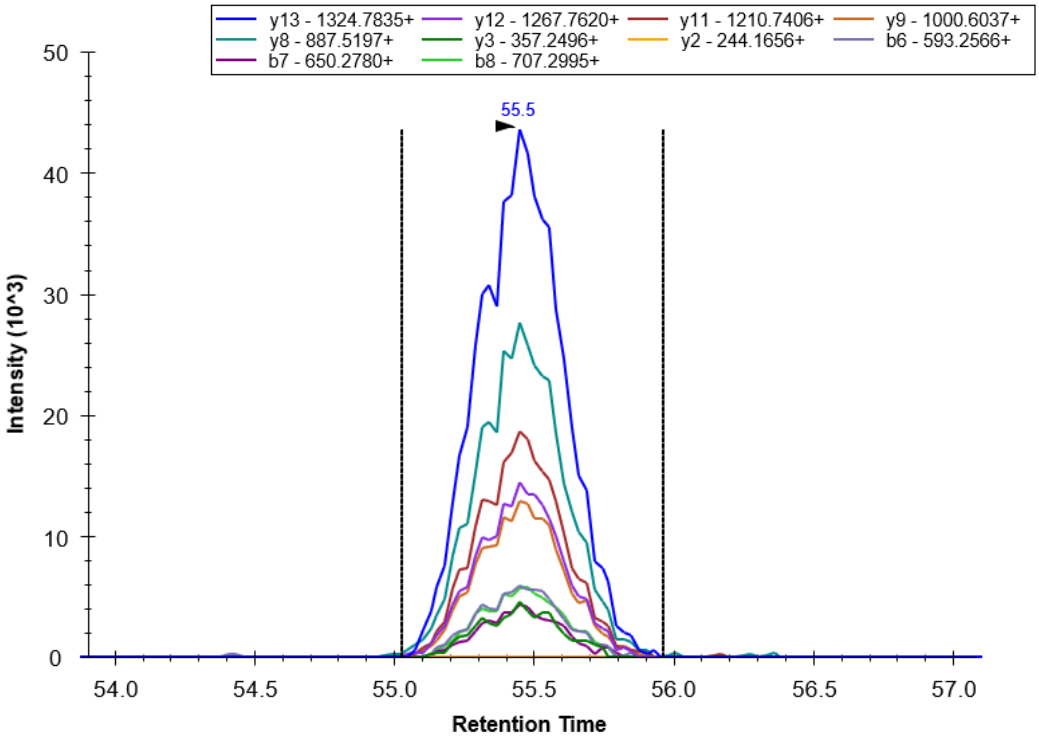

HNRNPK, LLIHQSLAGGIIGVK, 759.97195, 2+:

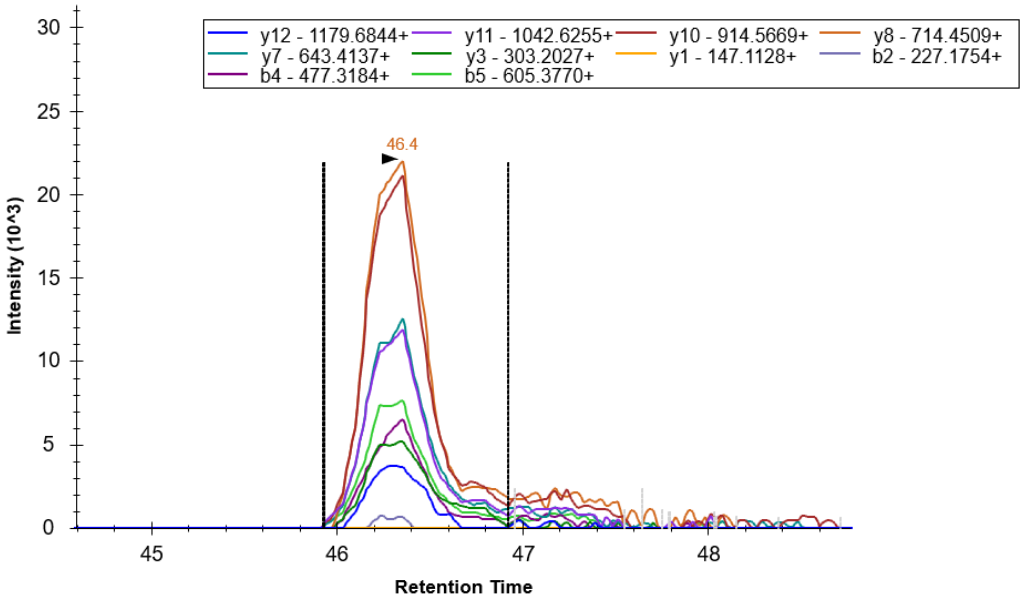

HNRNPK, TDYNASVSVPDSSGPER, 890.90284, 2+:

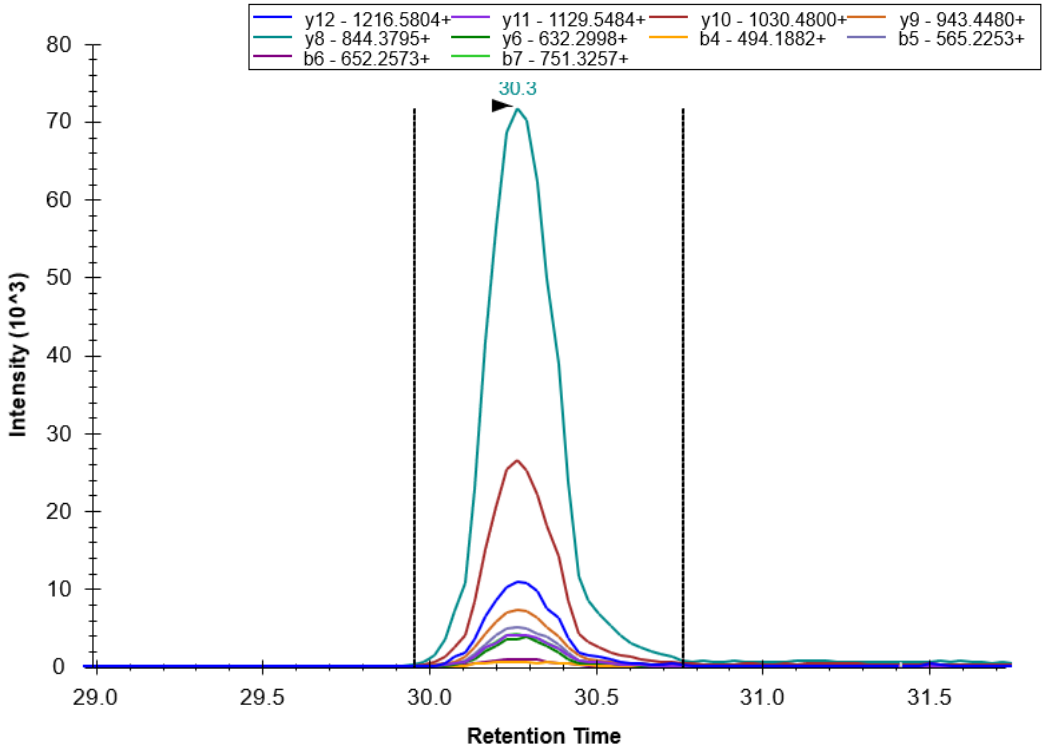

RPS16, LLEPVLLLGK, 547.86282, 2+

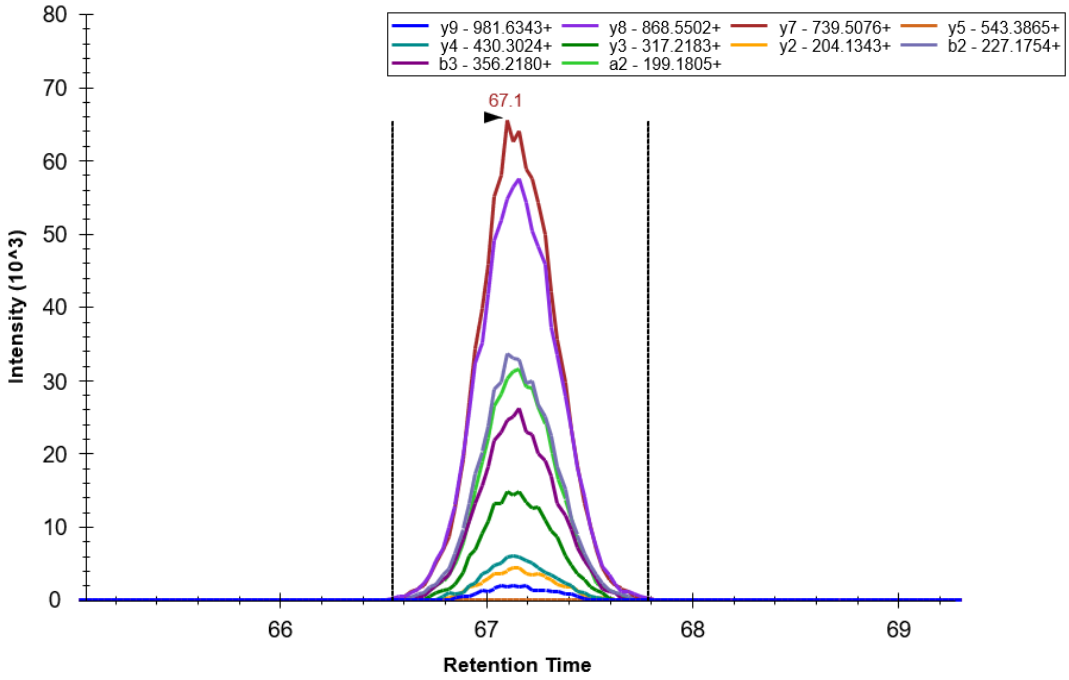

RPS16, GPLQSVQVFGR, 594.3302, 2+:

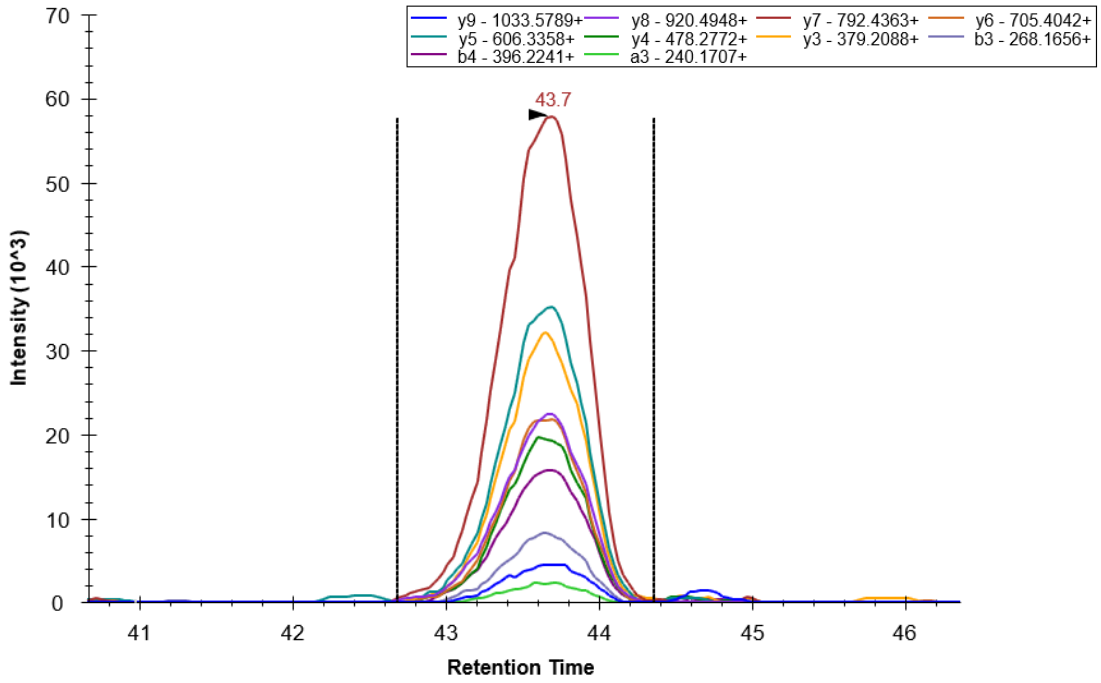

HNRNPA0, LFIGGLNVQTSESGLR, 845.95977, 2+:

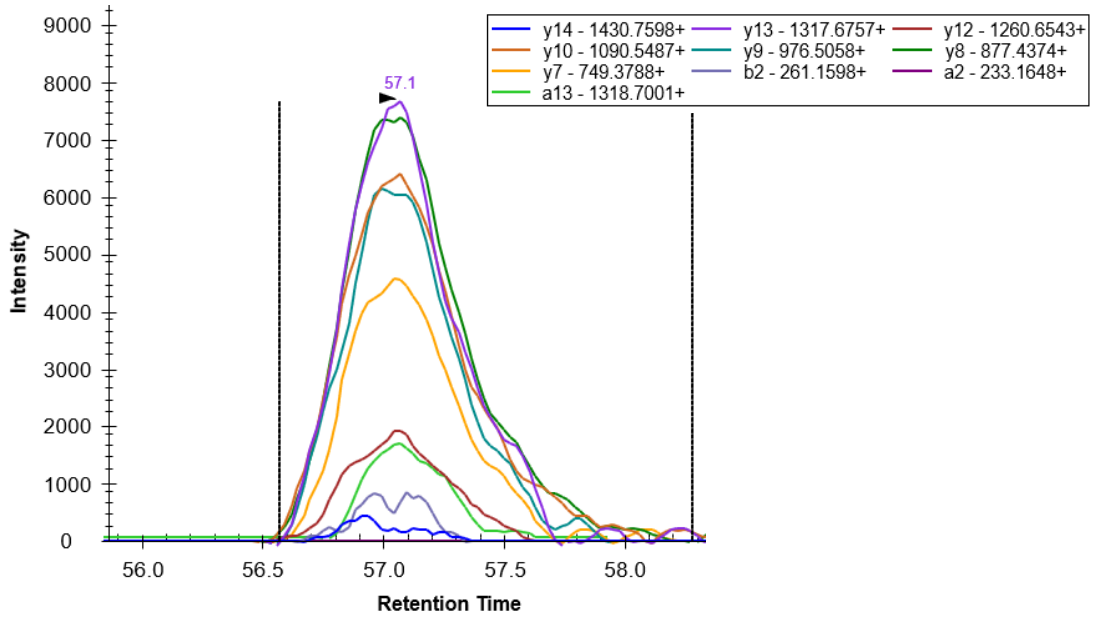

RACK1, VWQVTIGTR, 530.30092, 2+:

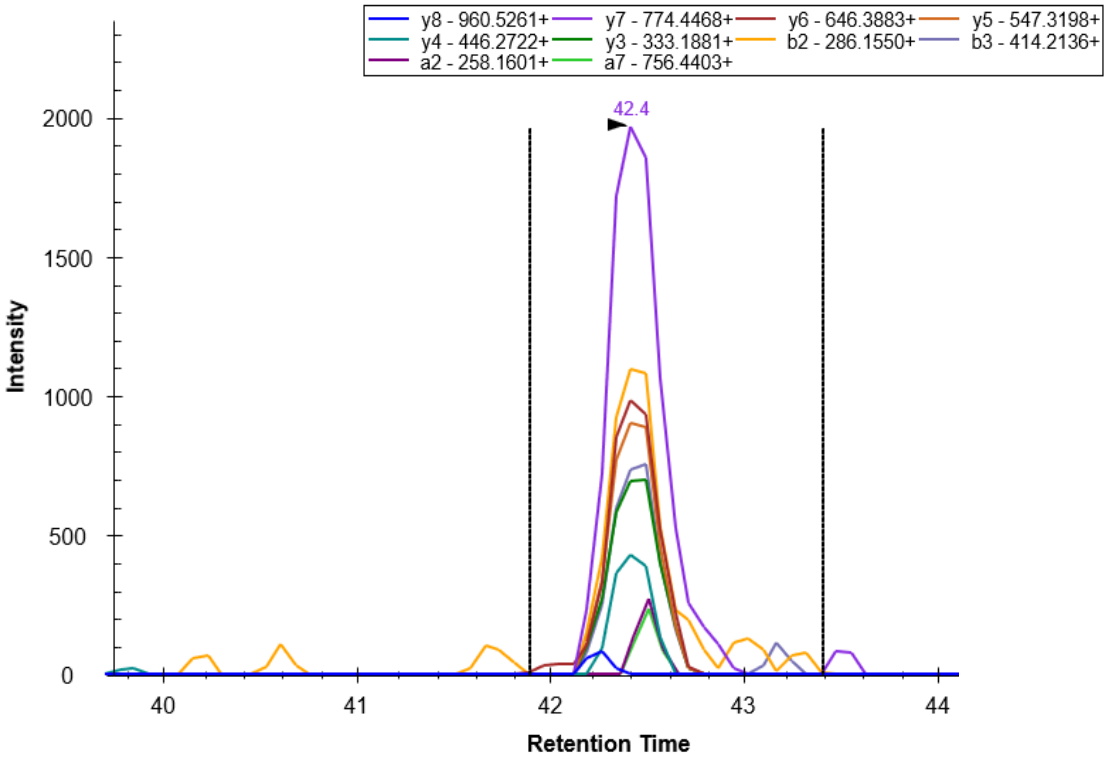

RACK1, DETNYGIPQR, 596.78328, 2+:

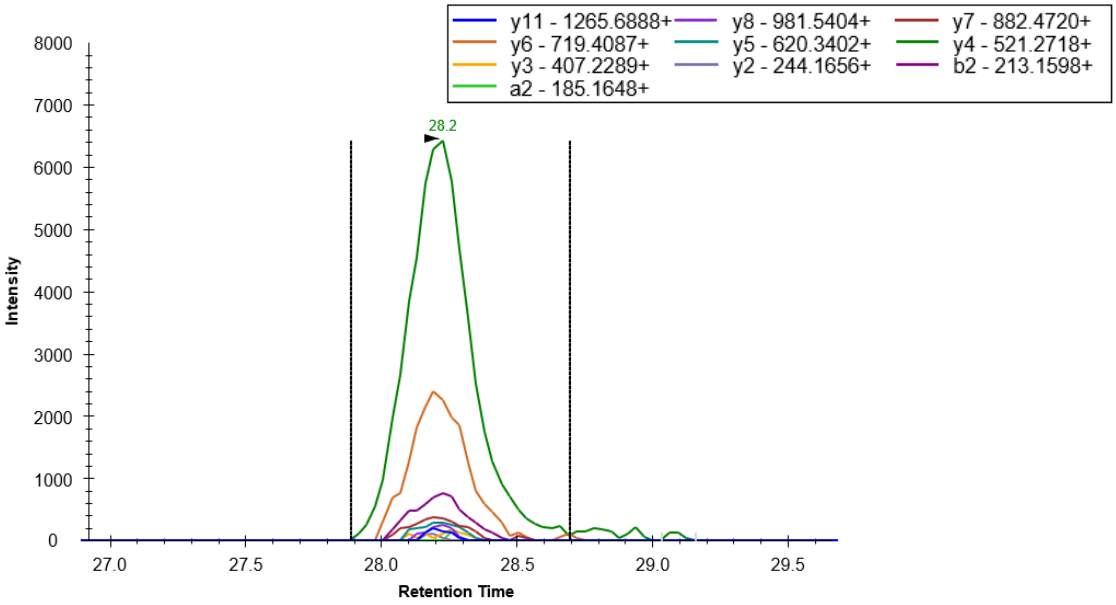

TARDBP, TSDLIVLGLPWK, 671.39247, 2+:

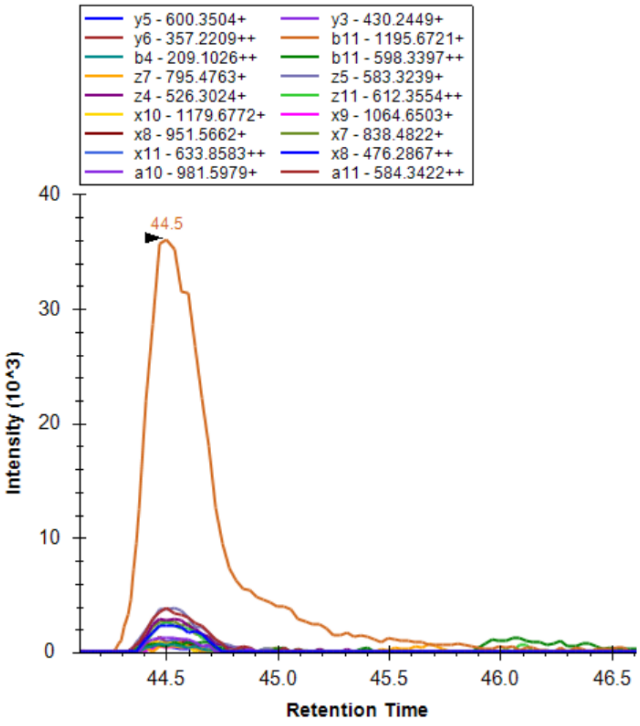

TARDBP, FGGNPGGFGNQGGFGNSR, 863.88767, 2+:

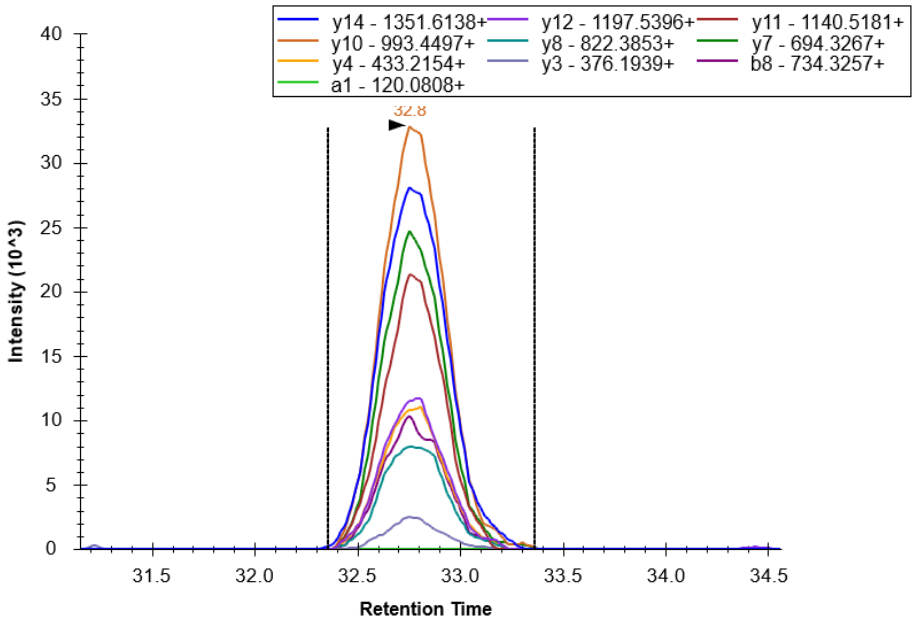

TARDBP, GISVHISNAEPK, 626.3382, 2+:

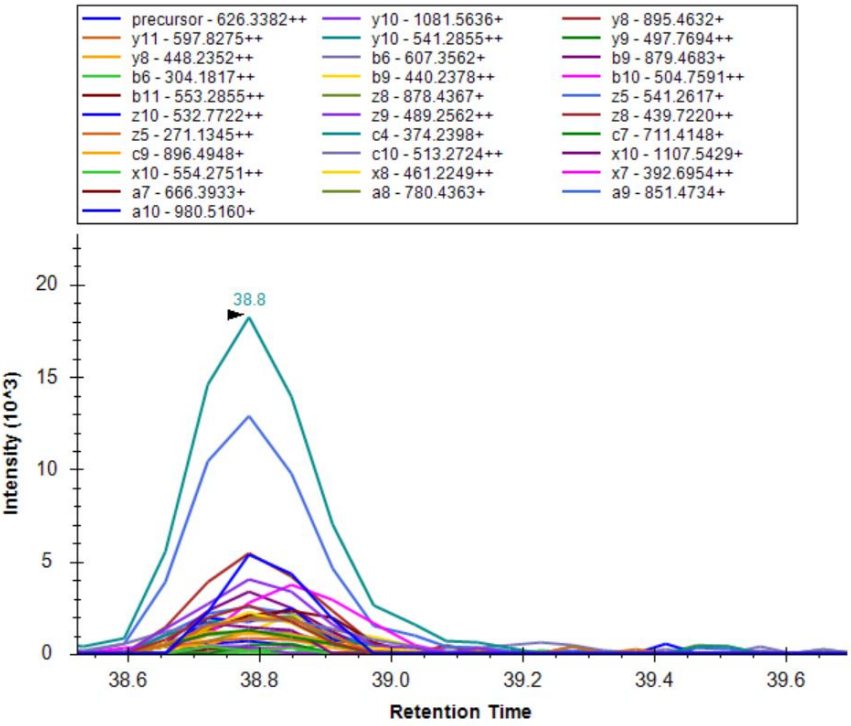

TARDBP, FTEYETQVK, 572.7797, 2+:

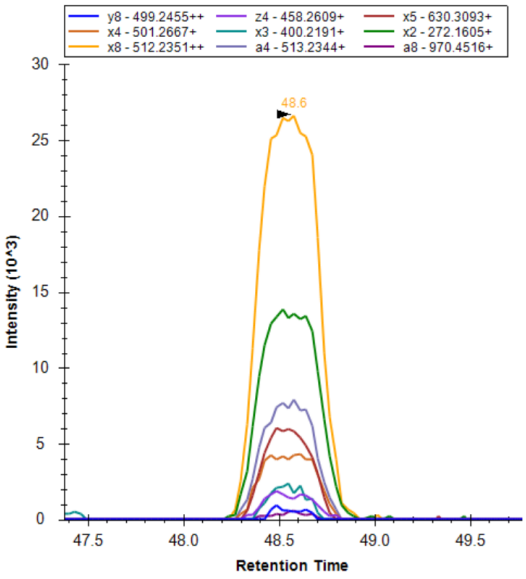

TARDBP, QSQDEPLR, 486.7409, 2+:

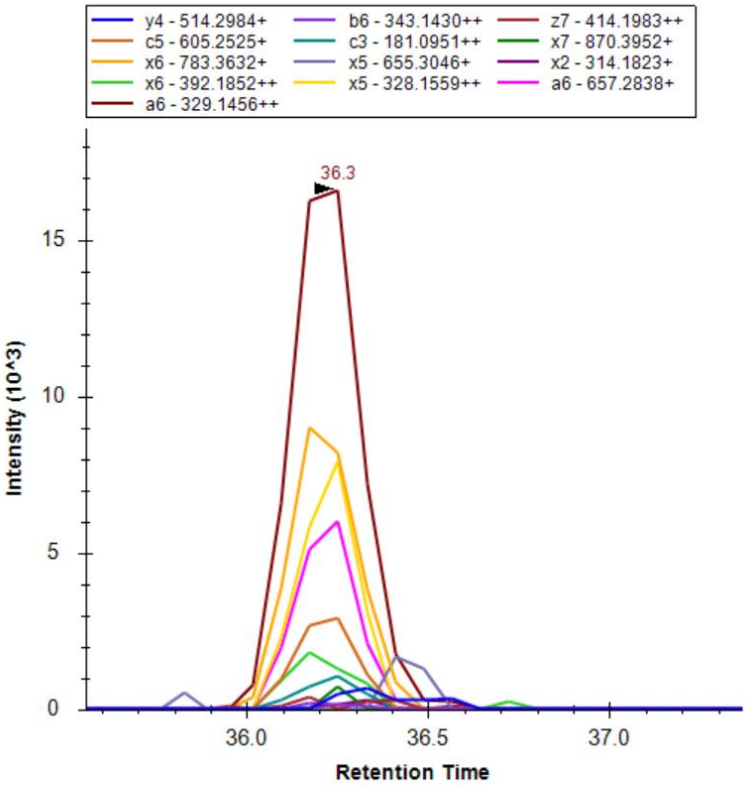

PDHA1, LEEGPPVTTVLTR, 706.3932, 2+:

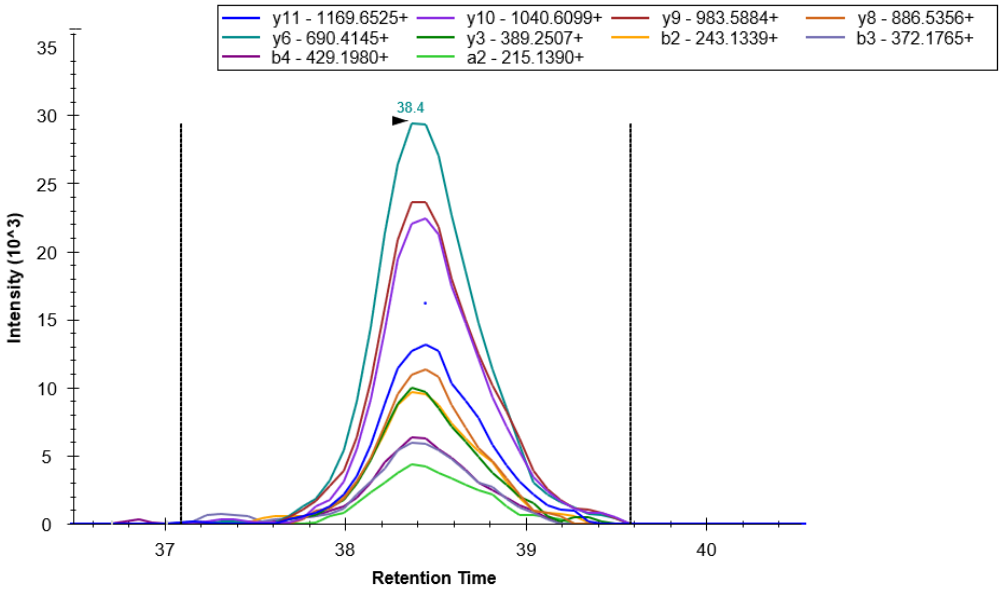

PDHA1, MVNSNLASVEELK, 717.3688, 2+:

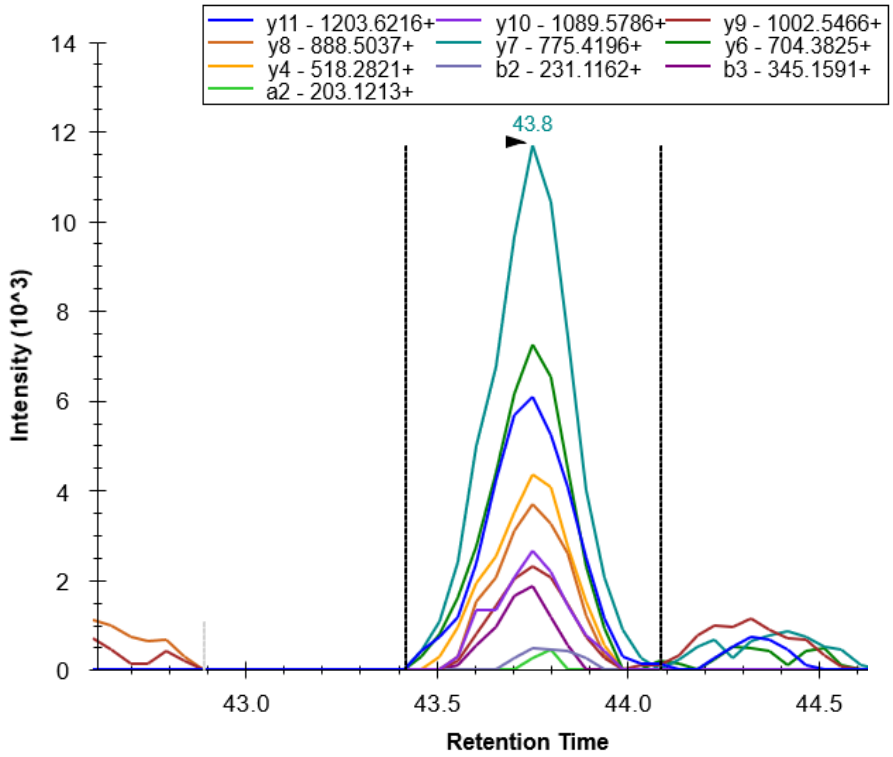

PDHA1, EILAELTGR, 501.2849, 2+:

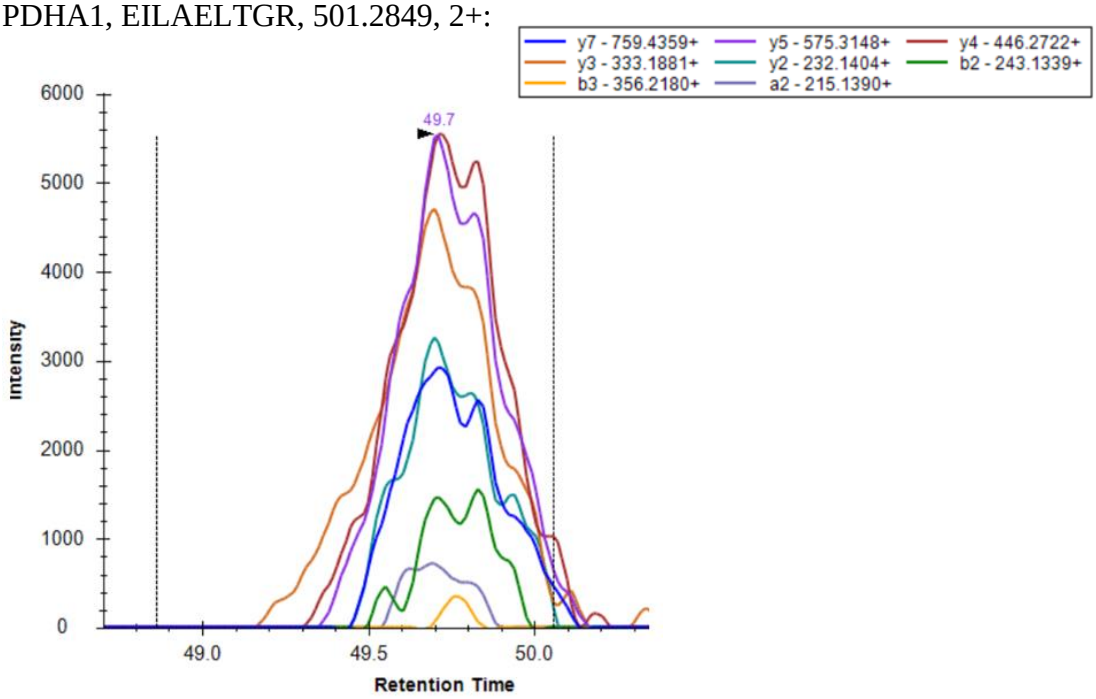

PDHA1, GPILMELQTYR, 660.8526, 2+:

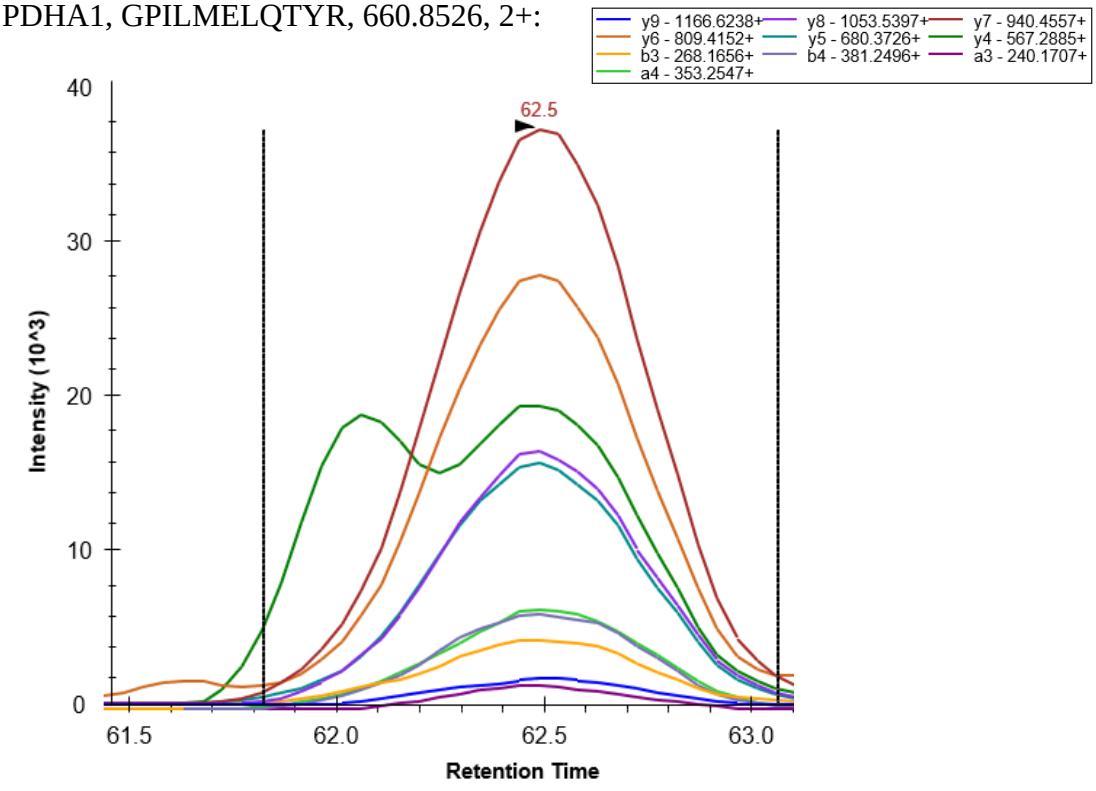

PDHB, TIRPMDMETIEASVMK, 926.4543, 2+:

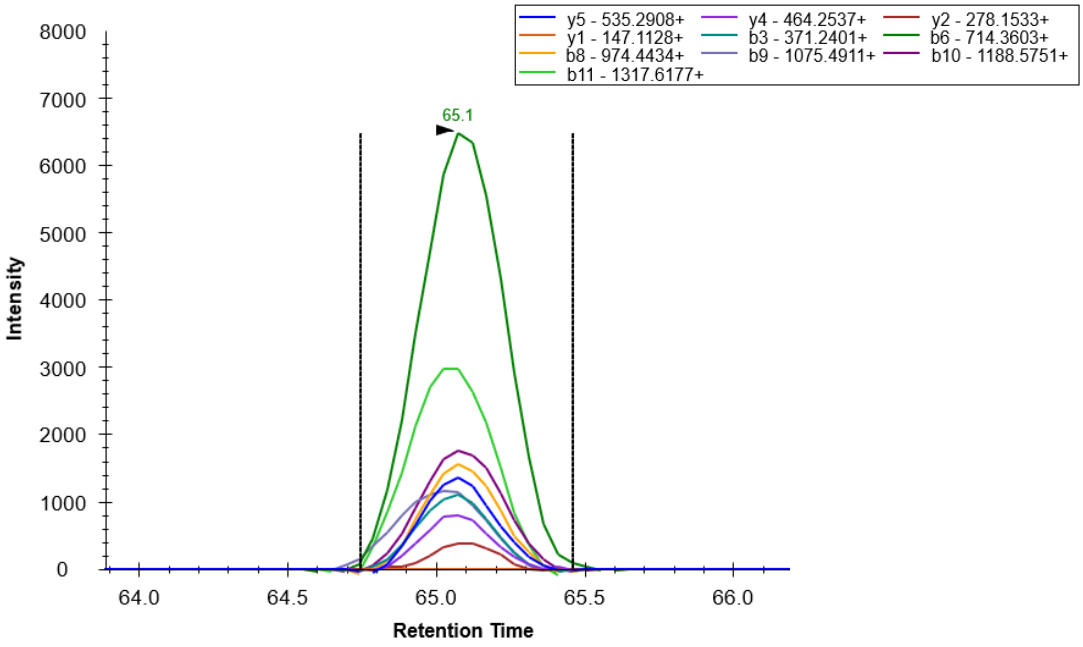

PDHB, VFLLGEEVAQYDGAYK,901.454, 2+

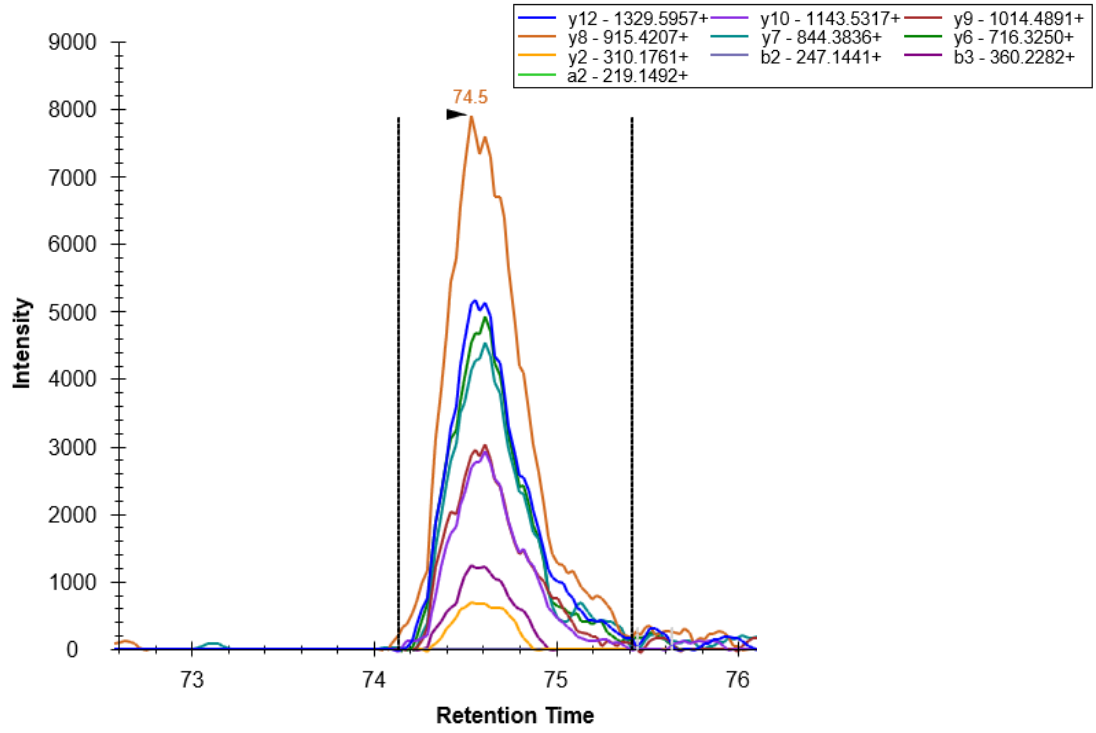

PDHB, IMEGPAFNFLDAPAVR, 874.4454, 2+:

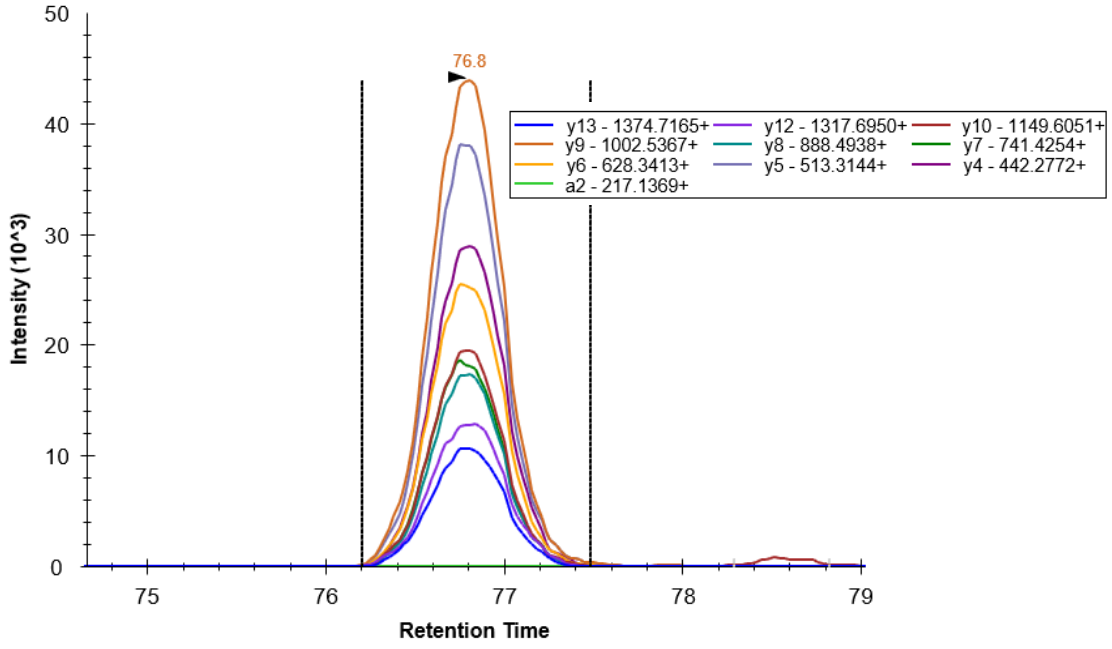

PDHB, DAINQGMDEELER, 760.3383, 2+:

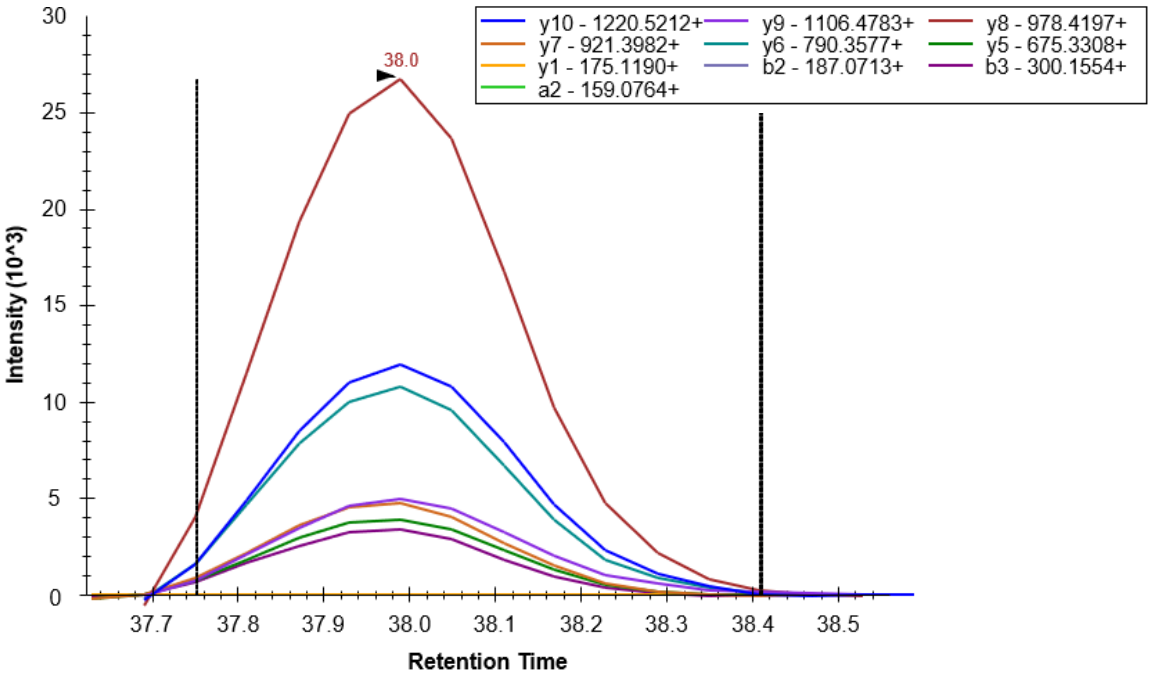

PDHB, ILEDNSIPQVK, 628.348, 2+:

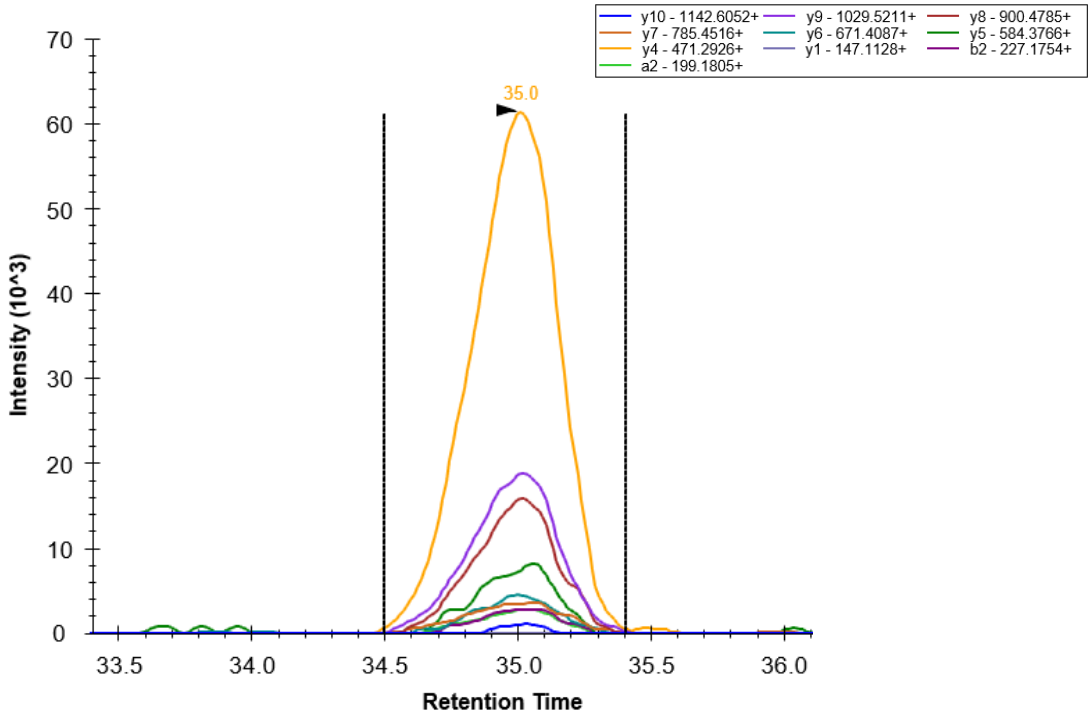

PDHB, DFLIPIGK, 451.7709, 2+:

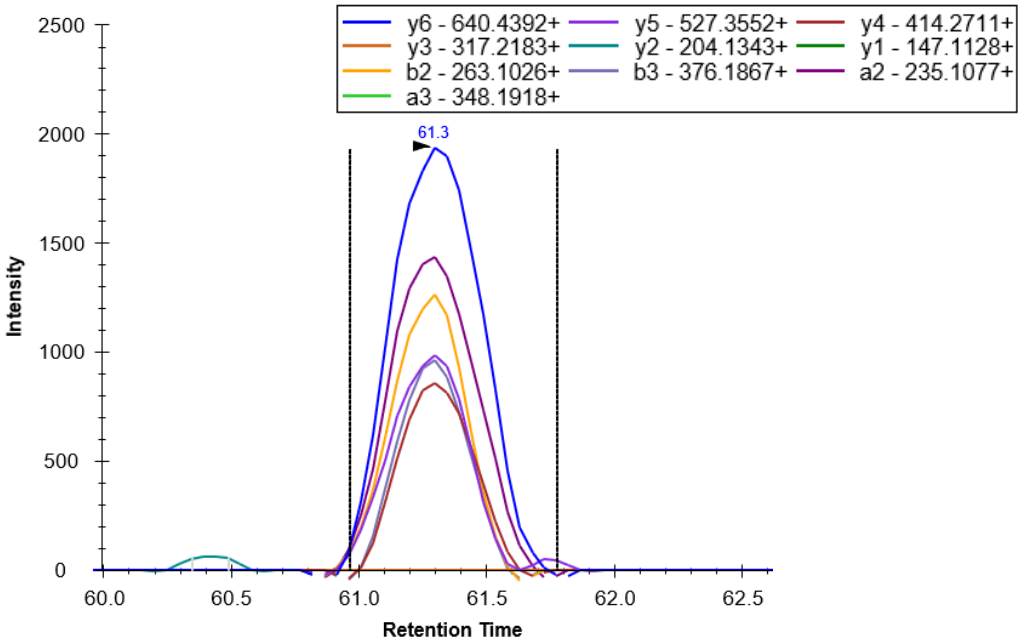

HNRNPK, 517.2223, 3+:

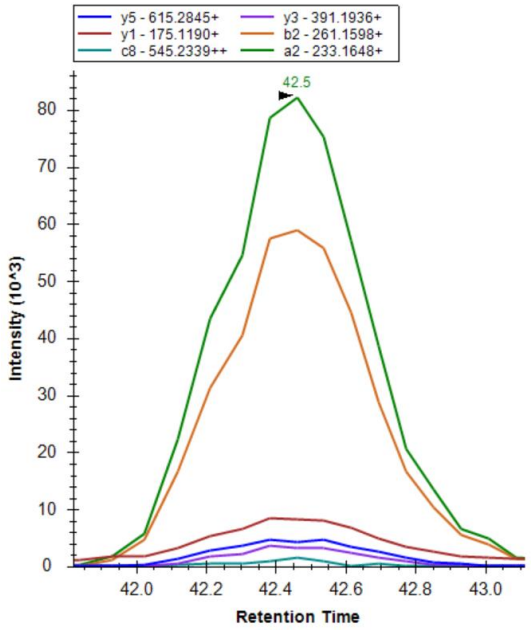

Internal Standard, VFFAEDVGSNK, 606.7984, 2+:

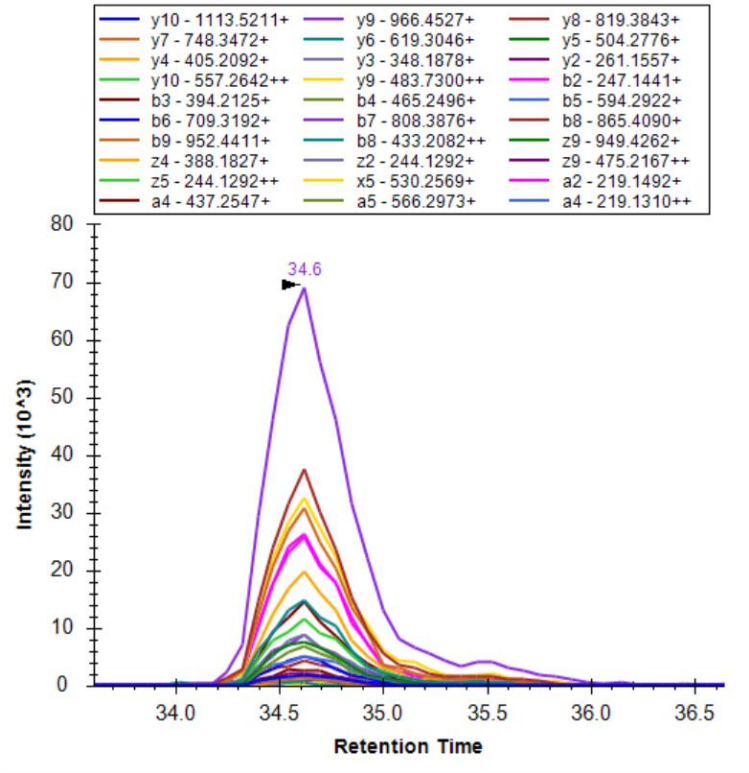

GAPDH, VVDLMAHMASK, 601.307 2+:

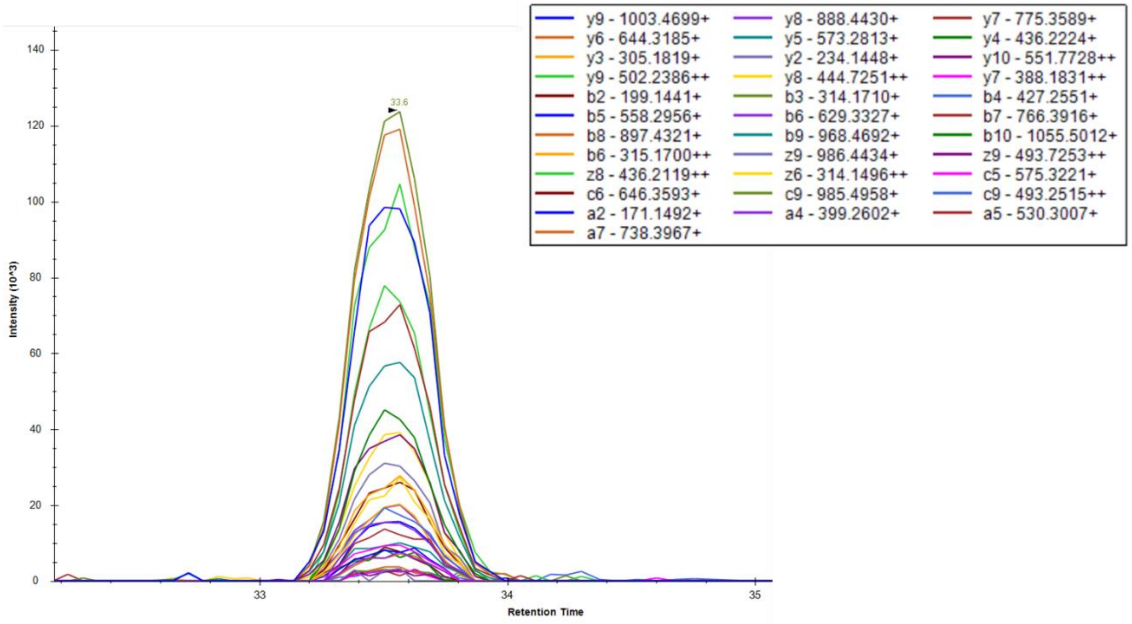

GAPDH, LVINGNPITIFQER, 807.4541 2+:

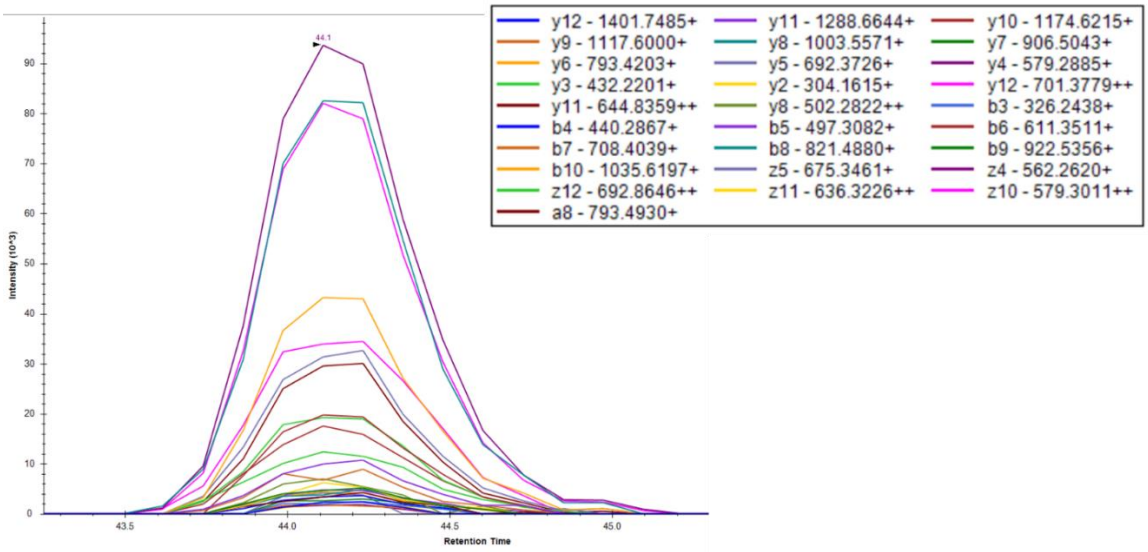

GAPDH, VPTANVSVVDLTCR, 765.9008, 2+:

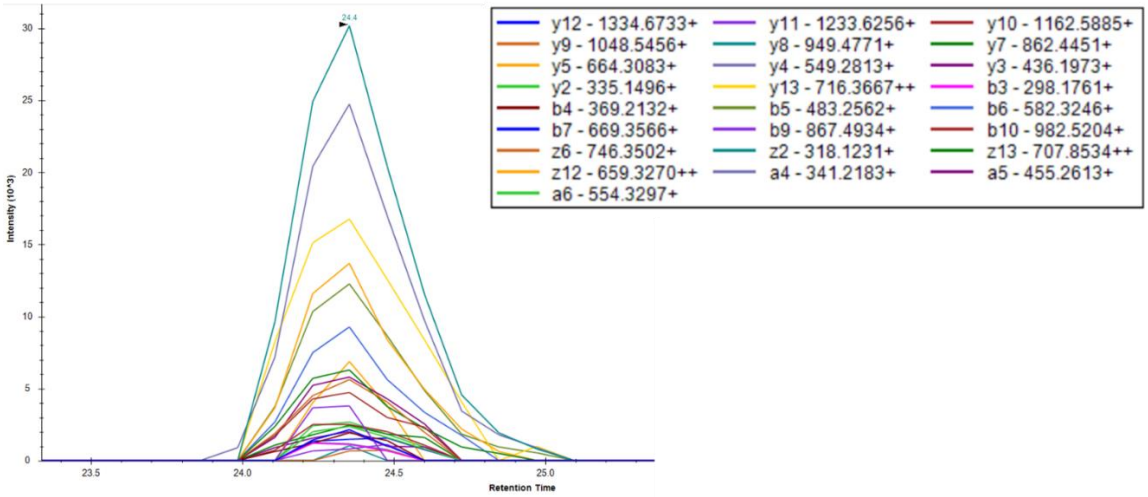

GAPDH, LISWYDNEFGYSNR, 882.4048, 2+:

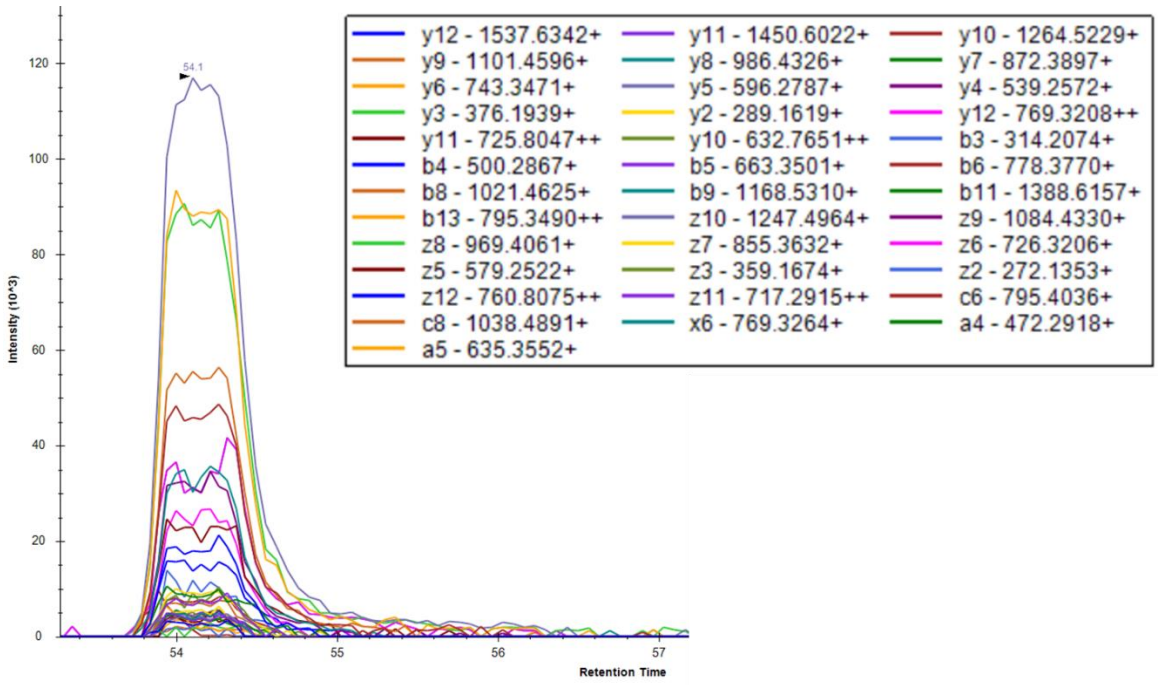

GAPDH, GALQNIIPASTGAAK, 706.3988, 2+:

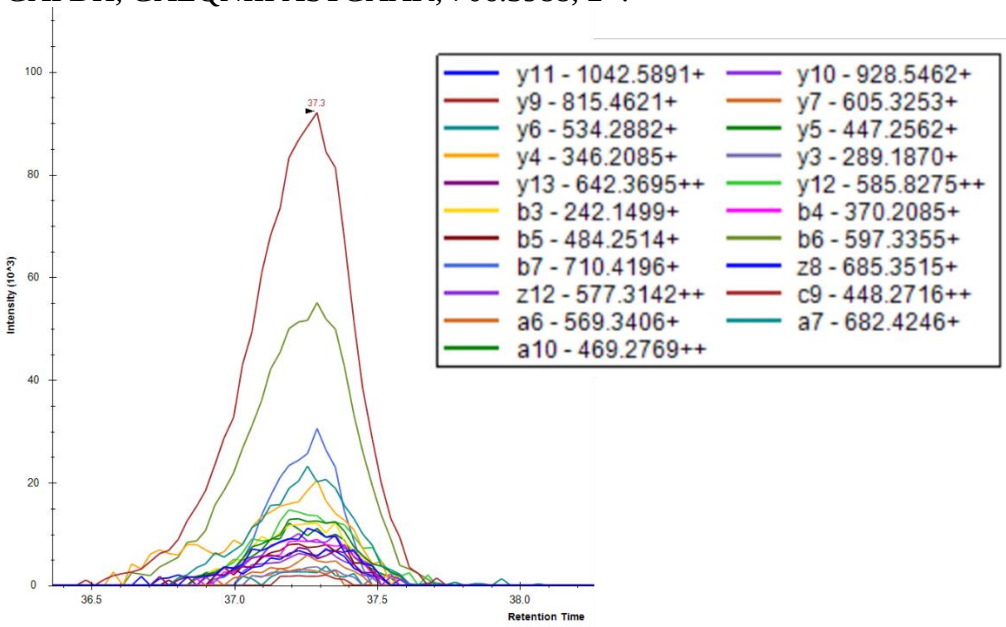

GAPDH, IISNASCTTNCLAPLAK, 917.4635, 2+:

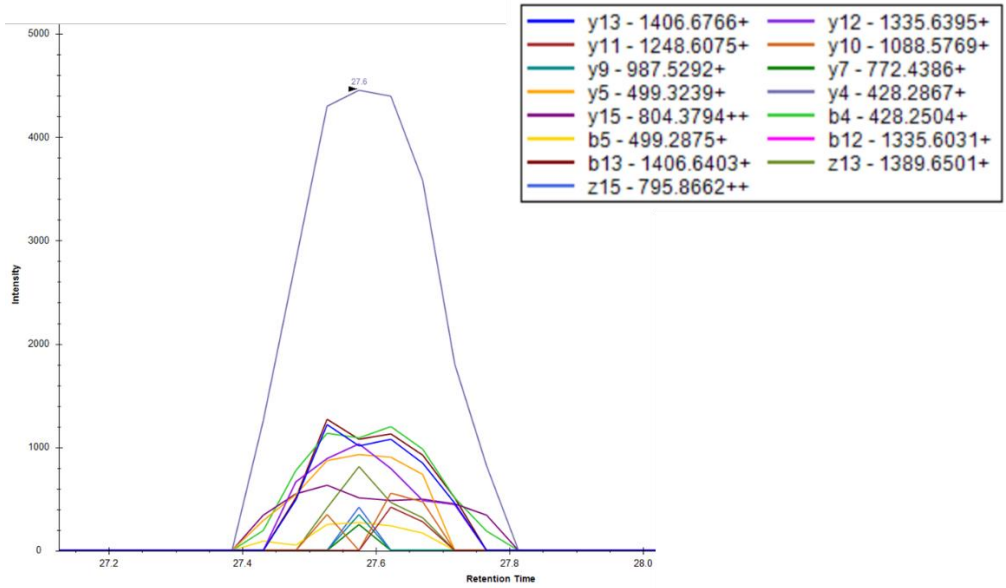

GAPDH, Propachlor Adduct-IISNAS**C**TTNCLAPLAK, 977.0065 2+:

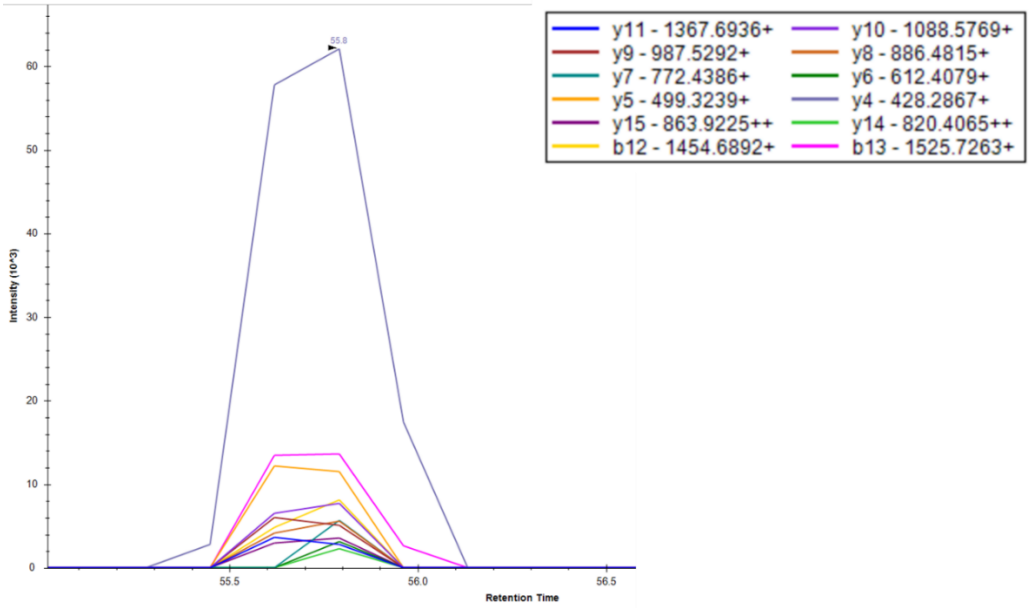

PARK7, GAEEMETVIPVDVMR, 838.4051 2+:

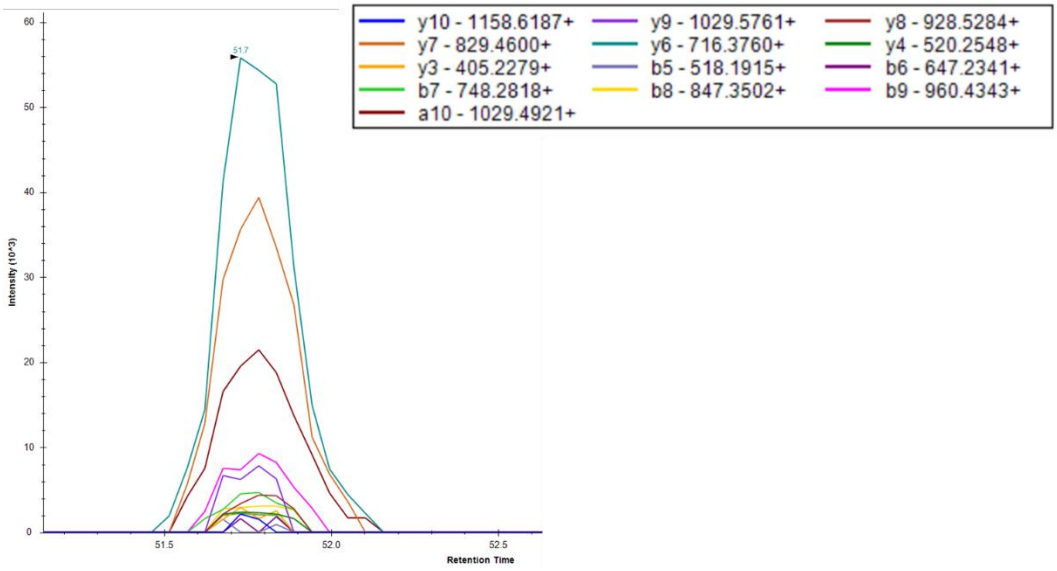

PARK7, DVVICPDASLEDAK, 766.369, 2+:

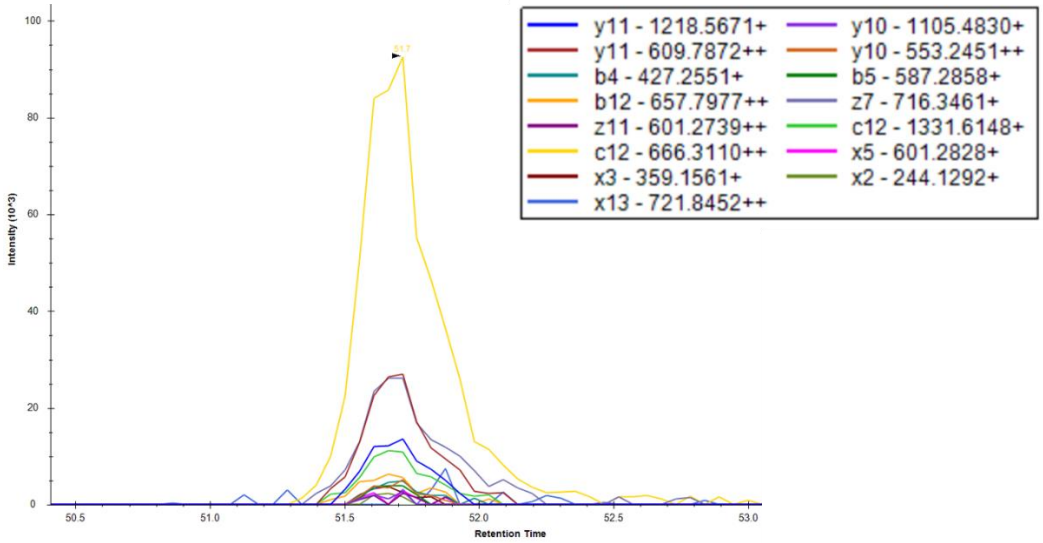

PARK7, VTVAGLAGK, 408.2529, 2+:

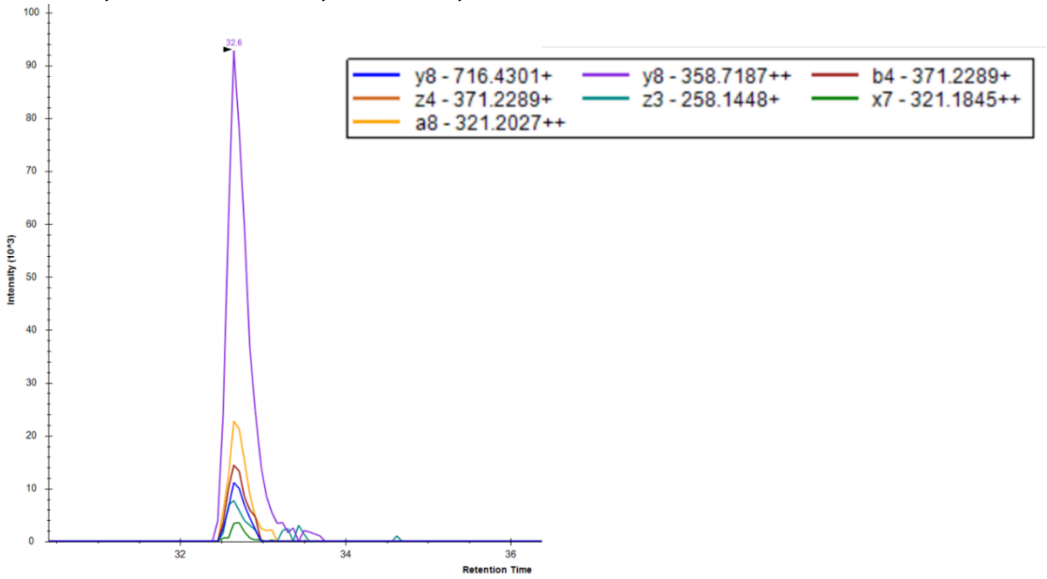

NKRF, TNPEYIYAPLK, 654.8453 2+:

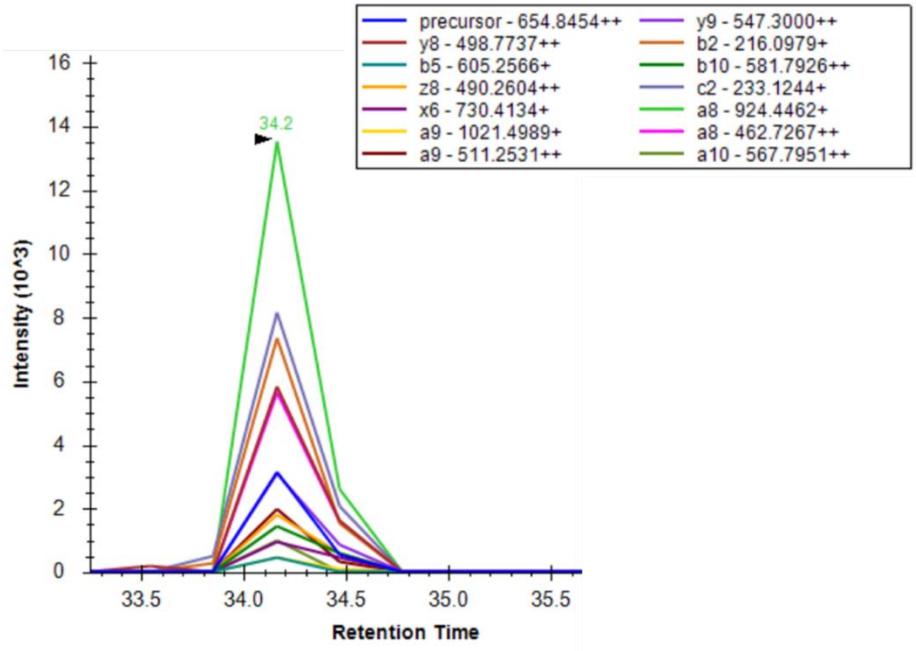

NKRF, SESHTDLTFSR, 640.2993 2+:

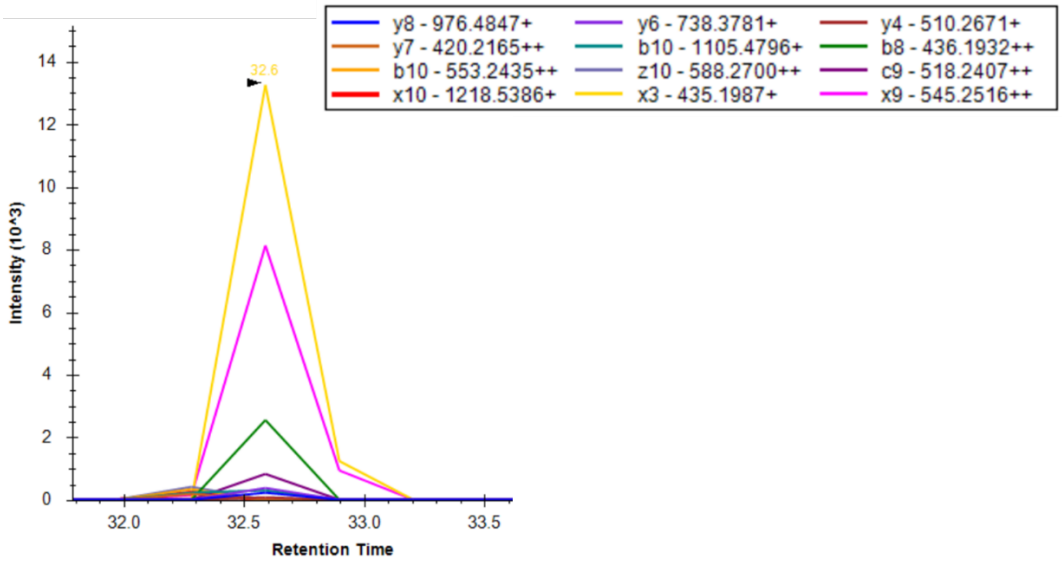

NKRF, MTVEYVYER, 595.2815 2+: